

THERMALLY STIMULATED DISCHARGE OF AMORPHOUS
POLYMERIC POLYVINYL BUTYRAL AND XEROGRAPHIC
SELENIUM LAYERS

by

KAMARULZAMAN BIN MOHAMED ZIN B.Sc.(Hons.), M.Sc.

A thesis submitted for the degree of
Doctor of Philosophy of the University of London
and for the Diploma of Imperial College

Solid State Electronics Group
Department of Electrical Engineering
Imperial College of Science and Technology
London SW7 2BT
March 1986.

ABSTRACT

Thermally Stimulated Discharge (TSD) of the following two materials or materials system were carried out: i) Polyvinyl butyral, a binder resin used in the pigment-resin-dye type of xerographic photoreceptors and ii) a double-layer a-SeTe/a-Se xerographic photoreceptor.

TSD of DC charged films of PVB reveal the presence of two different mechanisms of persistent electrical polarisation. The peak at 60 °C in the short-circuit current thermogram is attributed to the disorientation of permanent dipoles in the polymer. The position of this peak also coincides with the glass transition temperature, T_g , of the polymer. This signifies the close relationship between the dipole disorientation with the onset of segmental movements of the polymer chains.

A second peak observed at about 78 °C in the thermogram is due to a space charge polarisation arising from intrinsic ions that were previously immobilised at the near electrode regions. The appearance of the space charge peak in a temperature region which is above T_g reflects the dependence of the translational drift of the re-mobilised ions on the available free volume which is needed for the decay of the space charge polarisation. By correlating the relaxation time for the ionic transitions with the structural relaxation time that is expressed by the free volume theory, the values of the fractional free volume at T_g and the coefficient of expansion of the free volume are found.

TSD of the surface potential of unmetallised and corona charged samples of the films yield decay plots with distinctive two-step like curves corresponding to the dipolar relaxation and the neutralisation of the homocharges by the intrinsic electrical conduction of the polymer. The time derivative of the surface potential decay curve, which is the TSD displacement current thermogram, confirms that the intrinsic ionic conductivity of the polymer is the dominant parameter in determining the build-up or decay of any space charge polarisation in the PVB films.

The TSD of DC charged samples of a double layer a-SeTe/a-Se xerographic photoreceptor display two current peaks which are directly attributable to the heterogeneity in the sample structure.

The low temperature peak, centred at about -8°C , is due to the decay of a Maxwell-Wagner polarisation and is essentially a conductivity-determined peak. The second peak that is observed is broad, spanning between 30 to 50°C and is due to the release of trapped carriers from states that are associated with the physical junction of the a-SeTe and a-Se layers. The detrapping is closely related to the structural relaxations of the individual layers as evidenced by the proximity of the TSD current peak to the glass transition regions of the layers.

ACKNOWLEDGEMENTS

I am grateful to Dr.C Juhasz for his help, guidance and encouragement throughout the course of this project.

I wish to thank members of the Solid State Electronics Group for helpful suggestions, especially to Dr.S.O Kasap for the many stimulating discussions that we have had. Thanks are also due to Mr.K.G White for technical assistance.

I am grateful to the Government of Malaysia and Gestetner (Byfleet) Ltd.,U.K for financial support.

I would also like to thank Mrs.D Abeysekeera for her adept typing of the manuscript.

Finally, I acknowledge with the deepest gratitude the understanding and strength of my mother Zaharah. This work would not have been possible without her whole-hearted support and constant encouragement. I could never thank her enough.

In everlasting memory of Mohamed Zin bin Mahmud

CONTENTS

| | <u>Page No.</u> |
|------------------|--|
| CHAPTER 1 | POLYMERS |
| 1.1 | The Polymeric Solid State 10 |
| 1.2 | Morphology and Molecular Architecture 11 |
| 1.3 | Amorphous Polymers |
| 1.3.1 | The Glass Transition 14 |
| 1.3.2 | Relaxations in Amorphous Polymers 17 |
| 1.3.3 | The WLF equation 19 |
| 1.4 | Electronic Properties of Polymeric Solids |
| 1.4.1 | Introduction 20 |
| 1.4.2 | Extended Electronic States 21 |
| 1.4.3 | Localised States 23 |
| 1.5 | Electrical Transport in Organic Polymers |
| 1.5.1 | Introduction 24 |
| 1.5.2 | Intra-molecular Electronic Conduction 25 |
| 1.5.3 | Inter-molecular Electronic Conduction 27 |
| 1.5.4 | Ionic Conduction 29 |
| 1.5.5 | Displacement Currents 31 |
| 1.6 | Summary 32 |
| 1.7 | Aims of The Present Study and Lay-out of the Thesis 33 |
| CHAPTER 2 | THERMALLY STIMULATED DISCHARGE |
| 2.1 | Introduction 34 |
| 2.2 | Principles of the TSD technique 36 |
| 2.2.1 | Polarisation 36 |
| 2.2.2 | Depolarisation 36 |
| 2.2.3 | Mechanisms Contributing to TSD 37 |
| 2.2.4 | Freezing-in of the Polarisation 39 |
| 2.2.5 | Depolarisation and the Origin of TSD peaks 40 |
| 2.3 | Detection Efficiency of TSD current measurements 41 |
| | and Variations of the Method |
| 2.4 | TSD Theory involving Dipolar Processes |
| 2.4.1 | Dipole Disorientation with a single 43 |
| | Relaxation Time |
| 2.4.2 | Dipolar TSD with a Distribution of Relaxation 47 |
| | Times |
| 2.4.3 | Equivalent Frequency of Dipolar TSD measurements 40 |
| 2.5 | TSD Theory involving Space Charges |
| 2.5.1 | Introduction 53 |
| 2.5.2 | The Charge Motion Model 53 |
| 2.5.3 | A brief note regarding the Trapping Model 57 |

| | <u>Page No.</u> |
|--|-----------------|
| 2.6 TSD of Heterogenous Physical Systems | |
| 2.6.1 TSD of a Double-Layer Laminate | 59 |
| 2.6.2 TSD of a Homogenous Solid with an Air gap | 65 |
| 2.6.3 TSD of Surface Potential - "Charge" TSD | 68 |
| 2.6.3.1 Theory | 68 |
| 2.7 Evaluation of Data from TSD curves | |
| 2.7.1 Preliminary remarks | 71 |
| 2.7.2 Calculation of Activation Energies | |
| 2.7.2.1 Initial Rise Method | 72 |
| 2.7.2.2 Graphical Integration Method | 74 |
| 2.7.2.3 Methods based on the Variation of Heating Rates | 75 |
| 2.7.3 Calculation of Other Relaxation Parameters | 76 |
| 2.7.4 Notes for Distributed Processes | 77 |
| 2.7.5 Notes for the Charge Motion Model | 78 |
| | |
| CHAPTER 3 POLYVINYL BUTYRAL AND AMORPHOUS SELENIUM-BASED XEROGRAPHIC PHOTORECEPTOR | |
| 3.1 Polyvinyl butyral | |
| 3.1.1 Introduction | 80 |
| 3.1.2 Chemical Formula and Structure | 82 |
| 3.1.3 Infra-red Absorption | 82 |
| 3.1.4 Relaxational Properties | |
| 3.1.4.1 Introduction | 85 |
| 3.1.4.2 Dielectric Properties | 86 |
| 3.1.4.3 Dynamic Mechanical Properties | 90 |
| 3.1.4.4 TSD behaviour | 90 |
| 3.1.5 Summary | 95 |
| 3.2 Amorphous Selenium-based Multi-Layer Photoreceptor | |
| 3.2.1 Introduction | 98 |
| 3.2.2 Interfaces in Photoreceptors | 100 |
| 3.2.3 TSD of Xerographic Photoreceptors | 102 |
| 3.3 Experimental Objectives | 103 |
| | |
| CHAPTER 4 EXPERIMENTAL DETAILS AND PROCEDURES | |
| 4.1 Sample Preparation | |
| 4.1.1 Polyvinyl butyral | 105 |
| 4.1.2 a-Se based Multi-Layer Photoreceptor | 109 |
| 4.1.2.1 Te profile | 111 |
| 4.2 Experimental Set-up and Procedure | |
| 4.2.1 Surface Potential and "Charge" TSD Measurements | 113 |
| 4.2.1.1 Corona Charging Unit | 113 |

| | <u>Page No.</u> |
|---|-----------------|
| 4.2.1.2 Electrostatic Voltmeter and Measuring Probe | 115 |
| 4.2.1.3 Heating System and Temperature Control | 116 |
| 4.2.2 TSD Current Measurements | 118 |
| 4.2.2.1 The Cryostat, Sample Holder and Vacuum System | 118 |
| 4.2.2.2 Temperature Control | 120 |
| 4.2.2.3 Current Detection and Recording | 121 |
| 4.3 Materials Characterisation | 123 |
| 4.3.1 Differential Thermal Analysis | 123 |
| 4.3.2 Infra-red Spectrophotometry | 125 |
| CHAPTER 5 RESULTS AND DISCUSSIONS | |
| 5.1 Introduction | 127 |
| 5.2 Polyvinyl butyral | 127 |
| 5.2.1 TSD of DC charged PVB films | |
| 5.2.1.1 Preliminary | 127 |
| 5.2.1.2 Results | 128 |
| 5.2.1.3 The α -peak | 128 |
| 5.2.1.4 Origin of the α -peak | 130 |
| 5.2.1.5 Estimation of Other Relaxation Parameters | 140 |
| 5.2.1.6 The ρ -peak | 141 |
| 5.2.1.7 Origin of the ρ -peak | 142 |
| 5.2.1.8 Ionic Conduction and the Free Volume | 149 |
| 5.2.1.9 Conclusions | 153 |
| 5.2.2 TSD of Corona charged PVB films | |
| 5.2.2.1 Preliminary | 157 |
| 5.2.2.2 Results | 158 |
| 5.2.2.3 Discussions | 158 |
| 5.2.2.4 Conclusions | 168 |
| 5.2.3 TSD of Surface Potential - "Charge" TSD | |
| 5.2.3.1 Preliminary | 170 |
| 5.2.3.2 Results | 171 |
| 5.2.3.3 Discussions | 175 |
| 5.2.3.4 Conclusions | 181 |
| 5.2.4 Summary | 185 |
| 5.2.4.1 Significance to Xerography | 192 |
| 5.3 Double-Layer Xerographic Photoreceptor | |
| 5.3.1 Introduction | 194 |
| 5.3.2 Results and Discussions | 195 |

| | <u>Page No.</u> |
|------------------------------------|-----------------|
| 5.3.2.1 V _a positive | 195 |
| 5.3.2.2 V _a negative | 204 |
| 5.3.3 Conclusions | 206 |
| 5.3.3.1 Significance to Xerography | 211 |
| CHAPTER 6 FINAL CONCLUSIONS | 213 |
| APPENDIX | 219 |
| BIBLIOGRAPHY | 220 |

CHAPTER 1

POLYMERS

1.1 The Polymeric Solid State

Introduction

This section introduces the main features of the solid polymeric structures which will be of consequence to the discussion of electrical properties in later subsections.

Synthetic high polymers are characterised by their chain-like molecular physical structure, achieved by the repeated linking of small units, the monomer, to chains often a μm long, resulting in a typical length to diameter ratio reaching 10^4 to 1. The distinctive physical properties of polymers owes much to this phenomena.

The main characteristics of the chains are that the chemical bonding along the chain is the strong and directional covalent bonding while that between the chains, the intermolecular bonds, are of the weak Van der Waals type or occasionally, as in the case of polyamides, are hydrogen bonded. The number of repeat units, or degree of polymerisation in a typical polymer may reach 10^3 , therefore on average a typical polymer molecule may have a mean molecular weight of 10^5 . These macromolecules represent the largest class of matter to be characterised on a molecular level.

1.2 Morphology and Molecular Architecture

The large molecule built up from the polymerisation process may be linear, branched or interconnected to form a complex 3-dimensional network by extensive cross-linking. The physical structure of the individual chain will also depend on the configurational isomerism of the repeat units leading to trans- or cis-isomerism. When the repeat units are not symmetrical with respect to the central chain axis, then tacticity can be used to describe the polymer chain. Figure 1.1 shows the organic polymer, polypropylene in an isotactic and syndiotactic configuration. When a polymer is described as atactic, then a completely random configurational arrangement of the polymer sub-units is inferred.

Polymer chains may also adopt a helical structure if there are relatively bulky side groups to be accommodated or if there is a strong steric repulsion between side groups bearing a permanent dipole moment. An example of a helical vinyl polymer is shown in figure 1.2 where the substituent group X is attached to one point along the chain.

Tacticity is an important factor in determining the ability of the solid to crystallise. An atactic arrangement would obviously hinder crystallisation due to the high degree of inherent disorder. Atactic polymers generally tend to be non-crystalline although there could be exceptions to this (for e.g. poly vinyl alcohol, Bunn 1948) whilst stereo regularity greatly enhances the ability of the polymer chains to crystallise. Among the polymers that exhibit this approximate correlation are polypropylene (Natta and Corradini 1960), polystyrene

(Natta, Corradini and Bassi 1960) and poly methylmethacrylate (Stroupe and Hughes 1958).

In order for the polymer to crystallise, the chains must first be able to rearrange themselves from the highly disordered state of the melt or solution such that the short range intermolecular van der Waals forces could hold them together. For this to happen the chains must adopt a linearly extended configuration rather than be in a randomly coiled or a highly entangled state. This, however, will be thermodynamically unfavourable for the system of molecular chains since, consistent with the minimisation of the Gibbs free energy G , the molecular chains will adopt a configuration of maximum entropy S . The preferred state is one where the chains are randomly coiled since there is a higher number of configurations which are then available.

During crystallisation at a temperature T , the nett change in the Gibbs free energy,

$$\Delta G_c = \Delta H_c - T\Delta S_c \quad (1.1)$$

would be the sum of two opposing entities, ΔH_c the change in enthalpy and $T\Delta S_c$, the entropy factor. Compared to the metallic, ionic or covalently bonded solids, ΔH_c in polymeric solids is small since it is based on the relatively weak van der Waals forces. Highly perfect crystallisation is also impeded in polymeric solids due to the large entropy factor $T\Delta S_c$ with the final result that the availability of large, defect free polymeric single crystals becomes a rarity. Some aspects of polymer crystallisation has been described by Keith (1963).

Fig. 1.1 Stereo isomers of Poly propylene.
 a) Isotactic
 b) Syndiotactic

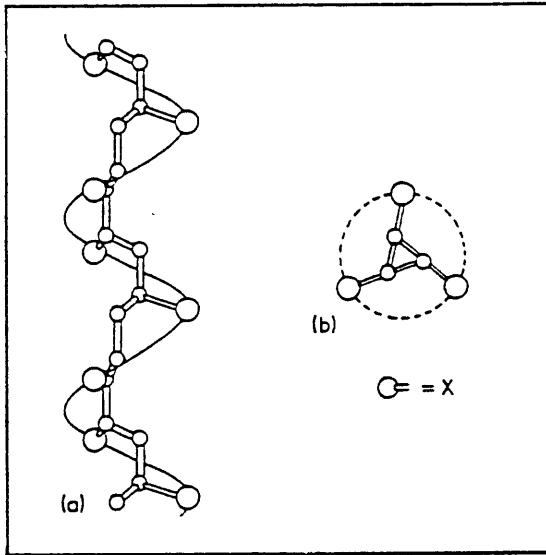
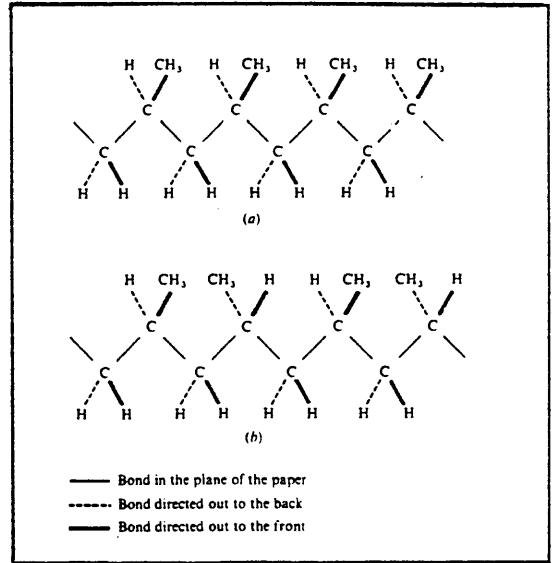
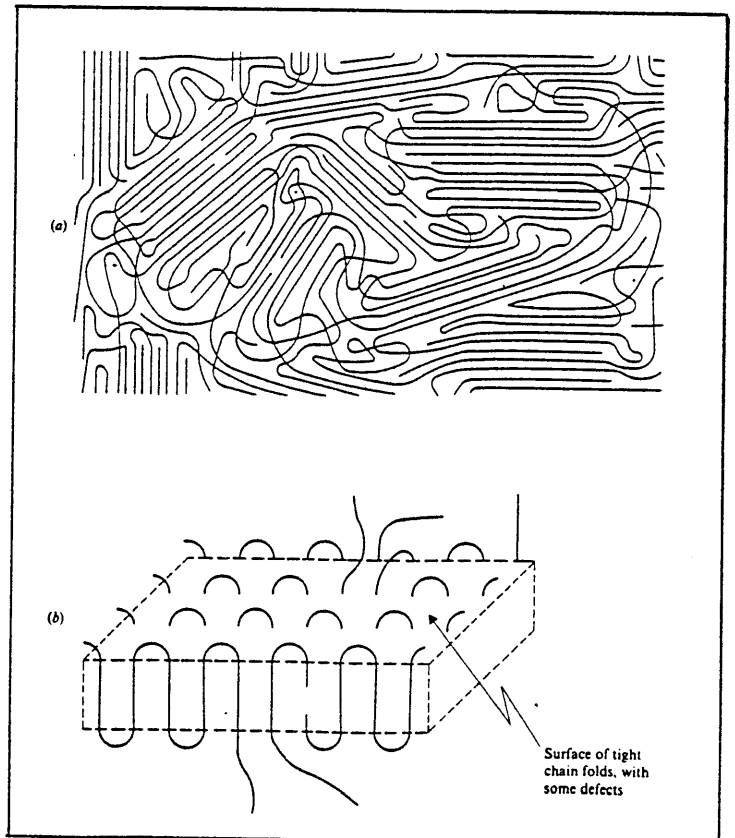


Fig. 1.2 Schematic representation of 3/1 helix for isotactic vinyl polymers of the type $(-CH_2-CHX-)_n$.

- a) Side view
 b) View along helix

The X groups are $-CH_3$, $-CH=CH_2$ etc.

Fig. 1.3 Polymer Crystallinity models.
 a) Fringed micelles
 b) Chain folded lamellae



Experimental studies on polyethylene have shown that in the solid, there were regions of high order interspersed in an essentially disordered phase (Flory 1953) which led to the fringed micelle picture as shown in figure 1.3 (a). A more recent theory is that the macromolecules, by chain folding, form crystallites of a lamellar structure as shown in figure 1.3(b) (Renecker and Geil (1960). The lateral dimensions of a lamella is of the order of 10-20 μm with a thickness of only 10 nm. A spherulitic structure may also be observed. In general, the morphology of a polymeric solid will depend on the intrinsic properties of the polymer like tacticity, stereoisomerism, molecular weight, size of side-groups, and also on the kinetics of the solidification process.

1.3 Amorphous Polymers

1.3.1 The Glass Transition

From the brief discussion on the crystallisation process above it is quite clear that solid polymers with bulky side groups like polyvinylbutryal would hardly be crystalline at all. The amorphous or disordered phase of a polymer normally shows a transition from a rubbery to a glassy state at some characteristic transition temperature called the glass transition temperature, T_g . There is a dramatic change in the properties of the solid at this transition region. The heat capacity, C_p , and the volume thermal expansion coefficient, α , both show a sharp, step-like increase when the rubbery state is approached (figure 1.4). Since $C_p = \left(\frac{\partial H}{\partial T}\right)_p$ and $\alpha = \frac{1}{V} \left(\frac{\partial V}{\partial T}\right)_p$ are derivatives of the fundamental thermodynamic quantities H(enthalpy) and V(volume),

the glass transition is often referred to as a 2nd order thermodynamic transition.

One of the most widely used methods of demonstrating the glass transition and determining T_g is by measuring the specific volume of the sample as it is gradually cooled down from the melt as shown in figure 1.5. In the vicinity of T_g , there is a change in the slope of the curve which occurs over a range of several degrees of temperature. T_g is normally taken as the point of intersection of the 2 extrapolations. Figure 1.5 also shows the variation of T_g with the rate of cooling, i.e. the vitrification process is a rate dependent phenomenon. This evidence favours the view that this transition is a kinetic process since a genuine 2nd order thermodynamic transition does not depend on the rate of cooling (Elias 1977). It is also still a matter of debate as to whether a limiting value of T_g could eventually be obtained if the rate of cooling is slow enough (e.g. Parthasarathy et al 1983).

In the glassy region the thermal energy is insufficient to surmount the potential energy for the translational and rotational motion needed for the conformations. The chain segments are essentially frozen-in below the glass transition temperature. As the temperature is raised, the thermal energy becomes comparable to the potential energy barriers for chain segment rotation/diffusion, allowing the segments to undertake short range diffusional motion as well as undergo micro-Brownian type of motions. A major change in the segmental mobility occurs at T_g , enabling a large scale reorganisation if the sample is subjected to a stress. At T_g , it can be said that the time constant for molecular re-arrangement becomes comparable to the time

scale of the experiment used to measure it.

There is some controversy over the development of a single theory for the glass transition due to the experimental observations that not only static and thermodynamic properties are affected during the transition, but that the rate and relaxational properties are also markedly influenced. This led to theories which have their origins in either thermodynamic or kinetic concepts, details of which will be beyond the scope of this thesis. This subject has been extensively reviewed, for example by Boyer (1963), Shen and Eisenberg (1970), Gee (1970) and Parthasarathy (1983).

Perhaps the most widely used concept in describing the glass transition is that of the free volume theory of Fox and Flory (1948, 1950). Here the liquid or solid is seen as having its total volume being partly occupied by its molecules and partly being unoccupied or free. This unoccupied volume consist of "holes" of molecular size or voids due to imperfections of the packing order of the molecules in the random array. It is into this unoccupied volume that molecules must be able to move into in order to adjust from one conformational state to another. In the glassy state, the free volume has a constant value and also remain fixed or frozen in. As the solid is gradually heated up through the glass transition this free volume will expand and hence the solid, now in the rubbery state, will for example, acquire a higher coefficient of volume expansion α as shown in figure 1.4. It was shown by Boyer 1963 that for organic polymers with molecular weight $> 10^4$ and also relatively free from side group movements, below T_g the value of the mean fractional volume which is "free" is

approximately 11.3% of the total volume of the glassy polymer. The free volume theory has been quite successful in quantifying many effects and properties of the transition behaviour of polymeric solids, however, as had been pointed out by Boyer 1963, its extension to organic polymers with a high degree of cross-linking or polymers with bulky side-groups has to be treated with caution.

1.3.2 Relaxations in amorphous polymers

The relaxational and transitional behaviour of a large number of polymers have been studied by a range of experimental techniques which includes dynamic mechanical measurements, dielectric response and nuclear magnetic resonance methods amongst others. Each of these methods influences the individual molecules in different ways resulting in different responses to the external stimuli. Some degree of polarisability is needed for the relaxation to be detected by a dielectric measurement, while mechanical measurements may be able to reveal the presence of completely non-polar groups. Equivalent rotational movements while easily detected by n.m.r. methods are however not detectable by mechanical techniques.

It is widely known that apart from the glass transition or the so called primary relaxation, amorphous polymers also exhibit other secondary relaxations below T_g . In the case of semi-crystalline polymers the situation could also be further complicated by a melting transition of the crystalline phase of the solid.

A typical loss spectrum for a dielectric or mechanical measurement for an amorphous polymer is shown schematically in figure 1.6. Loss peaks, characteristic of a molecular process are labelled somewhat arbitrarily (Deutsch, Hoff and Reddish 1954) as α , β , γ and so on in descending order of temperature. The α peak is normally

Fig. 1.4 Schematic variation of C_p , the heat capacity and α , the volume expansivity for a typical glass forming liquid with temperature.

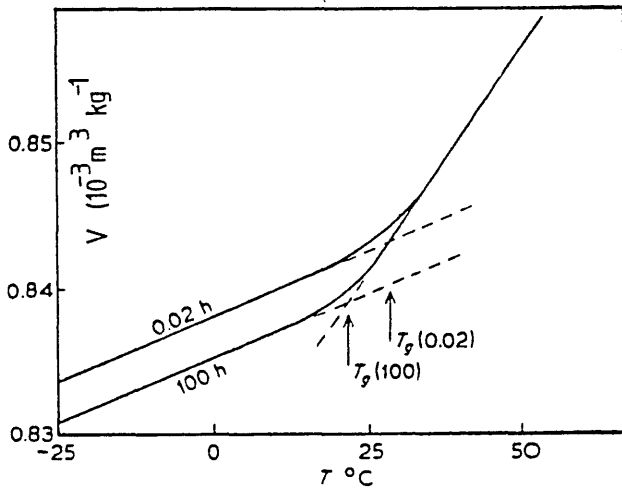
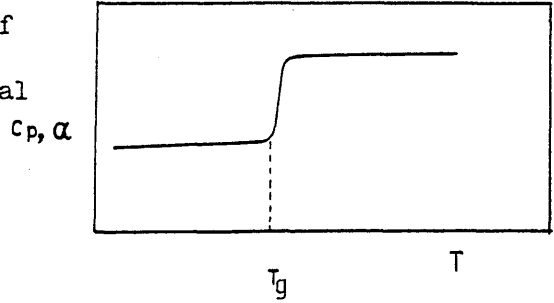


Fig. 1.5 Variation of the specific volume of poly vinylacetate at 2 different rates of cooling. (After Kovacs 1958) (h=hours)

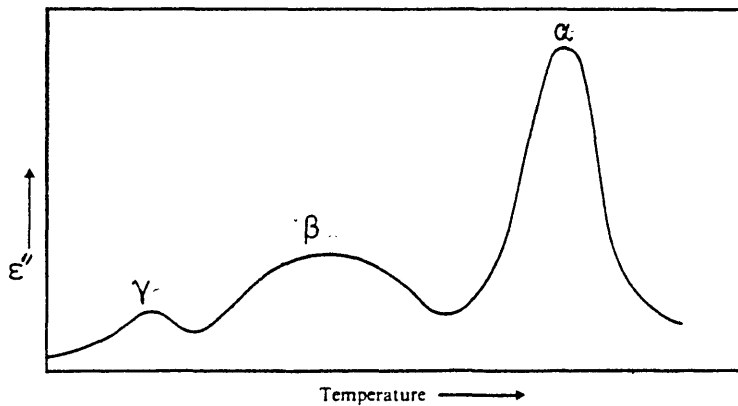


Fig. 1.6 A schematic representation of dielectric loss peaks as a function of temperature

associated with the major backbone chain movements at the glass transition, while the secondary peaks β , γ are due to local movements of the main chain and/or movements of the side groups (or within them) that were attached to the main chain. The molecular origins of these peaks have been an area of extensive research (for example Heijboer 1978, Roberts and White 1973). A simple schematic representation for some of the possible sub-molecular movements in the relaxation process is shown in figure 1.7. It is also worth noting that the assignment of secondary relaxation peaks for a particular type of molecular process has to be carried out with a satisfactory prior knowledge about the tacticity, isomerism, impurity content or degree of polymerisation etc. of the glassy polymer itself.

1.3.3 The WLF equation

Empirically, it was also found that above T_g (Williams, Landel and Ferry 1955) all electrical and mechanical relaxations at a temperature T could be related to that at a reference temperature, normally taken as T_g , by a shift factor a_T given by

$$\log a_T = - \left[\frac{17.44(T-T_g)}{51.6+T-T_g} \right] \quad (1.2)$$

a_T could be taken as the ratio of a relaxation time at temperature T to that at T_g for the solid in the temperature interval of T_g to ($T_g + 100$ K). Although the WLF equation was originally developed by curve fitting, it is now possible to justify it theoretically from consideration of free volume changes (see for e.g. Young 1981).

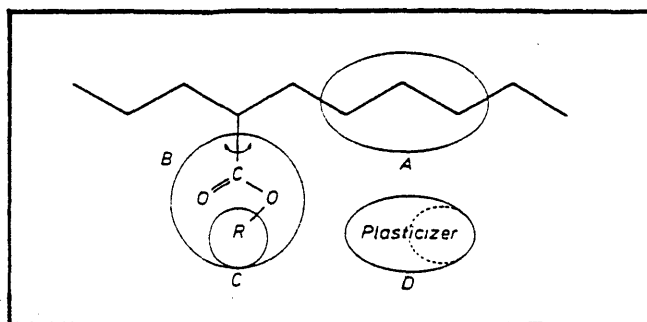


Fig. 1.7 Possible types of sub-molecular movements that can result in loss peaks. (After Heijboer 1978)

- A : Local chain movements
- B : Rotation of side-groups attached to the main chain
- C : Internal motions within the side-groups
- D : Motions of a small molecule (plasticizer, impurities etc.) embedded in the molecule.

1.4 Electronic Properties of Polymeric Solids

1.4.1 Introduction

The theoretical understanding of electronic states in polymeric solids is an essential precursor to the understanding of the range of interesting electrical phenomena that are experimentally observed in these solids. As an example, the electrical conductivity of some materials having a polymeric structure may vary from that of the excellent insulators to a state where their conductivities becomes comparable with the metallic conductors, as shown in figure 1.8. The discovery that polymeric single crystals of sulphur nitride $(SN)_x$ could behave like a metallic conductor (Walatka, Labes and Perlstein 1973) and the subsequent experimental demonstration that the material was superconducting below 0.3 K (Greene, Street and Suter 1975) instigated a renewed wave of interest, both theoretical and experimental, of the possible mechanisms of electrical transport in this class of solids. A recent review (Street and Clarke 1981) however has shown that there are still serious problems to be overcome before polymeric superconductors become a technological reality.

Additionally, the excellent insulating properties of polytetra fluoroethylene has found use in electret microphones (Sessler and West 1962) where obviously the long term charge storage ability of the films were important. Photoconductive organic polymers like poly-N vinylcarbazole (PVK) doped with 2,4,7-trinitro-9-fluorenone (TNF) is also used as photoreceptors in the xerographic industry (Gill 1976).

The use of materials with a polymeric structure in a diverse range of electrical applications is undoubtedly a reflection of the wide range of intrinsic electrical properties that these solids exhibit. It is obvious that a study of their electrical behaviour will be inter-disciplinary in nature.

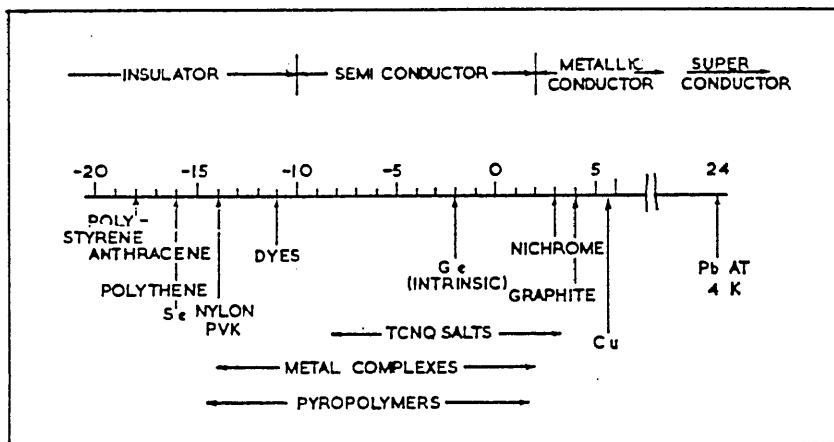


Fig. 1.8 Conductivity ranges of various types of material. The scale gives the logarithm of the conductivity ($\text{ohm}^{-1}\text{cm}^{-1}$) at 30°C . (After Goodings 1976)

1.4.2 Extended electronic states

As a consequence of the strong intramolecular covalent bonding and relatively weak intermolecular bonding, the electronic behaviour of polymers will be highly anisotropic. If each chain is envisaged as being made up of a large number of identical repeat units, each with molecular orbitals built up from their individual atomic orbitals, then the overlap of these molecular orbitals could give rise to bonding and

anti-bonding orbitals leading to the formation of valence and conduction bands respectively for the whole polymer chain (Gutmann and Lyons 1967). The polymeric solid is then treated as a semiconductor but with narrow band-widths. Some detailed calculations of the band structure of several polymers can be found (see Andre and Ladik 1975 and references there in).

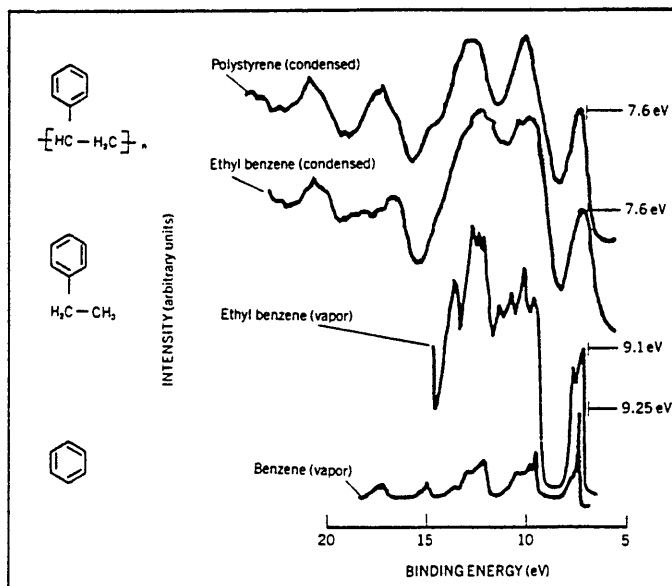
The results for a linear conjugated polymer, polyacetylene, is briefly described below. By using the tight binding model, Ritsko 1982 calculated that there exist a band gap of 1.52 eV and that the free carrier mobility along the chain was approximately $2 \times 10^2 \text{ cm}^2 \text{V}^{-1} \text{ s}^{-1}$. However this large value has yet to be experimentally verified, the strong influence of trapping and the necessary intermolecular chain hopping being cited as the main limiting factors for the carrier mobility. Calculations carried out for polyethylene, a linear saturated polymer which does not have the system of extensively delocalised π electrons as in polyacetylene, resulted in a mobility value of $\sim 34 \text{ cm}^2 \text{V}^{-1} \text{ s}^{-1}$, which is still a relatively large value. However Fabish 1979, has found that the calculated value was still about 5 orders of magnitude larger than that measured experimentally.

It can be said that measurements of electrical conductivity and mobility in real polymer samples may not always be useful tests of the theoretical mobility values based on band structure calculations. In fact, due to the narrow band widths, the application of band theory concepts to describe the electronic transport behaviour of these materials has to be treated with caution.

1.4.3 Localised states

Due to the reasons above it was proposed (Duke, Salaneck et al 1978, Duke 1978) that the electronic structure of organic polymers with narrow band widths will be better described by the individual states of the molecular sub-units. An extrinsic injected charge will thus be localised, forming a molecular anion or cation state depending on the polarity of the injected charge. The weakness of the inter-molecular interactions will also mean that the physical properties of the whole polymer will have a strong resemblance to that of their individual molecules. This was in fact shown from results of photo-emission experiments as seen in figure 1.9. Except for a gradual shift towards smaller values and a widening of the highest energy peaks, the ultra violet photoemission spectra of benzene (vapour), ethyl benzene (vapour and condensed phases) and polystyrene (condensed) exhibited a remarkable similarity.

Fig. 1.9 Ultra violet photo-emission spectra of benzene, ethyl benzene and polystyrene. With increasing condensation and structure, the peaks in the spectra widen and shift to smaller binding energies. To emphasise the similarity of the spectra, they have been shifted to align their highest energy peaks. (After Duke et.al 1978)



The shift towards lower energies was thought to arise from the polarisation of the surrounding molecules by the localised molecular cation or hole state (photoemission leaves a nett positive hole behind) (Salaneck 1978), while the widening of the peak maximum was attributed to the spread of the magnitudes of the polarisation in the condensed phase. The spread in polarisation energies was due to structural and chemical inhomogeneities of the solid, a source of "diagonal disorder" as was described by Anderson 1978. We note here that "diagonal disorder" refers to the variation of the on-site energies from a mean value while "off-diagonal disorder" refers to the variation associated with the magnitude of the transfer integrals between two adjacent sites. Since the magnitude of the "diagonal disorder" as approximated by the width of the ionization peaks of figure 1.9 was about 1 eV and that the band widths due to the intermolecular overlap is only about 0.1 eV, it was thus concluded that the charged electronic states of pendant group polymers will be highly localised.

1.5 Electrical Transport in Organic Polymers

1.5.1 Introduction

Compared to the ⁱⁿ⁻organic semiconductors and metals, knowledge about the electrical transport mechanisms in organic polymeric solids is still scant. Widely different experimental results and subsequently different transport mechanisms were proposed, each of which explaining results of a particular experiment but often failing to give a satisfactory interpretation in more generalised manner. This is a reflection of the complex nature of charge transport in these types of solids.

A good starting point for the discussion of electrical conductivity is by considering the phenomenological equation

$$\sigma(T) = \sum q_i n_i(T) \mu_i(T) \quad (\text{eqn. 1.3})$$

where q_i is the magnitude of charge on the i^{th} species, $n_i(T)$ is the density at temperature T and $\mu_i(T)$ is its effective mobility. Charge carriers in organic polymers could be ions, electrons and holes. The assignment of charge carriers in insulating polymers is a difficult problem due to the small magnitude of the conduction currents involved and the strong effects of impurities and defects in the solid. The dependence of the detected current on the pressure or temperature (especially near T_g) could also be employed in identifying the carrier species involved (for e.g. Saito et al 1968, Miyamoto and Shibayama 1973).

1.5.2 Intra-molecular electronic conduction

The discussion of intrinsic electronic conduction in organic polymers could be broadly classified into 2 sections, based on the structure of the backbone chain.

Type 1:

In this type, the chains are linked by σ -bonds, i.e. their linkages are saturated. This includes the linear polymers like polyethylene, polyvinyl chloride, polystyrene, polyvinyl butyral and

poly-N-vinyl carbazole amongst others (please see Appendix 1 for chemical formulae and structure). Polymers of this type generally have a low electronic conductivity along the main chain due to the localised nature of the σ electrons in the C-C bonds. Nevertheless, large aliphatic or aromatic substituents may cause a significant overlap of their intra-molecular orbitals such that electrons or holes can hop across these substituent groups thereby increasing the conductivity along the chain. Examples of such polymers are polystyrene and poly-N-vinylcarbazole (PVK). A large amount of work was carried out on PVK (Mort 1972, Pfister and Griffiths 1978) as the polymer is widely used as a photoreceptor material in the xerographic industry. A feature of these substituted polymers are that they adopt a helical structure (Natta and Corradini 1955, Kimura et al 1970) as compared to the planar zig-zag form of the parent polyethylene.

Type 2:

This consists of polymers with conjugated double bonds in the linear chain of which polyacetylene is the most studied example (Chiang et al 1977, Fincher et al 1978). Polymers in which aromatic or heterocyclic rings are part of the main chain like the poly-phthalocyanines and the poly-acene quinone radical (PAQR) polymers also belong to this type where there is a system of de-localised π -electrons along the main chains making electronic conduction highly favourable.

The energy, E_A , required to excite an electron from the ground state to the first excited state is related to the number of atoms N along the linear chain and is given by (Goodings 1976)

$$E_A \sim \frac{19(N+1)}{N^2} \quad \text{eV} \quad (\text{eqn.1.4})$$

which implies that the conductivity along the chain should increase as the length of the chain is increased. As found by Lichtmann and Fitchen 1979 however, this correlation was not easily observed due to the ubiquitous presence of defects and chain ends which produce a limited or broken sequence of electronic de-localisation. In addition to this, bond alternation starts to set in when long molecules are linked together. Here, instead of bonds of equal length, long and short bonds alternate for reasons of stability, thus making electron delocalisation a self-limiting process. This alternation is an example of the so-called Jahn-Teller stabilisation.

It is also desirable that for conjugation to be fully maintained, the molecules must remain planar. Pohl (1962) have used the terms "eka conjugation" when the conjugation is extensive along the chain and "rubi conjugation" when the conjugation is limited due to rotations about a bond or other steric consideration causing an insufficient overlap of the carbon P_z orbitals. It can also be said that even in the case where there is no steric hindrance, entropy considerations alone would limit any extensive conjugation in a chain due to the strong favouring of the out-of-plane conformations along these long chains.

1.5.3 Intermolecular electronic conduction

The discussion so far has centred on conduction along the chains of the polymer. As it is well known that single crystal macro-

molecules are a rarity, it is more likely that any electronic conduction in a polymeric solid will be dominated by the consequences of structural disorder. Electronic transport should be relatively easy long the polymer chains, or in the case of polymers with large side-groups, along the strings of the overlapping side groups. This is in contrast to the more difficult inter-molecular transfers between the chains. It is envisaged that the overall electrical conductivity of the polymeric solid is controlled by these difficult inter-molecular transfers (Meier 1974). Experimentally, most insulating polymers appear to exhibit a thermally activated mobility following the Arrhenius relation (for e.g. Lewis 1984)

$$\mu = \mu_0 \exp[-E_a/kT] \quad (1.5)$$

where E_a is an energy for activation and μ_0 is the trap-free mobility. The interpretation of the mechanism for E_a is highly complex. It is a quantity which depends on the type of polymer, its degree of crystallinity and the temperature range at which the measurements were carried out.

Our discussion of molecular ion states (see section 1.4.3) would suggest that electronic conduction may also proceed via discrete hops or tunnelling between the electron (or molecular anion) states or hole (molecular cation) states. Silinsh 1980 have suggested that these states are most likely to be distributed (in energy) according to a Gaussian form, where for holes it is given by

$$D(E_h) = (2\pi)^{-1/2} S_h^{-1} \exp\left[-(E_h - E_h^0)^2 / 2S_h^2\right] \quad (1.6)$$

where E_h^0 is the unperturbed energy of the molecular cation state and S_h is the standard deviation of the distribution. S_h is dependent on the structure as well as on the temperature of the polymer.

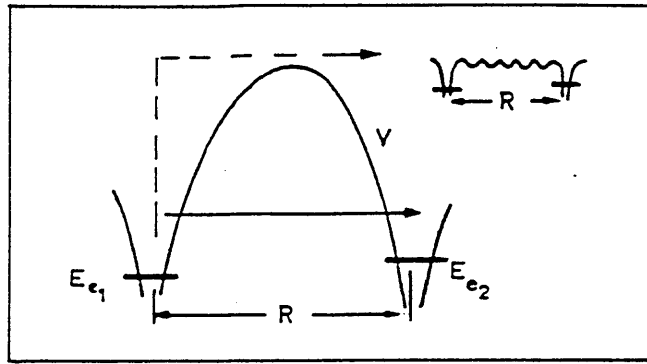


Fig. 1.10 Electron tunneling between negative molecular ion states through (—) or over (---) the potential barrier V . Inset shows tunneling via an extended polymer chain. (After Lewis 1984)

A simple expression for the tunnelling rate, p between two donor states, as shown in figure 1.10, can also be approximated by (Mott and Davis 1979)

$$p = \nu \exp[-2\beta R] \exp[-\Delta E/kT] \quad (1.7)$$

where ν is the frequency of attempts (10^{12} to 10^{13} s^{-1}), β is a parameter which accounts for the overlap of the wavefunction between 2 sites R distance apart and of energy difference ΔE . A range of allowable tunnelling pathways will be available for the carrier which, on the whole, will be towards energetically lower states.

The inverse of eqn. 1.7 gives the residence time at a particular energy level and by using representative values of ν and βR , Lewis 1984 demonstrated that if $\Delta E = 0.2 \text{ eV}$, then $1/p$ is $\sim 10^{-9}$ ses. while if $\Delta E = 1.0 \text{ eV}$, $1/p$ is ~ 6 hours. It can be seen that the deeper trapping sites have a considerable influence on the transport properties of the bulk solid.

1.5.4 Ionic conduction

The presence of impurities, fragments of polymerisation catalysts, degradation and dissociation products, absorbed water and other ionisable species may contribute to an externally detected electric current when an electrical stress is applied to a solid

polymer. The detection of electrolysis products at the electrodes, which will provide conclusive evidence for an ionic conduction, is extremely difficult due to the minute quantities involved.

A simple treatment for ionic conductivity based on a simple ionic dissociation and the law of mass action would yield for the ionic conductivity (Blythe 1979)

$$\sigma = (K_0 n_0)^{1/2} \{e(\mu_+ + \mu_-)\} \exp \left[- \frac{\Delta W}{2\epsilon_s kT} \right] \quad (1.8)$$

where K_0 is a constant which amongst others includes the entropy term for the ionic dissociation, n_0 is the initial concentration of the ionic compound, μ_+ , μ_- are the mobilities of the positive and negative ions respectively, ΔW the work required to separate the ions in a medium of unit dielectric constant and ϵ_s is the dielectric constant of the medium.

Based on a simple model (Mott and Gurney 1948), it also follows that the ionic current j could also take the form

$$j \sim \exp \left[- \left[\frac{\Delta W}{2\epsilon_s} + \Delta u \right] / kT \right] \sinh \left\{ \frac{eaF}{2kT} \right\} \quad (1.9)$$

where F is the applied field and Δu is the barrier height for an ionic jump and a is the distance between two available sites along the direction of the applied field. A good agreement of equation 1.9 with experimental results was obtained for poly vinyl chloride (Kosaki, Sugiyama and Ieda 1971) who also found that the jump distance a equals 1.2 nm, a typical value for molecular spacings.

Generally the contributions to the experimentally detected currents by either ions or electrons/holes could be unravelled by vary-

ing certain experimental parameters like temperature, illumination, pressure, degree of crystallinity etc. An increase in the ambient pressure would cause a reduction in the free volume and thus, would suppress ionic conduction. This at the same time will increase any electronic conduction due to the increase in the overlap of the intermolecular hopping integrals. At temperatures near and above the glass transition where there is a sharp increase in the free volume, ionic mobility is also enhanced (Kosaki et al 1971). An increase in the degree of crystallinity would also suppress ionic conduction due to a closer and more ordered molecular packing.

1.5.5 Displacement currents

When a static electric field is applied between an electroded polymer sample a displacement current may be detected. In practice the current transient will consist of an initial pulse corresponding to the relatively "instantaneous" electronic and atomic polarisations which is then followed by a decaying current due to a dipolar orientation if there are groups of atoms with permanent dipole moments. If the intrinsic conductivity of the solid is low, the displacement current due to the dipole orientation may swamp the true conduction current. The dipole orientation process is usually distributed over an extended period of time due to the possible different local environments and rotational masses involved (Daniels 1967).

The decaying displacement current follows the relationship (Wintle 1974, Adamec and Calderwood 1978)

$$I \propto t^{-n} \quad (1.10)$$

where $n > 1$.

The transient displacement current detected after the application of a step voltage is usually called the anomalous charging current while the current transient (of the opposite sign) that is detected upon removal of the step voltage is called the discharging or absorption current (Baird 1968).

1.6 Summary

In this chapter we have attempted to present a brief synopsis of the wide range of different electrical phenomena that may be exhibited by the organic polymers in general. The electrical properties of an organic polymer is intimately linked to its physical morphology and stereo-structure, its temperature, as well as the time at which the observation was made (with regards to time at which the stimulus was first applied).

In addition to the observation of transient polarisation effects (electronic, atomic or dipolar) or a steady-state conduction current, charge accumulation in the polymer bulk or at the electrode boundaries may also give rise to space charge limited currents. Photoconductivity in some organic polymers is a subject of interest due to their use in the xerographic industry (for e.g. Mort and Pfister 1982 and references therein). Static electrification is a well documented but little understood phenomena exhibited by the insulating polymers. It can be said that the study of electrical phenomena in polymer dielectrics is a vast area of research encompassing widely different experimental techniques.

1.7 Aims of the Present Study and Lay-out of the Thesis

The aim of this present study is the investigation of the persistent electrical polarisation in two materials/materials system that are used in the field of xerography using the technique of Thermally Stimulated Discharge.

Poly vinylbutyral is a polar polymer which is often used as a binder resin in a pigment-resin-dye type of photo-sensitive element used in xerography. Also, when impregnated with carbon black, particles ($\sim 10 \mu\text{m}$ diameter) of the polymer are also used as toners for image reproduction.

Electrical polarisation in a two-layer photoreceptor based on amorphous Selenium is also investigated. This type of photoreceptor is a relatively recent development and is usually designed to operate in printers that utilise semiconductor lasers or LED arrays.

In use, these materials (in their appropriate device configurations) are often alternately charged and photo-discharged at high speeds (\sim few secs.) i.e, electrical polarisation is an important part of their operation. An understanding of the mechanisms involved in the build-up and decay of the electrical polarisation in these materials/materials system would be useful for the improvement of its xerographic performance.

Chapter 2 of the thesis describes a phenomenological theory for the TSD of several types of persistent electrical polarisation and of several sample configurations. A review of past work carried out on the materials is given in chapter 3. Chapter 4 describes the details of the experimental set-up. This also includes some results of the complementary experiments that were carried out. The results of the TSD experiments are presented in chapter 5. Chapter 6 gives the final conclusions that could be drawn from the work carried out. An appendix giving a brief description for some of the more common commercial organic polymers can be found at the end of the thesis.

CHAPTER 2

THERMALLY STIMULATED DISCHARGE

2.1 Introduction

The principal concern of this thesis is the study of the decay of the persistent electrical polarisation of solid polymeric dielectrics by using the method of thermally stimulated discharge. Assuming that the processes determining the decay of the polarisation are thermally activated then it is assumed that by heating the solid at a constant rate, the restoration towards charge neutrality will be accelerated. Thus the state of the polarisation can be studied as a function of temperature instead of time.

During the thermally stimulated discharge (TSD) of a previously polarised and electroded dielectric sample, a current displaying a number of peaks may be generated. The locations of these peaks along the TSD current spectrum are characteristic of the particular mechanisms for the decay. Systematic analysis of these current peaks will yield information on, for example, dipolar relaxation characteristics, activation energies for intrinsic conduction or trapping parameters of electronic charges in the solid.

The use of thermally accelerated decay of the persistent polarisation in a dielectric can be traced back to the early works of Frei

and Groetzinger (1936), Gross (1949), Murphy (1963) amongst others who applied the technique to diverse dielectric materials such as the naturally occurring waxes, resins, and synthetic polymer plastics. These materials, due to their sheer physical and chemical complexity, limit somewhat the proper identification of the fundamental mechanisms involved. Some of the earliest study of the phenomenon are the works of Bucci and Fieschi (1964) and Bucci et al (1966) on point defect dipoles in ionic crystals which they called ionic thermocurrents. Thereafter, several terms were used to describe essentially identical techniques that were reinitiated or redeveloped by independent workers (e.g. Takamatsu and Fukada (1970), Creswell and Perlman (1970), Nedetzka et al (1970), Simmons and Taylor (1972) and Moran and Fields (1974).

The method also has its analogue in other branches of solid state physics or physical chemistry viz. thermoluminescence, thermally stimulated conductivity, partial thermoremanent magnetisation and thermal desorption to name a few. A review by Chen 1976 gives an interesting inter-relation of the methods mentioned above. The application of the TSD techniques as a major tool in explaining the complex electrical processes in polymeric solids could be accredited to Van Turnhout (1971, 1975). In his extensive work (1975), the author has shown that TSD could be used as a powerful complementary technique to the more traditional methods like dielectric measurements and current-voltage-temperature methods in the study of electrical phenomena in polymer dielectrics. Used in conjunction with the physico-chemical methods of differential scanning calorimetry and differential thermal analysis, the technique can also be useful in identifying certain molecular or sub-molecular relaxation processes.

2.2 Principles of the TSD Technique

The basic principles of the technique can best be illustrated by figure 2.1 where the schematic evolution of the experimental parameters i.e. a) field across the electroded sample b) temperature of a sample and c) observed output across the electrodes (current) during the polarization and depolarisation stages are plotted as a function of time. These stages are briefly described below.

2.2.1 Polarisation

The sample, after being electroded is first heated up to some elevated temperature T_p (normally slightly above T_g of the polymer) where it is held at a constant value. A DC bias field E_p , is then applied across the electrodes up to a time t_p after which the temperature of the sample is quickly reduced to a low value T_d (normally below room temperature) and held constant. The static field E_p which was still applied during the cooling down period is then switched off after a total elapsed time t_s . The sample is then short-circuited through a sensitive current meter where it will then be depolarised.

2.2.2 Depolarisation

The temperature is raised next (from time t_d) at a constant rate r (typically $\sim 4^\circ\text{C min}^{-1}$) up to and beyond the temperature at which the particular relaxation process under study has ceased to dominate. In most cases the sample under study would be discarded after a single TSD cycle.

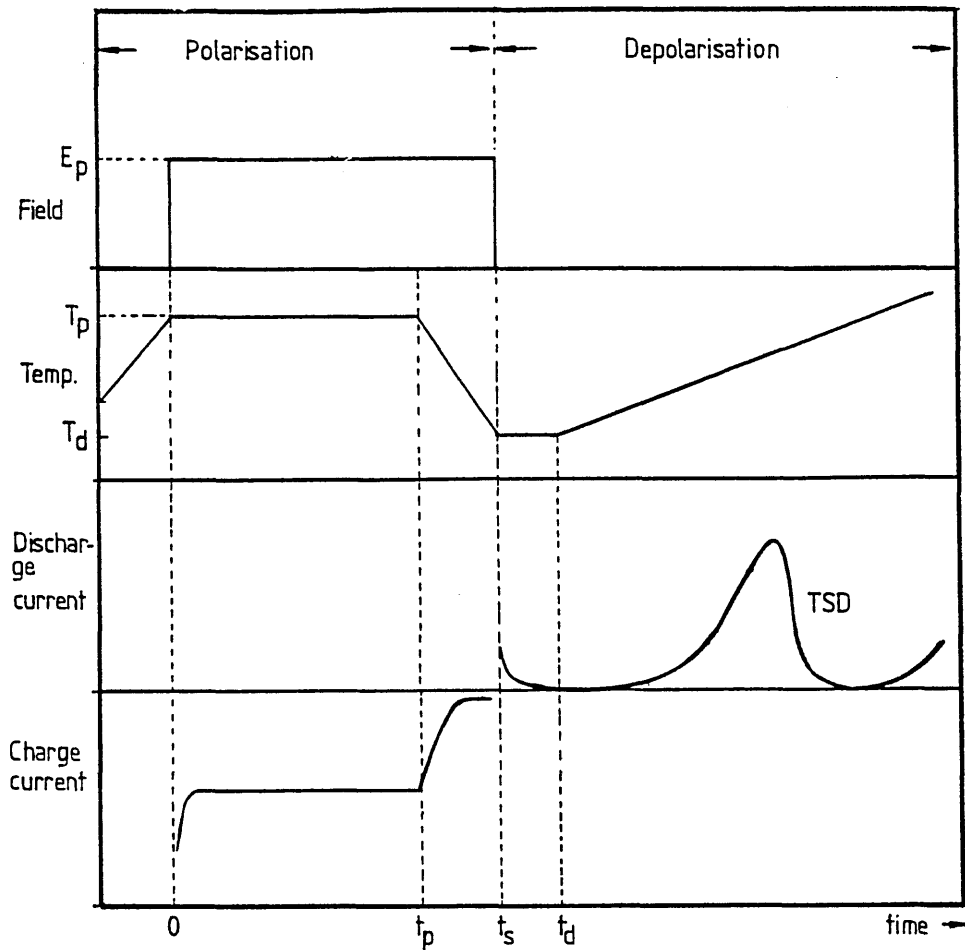


Fig. 2.1 Principles of the TSD technique.

2.2.3 Polarisation mechanisms contributing to TSD

The identification of the physical origins of the observed TSD current peaks is a complex task. Information about the dipolar polarisability of the polymer studied, the structural or physical homogeneity of the solid, the nature of the contacting electrodes and the polarisation and depolarisation conditions are some of the variables that need to be considered before any conclusive identification can be inferred.

On the application of E_p , a number of polarisation mechanisms may occur in the solid involving either microscopic or macroscopic charge displacements. These are:

- i) Deformation of the electronic shells of the individual atoms causing an electronic polarisation.

- ii) Deformation of heteropolar bonds causing atomic displacements in the molecule. Processes (i) and (ii) may have response times of the order of 10^{-12} seconds, times which are much too fast for TSD observations.
- iii) Orientational or dipolar polarisation in materials containing permanent molecular or ionic dipoles. The response time of these entities can be as fast as 10^{-12} secs. or as slow as 10^3 secs., depending on the frictional resistance of the medium.
- iv) Displacement of intrinsic free charges in the solid over macroscopic distances and subsequent trapping, especially near electrode boundaries which are partially or completely blocking. This effect causes an overall polarisation which is usually called translational or space charge polarisation.
- v) A polarisation similar to iv) but of extrinsic origin. Injection of excess carriers at high fields (e.g. Schottky emission) or a Townsend breakdown due to imperfect electrode-dielectric contact will also cause a polarisation in areas near the electrodes. An important point to note is that unlike iv), the sign of the charges is the same as that of the corresponding forming electrode, i.e. they are homocharges. The charges due to mechanisms iii) and iv) are referred to as heterocharges.
- vi) A Maxwell-Wagner polarisation, characteristic of a heterogeneous system of different layers or phases in the solid dielectric. The unequal conduction currents in the various phases will result in the formation of charged layers at their boundaries, leading to interfacial polarisation. Such physical heterogeneities may result from grain boundaries in polycrystalline

solids or fabricated laminates of different amorphous materials such as in the multilayered xerographic photoreceptors.

Due to the large intrinsic resistivities of polymeric dielectrics, the high probability of carrier immobilization due to trapping effects and hindered re-orientation of any dipolar groups in the bulk at room temperature, removal of the applied field will still leave a persistent polarisation that is slow to decay compared to the time scale of the experiment. This is the so-called "electret" effect, an expression first used by Heaviside (1892). It has been recently suggested (Mascarenhas 1980) that a substance can be said to be an electret if the decay time of its stored polarisation is long in relation to the characteristic time of experiments performed on the material.

2.2.4 Freezing-in of the Polarisation

Heating a dielectric to an elevated temperature T_p will markedly reduce the response time for a dipole orientation or charge displacement process which will mean that the attainment of an equilibrium polarisation in those conditions can be achieved in a reasonably short time. The equilibrium polarisation that was attained at T_p can effectively be "frozen-in" if the temperature of the sample is cooled down to sufficiently low value, T_d , (with the field on) such that at that temperature the relaxation times of the immobilised charges and aligned dipoles are much longer than the time scale of the experiment. Consequently, on removal of the electric field at this lowered temperature, only the "instantaneous" electronic and atomic polarisations adjust to the new conditions since they are intra-molecular and thus nearly temperature independent effects.

2.2.5 Depolarisation and the origin of TSD peaks

In the non-isothermal discharge of the thermoelectret (an electret formed by a thermal and applied field cycle such as in figure 2.1), the depolarisation processes are gradually speeded up as they respond to the temperature rise. In a polar polymer the increasing thermal agitation will first initiate the low energy local re-orientation of the dipoles (β -type of relaxations) followed by the α -type of relaxation at temperatures approaching T_g . The decrease in the internal dipolar polarisation will release image charges at the electrodes which will then flow in the external circuit. During TSD this current will first increase as the dipole disorientation process increases in intensity after which the current will decrease corresponding to the gradually vanishing polarisation. Thus a peak in the TSD current spectrum due to a dipole disorientation will result.

The decay of a space charge polarisation due to electrons, holes or ions may proceed via several different processes. Thermally generated (intrinsic) carriers in the bulk may neutralise the immobilised space charges (or excess charges), driven by the internal fields. Another mode of decay is that the excess charges may drift towards the electrodes or their oppositely charged counterparts as they regain their mobilities with the temperature rise. In addition to their drift, the excess charges may also diffuse away from regions of high concentration, spreading out in the bulk solid. The origin of TSD current peaks due to processes involving space-charges is much more complex phenomena than that due to a dipole re-orientation. A generalised theory for this requires taking into consideration at least four identifiable basic processes, namely their field induced motion or drift, their

diffusion induced motion, recombination during their transport as well as formation of new carriers by dissociation. Obtaining simple TSD current expressions is therefore dependent on a number of simplifying assumptions which at best can be expected to predict only some qualitative characteristics of the TSD current spectrum.

2.3 Detection Efficiency of TSD Current Measurements and Variations of the Method

The magnitude of the TSD current will depend on the effective charge retained by the electret, however not all of the decay processes will contribute fully to the external current. Dipolar disorientation have a theoretical efficiency of 100% because each unit change of polarisation in the sample bulk will release the corresponding image charges on the electrodes that could then flow in the external circuit. However, for decay processes involving space charges only part of the decay will be observed between the shorted electrets. This experimental characteristic may be due to either one or a combination of the following reasons (Van Turnhout 1973).

- i) Some of the charges could be neutralised by an internal ohmic conduction which will pass unnoticed by the external circuit. This will be especially true for materials of relatively high intrinsic conductivity like polar polymers.
- ii) Some of the charges may recombine with their image charges at the non-blocking electrodes, therefore only part of the total induced image charge will be free to flow into the external circuit. The nature of the dielectric-electrode interface

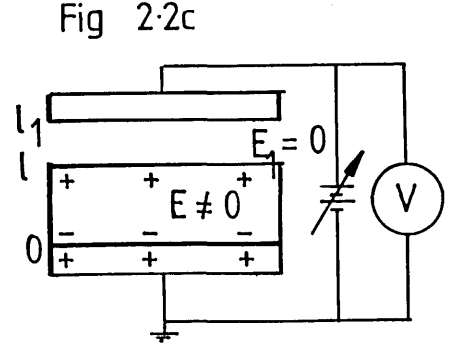
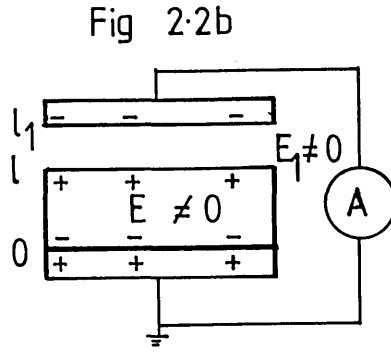
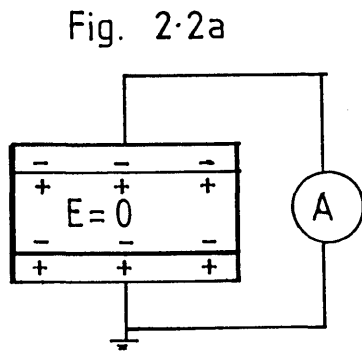


Table 2.1

Characteristics of the Different TSD methods

| | | |
|----------|---------------------------------|---|
| Fig.2.2a | Current TSD of shorted electret | $\int_0^1 E dx = 0, j^* \neq 0$ |
| Fig.2.2b | Current TSD with an air gap | $\int_0^{1+l_1} E dx = 0, \int_0^1 E dx = 0,$ $j^* \neq 0$ |
| Fig.2.2c | "Charge" TSD with an air gap | $V = \int_0^{1+l_1} E dx = \int_0^1 E dx,$ $j = 0$ |

The experimental quantities measured are marked with an asterisk.

will thus play an important part in the efficiency of the TSD current measured.

- iii) Current released by diffusion of the excess charges will depend on the blocking nature of the electrodes. A zero external current would result if completely non-blocking electrodes are used.

In general, the detection efficiencies for processes involving space charges may be improved by incorporating a highly blocking layer between sample and electrode such that any charge exchange across the electrode-dielectric interface will be blocked. Such a physical arrangement can be easily realised by utilising an air gap as the blocking layer as shown in figure 2.2 (b). Also, since the nett field in the solid is now non-zero, the decay of excess charges by ohmic conduction can be observed. Van Turnhout (1975) has shown that for such physical systems decay of the excess charges by internal ohmic conduction will dominate that of drift and diffusion. TSD measurements of this type are often called air-gap TSD or open circuit TSD.

Alternatively, in such systems the measurement of the voltage induced on the non-contacting electrode would also be useful in the study of the persistent polarisation in the sample bulk (figure 2.2(c)). This method can be named "charge TSD" since it now measures the evolution of the effective surface charge on the electret as it is being heated up. Compared to the TSD current measurements where the measured signals are very small (10^{-13} to 10^{-7} Amps, typical), charge TSD has the advantage of measuring large voltage signals (10 to 10^3 volts). The variants of the possible TSD measurements and the quan-

titles measured are summarised in table 2.1. Further details of the methods will be discussed in the appropriate subsections.

2.4 TSD theory involving Dipolar Processes

Introduction:

This section considers the TSD behaviour of a homogenous, electroded sample. It is assumed that the contacts are intimate, i.e. there is no intermediate medium between the electrode and the dielectric. Similar to conventional conductivity measurements, they must ideally be provided with a guarded electrode in order to avoid field fringing and surface conduction when a static electric field is applied. We also assume that the sample is polar and when subjected to the forming scheme of figure 2.1, a persistent dipole polarisation $P(t)$ can be formed in the sample bulk.

2.4.1 TSD due to Dipole Disorientation with a Single Relaxation Time

The discharge of the frozen-in dipole polarisation $P(t)$ in a short-circuited polar electret under a linear heating rate r is considered below. Assuming that the polarisation $P(t)$ decays with a single temperature dependent relaxation frequency $\alpha(T)$ according to the Debye rate equation we have,

$$\frac{dP(t)}{dt} + \alpha(T)P(t) = 0. \quad 2.1$$

Integration of the above yields

$$P(t) = P_e \exp \left[- \int_{t_d}^t \alpha(T) dt \right] \quad 2.2$$

where t_d is the time of commencement of TSD.

P_e is the attained equilibrium polarisation before the start of the TSD and could be expressed by

$$P_e = Np \overline{\cos \theta} \quad 2.3$$

where N is the density of dipoles, p is the electric dipole moment and θ is the angle the dipoles subtend with the applied field. For a low concentration of dipoles, the average orientation can be expressed as

$$\overline{\cos \theta} = \frac{pE}{3kT_p} \quad 2.4$$

The current density $j(t)$ due to the decay of the polarisation is

$$j(t) = \frac{-dP(t)}{dt} = \alpha(T)P(t) \quad 2.5$$

Using 2.2, this can be expressed as

$$j(t) = \alpha(T) P_e \exp \left[- \int_{t_d}^t \alpha(T) dt \right] \quad 2.6$$

In a TSD run, the temperature T is raised at a rate $r = \frac{dT}{dt}$, therefore we can express the released current as;

$$j(T) = \alpha(T) P_e \exp \left[- \frac{1}{r} \int_{T_d}^T \alpha(T) dT \right] \quad 2.7$$

using the conditions that at the start of the run, $t = t_d$, $T = T_d$.

The relaxation frequency for the dipole disorientation, $\alpha(T)$ is often envisaged to follow an Arrhenius shift

$$\alpha(T) = \alpha_0 \exp[-A/kT] \quad 2.8$$

where α_0 is the characteristic relaxation frequency ($T \rightarrow \infty$) and A is the activation energy for dipole disorientation. Equation 2.8 can be applied to describe the temperature shift of the relaxation frequency of well-characterised dipole groups normally associated with the β -type of relaxations. For dipole groups where disorientation are brought about by the segmental and cooperative movements of segments of the main chains, the frequency shift can be better described by the WLF shift (applicable for $T > T_g$)

$$\alpha(T) = \alpha_g \exp \left[2.303 C_1 (T - T_g) (C_2 + T - T_g)^{-1} \right] \quad 2.9$$

where for most amorphous polymers

$$\alpha_g = 7 \times 10^{-3} \text{ s}^{-1}, C_1 = 17.44 \text{ and } C_2 = 51.6 \text{ K}$$

(van Turnhout 1971).

Combining equations 2.7 and 2.8 we have the expression for the TSD current density

$$j(T) = \alpha_0 \exp[-A/kT] P_e \exp \left[-\frac{1}{r} \int_{T_d}^T \alpha(T) dT \right] \quad (2.10)$$

or substituting for P_0 using 2.3 and 2.4,

$$j(T) = \frac{\alpha_0 N p^2 e_0 E_p}{3kT_p} \exp[-A/kT] \exp \left[\frac{-\alpha_0}{r} \int_{T_d}^T \exp(-A/kT') dT' \right] \quad \dots \quad (2.11)$$

Equation 2.11 describes the depolarisation current density released due to a dipolar depolarisation in a shorted electret. The first exponential, which dominates the expression at low temperatures, describes the initial increase of the depolarisation current as the frozen-in dipoles gradually becomes disoriented. The second exponential which dominates at high temperatures will gradually depress the current released until a maximum output current is reached, after which the current rapidly falls as the induced polarisation is exhausted. The current peak is thus asymmetric, having a steeper slope on its high temperature side. The theory of TSD due to dipolar disorientation as described above is credited to Bucci and Fieschi 1964. Since then, the theory has been extended to include systems with a distri-

bution in relaxation times (for e.g. Gross 1968, Van Turnhout, 1971, 1975 and Lacabanne and Chatain 1973).

The peak temperature T_m for the current peak can be found by differentiating equation 2.10 and also substituting for $\alpha(T)$ from 2.8 we have

$$T_m = \left[\frac{rA}{k\alpha_0} \exp\left(\frac{A}{kT_m}\right) \right]^{\frac{1}{2}} \quad 2.12$$

From the above it can be seen that T_m will shift towards a higher temperature if a higher heating rate r is employed. Also, for a fixed heating rate, the position of the peak (i.e. along the temperature axis) will be an increasing function of A , the activation energy for disorientation as well as the natural relaxation time $\left(\frac{1}{\alpha_0}\right)$ for the process. An interesting conclusion that can be drawn from 2.12 is that T_m is independent of the forming conditions E_p and T_p provided the equilibrium polarisation has been attained.

2.4.2 Dipolar TSD with a distribution of relaxation times

In the essentially non-crystalline polymeric solid, different conformations that the macromolecules may adopt will result in an environment that can offer different resistances to the disorientating or rotating dipoles in different areas of the bulk. The dipoles then will have to surmount different activation energies resulting in different relaxation frequencies, $\alpha_i(T)$. Assuming that they still obey an Arrhenius shift, -this can be written as

$$\alpha_i(T) = \alpha_0 \exp[A_i/kT] \quad 2.13$$

Different relaxation frequencies may also arise from different values of α_0 , for this we have

$$\alpha_i(T) = \alpha_{0i} \exp[A/kT] \quad 2.14$$

A distribution of the type described by 2.13 is usually encountered in β -type of relaxations. The type described by 2.14, is more likely to arise from relaxations associated with movements of the dipolar groups that move in unison with the micro-Brownian motions of the main chain segments like the α -relaxation near T_g (McCrum et al 1967). Here different masses for the relaxing segments are most likely to be involved.

Assuming that distributions in α_0 or A are continuous, their contributions towards the polarisation $P(t)$ could be expressed as

$$P(t) = P_e \int_0^\infty f(\alpha_0) \exp \left[-\alpha_0 \int_{t_d}^t \exp(-A/kT) dt \right] d\alpha_0 \quad 2.15$$

for a distribution in α_0 . For a distribution in A , this can be written as

$$P(t) = P_e \int_0^\infty g(A) \exp \left[-\alpha_0 \int_{t_d}^t \exp(-A/kT) dt \right] dA. \quad 2.16$$

The distribution are also normalised such that

$$\int_0^{\infty} f(\alpha_0) d\alpha_0 = \int_0^{\infty} g(A) dA = 1 \quad .$$

The corresponding expressions for the current can be found by differentiating 2.15 and 2.16, yielding

$$j(t) = P_e \exp(-A/kT) \int_0^{\infty} \alpha_0 f(\alpha_0) \exp \left[-\alpha_0 \int_{t_d}^t \exp(-A/kT) dt \right] d\alpha_0$$

... 2.17

and

$$j(t) = P_e \int_0^{\infty} \alpha_0 g(A) \exp \left[\left[-A/kT \right] - \alpha_0 \int_{t_d}^t \exp(-A/kT) \right] dA \quad .$$

... 2.18

The equations above also show that the TSD currents are independent of the forming conditions provided that the fullest possible polarisation has been reached. If this condition is not achieved, say due to too short a polarisation time t_p or too low a temperature T_p , then an effective distribution can be defined by

$$f^*(\alpha_0) = f(\alpha_0)FS(\alpha_0) \quad 2.19$$

or
$$g^*(\alpha_0) = g(A)FS(A) \quad 2.20$$

where $FS(\alpha_0)$ or $FS(A)$ refers to the "filling state" of the polarisation. For a completely filled state, i.e. one where the electret has been polarised to its equilibrium polarisation value P_e , the parameter FS equals unity.

FS can also take into account the loss of polarisation during the cooling phase (t_p to t_s) and isothermal storage (t_s to t_d) of the TSD run. Expressions for FS for partial polarisations can be found in the works of Van Turnhout 1971, Ong and Van Turnhout 1973 and we refer the reader to the quoted works for details.

Finding empirical expressions for the distributions in α_0 or A has been a subject of wide interest and details of these can be found in texts of dielectric theory (e.g. Daniels 1967). Analysis of TSD currents using some of these empirical distributions are quite complex (Thurzo et al 1975, Van Turnhout 1975). It was also found that the low temperature β and γ peaks of polymers were best described by the Cole-Cole, Fuoss-Kirkwood and Wagner distributions. The high temperature α -peak was also found to be best fitted using the asymmetric distributions of Cole-Davidson or Havriliak-Negami.

2.4.3 Equivalent Frequency of Dipolar TSD Measurements

Dipolar TSD peaks can be correlated with ϵ'' vs T measurements via the temperature at which the dielectric loss factor ϵ'' is maximum. For a single Debye relaxation, the loss peak satisfies the condition

$$\omega\tau = 1$$

where ω is the angular frequency of the measurement and τ is the relaxation time of the dipoles $\left(\tau = \frac{1}{\alpha}\right)$. Assuming an Arrhenius shift allows us to use equation 2.12, the equation relating T_m to $\alpha(T)$. Using this and 2.21 results in an equivalent frequency for the TSD measurement which is given by

$$f_{eq} = \frac{\omega}{2\pi} = \frac{rA}{2\pi kT_m^2} \quad . \quad 2.22$$

The meaning of equation 2.22 is that f_{eq} is the frequency at which the dielectric measurement should be performed in order to obtain a loss peak at the same temperature, T_m , which is equivalent to its TSD current maximum. For relaxation obeying the WLF shift, f_{eq} is given by

$$f_{eq} = \frac{1}{2\pi} \left[\frac{rC_1C_2}{(C_2+T_m-T_g)^2} \right] \quad 2.23$$

where C_1, C_2 are constants defined in Equation 2.9.

Using typical values of r , the heating rate, as well as T_m and T_g , equation 2.23 would yield equivalent frequencies of 10^{-4} to 10^{-1} Hz which are in the ultra-low region of dielectric measurements. This also implies that for a good correlation to be made, TSD data should be compared with ϵ'' vs T measurements that were carried out at low frequencies. This is important if there are overlapping loss peaks in the dielectric spectrum since these peaks usually merge into a broadened hump when high measuring frequencies are employed.

It is also possible to calculate ϵ'' vs T data from a single TSD curve by extending Hamon's (1952) and Schwarzl and Struik's (1967) approximation methods for isothermal transient currents as was shown by Van Turnhout (1975). Perlman and Unger (1974) and Hino (1975) has also calculated ϵ'' vs f data from TSD measurements requiring the isolation of the individual TSD peaks if it is known that there is an overlap.

The TSD current thermograms could also be compared with dynamic mechanical measurements especially those that were carried out at low frequencies. A comparison of the results of three different techniques on the polymer PMMA is shown in fig.2.3. The curves for the dielectric loss ϵ'' , the dynamic mechanical loss G'' and the TSD current thermogram display a good agreement in the positions of their peaks. The TSD current thermogram however also display an extra high temperature peak (designated as ρ) in the comparative plots. This peak is believed to be due to the drift of space charges in the polymer. Due to the overwhelming conduction effects, this peak was not displayed in the dielectric loss curve.

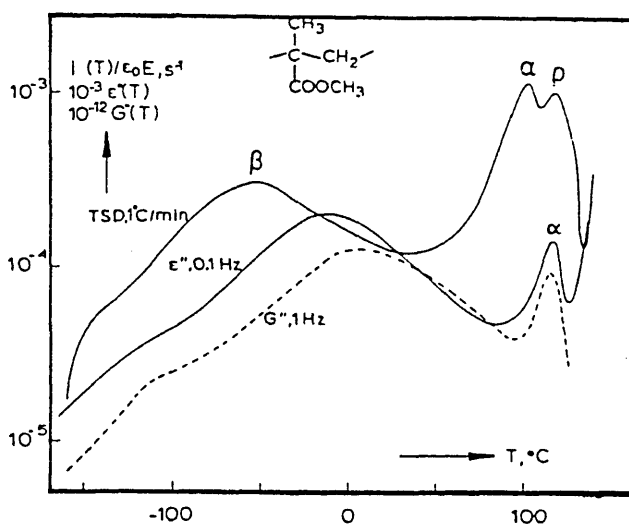


Fig.2.3
Comparison between dielectric ϵ''
dynamic mechanical G'' and TSD
current measurements on PMMA
(after Van Turnhout 1975)

2.5 TSD theory involving Space Charges

2.5.1 Introduction

The TSD decay of a polarisation due to excess electrical charges is a much more complex phenomena than that of a decaying dipole polarisation. For an understanding of the observed TSD current curves, a satisfactory analytical theory of the movement of excess charges in the dielectric need to be known. In addition to the uncertainties in the actual physical processes accompanying the space charge decay, the theory also leads to the need to solve partial differential equations in the spatial and temporal parameters for the space charge distribution. No general solution could be derived for the non-linear partial differential equations involved without making simplifying assumptions regarding the charge decay mechanisms involved. A detailed and thorough discussion of the mathematics involved could be found in the works of Calderwood and Scaife 1970, Van Turnhout 1975 and Gross 1980. In this thesis however only the results of some very simple treatments will be quoted.

Two basic models are usually considered as starting points for a TSD theory involving space charges. In the charge motion model the current is assumed to be essentially governed by the bulk conductivity of the material (electronic or ionic), irrespective of its possible trapping properties. In the trapping model, the current is assumed to result only from carriers (usually electronic) released into the conduction (or valence) band as the charge distribution returns to equilibrium.

2.5.2 The Charge Motion model

The decay of a positive space charge of density $\rho(x,t)$ in non-polar medium during TSD can be expressed, using the continuity equation as

$$\frac{\partial \rho(x,t)}{\partial t} = -\mu(T) \partial \rho(x,t) E(x,t) / \partial x - \sigma(T) \partial E(x,t) / \partial x \quad 2.24$$

causing the polarisation where $\mu(T)$ is the drift mobility of the space charges and $\sigma(T)$ is the intrinsic ohmic conductivity of the medium. Both $\mu(T)$ and $\sigma(T)$ are assumed to be thermally activated and obey the Arrhenius shift. The decay of charges via diffusion is neglected in this model. The first term on the right hand side accounts for the decay of the space charges via a drift (hopping over a single potential barrier) motion while the second term accounts for the decay by ohmic conduction. The electric field E and the space charge density ρ is related by the Poisson equation,

$$\frac{\partial E(x,t)}{\partial x} = \frac{\rho(x,t)}{e_0 e} \quad 2.25$$

The current density released by the space charge motion is then given by (Van Turnhout 1975),

$$j(t) = e_0 e \frac{\partial E(x,t)}{\partial t} + \left[\mu(T) \rho(x,t) + \sigma(T) \right] E(x,t) \quad 2.26$$

Also, since the sample is short circuited,

$$\int_0^{\ell} E(x,t) dx = 0 \quad 2.27$$

where ℓ is the thickness of the sample. By integrating with respect to x and using 2.25, equation 2.26 can be rewritten as

$$j(t) = [e_0 e \mu(T) / 2\ell] [E^2(\ell,t) - E^2(0,t)] \quad 2.28$$

where $E(0,t)$ and $E(\ell,t)$ are the values of the electric field at the electrodes obtained by the integration of eqn.2.25 and using eqn.2.27.

The expression for the current density (eqn.2.28) also show that both the displacement and ohmic conduction currents do not contribute to the external current during the TSD.

The partial differential equations describing the actual motion of the space charges can only be solved analytically for very simple charge distributions. Van Turnhout 1975 obtained the expression

$$j(t) = -\mu(T)\rho^2(x_0,t)f(t)^2[1-f(t)/l] / 2\epsilon_0\epsilon_l \quad 2.29$$

for the case of a box distribution of a space charge cloud whose initial charge density $\rho(x,0)$ is constant up to a depth f_0 . During the decay, the cloud expands into the sample bulk, its leading front $f(t)$ heading towards the opposite electrode ($x=l$) at a velocity,

$$\frac{df(t)}{dt} = \mu(T)E(f,t) \quad 2.30$$

$x_0(t)$ is the zero field point, i.e. E at $x_0(t) = 0$, in the sample bulk. From 2.29 it is also clear that once $f(t)$ reaches the back electrode, at l , the current released will abruptly drop to zero. A transit time t_λ is thus defined by the time taken by the leading front, initially at f_0 to drift across the sample towards l , the back electrode.

For a highly resistive medium ($\sigma(T) \sim 0$) and $t < t_\lambda$, equation 2.26 can also be written as

$$j(t) = \epsilon_0\epsilon \frac{dE}{dt} (l,t) \quad 2.31$$

since $\rho(l,t) = 0$ because no charge has reach the back electrode at l .

The total charge that is released can be found by integrating equation 2.31 yielding

$$Q(t_\lambda) = \epsilon_0 e [E(l, t_\lambda) - E(l, 0)] \quad 2.32$$

In this model, the amount of charge released will be dependent on the initial depth of penetration of the excess charges, f_0 , and that the total charge recovered will be a small percentage of the initial charge stored. This percentage would be smaller still if $\sigma(T) \neq 0$ since internal neutralisation via ohmic conduction have to be accounted for.

Distributions other than that of the box model above have also been considered. For a floating space charge layer i.e. one that is touching neither electrodes, Leal Ferreira and Gross (1973, 1974) have shown that for the case $\sigma(T) = 0$, the TSD current during $0 \leq t \leq t_\lambda$ can be expressed as

$$j(t) = [\mu(T)\hat{Q}_0/l] [E(l, 0) - \hat{Q}_0/2\epsilon_0 e] \exp \left[(\hat{Q}_0/\epsilon_0 e l) \int_0^t \mu(T) dt \right] \quad 2.33$$

$$\text{where } \hat{Q}(t) = \int_0^l \rho(x, t) dx$$

$$= \epsilon_0 e [E(l, t) - E(0, t)] \quad 2.34$$

is the total space charge stored and that

$$\hat{Q}(t) = \hat{Q}_0 \quad \text{for } t < t_\lambda.$$

Equation 2.33 above has a temperature dependence similar to that of a single dipole relaxation which implies that the initial part of the TSD plot due to the drift of the space charges can be analysed in the

same way as that of the Debye peak of a dipole depolarisation. In contrast to the latter however, the current does not have a linear dependence on the initial magnitude of polarisation stored. Another characteristic of the TSD current plot due to the drift of excess charges is that the temperature of the TSD current peak will shift towards a lower temperature as the initial density of stored charges is increased. With a higher density of stored charges, the resulting driving field will be stronger, thus accelerating the drift of the charges towards the electrodes. This results in a faster discharge of the sample.

2.5.3 A brief note regarding the trapping model

Our previous discussions of the main features of the charge motion model have assumed that the discharge current was essentially governed by the drift mobility of the excess charges as well as the intrinsic conductivity of the medium. Any possible trapping effects were neglected by this model. The theory of TSD currents based on trapping models have been quite extensively discussed by many authors (e.g. Creswell and Perlmann 1970, Van Turnhout 1975, Sessler and West 1976) where it was generally assumed that band theory concepts were applicable. In this model, a TSD current peak would correspond to a group of electronic carriers that had been previously released from a set of trapping levels within the forbidden gap that were now driven by the internal field towards the electrodes. Unlike the space charge motion model which predicted the appearance of only one TSD current peak, a model based on the trapping model can account for the appearance of several TSD current peaks each originating from an ever energetically deeper set of traps.

During the passage of the thermally released carriers towards the shorted electrodes, some of the carriers may experience a series

of retrapping/detrapping events or even recombine. The motion of a carrier with fast retrapping can be thought of as a hopping motion and as such the TSD current expression will be quite similar to the charge motion model as described in the previous section (Van Turnhout 1975). The only difference between the two formalisms is that in the trapping model, carrier recombination replaces intrinsic conduction as one of the internal neutralisation processes. This similarity of the TSD current expression however again reiterate the caution needed in interpreting TSD data, failure of which will lead to erroneous conclusions.

The case for slow re-trapping has been discussed by Creswell and Perlman 1970, Sessler and West 1976, Sessler 1976 and again it is noted that for manageable TSD expressions to be obtained certain drastic simplifying approximations regarding the trapping kinetics, initial charge distribution and nature of electrodes has to be made. Van Turnhout (1975) has also pointed out that unlike the case of a fast re-trapping where the TSD current plots are dependent on the initial depth of the excess charge penetration, the TSD plots for the case of slow re-trapping is independent of the initial depth of charge, allowing an experimental distinction to be made.

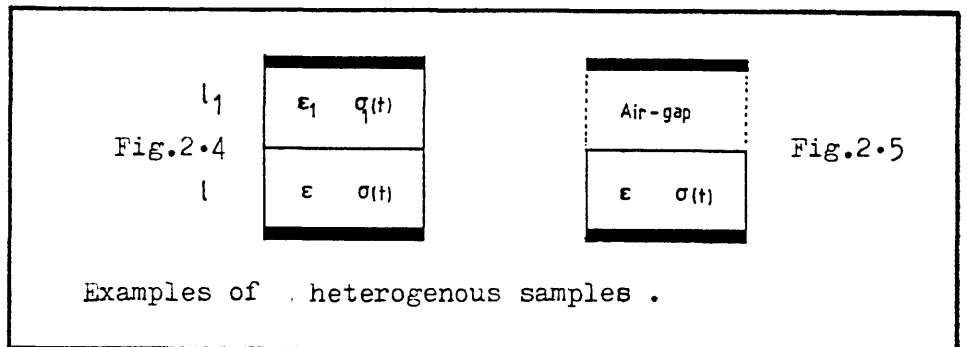
2.6 TSD of Heterogeneous Physical Systems

Introduction:

This section considers the TSD behaviour of 2 types of heterogeneous systems. In the 1st type, the sample itself is a laminate of 2 different materials (figure 2.4) sandwiched between intimately contacting electrodes while in the 2nd case the homogeneous solid sample is electroded on only one of its surfaces. If an electrode is brought close and parallel to the free surface, then this physical arrangement can be considered similar to the 1st case but now with an air-gap as one component of the laminate (figure 2.5).

2.6.1 TSD of a Double layer laminate

When a heterogenous structure such as that shown in figure 2.4 is subjected to a forming process as that described in section 2.1, a space charge layer will be formed at the boundary of the layers. This is usually called a Maxwell-Wagner polarisation and is caused by the unequal magnitudes of the ohmic conduction currents entering and leaving the interface, resulting in a nett accumulation of charge which may be frozen-in upon cooling of the sample. Upon removal of the applied field and heating, the accumulated charges can be neutralised by ohmic conduction currents flowing in opposite directions in the respective layers. This neutralisation of the interfacial charges will give rise to a peak in the TSD current spectrum. The charging and discharging behaviour of the system is briefly described below.



Charging

Both layers are assumed to be non-polar and have temperature dependent conductivities $\sigma(T)$ and $\sigma_1(T)$ and dielectric constants ϵ and ϵ_1 (assumed temperature independent) respectively. If an applied voltage V_a is applied across the electrodes, the equilibrium current density within the two layers can be expressed as

$$j(t) = \epsilon_0 \epsilon_1 \frac{dE_1(t)}{dt} + \sigma_1(T)E_1(t)$$

2.35

$$= \epsilon_0 \epsilon \frac{dE(t)}{dt} + \sigma(T)E(t)$$

where $E_1(t)$ and $E(t)$ are the time dependent electric fields in the layers. These can be related to the applied voltage V_a by

$$V_a = E_1(t)\ell_1 + E(t)\ell \quad 2.36$$

where ℓ_1 and ℓ are the thicknesses of the layers.

At the interface, there will be a gradual build-up of a space charge, $Q(t)$, which is assumed to be confined to a thin layer. This means that $E_1(t)$ and $E(t)$ are uniform quantities within their layers and also $Q(t)$ is essentially a surface charge. The build-up of this charge can be described by using the continuity equation, yielding

$$\frac{dQ(t)}{dt} = \sigma_1(T)E_1(t) - \sigma(T)E(t). \quad 2.37$$

Also, Gauss law will yield for the interface,

$$Q(t) = \epsilon_0 \epsilon E(t) - \epsilon_0 \epsilon_1 E_1(t) . \quad 2.38$$

From 2.35 and 2.36, the potential difference across layer 1 can be written as a differential equation

$$\frac{dV_1(t)}{dt} + \beta_g(T)V_1(t) = \beta(T)V_1(0) \quad 2.39$$

where

$$\beta(T) = \frac{\sigma(T)}{\epsilon_0 \epsilon} \quad 2.40$$

$$\beta_g(T) = \frac{\frac{\sigma_1(T)}{\ell_1} + \frac{\sigma(T)}{\ell}}{\epsilon_0 \left(\frac{\epsilon_1}{\ell_1} + \frac{\epsilon}{\ell} \right)} \quad 2.41$$

$V_1(0)$ is the capacitively divided value of the applied voltage, i.e. at $t=0$. This can also be written as (from 2.36),

$$V_1(0) = V_a \left(1 + \frac{\epsilon_1}{\ell} / \epsilon \ell_1 \right)^{-1} \quad 2.42$$

The solution for 2.36 can be shown to be

$$v_1(t) = [V_1(0) - V_1(\infty)] \exp \left[- \int_0^t \beta_g(T) dt \right] + V_1(\infty) \quad 2.43$$

Using equations 2.36 and 2.37 and the fact that as $t \rightarrow \infty$; $\frac{dQ}{dt} \rightarrow 0$,

the final equilibrium value of $V_1(t)$, i.e. $V_1(\infty)$ can be expressed as

$$V_1(\infty) = V_a \left(1 + \frac{\sigma_1(T)/\ell}{\sigma(T)/\ell_1} \right)^{-1} \quad 2.44$$

Using 2.44, 2.36, 2.37 and 2.38, then as $t \rightarrow \infty$, the final charge density established at the interface is given by

$$Q(\infty) = \left(\frac{1 - \epsilon_1 \sigma(T) / \epsilon \sigma_1(T)}{1 + \ell_1 \sigma(T) / \ell \sigma_1(T)} \right) \left(\frac{\epsilon_0 \epsilon}{\ell} V_a \right) \quad 2.45$$

The magnitude and sign of $Q(\infty)$ will depend not only on the applied voltage V_a but also on the ratio $\epsilon_1 \sigma(T)/\epsilon \sigma_1(T)$ being greater or smaller than unity. For a given value of V_a , a homocharge or a heterocharge may be obtained at the interface. The sign and magnitude of $Q(\infty)$ will depend on the temperature of the sample via the temperature dependences of $\sigma_1(T)$ and $\sigma(T)$ (assuming ϵ_1, ϵ are temperature independent). In the particular case when the individual conductivity curves ($\sigma(T)$ vs T) intersect, the temperature of formation of the electret becomes an important parameter in determining the nature of the interfacial charges that can be stored.

From 2.45 we also note that $Q(\infty)$ is large when $\sigma_1(T)$ and $\sigma(T)$ differ significantly. For example in an air-gap system where the condition $\sigma_1(T) \gg \sigma(T)$ may be applicable, we have

$$Q(\infty) = \frac{\epsilon_0 \epsilon V_a}{l} \quad 2.46$$

i.e. the magnitude of the stored charge will be independent of the forming temperature.

Discharging

During TSD, the frozen-in charges at the interface will be neutralised by thermally generated carriers of the opposite sign which are conveyed to the interface by ohmic conduction. Since now the applied voltage is removed,

$$V_1(t)l + V(t)l = 0 \quad 2.47$$

and also

$$\frac{dV_1(t)\ell_1}{dt} + \beta_g(T)V_1(t) = 0 \quad 2.48$$

The similarity of the above equation with equation 1 of section 2.4.1 also means that the decay of the interfacial charges will behave like a Debye relaxation. The decay of $V_1(t)$ found from the solution of 2.48, as a function of temperature T is given by

$$V_1(T) = V_1(t_d) \exp \left[-\frac{1}{r} \int_{T_d}^T \beta_g(T) dT \right] \quad 2.49$$

$V_1(t_d)$ is the potential difference across layer 1 at the start of the TSD and can be related to the stored interfacial charges by using 2.36 and 2.38, yielding

$$V_1(t_d) = \frac{-Q(t_d)}{e_0(e_1/\ell_1 + e/\ell)} \quad 2.50$$

The current released during TSD is found by substituting 2.49 into 2.35,

$$j(T) = \left(\beta_1(T) - \beta_g(T) \right) \left(e_0 e_1 \frac{V_1(T)}{\ell_1} \right)$$

where

$$\beta_1(T) = \frac{\sigma_1(T)}{\epsilon_0 \epsilon_1} \quad .$$

Substituting for $\beta_1(T)$ and $\beta_g(T)$ into 2.51 we finally have the TSD current density

$$j(T) = \left(\frac{\epsilon \sigma_1(T) - \epsilon_1 \sigma(T)}{\epsilon_1 \ell + \epsilon \ell_1} \right) V_1(T) \quad . \quad 2.52$$

From the above equation it can be seen that the TSD current is the algebraic sum of 2 opposing currents in the layers. The TSD current is largest (hence measuring efficiency highest) when $\epsilon \sigma_1(T)$ and $\epsilon_1 \sigma(T)$ differ significantly. The direction of the TSD current will depend on $V_1(T)$ and on the relative magnitudes of $\epsilon_1 \sigma(T)$ and $\epsilon \sigma_1(T)$. A current reversal in the course of a TSD run will also be possible if the conductivity curves ($\sigma(T)$ vs T) of the layers intersect as the temperature is increased. This means that the charges are first dominantly neutralised by the ohmic dissipation currents in one layer followed by the dissipation currents in the second layer which is in the opposite direction. When the conductivity curves do not intersect, the TSD current will usually be represented by one asymmetrical peak, the position of its current maximum being determined by the faster of the two ohmic dissipation process. It can also be shown that the temperature of the current maximum can be expressed as

$$T_m = \left[\frac{\epsilon_0 r (\epsilon_1 \ell + \epsilon \ell_1) [\epsilon_1 \sigma(T_m) A - \epsilon \sigma_1(T_m) A_1]}{k [\sigma_1(T_m) \ell + \sigma(T_m) \ell_1] [\epsilon_1 \sigma(T_m) - \epsilon \sigma_1(T_m)]} \right]^{1/2} \quad \dots \quad 2.53$$

where A and A_1 are the energies of activation for intrinsic conduction in the respective layers.

The Debye-like character of the decay of the interfacial charges also allow the evaluation of the activation energy for the Maxwell-Wagner relaxation to be approximated by methods that are similar to those used for dipolar disorientation (Van Turnhout 1975). This will be discussed further in section 2.7.2.

The model of a Maxwell-Wagner TSD based on a 2 layered laminate is obviously a very special case. In real polymers, owing to the ill defined structural inhomogeneities or regions of crystalline and amorphous domains, the equations describing the TSD will be more complex.

2.6.2 TSD of a Homogenous Solid with an Air Gap

The TSD of a sample having a configuration as shown in figure 2.5 is considered below. Recalling our discussions of the previous section, we can assume $\sigma_1(T) = 0$ and $\epsilon_1 = 1$ since the layer is now an air-gap. We also assume that the solid is polar, therefore in addition to the build up of a surface charge due to an ohmic conduction in the solid, there will also be a dipole polarisation, $P(t)$, when V_a is applied across the air-gap and solid. The dipole polarisation can be accounted for by introducing $P(t)$ in the equations containing $E(t)$.

Equation 2.35 for the current during charging can be expressed as

$$\begin{aligned}
 j(t) &= \epsilon_0 \frac{dE_1(t)}{dt} \\
 &= \epsilon_0 \epsilon_\infty \frac{dE(t)}{dt} + \frac{dP(t)}{dt} + \sigma(T)E(t)
 \end{aligned}
 \tag{2.54}$$

Equation 2.38 becomes

$$\begin{aligned}
 Q(t) - P(t) &= \epsilon_0 \epsilon_\infty E(t) - \epsilon_0 E_1(t) && 2.55 \\
 &= \epsilon_0 \epsilon_\infty \frac{V_a}{l} - \epsilon_0 \left(\frac{l}{l_1} + \frac{\epsilon_\infty}{l} \right) V_1(t) \\
 & \dots && 2.56
 \end{aligned}$$

where $E(t)$ was substituted from 2.36. The differential equation describing the build-up of $Q(t)$ at the interface can be written using equations 2.54, 2.36 and 2.56 to yield

$$\frac{dQ(t)}{dt} + \beta_h(T)Q(t) = \beta_h(T)P(t) - \sigma(T)V_a(l + \epsilon_\infty l_1)^{-1}$$

2.57

where $\beta_h(T) = \beta(T) \left(1 + \frac{l}{\epsilon_\infty l_1} \right)^{-1}$,

i.e. the presence of $P(t)$ has reduced the relaxation frequency of the

solid by $\left(1 + \frac{l}{\epsilon_\infty l_1} \right)^{-1}$.

If we assume that $P(t)$ obeys a Debye-like relaxation with a single frequency $\alpha(T)$ and substituting for $E(t)$ using 2.56 and 2.36 we may also write

$$(\epsilon + \epsilon_\infty \lambda_1) \frac{dP(t)}{dt} + (\lambda + \epsilon \lambda_1) \alpha(T) P(t) = (\epsilon - \epsilon_\infty) \alpha(T) \left(\epsilon_0 V_a + \lambda_1 Q(t) \right) \quad 2.58$$

Equations 2.57 and 2.58 both show that the build-up of the interfacial charges $Q(t)$ and dipole polarisation $P(t)$ do not proceed independent of each other and would have to be solved numerically to yield the appropriate quantities.

During discharge, the equations describing the decay of $Q(t)$ and $P(t)$ can be found from 2.57 and 2.58 respectively by making $V_a = 0$. These could be written as

$$\frac{dQ(t)}{dt} + \beta_h(T) Q(t) = \beta_h(T) P(t) \quad 2.59$$

and

$$(\epsilon + \epsilon_\infty \lambda_1) \frac{dP(t)}{dt} + (\lambda + \epsilon \lambda_1) \alpha(T) P(t) = (\epsilon - \epsilon_\infty) \alpha(T) [\lambda_1 Q(t)] \quad 2.60$$

The discharge current during TSD can be found from 2.54 and 2.55 and the condition that $V_a = 0$. We then have

$$j(t) = \frac{d}{dt} [P(t) - Q(t)] \left[1 + \epsilon_\infty \frac{\lambda_1}{\lambda} \right]^{-1} \quad 2.61$$

The TSD current generated is proportional to the rate of fall of the quantity $[P(t) - Q(t)]$. In order to evaluate the actual course of the TSD current it is necessary to know the individual behaviours of $P(t)$ and $Q(t)$. Equations 2.58 and 2.59 will then have to be solved simultaneously.

It will be possible that the TSD current will exhibit two peaks, first, due to a dipole reorientation followed by one due to the neutralisation of the surface charges by ohmic conduction in the sample.

2.6.3 TSD of Surface Potential - "Charge" TSD

Introduction:

By measuring the persistent effective charge on the unmetalised surface of the polymer electret during a thermal rise, a charge TSD will be recorded. As will be discussed briefly in section 2.1.2 of chapter 4, throughout the course of the measurement the field between the measuring electrode and the charged surface is always made zero. Thus in the schematic representation of 2.2(c), the field $E_1(t) = 0$, a condition which we will note in our discussions of the theory of charge TSD.

2.6.3.1 Theory

We assume that the sample is polar and has an effective surface charge density $[Q(t) - P(t)]$. This effective surface charge will manifest itself as a surface potential, $V_s(t)$, which will decay as

both the dipole polarisation becomes disoriented and the excess

homocharges on the surface become neutralised by thermally generated carriers from within the sample bulk. Using the condition that, $E_1(t)=0$ during the surface potential measurement, equation 2.55 becomes

$$Q(t) - P(t) = \epsilon_0 \epsilon_\infty E(t) \quad 2.62$$

From the above we can also write for the surface potential,

$$V_s(t) = [Q(t) - P(t)] \frac{\ell}{\epsilon_0 \epsilon_\infty} \quad 2.63$$

During a TSD measurement the actual behaviour of $V_s(t)$ will be determined by the individual responses of $Q(t)$ and $P(t)$. These quantities can be approximated from equations 2.59 and 2.60 respectively but with an additional condition that since $E_1(t) = 0$, the gap distance ℓ_1 can be approximated by $\ell_1 \rightarrow \infty$. With this approximation, the equations reduce to

$$\frac{dQ(t)}{dt} + \beta(T)Q(t) = \beta(T)P(t) \quad 2.64$$

since now $\beta_h(T) \rightarrow \beta(T)$ as $\ell_1 \rightarrow \infty$

and

$$\frac{dP(t)}{dt} + \alpha(T)P(t) = (\epsilon - \epsilon_\infty)\alpha(T)Q(t) \quad 2.65$$

since $\ell \ll \infty$.

The experimental plot of the drop of the surface potential vs T will be a curve with 2-steps but normally the plot of the derivative will be more structured and informative. This is preferred for analysis since it displays the changes in Q(t) and P(t) more clearly.

Differentiating 2.63 with respect to time we have

$$\frac{dV_s(t)}{dt} = \frac{l}{\epsilon_0 \epsilon_\infty} \frac{d}{dt} [Q(t) - P(t)] \quad 2.66$$

Comparing 2.66 with the equation for the released current as in the TSD with an air gap of section 2.6.2, we have

$$\frac{\epsilon_0 \epsilon_\infty}{l} \frac{dV_s(t)}{dt} = - \left[1 + \frac{\epsilon_\infty l_1}{l} \right] j(t) \quad 2.67 \text{ where}$$

$j(t)$ is the TSD current of the air-gap configuration as defined by equation 2.61. Thus except for the factor $-[1 + \epsilon_\infty l_1/l]$, the expression will be similar to the air-gap TSD current density. From this similarity we will expect the plot of the time derivative of the persistent surface potential versus temperature will exhibit peaks that correspond with those of the TSD current plots.

Using equations 2.62, 2.63 and 2.66 it can also be shown that in the temperature range of the 2nd peak (i.e. when the dipole polarisation has essentially vanished) the following relation will hold,

$$\frac{1}{V_s(T)} \frac{dV_s(T)}{dT} \sim \beta(T) \quad 2.68$$

This can be re-written as

$$\frac{1}{V_s(T)} \frac{dV_s(T)}{dT} = \frac{-\sigma_0}{r \epsilon_0 \epsilon_\infty} \exp\left[\frac{-A_c}{kT}\right] \quad 2.69$$

where it was assumed that the conduction in the sample is thermally activated following an Arrhenius relation with r being the heating rate. Thus the activation energy for ohmic conduction, A_c , for the solid can be experimentally found by plotting $\ln\left[\frac{1}{V_s(T)} \frac{dV_s(T)}{dT}\right]$ vs $\frac{1}{T}$ in the temperature range when the dipoles have all been depolarised.

2.7 Evaluation of data from TSD curves

2.7.1 Preliminary remarks

In view of the complexity of the charge storage mechanisms in polymeric materials and the uncertainties associated with their physical structures in general, the interpretation of their current or charge TSD spectrums has to be carried out with some knowledge about the possible underlying microscopic processes involved. This is important since most models usually adopted for describing dipolar, ionic and electronic processes predict similar functional relationships which can lead to TSD peaks that look deceptively similar. The interpretation of the TSD results will be greatly facilitated if relevant factors such as physical structure, chemical content, thermodynamic behaviour etc. are reasonably well known from other complementary experiments.

2.7.2 Calculation of Activation Energies

Introduction

In theory, the activation energy of a non-distributed relaxation process can be calculated from a single TSD curve by means of some characteristic elements of the peak such as its half-width, inflection point or initial part of the current rise. Other methods based on utilising the whole current-temperature curve or that which uses several heating rates are also available. Most of these methods, except for the one using the whole of the TSD plot, were derived from methods based on the early works of thermoluminescence or thermally stimulated conductivity (see for e.g. Kivits and Hagebeuk 1977, Sessler 1979). It is noted that some of the methods to be described below are also very similar to those used for thermal analysis (for e.g. Daniels 1973, Wenlandt 1974).

2.7.2.1 Initial Rise Method

This method is credited to Garlick and Gibson 1948 and is based on the fact that the 2nd integral term in the $j(T)$ expression (equation 2.11) is negligible at temperatures $T < T_m$. Thus, differentiating with respect to $1/T$, one obtains for the initial portion of the current rise,

$$\frac{d}{d(1/T)} \ln j(T) = -A/k \quad 2.70$$

where A is the activation energy. By plotting $\ln j(T)$ vs $1/T$, A can be determined. This procedure is generally advocated to be satisfactory and is widely used. It does not necessitate a linear heating rate nor a precise knowledge of the absolute temperature.

The approximation that at $T < T_m$ the TSD current can be simplified into $j(T) \sim \text{constant} \cdot \exp[-A/kT]$ may not be true if the magnitude of the TSD signal in the rising portion of the plot is large when compared to the peak height. When this happens, then the plot of $\ln j(T)$ vs $1/T$ ceases to be linear and the value of A (obtained from the slope) has to be corrected. Christodoulides (1985b) has proposed an expression for the corrected value of A as given below.

$$A_{\text{corrected}} = (1 + 0.74d_1 + 0.092d_2)A - (2d_1 + 0.22d_2)kT_m. \quad 2.71$$

Here A is the value obtained from the least-squares-fitted plot of $\ln j(T)$ vs $1/T$ with experimental values of $j(T)$ that had been culled between two values of the current $j(T_2)$ and $j(T_1)$ where $T_1 < T_2 < T_m$. The parameters d_1 and d_2 are defined as

$$d_1 = \frac{j(T_1)}{j(T_m)} \quad ; \quad d_2 = \frac{j(T_2)}{j(T_m)} .$$

The ranges of applicability of equation 2.71 are $d_2 \leq 0.5$, $d_2/d_1 \geq 5$ and

$$10 \leq \frac{A_{\text{corrected}}}{kT_m} \leq 100.$$

2.7.2.2 Graphical Integration Method

This method was independently forwarded by Bucci et al (1966) and Laj and Berge (1966). It directly follows from 2.5 that the relaxation time $\tau(T)$ ($= \frac{1}{d(T)}$) can be written as

$$\tau(T) = \frac{P(T)}{J(T)} = \frac{1}{r} \left[\int_T^{\infty} J(T') dT' \right] \frac{1}{J(T)} \quad 2.72$$

or

$$\ln \tau(T) = \ln \left[\frac{1}{r} \int_T^{\infty} J(T') dT' \right] - \ln J(T). \quad 2.73$$

Assuming an Arrhenius shift for $\tau(T)$, we have

$$\ln \tau(T) = \ln \tau_0 + A/kT \quad . \quad 2.74$$

The quantity $\tau(T)$ can be calculated by using 2.73 where we have taken the integral term to be easily evaluated by graphical integration of the area of the TSD peak from $T \rightarrow \infty$. Knowing $\ln \tau(T)$ and plotting it against $1/T$, a straight line may be obtained, yielding the activation energy A . This straight line is usually called the BFG plot after Bucci et al 1966. Like the initial rise method this procedure does not presume a linear heating rate, but unlike the former it utilises data from the whole of the TSD peak. The BFG plot is to be preferred if the TSD plots exhibit large parasitic background currents which may be difficult to eliminate from the small current signal portion of the initial rise.

2.7.2.3 Methods based on the Variation of Heating Rates

These methods are based on the shifts of the TSD current maximum with the heating rates employed. Several ways of plotting the results have been proposed (Booth 1954, Bohun 1954). It can be readily seen that from 2.12

$$A = \frac{kT_{m_1} T_{m_2}}{T_{m_1} - T_{m_2}} \ln \left[\frac{r_1 T_{m_2}^2}{r_2 T_{m_1}^2} \right] \quad 2.75$$

i.e., if the heating rate is changed from r_1 to r_2 , the activation energy for the relaxation can be calculated from the corresponding shift of the peak temperature T_{m_1} to T_{m_2} .

A better procedure utilising a series of heating rates, r , (resulting in corresponding T_m 's) was also suggested by Hoogenstraaten (1958) whereby the plot of $\ln\left(\frac{T_m^2}{r}\right)$ against $1/T_m$ should yield a straight line, from the slope of which the activation energy can be found. The accuracy of these methods will depend on the accurate control of the heating rates employed and also on the magnitude of the actual shifts of the T_m 's. Therefore it can be seen from equation 2.12 that the method is less suitable for relaxations with large activation energies, A , since the shifts of the current maxima will be smaller and experimentally more difficult to measure.

Several other methods to calculate the activation energy based on utilising the shape or symmetry of the TSD peak can also be found (for e.g. Grossweiner 1953, Halperin and Braner 1960, Chen

1969a, 1969b). Christodoulides 1985a has briefly reviewed some of the techniques and also proposed a new procedure to obtain a more accurate value for the activation energy.

2.7.3 Calculation of other relaxation parameters

If the activation energy for the relaxation is known by using the procedure described above, then the characteristic frequency

factor $\alpha_0 = \frac{1}{\tau_0}$ can be calculated from equation 2.12 if T_m is noted from the experimental peak. α_0 can also be directly determined from the BFG plot (section 2.7.2.2).

The equilibrium polarisation P_e for the electret may also be obtained by integrating the area underneath the $j(T)$ curve, assuming that there was no loss or change of polarisation during the cooling and isothermal stages of the TSD run, i.e.

$$P_e = P(T_p) = P(T_d) . \quad 2.76$$

Hence

$$P_e = \int_{T_d}^{\infty} j(T) dT . \quad 2.77$$

Also using the relation for the relaxation strength,

$$\begin{aligned} \Delta\epsilon &= \epsilon_s - \epsilon_{\infty} \\ &= \frac{P_e}{\epsilon_0 E_p} \end{aligned} \quad 2.78$$

where E_p is the field applied during formation. From the above equation and using equations 2.3 and 2.4 we can relate the experimentally observed quantity, $\Delta\epsilon$, with the molecular parameters, N , the dipole density and p , the dipole moment. This is expressed as

$$\Delta e = \frac{Np^2}{3\epsilon_0 kT_p} \quad 2.79$$

where T_p is the temperature of formation of the electret. If either quantity N or p , is known, then the other can be calculated using 2.79. The obvious condition is that P_e is adequately described by the Langevin equation and that it is recovered fully during the TSD.

2.7.4 Notes for distributed processes

The methods described previously to calculate the activation energy only holds strictly for relaxations of a single, well-defined frequency. For a distributed relaxation, the initial rise method for the calculation of the activation energy would theoretically yield too low a value by over emphasizing the role of the components with the slowest relaxation times. The graphical integration method will also have the same systematic error as a result of taking into account of too high a number of components.

Van Turnhout (1975) has shown that the initial rise method can still be applied to the case where there is a symmetrical distribution in $\frac{1}{\alpha_0}$. Up to the lower half-width temperature, the TSD current was shown to obey approximately

$$\ln J(T) \sim \text{const} - \frac{WA}{kT} \quad 2.80$$

where W is a constant whose value will depend on the type of the distribution describing $\frac{1}{\alpha_0}$. Equation 2.80 also show that A can

still be calculated by the initial rise plot.

The methods based on the variations of the heating rates are still theoretically applicable, without modification, for the distributed process. This is so because the peak of the TSD current plot is determined essentially by the components with the average value of the activation energy. However, a problem would exist in the exact determination of T_m 's and their shifts due to the broad nature of the TSD plots of the distributed systems.

The determination of other relaxation parameters such as the characteristic frequency, equilibrium polarisation and relaxation strength is little affected by the existence of a distribution in relaxation times. The quantities can still be approximated by the equations of section 2.7.3 (Vanderschueren and Gasiot 1979).

2.7.5 Notes for the Charge Motion Model

Assuming that the decay of a uniform distribution of the excess charges obeys first order kinetics with a single relaxation time, then the classical methods (initial rise, variable heating rate methods) used to evaluate the TSD parameters are still applicable. This follows from the similar functional relationship of the $j(T)$ expression for the different decay processes that was briefly discussed in the preceding sub-sections.

For a spatially non-uniform distribution of space charges Wintle (1971) has proposed a modification to the graphical integration method. Here the quantity

$$\left[\int_{T_d}^T j(T') dT' \right] \left[\int_T^{\infty} j(T') dT' \right]^{-1}$$

is plotted against $\frac{1}{T}$ to yield the effective activation energy for the decay (compare with the BFG plot of section 2.7.2.2). Van Turnhout (1975) has also discussed a method where the quantity

$$\left[T_m^2 \int_{T_d}^T j(T') dT' \right] \left[T^2 \int_T^{\infty} j(T') dT' \right]^{-1}$$

is plotted against $\frac{1}{T}$. The methods mentioned above are applicable

in the low temperature region of the current plots.

The linearity of the latter plot is also suggested as being used as a good test as for the applicability of the charge motion model. The linearity of this plot is unique to the decay of a space charge polarisation via their self-drift.

In the charge motion model, it is also expected that the activation energy calculated from TSD data will be closely related to that for the dark conductivity mechanism in the medium (Kessler and Caffyn 1972, Agarwal 1974) and as such the method can be used as a good complement to the traditional current-voltage-temperature method, particularly when blocking electrodes could not be avoided.

CHAPTER 3

POLYVINYL BUTYRAL AND AMORPHOUS SELENIUM BASED XEROGRAPHIC PHOTORECEPTOR

The aim of this chapter is to present a brief introduction to the physical and electrical properties of polyvinyl butyral and an example of a commercial multi-layer xerographic photoreceptor. A brief survey of previous work carried out on the materials is also presented.

3.1 Polyvinyl butyral

3.1.1 Introduction

Polyvinyl butyral from now on referred to as PVB, belongs to a generic group of polymer resins, the poly vinyl acetals which are derived from the acetalisation of poly vinylalcohol with aldehydes. Several methods for the commercial manufacture of PVB exist, and indeed the final product have different trade names (Lindemann 1969). There are two different processes that are normally used in the commercial manufacture of PVB. This could be broadly classified as the Du Pont processes (Rombach 1964) and the Monsanto process (Voss and Starck 1930). In general, the physical and chemical properties of the PVB product will depend on the degree of hydrolysis and molecular weight of poly vinylalcohol that was used as well as the amount and grade of the butyraldehyde. Several commercial grades of PVB are normally manufactured (e.g. Monsanto Co. 1977) each with a slightly different set of physical properties. Table 3.1 lists some properties of Butvar B79, one of the many forms of commercially available PVB.

Table 3.1 Some properties of commercial Polyvinyl butyral (BUTVAR B79)
(After Monsanto Co. 1977)

| | |
|--|----------------------------|
| Type | Butvar B79 |
| Form | White, free flowing powder |
| Weight-average Molecular weight | 34,000-38,000 |
| Specific Gravity | 1.083 |
| Butyral content expressed as % poly vinyl butyral | 88% |
| Hydroxyl content expressed as % poly vinyl alcohol | 9.0 - 13.0 % |
| Acetate content expressed as % poly vinyl acetate | 0 - 2.5 % |
| Water absorption (24 hours) % | 0.3 % |
| Apparent Glass Transi- tion temp. (ASTM D 1043-51) | 48 - 55 ° C |

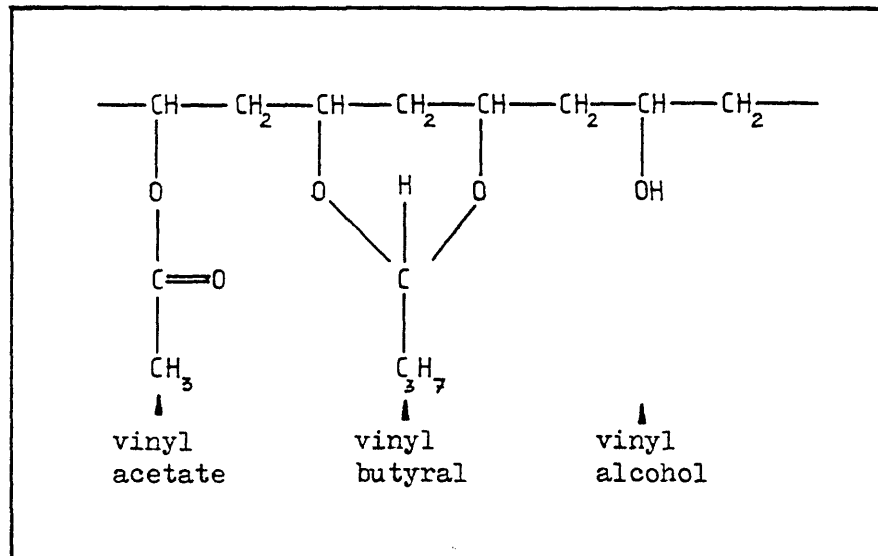


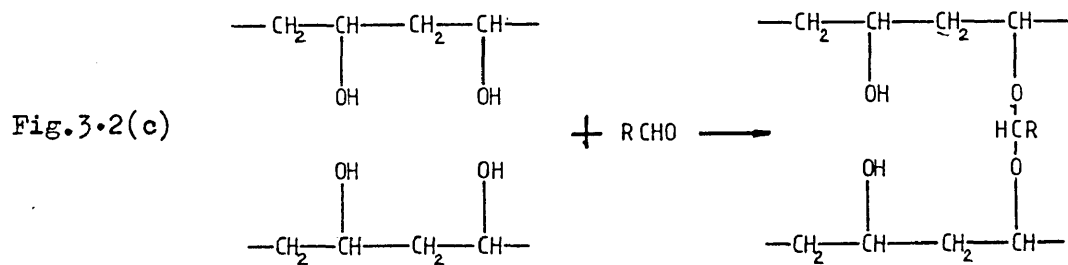
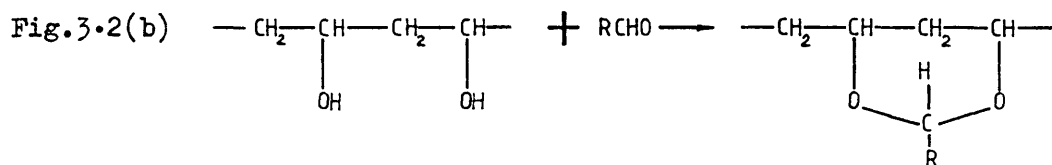
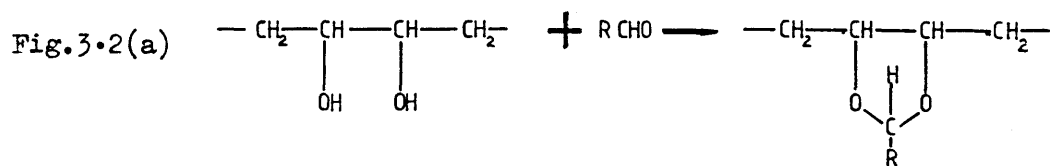
Fig.3.1 Poly vinylbutyral monomer unit showing residual vinyl acetate and vinyl alcohol units

3.1.2 Chemical Formula and Structure

Commercially manufactured PVB will normally have a chemical structure as shown in figure 3.1. Typically, the resin will still possess residual vinyl acetate and vinyl alcohol groups in the repeat unit since a 100% acetalisation of the parent poly vinylalcohol would be difficult to achieve (Flory 1938). The structure of PVB may also show different conformations, depending on the different modes of acetalisation as shown in figures 3.2 (a,b,c). Reactions 3.2(a) and 3.2(b) will result in 6-membered and 5-membered intra-molecular acetal rings between adjacent hydroxyl groups. The reaction specified in figure 3.2(c) also presents another possibility in which inter-molecular acetal links are formed, resulting in cross-linked structures. The properties of PVB thus may also vary with the reaction kinetics of the acetalisation process even though the final degrees of acetalisation are identical. It is also worth noting at this point that the manufacture of PVB by the Monsanto process (for Butvar B-series) results in high degrees of acetalisation, favouring intra-molecular acetalisation (reactions 3.2(a) and 3.2(b)). As was shown by Toyoshima 1973, this may also result in a more uniform distribution of acetal groups along the chain.

3.1.3 Infra-Red Absorption

The infra-red absorption spectrum of PVB is normally characterised by the presence of band combinations at 7.23, 8.8, 9.0, 9.5, 10.0 and 10.3 μm as shown in figures 3.3(a) and 3.3(b). Accord-



Acetalisation of Poly vinylbutyral. $\text{R} = \text{C}_3\text{H}_7$

3.2(a) Intramolecular acetalisation of the 1,2-glycol group

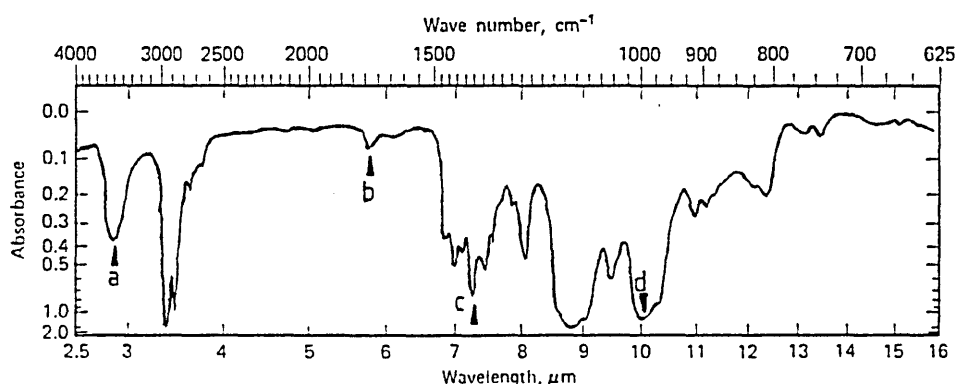
3.2(b) Intramolecular acetalisation of the 1,3-glycol group

3.2(c) Intermolecular acetalisation

ing to Hummel and Scholl 1971, PVB is primarily characterised by the two very intense absorption band complexes centred around 8.9 μm and 10.1 μm , the latter being due to the vibrations of the 1,3 dioxane ring.

The presence of other vinyl units like vinyl alcohol and vinyl acetate in commercially available PVB are to be expected due to their inherent presence during the manufacturing process. The presence of these units are also shown in the figures below.

Fig.3.3(a) Infra-red absorption of Poly vinylbutyral containing ~88% vinyl butyral, ~9-13% vinyl alcohol and 2.5% (max.) vinyl acetate.(After Hummel and Scholl 1971,Spectrum 1015)



- a O-H stretching in vinyl alcohol
- b C=O stretching in vinyl acetate
- c C-H₃ bending in vinyl acetate
- d 1,3 dioxane ring vibration in vinyl butyral

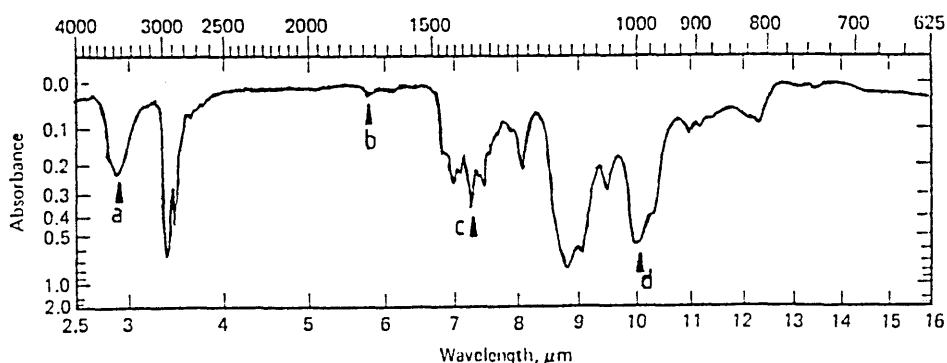


Fig.3.3(b) Infra-red absorption of Poly vinyl butyral containing ~80% vinyl butyral, 17.5-21% vinyl alcohol and 2.5% (max.) vinyl acetate units.(After Hummel and Scholl 1971,Spectrum 1017)

3.1.4 Relaxational Properties

3.1.4.1 Introduction

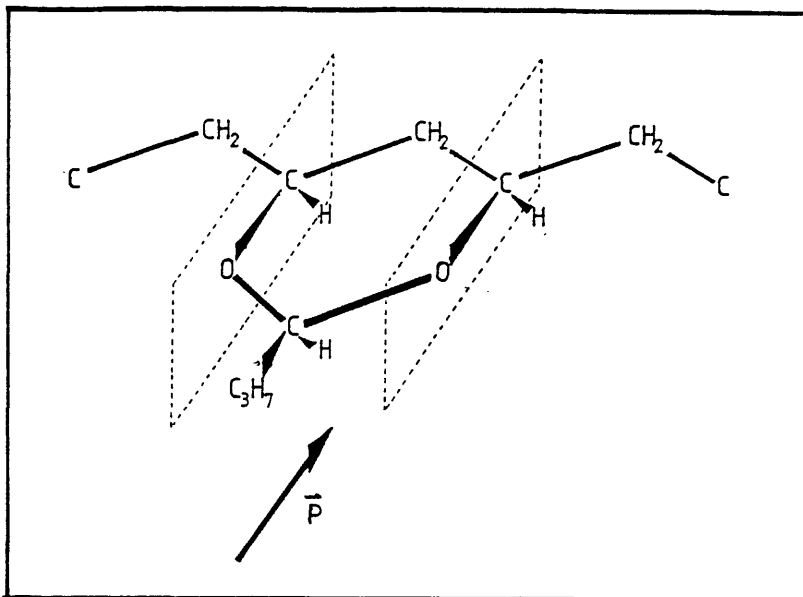
The dielectric properties of PVB were first studied by Funt (1952) and Schulz and Muller (1952). Relatively few electrical studies were carried out on PVB when compared to the other commercial organic polymers. This is believed to be due to the relative unimportance of the polymer as an electrical material. Its excellent adhesive properties to glass (Weihe 1941, Huntsberger 1981) has resulted in the material being used as a laminate in the safety glass industry. This is by far, the major consumer of all the PVB produced today.

Other uses of PVB include its use as a binder resin in electrical materials systems such as pigment-resin-dye based xerographic photoreceptors (Schaffert 1975) or high density magnetic recording films (Nakamae et al 1984). Fine particles of PVB impregnated with carbon black are also used as a toner material for xerography (O'Reilly and Erhardt 1973).

Apart from its technological applications, PVB is also interesting from the scientific point view. The monomer unit contains a polar side-group attached to two points along the main carbon chain, causing any rotary movements which are independent of the main chain to be severely inhibited (fig.3.4). In addition to this, residual polar hydroxyl and polar acetate groups are also present in the molecule, though in smaller amounts. The presence of these groups could also influence the electrical properties of the polymer such as dielectric loss, polarisation and depolarisation behaviour and electrical conductivity.

Fig.3.4 Schematic representation of PVB showing position of polar group relative to the main vinyl chain. \vec{p} is the dipole moment.

The 1,3-dioxane ring can be clearly seen.



3.1.4.2 Dielectric Properties

Funt (1952) investigated the dielectric properties of hot pressed PVB films in the temperature range of 20°C to 140°C and found that a single loss peak was present for frequencies between 0.3 Hz and 100 Hz (figure 3.5). It was also found that the loss factor ϵ'' was both frequency and temperature dependent, the maxima shifting to higher temperature as the frequency is increased. The plot of $\ln \tau$ vs $1/T$ where τ is the reciprocal of the angular frequency of maximum absorption, was found to be straight line within the temperature range that was used (figure 3.6). By observing the linearity of this plot and using the theory of Absolute Rates (Eyring, 1941), the slope of the plot was used to define the activation enthalpy, ΔH^* for the relaxation.

The loss peaks were attributed to the rotations of the polar

side groups (1,3 dioxane structure) and on the evidence of the relatively high values of ΔH^* for the relaxation process, he concluded that the dipole rotations must be severely restricted. This was a consequence of the bonding of the polar groups to two points along the main chain. He also suggested that from the observation of the large values of the change in the entropy, ΔS^* , approximately 10 monomer units must be rotating together, a situation which was only possible when the glass transition temperature of the polymer is approached.

Funt also noted the deviations of the results from the quantitative predictions of the Debye theory, and suggested that this was due to the distributed nature of the relaxation times of the dipoles involved. A sharp increase at higher temperatures in the ϵ'' curves (figure 3.5) were also observed with the possible occurrence of another relaxation peak being not discounted.

Takahashi(1961a) carried out dielectric measurements on heat treated PVB films in the temperature range of -70°C to 120°C using frequencies, f , ranging from 0.3 Hz to 10^6 Hz and reported the occurrence of two dispersions in the ϵ'' vs $\ln f$ curves. These dispersions are shown in figure (3.7(a) and 3.7(b), which were plotted separately for their low and high temperature zones. These peaks, labelled α and β in descending order of temperature, can be seen to exhibit a strong temperature dependence especially in the high temperature zone (i.e for the α -relaxation). The plot of $\ln f_m$ vs $1/T$, where f_m is the frequency where ϵ'' is maximum showed a deviation from a straight line for the α -relaxation but for the β -relaxation a straight line was obtained. The deviation from the simple Arrhenius law for the α -dispersion was attributed to the cooperative behaviour of the

Fig.3.5
 ϵ'' vs. Temperature for
 several measurement
 frequencies.
 (After Funt 1952)

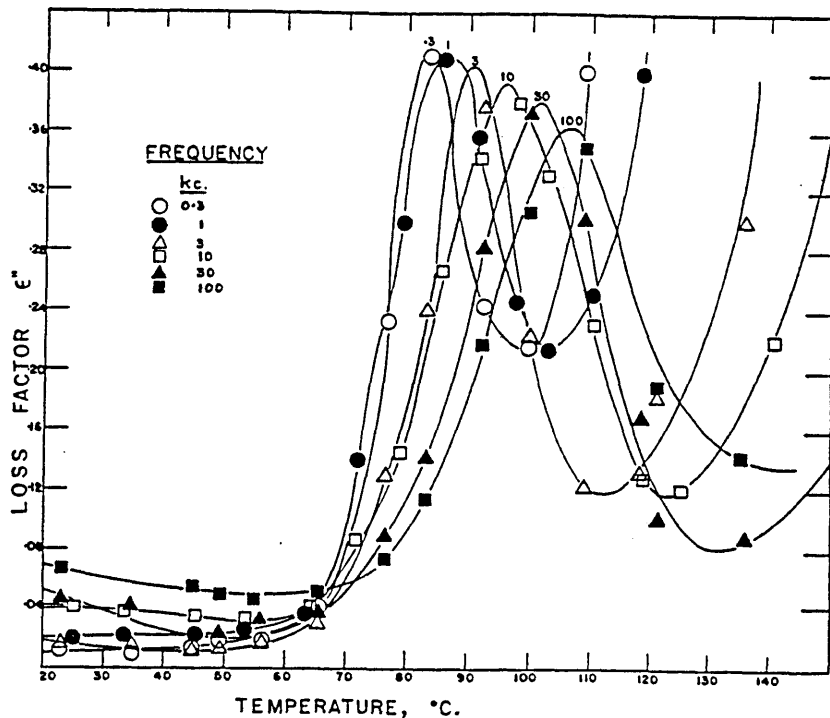


Fig.3.6 Logarithmic plot of
 relaxation time vs. reciprocal of
 absolute temperature. (After Funt 1952)

$\Delta H^* = 65.2 \text{ kcal.mole}^{-1} (2.83 \text{ eV})$

$\Delta S^* = 139 \text{ entropy units.mole}^{-1}$
 or $6.02 \text{ eV}^\circ\text{C}^{-1}$

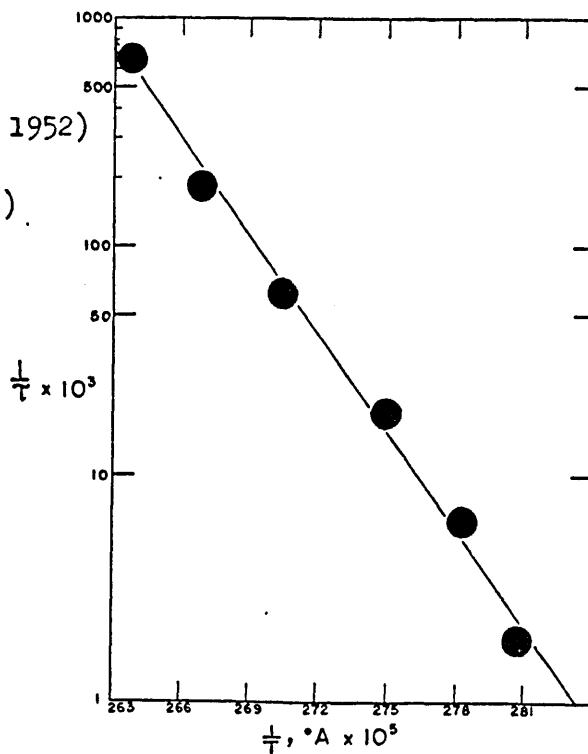


Fig.3.7 Frequency dependence of the loss factor ϵ'' for PVB films
 a : Low temperature region
 b : High temperature region
 (After Takahashi 1961 a)

Fig.3.7 (a)

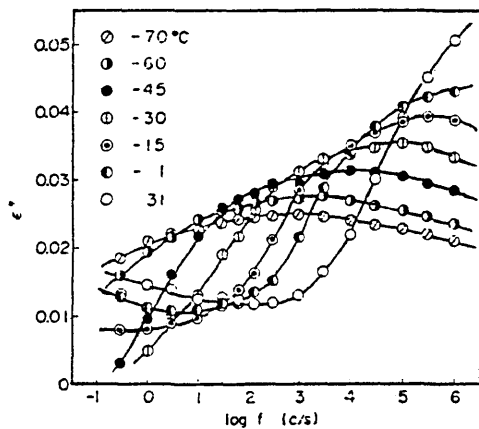


Fig. 3.7 (b)

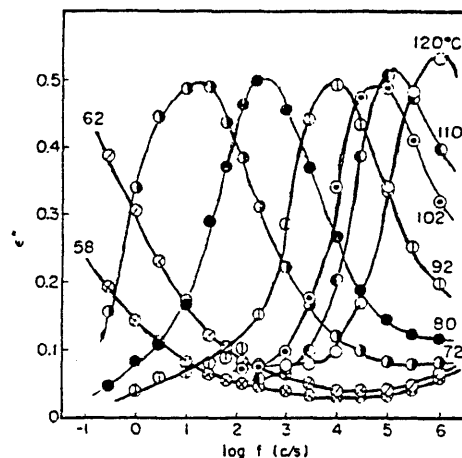


Fig.3.7 (c) Plot of logarithmic dispersion frequency vs. reciprocal of absolute temperature.

α -dispersion : $\Delta H^* = 4.03 \text{ eV (80}^\circ\text{C)}$
 $= 1.40 \text{ eV (120}^\circ\text{C)}$
 β -dispersion : $\Delta H^* = 0.52 \text{ eV}$

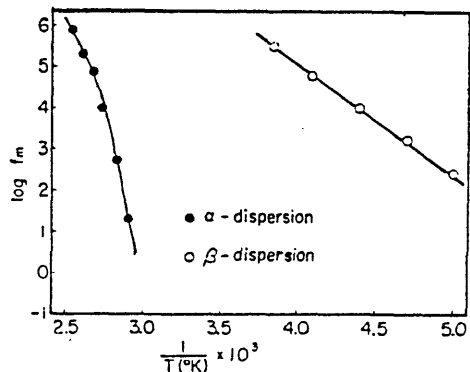


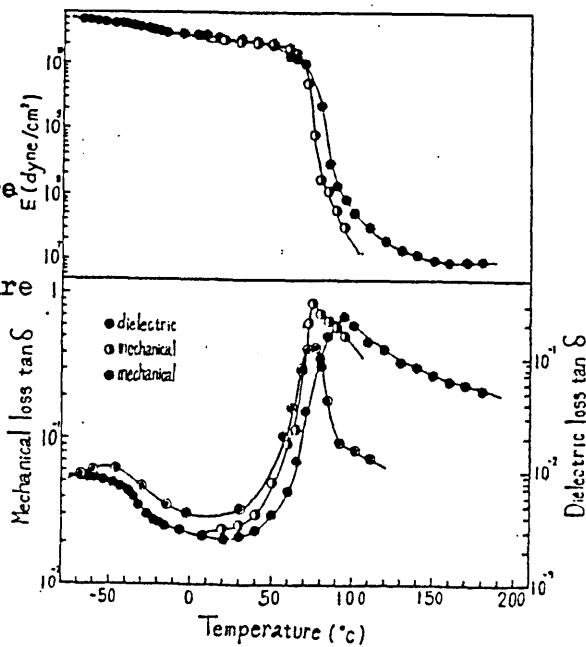
Fig.3.8 (After Takahashi 1961 b)

Top : Dynamic elastic storage modulus of PVB as a function of temperature

Bottom : Mechanical Loss and Dielectric Loss as a function of temperature

Legend:

- Dielectric, sample cured at 200 °C for 30 mins.
- Mechanical, sample cured at 200 °C for 30 mins.
- ◐ Mechanical, sample cured at 170 °C for 30 mins.



segmental movements of the main chain. Values of the activation enthalpy, ΔH^* , for the α -relaxation which were calculated using the WLF equation (Williams, Landel and Ferry 1955) are shown in figure 3.7(c).

In contrast to the behaviour of the α -dispersion, the β -relaxation peak exhibited a constant ΔH^* value. This peak was believed to be due to the local movements of the polar side groups of the polymer while the main chains were still rigid.

3.1.4.3 Dynamic Mechanical Properties

Dynamic mechanical measurements at 60 Hz carried out over the temperature range of -70°C to 200°C (Takahashi 1961(b)) also revealed two dispersions which exhibited a good correlation with the dielectric measurements. The plots of the mechanical loss and dielectric loss as functions of temperature are shown in figure (3.8) where both the β and α dispersions could be observed. It was noted that the samples of PVB used in the mechanical measurements contained a high percentage of vinyl alcohol units (~ 30%). The shift of the α -peak for the mechanical measurements was thought to be due to the different vinyl alcohol contents of the differently sourced PVB samples.

3.1.4.4 TSD Behaviour

The first studies on the electrical charge storage properties of the PVB by using the technique of thermally stimulated discharge currents were carried out by Jain et al (1974). The depolarisation characteristics of thin ($< 1\mu\text{m}$) layers of PVB were studied as

functions of polarising field, E_p and iodine concentration. The purified PVB films used were reported to exhibit a glass transition temperature at 85°C and a melting temperature at 172°C. The samples used were fabricated as planar surface cells.

After polarisation of the samples at $T_p = 92^\circ\text{C}$ for about 60 minutes, they were cooled down to room temperature at a very slow rate of approximately $1.5^\circ\text{C min}^{-1}$. By using a heating rate of 6°C min^{-1} , two thermally stimulated discharge current peaks were observed at 77°C (labelled β) and 157°C (labelled α). Both peaks did not exhibit any significant temperature shift with different polarising fields, E_p . The magnitude of the maximum currents and the total charge release increased linearly with increasing E_p . Using the initial current rise method, the activation energies for the β and α peaks were found to be 0.19 eV and 0.53 eV respectively.

The β -peak was attributed to the local rotations of the polar side groups around their equilibrium positions while the α -peak was believed to be due to the re-orientation of dipoles as a result of main-chain conformational movements in the polymer bulk. It was also stated that the possibility of the α -peak originating from the de-trapping of trapped charges could be ruled out. The observation that the peak occurred at a temperature well above the glass transition temperature of the polymer, (157°C, as compared to $T_g = 85^\circ\text{C}$) where one would expect the α or dipole peak to occur, was not discussed.

Jain, Kumar and Mehendru 1979 has also reported the observation of two peaks, labelled I and II, at 74°C and 150°C respectively

in the TSD of PVB films. The films used by them were reported to contain approximately 17% hydroxyl and less than 3% acetate groups and were reported to exhibit a glass transition at 77°C. Both sandwich and surface cell sample structures were fabricated, but the general TSD current spectra detected were reported to be independent of this difference in sample structures.

Peak I at 74°C was reported to be due to a dipole re-orientation displaying a non-distributed relaxation. The energy of activation for this relaxation was found to be 0.36 eV by the initial rise method. Due to this apparently low value, it was concluded that the dipole species involved in this relaxations were the hydroxyl and acetate groups, in view of their respectively less hindered movements/rotations with respect to their bondings to the main chain. The significance of the position of this peak near the glass transition temperature, (77°C), where the onset of segmental chain motions were most likely, was not taken into account. Thus, the contribution of the polar butyral side groups (contributing to about 80% of the weight of the polymer) were neglected.

The origin of the 2nd peak at 150°C was attributed to the release of trapped electronic carriers due to continuous thermal agitation of the sample. The possibility of an ionic nature of the charge carriers was deemed unlikely due to the relatively low energy of activation of the peak, 0.70 eV, as found by the initial rise plot. It was also reported that this relaxation peak exhibited a shift with the forming conditions and hence was probably distributed in its relaxation parameters.

Further work was also carried out on the TSD relaxation of PVB with different degrees of polymerisation (Mehendru, Jain and Kumar 1980). It was expected that due to molecular origin of the TSD peaks, any change in the physical structure of the polymer e.g. chain length, density of end-groups and molecular packing would cause a change in the eventual thermally stimulated relaxation behaviour.

Two TSD peaks were observed, centered at 74°C and 150°C, labelled β and α respectively. Their positions and magnitudes were studied as a function of the degrees of polymerisation, n , of the PVB films used ($n = 300, 900$ and 1600). The β peaks, associated with the local movements of side groups, were found to decrease in height as n is increased. This observation led the authors to conclude that with a decrease in the number of end-groups in the polymer bulk, which was brought about by a higher degree of polymerisation, a smaller number of polarisable species would be available to contribute to the β -relaxation process.

The α -peak, centred at 150°C was attributed to the release of electrons/holes in the bulk of the polymer. With an increase in the degree of polymerisation, n , the heights of the peaks decreased but their widths was found to increase proportionately, maintaining a constant total amount of charge released during the relaxation process. It was argued that this indicated that the volume distribution of traps in the polymer remain unaffected by the increase in the average chain lengths in the polymer. The observed widening of the α -peak was attributed to the increase in the molecular packing leading to an

increased interaction between the charge carriers. The increase in chain lengths was also deemed responsible for the slight increase in the calculated activation energies for the α -relaxation.

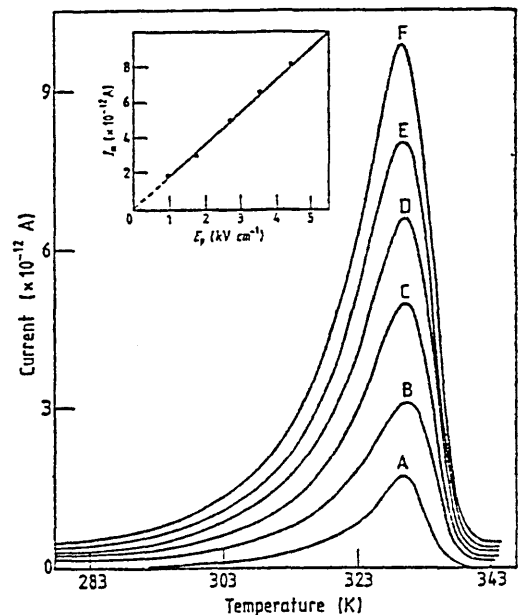
The TSD properties of thin PVB films were also investigated (Gil-Zambrano and Juhasz 1981) as functions of charging fields E_p , charging temperature T_p and heating rate r . A single relaxation peak was observed centred at about 58°C within the range of experimental variables used and this was designated as the α -peak.

It was found that the peak displayed the characteristics of a dipolar re-orientation, viz. linear dependencies of the magnitude of the peak current and the total amount of charge released on the polarising field (figure 3.9). The use of the thermal sampling technique (Zielinski and Kryszewski 1977) also revealed that the α -peak actually consisted of a distribution of overlapping TSD peaks, thus experimentally proving that the relaxation processes was distributed. It was found that the apparent activation energies for the thermally sampled peaks increased as the polarising temperatures were raised, indicating a spread in the activation energies for dipole disorientation.

Fig.3.9 (After Gil-Zambrano & Juhasz 1981)
TSD spectra of PVB films polarised
at 80 C for 4 mins. r is 4°C min^{-1} .

| | | | | |
|-----|-------|---|-------------------|--------------------|
| A : | E_p | = | 1.0×10^3 | V.cm^{-1} |
| B : | " P | = | 1.8 | " " " |
| C : | " | = | 2.7 | " " " |
| D : | " | = | 3.6 | " " " |
| E : | " | = | 4.5 | " " " |
| F : | " | = | 5.4 | " " " |

Inset shows plot of TSD peak current vs.
magnitude of polarising field.



3.1.5 Summary

Relatively few studies were carried out on the electrical properties of PVB compared to the other commercially important polymers like polyethylene, polyvinylidene fluoride or polyethylene terephthalate. Table 3.2 summaries the data available on the relaxational properties of the polymer. It was discussed earlier that the presence of residual vinyl alcohol and vinyl acetate do to a certain extent effect the physical and electrical properties of the PVB samples. These concentrations are also tabulated (where known).

Table 3.2 is divided into temperature zones and the observed relaxations are grouped under their respective temperatures of maximum responses (TSD current peaks, dielectric and mechanical loss maxima). A relaxation at about -50°C was detected by both dielectric and dynamic mechanical measurements (Takahashi 1961a, 1961b). A good correlation was observed between the two methods. These β -relaxations were believed to be due to the local movements of the side-groups (butyral, acetate, alcohol) about their equilibrium positions while the main polymer chains were still rigid. The apparent activation energies involved are of the order of 0.52 eV. A single activation energy seemed to characterise these relaxations implying well-defined entities under-going the relaxation process.

As the temperature of observation is increased, another relax-

Table 3.2

Summary of previous works that were carried out on PVB. Maximum responses are shown as a function of temperature.

| EXPT'L METHOD & REMARKS | TEMP. OF MAXIMUM RESPONSE | -50°C | 0°C | 50°C | 100°C | 150°C | 200°C |
|---|---------------------------|-------|--|------|--|-------|--|
| Funt B.L. (1952) Dielectric. 0.3 to 100 Hz. 20° to 140°C Butyral: 38.3% Acetate: 0.3% Hydroxyl: 7.0% Vinyl: 54.4% | | | | | ε" loss peak. Rotation of butyral side-groups ΔH = 2.83 eV (0.3 Hz) | | Sharp increase in ε" observed |
| Takahashi Y (1961 a) Dielectric. 0.3 to 10 ⁶ Hz. -70 to 120°C | | | β-dispersion Movements of side-groups (local) ΔH = 0.52 eV | | α-dispersion Segmental movements of the main chain ΔH = 4.03 eV (80°C) 1.40 eV (120°C) | | |
| Takahashi Y (1961 b) Dynamic mechanical. 50 Hz. -70 to 200°C Vinyl butyral: 61.3% " alcohol: 36.6% " acetate: 2.1% | | | β-dispersion Secondary loss due to local movements of side-groups | | α ₁ -dispersion Primary loss associated with 2nd. order transition. | | |
| Jain K et.al (1974) TSD Currents (surface cells) Slow cooling (-1.5°C min ⁻¹) | | | | | T _g = 85°C β-relaxation peak Local rotations of side-groups Activation energy = 0.19 eV | | T _m = 172°C α-relaxation peak Conformational movements of the main chain Activation energy = 0.53 eV |
| Jain K et.al (1979) TSD Currents Hydroxyl: 17% Acetate: < 3% | | | | | T _g = 77°C Reorientation of acetate and hydroxyl groups Activation energy = 0.36 eV | | Release of electrons/holes from traps. Activation energy = 0.66 eV Distributed process |
| Mehendru PC et.al (1980) TSD Currents Degrees of polymerisation = 300, 900, 1600. | | | | | T _g = 77°C β-relaxation peak Reorientation of acetate and hydroxyl groups. Peak shifted to lower temp. as degree of polymerisation increases | | α-relaxation peak Release of electrons or holes from traps. No shifts of peak. |
| Gil Zambrano J.L & Juhasz C (1981) TSD & TSP Currents (low charging fields) Diff. Thermal Analysis | | | | | T _g = 61°C α-relaxation peak. Conformational movements of chain segments with attached polar groups due to 2nd. order transition. Energy of activation = 2.0 eV | | |

ation peak is obtained, this involving large scale movements of about 20-50 carbon atoms in lengths. This relaxation is largest in the region of the glass transition of the polymer. At this temperature region the polymer chains gradually become unfrozen, allowing conformational movements/rotations of the polar butyral side group to take place. The relaxation process is characterised by a distribution in its relaxation frequencies as well as its energies of activation owing to the different possible lengths of the relaxing segments of the main chains to which the butyral groups were attached.

Taking into account the different T_g 's of the samples used by the different workers, which were possibly caused by the different amounts of residual side groups, a relaxation peak at this temperature were reported by all the workers (table 3.2). Funt (1952), Takahashi (1961a) and Gil-Zambrano and Juhasz (1981) all attributed this peak to the conformational movements of segments of the main chains to which the relatively large butyral groups were attached. However, the conclusions of Jain et al (1974), (1979) and Mehendru P.C. et al (1980) were in disagreement with the other workers. They attributed this relaxation peak to the local rotations/movements of the hydroxyl and acetate side groups, inherently implying that the main chains of the polymer were still rigid despite the experimental fact that the observed peaks were very close to T_g .

Jain et al (1974), (1979) and Mehendru P.C. (1980) all reported the observation of a TSD relaxation peak centered around 150°C. In

their first paper, Jain K. et al (1974) attributed this to the depolarisation of dipoles (the butyral group) explicitly ruling out any possibility of the peak being electronic or ionic in nature. However in subsequent papers Jain et al 1979, Mehendru 1980 both concluded differently, namely the origin of the observed peaks were attributed to the release of electronic carriers from deep traps.

3.2 Amorphous Selenium Based Multi-Layer Photoreceptor

3.2.1 Introduction

The remarkable dielectric and photoconductive properties of amorphous selenium (a-Se) has resulted in the material being used as the principal photoreceptor material of the xerographic industry today. A large amount of published work on a-Se can be found (e.g. standard textbooks by Zingaro and Cooper (eds.) 1974, Gerlach and Grosse (eds.) (1979). The techniques of Time-of-Flight and Xerographic Time-of-Flight are often used in determining the xerographic parameters of the material. Theoretical as well as experimental details of these methods can be found in the works of Owen and Spear 1976, Dolezalek 1976, Pfister 1979 and Berger 1979 amongst others. For a description of the physics of xerography, the reader is referred to the works of Dessauer and Clark 1965, Schaffert 1975, Watson 1979 and Williams 1984.

Other photoreceptor materials or materials systems that are also commercially used are the pigment-resin-dye layers and those based on organic photoconductors like poly vinyl carbazole (PVCz) and poly-N-vinyl carbazole (PVK) (see Schaffert 1975 and references therein). The possible use of hydrogenated amorphous silicon films as xerographic photoreceptors has also been a subject of recent interest (Shimizu 1980, Mort et al 1980, 1984) however this has not yet proven to be commercially viable.

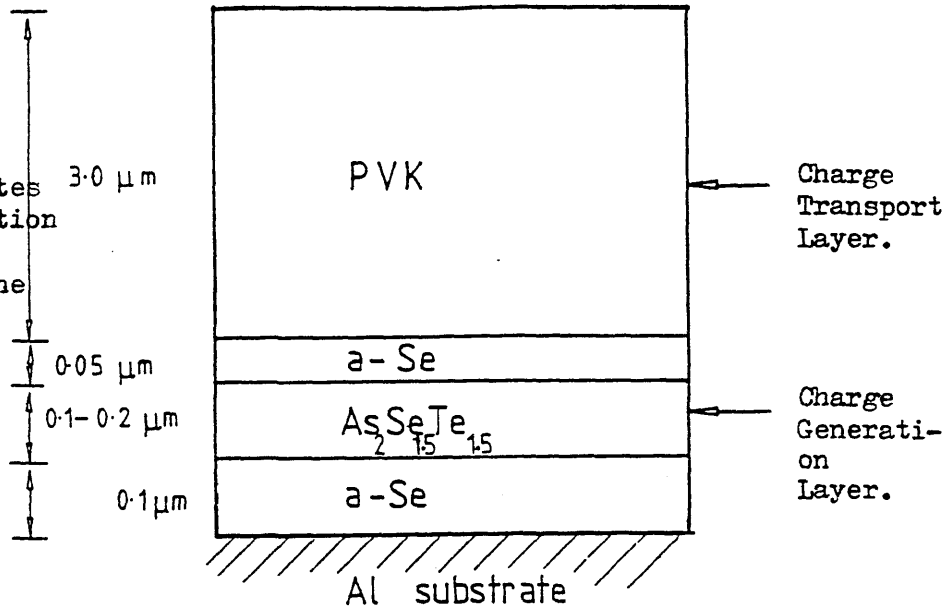
The significant changes in the xerographic properties of a-Se with alloying or doping (Fotland 1960, Schottmiller 1970, Tabak and Hillegas 1971, Kasap 1982) renders the material attractive as a photo-receptor whose response can be tailored to meet specific design considerations. Increased speeds in duplication demands that the photo-receptor have a fast photo-discharge and exhibit excellent cyclic stability. The use of electrophotographic technology in printers utilising arrays of LED's or semiconductor lasers also require that the spectral response of the a-Se based photoreceptors be extended towards longer wavelengths (750-850 nm).

Apart from the desirable effects such as the improvement of the photosensitivity or preventing re-crystallisation of the amorphous films, the doping or alloying of a-Se with certain impurities or elements may also cause an increased rate of dark decay due to the increase in the intrinsic conductivity of the alloy. In order to overcome some of the undesirable effects of alloying, xerographic photoreceptors with functionally separated layers were developed. These are layers where the different xerographic processes of photo-generation and transport of the excess charges are performed by physically different layers of the photoreceptor structure. The multilayered photoreceptors utilise varying geometrical configurations based on layers of a-Se, PVK:TNF, a-SeTe alloy or organic dyes (Neyhart 1966, Ing and Chiang 1967, Regensburger 1968 and Schaffert 1975). Some recent examples of photoreceptors that are designed to operate with commercial laser diodes can result in rather complex physical geometries (for e.g. Ishiwata et al 1980, Kiyota et al 1980, Taniguchi 1981, Tateishi and Hoshino 1984, Kato 1985), one example of which is schematically shown in figure 3.10.

Fig.3.10

An example of a multi-layer photo-receptor. The thin a-Se layer between the CGL and CTL facilitates efficient hole injection from CGL to CTL. The a-Se layer between the CGL and Al. substrate acts as a blocking layer to holes that may be injected from the substrate.

(After Ishiwata et.al 1980)



3.2.2 Interfaces in Photoreceptors

The presence of physically discontinuous layers of different materials in the photoreceptor structure may lead to a gradual build-up of a space charge at the interfaces of the layers which may have adverse effects on the xerographic performance of the photoreceptor. The transport of the excess, photogenerated charge towards the metal substrate may be influenced by the non-uniformity of the electric field in the photoreceptor bulk. Incomplete photo-discharge of the deposited surface charges may also result in large values of the persistent surface charge or residual potential which is detrimental to obtaining a good contrast for the latent electrostatic image on the photoreceptor surface.

The use of transient photoconductivity techniques which yield reliable quantitative results for the evaluation of transport parameters in a homogenous, single-layer and non-dispersive material becomes more difficult when it is applied to highly dispersive (i.e. where the transport of mobile carriers cannot be characterised by a

single, well defined drift mobility) or multilayered structures. This is exemplified in figures 3.11(a) and 3.11(b). The transient current profile will deviate from the ideal quasi-rectangular pulse with a trailing edge (figure 3.11(a)) into a distorted profile which qualitatively evidences the presence of different layers with different effective mobilities for the excess photogenerated carriers (figure 3.11(b)). In the latter figure, the transport of the carriers through the individual layers can be observed. The narrow initial pulse is attributed to the transport in the high mobility top a-Se layer followed by a low amplitude signal due to the transport in the thin low mobility a-Se Te layer which is then finally followed by the transport in the bottom a-Se layer (Cheung et al 1982). Due to the absence of a well defined "break" in the current trace, the quantitative analysis of the transient data becomes more ambiguous.

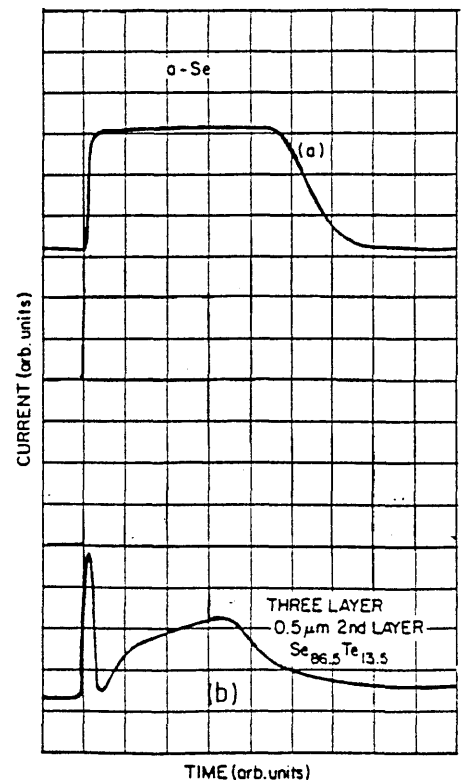
Fig. 3.11

Xerographic Time-of-Flight traces of several photoreceptor structures.

- a) Single layer pure a-Se film.
- b) Three-layer structure with a middle layer of $\text{Se}_{86.5}\text{Te}_{13.5}$, 0.5 μm thick.

The quantitative analysis of the current trace becomes more difficult due to the absence of well-defined breaks in the transient.

(After Cheung et.al. 1982)



For a well-behaved plot such as that shown in fig.3.11(a), the XTOF technique is also capable of revealing locations and densities of bulk space charge in the sample. Basically this involves the transformation of the current transient into a spatial dependence of the electric field and thereby, through Poisson's equation, the distribution of any trapped space charge. However, the success of this procedure would depend on the reliable determination of effective drift mobility of the photo-generated charges from the current transient data, a pre-requisite which would be difficult to satisfy when the experimentally observed current transients are complicated and exhibit undefineable transits. Some aspects of the determination of bulk space charge distribution from XTOF transits has been discussed by Berger et.al 1979 and Berger and Enck 1980.

3.2.3. TSD of Xerographic Photoreceptors

TSD studies of homogenous single layer films of a-Se has been carried out (Street and Yoffe 1972, Guillaud et.al.1977 and Hoshino and Miyata 1981) however to the best of the author's knowledge there has been no reported work on the application of the said technique to the multi-layer photoreceptors. It is believed that this absence can partly be attributed to the relatively recent development of the semiconductor-laser based printers that utilise these classes of photoreceptors (Shahbazian 1984).

The TSD of a photoreceptor belonging to the pigment-resin-dye type has revealed that trapping sites are present at the boundaries of the embedded pigment particles with the resin binder (Hoshino 1981). The TSD peak that was observed is thought to be due to the release of electronic carriers from states associated with the physical interfaces of the pigment/resin.

For the multi-layer photoreceptors, it is reasonable to assume that due to the heterogeneity in the sample structure, several polarisation effects could be observed when the sample is subjected to an electret formation cycle.

The discontinuities in the intrinsic conductivities and dielectric constants within the photoreceptor structure will lead to the accumulation of space charges at the interfaces of the individual layers whenever the system experiences an electrical stress for a period of time which is of the order of its effective dielectric relaxation time. Charge trapping by states associated with the physical heterogeneities of the structure will also cause an electrical polarisation in the sample.

A persistent internal polarisation caused by space charges will have a significant impact on the xerographic performance of the photoreceptor. The application of the TSD technique to the multi-layer photoreceptor structures will be particularly useful as it is capable of revealing the density as well as the kinetics of the space charge polarisation involved.

3.3 Experimental Objectives

The review of the work that has been carried out on PVB has allowed the objectives of this work to be defined more clearly. It is quite clear that from the works of Jain et.al. 1974, 1979 and Mehendru et.al. 1980 the origin of the high temperature peaks that were observed by them are far from clear. The aim of this work is to investigate the possibility of the occurrence of a high temperature peak ($T > T_g$) relaxation peak in the films of the PVB (Butvar B 79). As it is generally known that polar polymers generally exhibit significantly large ionic conductivities, a space charge polarisation due to the accumulation of the intrinsic ionic charge carriers is expected to be observed.

The use of corona charging as a means to polarise the PVB films also allows higher polarisation fields to be used without the frequent sample breakdowns that are usually encountered when metallised samples are polarised with relatively high values of the applied field. Corona charging also simulates the conditions where the polymer is polarised when it is being used as a binder resin in a xerographic photoreceptor.

Thermally stimulated surface potential decay or "Charge" TSD of the PVB films would also allow the observation of the decay processes without the need for a top electrode, thus also avoiding the rigours of the metallisation process. In particular, due to the non-zero average internal field, the decay of a space charge polarisation by the internal conduction of the polymer could then be observed.

For the heterogenous multi-layer photoreceptor structures, the use of the TSD technique would yield information on the effect the interfaces would have on the build-up of any space charge polarisation in the sample bulk. As was discussed in the previous sub-section (sect. 3.2.3), the identification of the possible polarisation mechanisms in these physical structures would undoubtedly be of use to the design of multi-layer photoreceptors in general.

CHAPTER 4

EXPERIMENTAL DETAILS AND PROCEDURES

Introduction

In this chapter the details of the sample preparation are first described. This is then followed by a description of the experimental set-ups that were used for experiments on surface potential decay (isothermal as well as thermally stimulated) and TSD current measurements. Other complementary materials characterisation experiments are also briefly mentioned.

Sample films that were investigated in this work were either prepared in the laboratory or, in the case of the a-Se based xerographic layers, were cut from photoreceptor drums that were manufactured by Gestetner (Byfleet) Ltd., Surrey, U.K.

As virgin samples were used for each experimental run, the total number of sample films fabricated numbered in the hundreds. Each experimental observation (per experimental variable) required several runs (about 5 being typical) to confirm its validity. It is therefore noted that the results that are presented in this thesis were culled from experimental observations that were considered to be representative of the particular behaviour investigated.

4.1 Sample Preparation

4.1.1 Polyvinyl butyral

Granules of PVB resin were obtained as a white, free flowing powder (Monsanto, Butvar B79). The method of preparation of the polymer films used was similar to the one described by Gil-Zambrano (1981). 10% by weight of PVB granules were dissolved in a solvent

having a volumetric ratio of 4:1 Toulene:Methyl Ethyl Ketone. Continuous stirring of the solution was maintained for about 5 hours at room temperature to ensure that a homogeneous polymer solution was obtained. The stirrer used was a Gallenkamp magnetic stirrer.

Ultrasonically cleaned microscopic glass slides measuring approximately 35 mm. long, 25 mm. wide and 0.8 mm. thick were used as the supporting substrate for the polymer films. Aluminium or silver were vacuum evaporated on the glass slides to act as the bottom electrode.

Metallisation of the glass substrates was carried out at pressures of 1×10^{-5} torr in a conventional water cooled diffusion pump and rotary pump vacuum unit to a thickness of $\sim 1000\text{\AA}$. A multi-stranded helical tungsten coil was used as the source heater for the evaporation of aluminium but for silver, a molybdenum coil was used instead, the reason being that the silver metal would not wet tungsten. A nomograph by Bond (1954) was used to determine the weight of evaporant metal needed and the corresponding evaporant to substrate distance to obtain the desired thickness of the electrodes. This method was found to be accurate as measurements of the thickness of the evaporated metal coatings with a Talysurf (Taylor-Hobson Talysurf model 4) showed.

The fabrication of the polymer film over the electroded glass slides was similar to the method described by Booth (1968). A rod coater unit as shown in figure 4.1(a) was used to form the films. Basically, the unit consisted of a stainless steel rod of diameter

6.3 mm. with 0.6 mm. diameter wire wound closely over it. This unit is supported over a smooth metal platform. The gap between this flat platform and the bottom edge of the wire wound rod could be selected by the means of two screws which raised or lowered the level of the platform with respect to the whole supporting structure. The fabrication of the PVB films is schematically shown in figure 4.1(b). The thickness of the films obtained could be chosen by varying both the number of droplets of polymer solution used for fabrication and the gap between metallised glass slide and bottom edge of the wire-wound rod. Films of thickness varying between 10 μm and 25 μm could easily be fabricated this way.

After fabrication, the samples were left in a vacuum oven for about 24 hours, at room temperature and pressure. This was to ensure that no sudden boiling off of the solvent could occur thus causing pin holes or voids in the polymer films. The occurrence of pin holes in the films would render them useless, since the subsequent metallisation of the top electrodes (for metallised sandwich structures) would cause a short circuit in the sample. After this period of 24 hours the oven was evacuated to 10^{-2} torr for about 5 hours to drive out any remaining solvent from the polymer film.

After the above treatments were completed, the samples were then ready for testing in open-circuit configuration, i.e. surface potential decay studies. However for the experiments in the short circuit mode, top electrode metallisation of the samples were subsequently done. A guard-ring configuration was used for the top electrode as shown in figure 4.2. The size of the inner top electrode used was 1.63 cm^2 with an outer guard-ring of internal diameter 1.55 cm

Fig.4.1(a) Rod Coater Unit

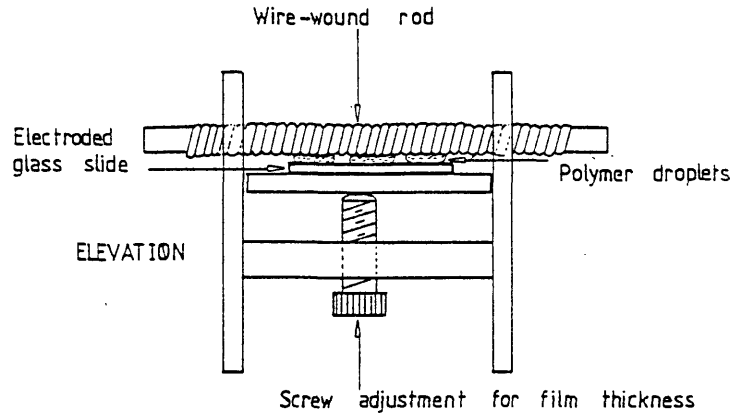


Fig.4.1(b) Fabrication of PVB film.

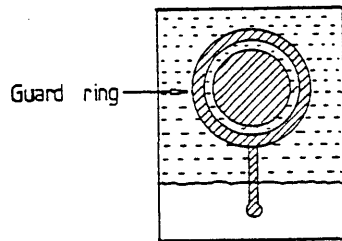
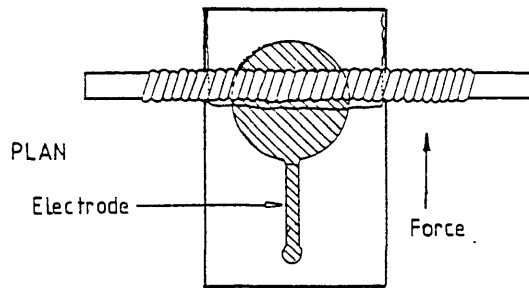


Fig.4.2 Sample Configuration

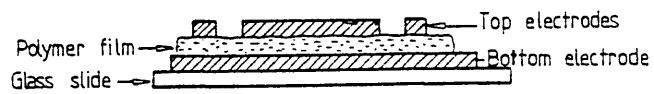
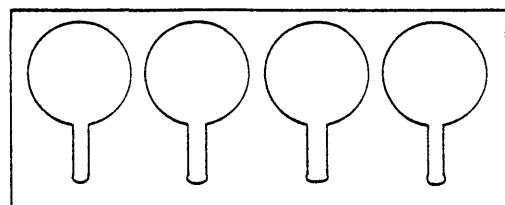


Fig.4.3 Masks for Electrode evaporation



and 0.38 cm wide. The masks used for the evaporation of the top metal electrodes were made of aluminium or perspex and had a configuration as shown in figure 4.3. Aluminium masks were employed when uncharged polymer films were to be evaporated upon while for samples that had been exposed to a corona discharge, perspex masks were used. This was to minimise the chances of the neutralisation of the surface charges on the films if there was an accidental contact during the evaporation process.

During the evaporation of the top electrode, care had to be taken such that the sample temperature did not exceed 60°C, the glass transition temperature of the PVB polymer films, as this may possibly cause changes in the surface morphology of the sample. The source to substrate distance used for the top electrode metallisation was approximately 20 cm. Initial calibration experiments has shown that this distance was sufficient in maintaining the above mentioned condition.

4.1.2 a-Se based Multi - Layer Photoreceptor

The samples of photoreceptors were obtained from Gestetner (Byfleet) Ltd, Surrey. Homogenous a-Se based single layer and heterogenous multilayer photoreceptors were available.

The photoreceptors were prepared by vacuum evaporation of 99.999% pure selenium or pre-alloyed mixtures of doped or alloyed selenium pellets. The substrates used are normally aluminium open-ended cylindrical drums of 11.5 cm. internal diameter and 29.5 cm.

length, a typical configuration that is employed in a commercial xerographic machine. Overall photoreceptor thickness of approximately 50 to 60 μm are normally evaporated onto these drums.

For our experimental measurements, samples approximately 2.5 cm square were first cut from the photoreceptors drums, discarding those originating from the drum edges as these were known to yield non-uniform thicknesses and in the case of layered photoreceptors, exhibiting undefinable material interfaces. During the cutting of the samples, care was taken such that there was no excessive overheating of the samples as this may cause a re-crystallisation of the essentially amorphous photoreceptors films.

The samples were subsequently evaporated with $\sim 1000 \text{ \AA}$ thick aluminium top electrodes with a guard-ring configuration. Again, care was taken such that during evaporation, the surface of the photoreceptor films did not exceed its glass transition temperature ($\sim 50^\circ\text{C}$) in order to avoid the possible occurrence of structural changes in the films.

After metallisation of the top electrodes, the samples were mounted on to glass slides by using silver dag (figure 4.4), the whole structure then being placed in the cryostat for TSD current measurements. All measurements were carried out at pressures of $\sim 1 \times 10^{-5}$ torr and in the dark. Samples are normally dark rested in the cryostat for periods up to 12 hours before measurements were commenced.

4.1.2.1 Te Profile

For the heterogenous a-Se-Te/Se photoreceptor structures, the Te impurity profile, expressed as percentage by weight was determined by the Scanning Auger Microprobe technique at the Wolfson Institute, University of Nottingham.

As can be seen in figure 4.5, the heterogenous structure of the films is in evidence. At about 8.6 μm below the top surface, the T_e concentration is largest (~ 20 wt. %) after which it gradually decreases to about 5 wt. % at 35.4 μm below the surface. The total thickness of the heterogenous structure is 56 μm . The interface between the a-Se and a-SeTe layers is therefore seen to be abrupt at about 8.6 μm below the top surface while the interface at 35.5 μm is more gradual, this is believed to be due to fractionation effects after the sample evaporation.

As a xerographic photoreceptor, the top few microns of a-Se would perform the functions of surface protection as well as charge retention due to its superior physical strength and higher electrical resistivity. The a-SeTe layer (between 8.6 μm and 35.4 μm) would act as the CGL while the bottom a-Se would be the CTL. Due to relatively thick a-SeTe layer, one could anticipate that this particular photoreceptor structure would have a significant rate of dark decay which could lead to problems with latent image stability. Unfortunately, no data on xerographic measurements were available to confirm this.

Fig.4.4
Sample configuration
for a-SeTe/a-Se
photoreceptor.

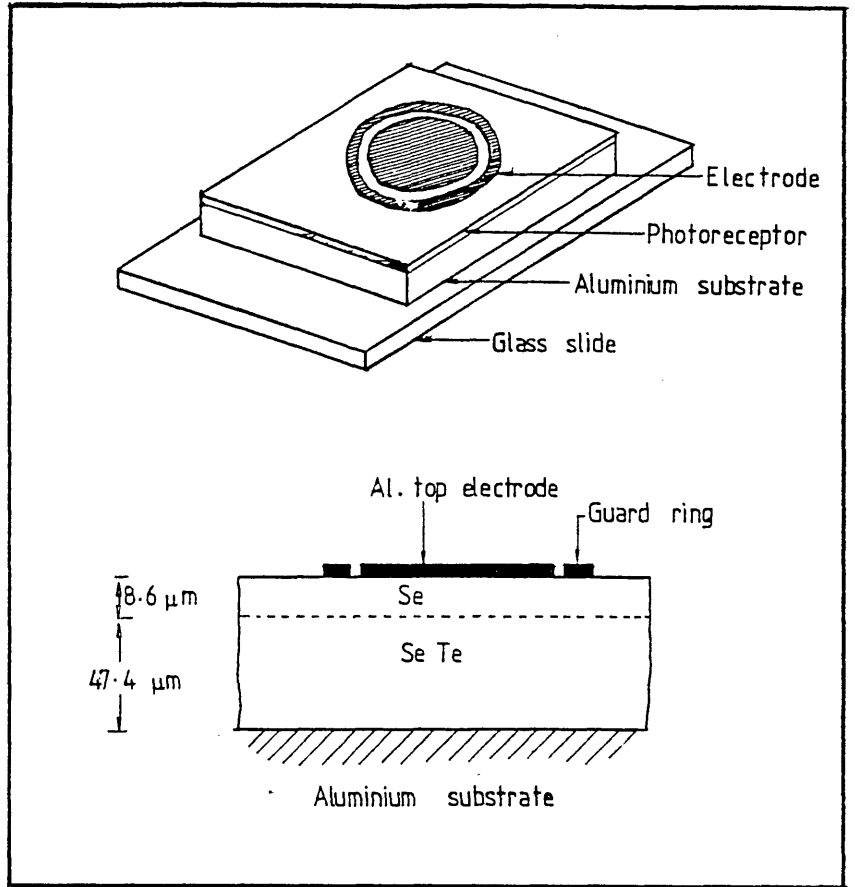
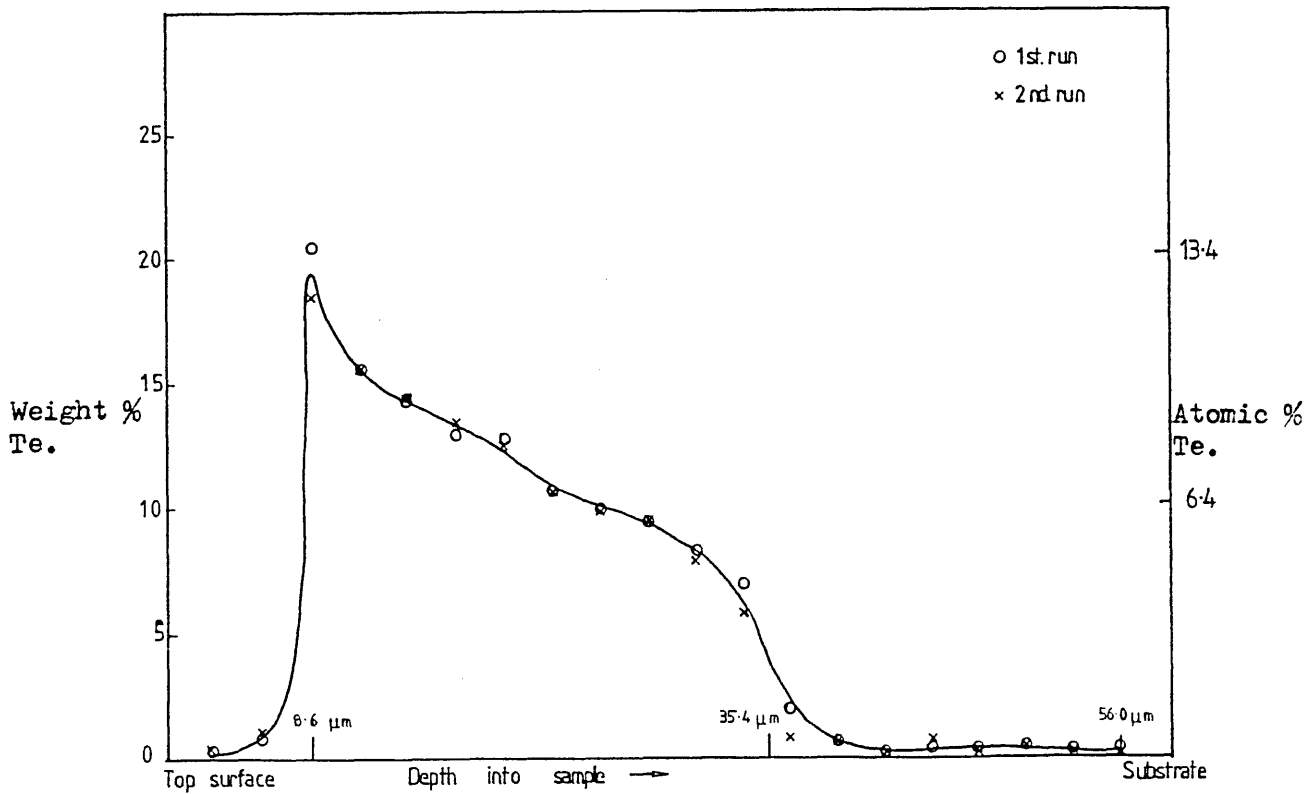


Fig.4.5 Concentration Profile of Tellurium
in a-SeTe/a-Se double-layer photoreceptor.



4.2 Experimental Set-up and Procedure

4.2.1 Surface Potential and "Charge" TSD Measurements

Isothermal as well as thermally stimulated surface potential decay measurements were carried out on the PVB films. The surface of the polymer films were charged either positively or negatively to surface voltages ranging from ± 25 volts to ± 1000 volts by using a DC corona discharge. The value of the initial surface voltage was controlled by a DC bias voltage V_g applied to a wire mesh grid situated between the corona wires and the sample. Charging times of 1 minute duration were normally carried out with the sample substrate temperature varied between 5°C and 100°C .

The measurement of the surface potential was carried out with an electrostatic voltmeter held about 2 mm above the charged polymer film. In isothermal measurements, the sample temperature was held constant and the surface potential decay was monitored with respect to time. In charge TSD measurements, the decay of the surface potential was accelerated by imposing a linear temperature programme on the sample. Values of the linear temperature programme employed ranged from 1°C min^{-1} to 6°C min^{-1} . A schematic representation of the experimental set-up used for the experiments on the non-metallised sample structures is shown in figure 4.6.

4.2.1.1 Corona Charging Unit

The corona charging unit is shown in detail in figure 4.7. A twin corona wire configuration was found to be suitable and was found to

Figure 4.6 Experimental set-up for Surface Potential measurement.

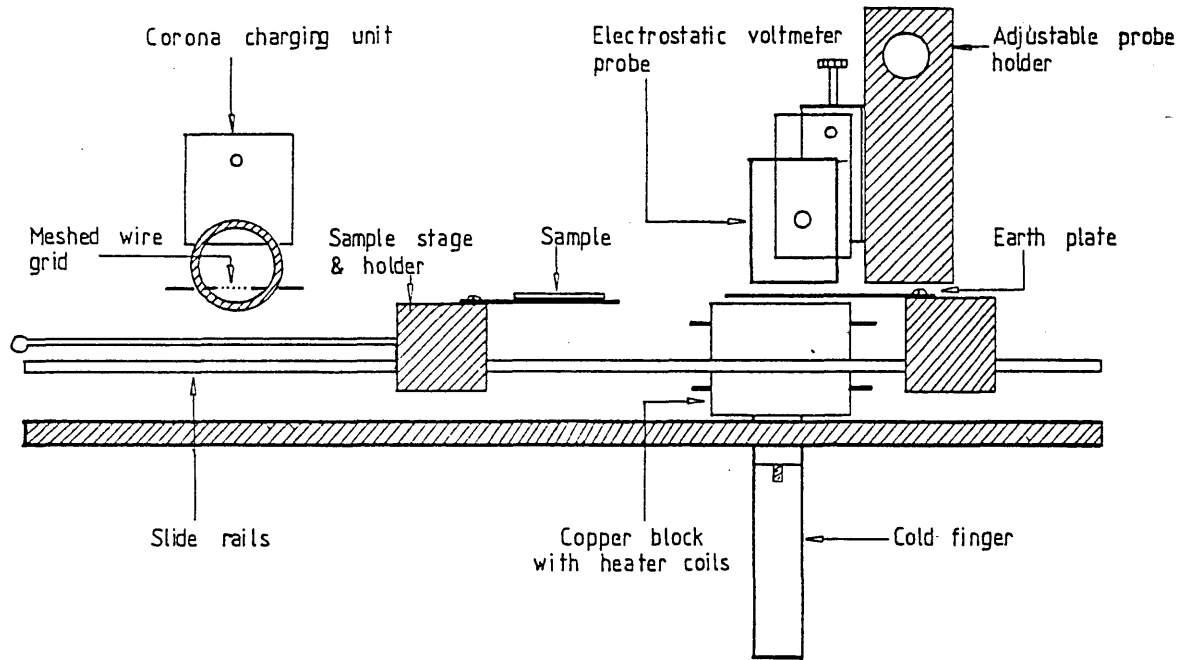
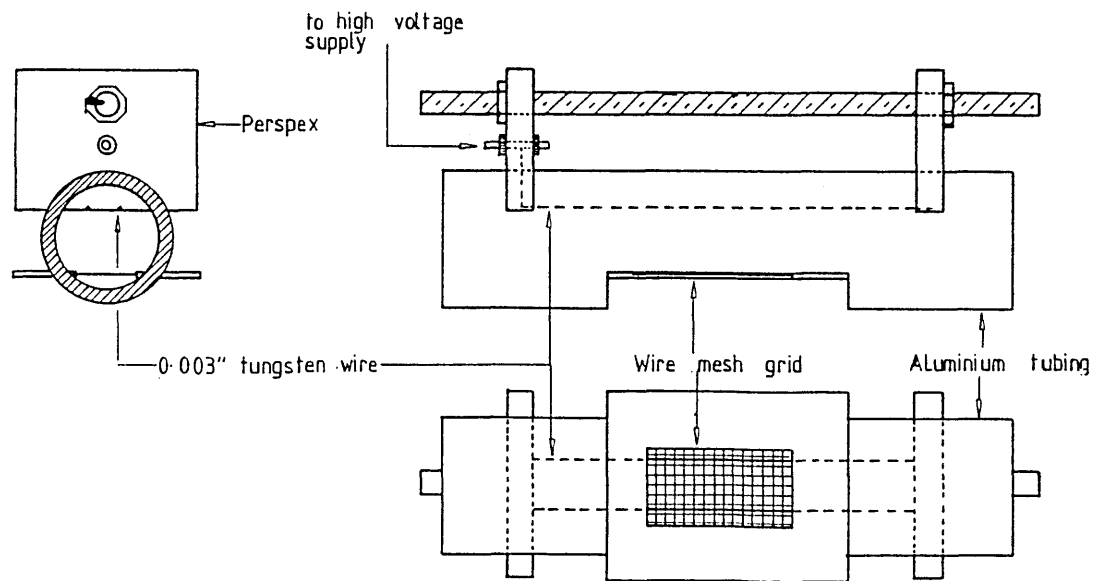


Figure 4.7 Details of Corona Charging Unit.



give a fairly uniform surface charge distribution on the polymer surface. The corona wire used was 0.003" diameter tungsten wire spaced 1.0 cm apart between two^{end-}pieces of perspex and held under tension by a threaded steel rod.

The earthing shroud was constructed out of a large aluminium tubing measuring 18.0 cm long and 2.5 cm external diameter. The bottom part of the tubing was sectioned out to accommodate the grid mounting. The grid was made out of a piece of nickel wire mesh having a spacing of 0.25 mm square which was held between two pieces of perspex 0.95 mm thick. The whole structure was then permanently glued to the bottom section of the aluminium tubing earth shroud. By fixing the grid structure this way, the corona wire to grid distance could be maintained constant and this distance was fixed to be 1.0 cm. The whole corona unit was then mounted on an aluminium base plate by two steel studs which rendered the unit adjustable for height with respect to the base.

The high voltage power supply for the negative corona charging was an ITT 484LFE927A coupled to an Advance Industrial Electronics PP-32A acting as the primary energising unit. For positive coronas, the high voltage was provided by a Brandenburg 532A power supply. The biasing voltage to the wire mesh grid was applied through a 10k resistor by a Fluke model 412B.

4.2.1.2 Electrostatic Voltmeter and Measuring Probe

The decay of the surface potential was detected by a Monroe

Electronics Electrostatic Voltmeter model 144S1E coupled to a detecting probe head model 1009B. The probe head was suspended by a mounting which was adjustable in both the horizontal and vertical planes which allowed the surface of the sample under study to be scanned. The distance between the sensitive aperture of the probe and the top surface of the polymer film was kept constant throughout the course of the experiment. This distance was of the order of 2.0 mm.

The electrostatic voltmeter set-up has a speed of response of 7.5 ms/kV, however this was not crucial considering the relatively slow decay of the surface potential of the polymer films investigated. The output of the electrostatic voltmeter was connected to a recorder (Bryans Instruments Ltd, model 2700).

The measurement of the surface potential which was performed by the Monroe electrostatic voltmeter follows the principles of the vibrating electrode method (Vosteen 1974). Here the voltage induced on the vibrating electrode by the field which arise from the effective surface charges on the dielectric is continuously compensated by a backing voltage with the result that the magnitude of this backing voltage equals the surface potential of the sample under study (Legros and Lewiner 1973, Dreyfus and Lewiner 1974). Effectively, the field between the charged surface and the measuring probe will be zero throughout the surface potential measurement.

4.2.1.3 Heating System and Temperature Control

The temperature of the sample under test was controlled by coupling the sample holder to a heat source/heat sink. The sample holder consisted of a piece of copper plate 4.0 cm. long, 4,9 cm. wide

and 0.22 cm thick which was attached to a system of sliding rails which allowed it to be moved from the charging station to the measuring station, 9.5 cm. apart. To perform the measurement of the surface potential after charging, the sample holder was manually pushed along the rails to come to rest directly beneath the measuring probe. The elapsed time between charging and measurement was of the order of 1 second, however this was not considered crucial as the decay times of the detected surface voltage was much longer (\sim several minutes). During charging and measurement, the bottom electrode of the sample remained grounded at all times.

The heat source/heat sink was made out of a rectangular block of copper measuring 4.0 cm long, 5.0 cm. wide and 3.3 cm. high with a cylindrical copper rod of 1.80 cm diameter and 4.5 cm. long hard soldered to its base. The controlled heating of the copper block was achieved by passing a pulsed current driven by a programmable temperature controller (Stanton Redcroft Temperature controller model 681) via a Phillips co-axial heater wire. A platinum resistor temperature detector was utilised as a temperature sensor which provided the necessary feedback signal for the temperature controller.

A screwed-on extension cylindrical copper rod was utilised to facilitate fast cooling of the copper block. This was achieved by immersing the copper rod into a dewar of liquid nitrogen. With this arrangement, the temperature of the copper block and hence the sample, could be held constant between -2°C and -200°C or, when it was needed, it could be increased at linear rates ranging from $1^{\circ}\text{C min}^{-1}$ to $6^{\circ}\text{C min}^{-1}$. Good thermal contacts between sample to sample holder, sample

holder to heat source/heat sink were achieved by using a thermal joint compound (Thermacote, Thermalloy Company Texas).

The actual temperature of the polymer film was deduced from a calibration curve as there was a temperature difference between the top surface of the polymer film and the bulk of the heat source/heat sink. This calibration curve is shown in figure 4.8.

4.2.2 TSD Current Measurements

Thermally Stimulated Discharge Current measurements were carried out on both PVB films as well as photoreceptor films. All measurements were carried out in the dark at pressures of $\sim 1 \times 10^{-5}$ torr.

A schematic lay-out of the measurement system is shown in figure 4.9. The basic equipment consisted of a cryostat where the sample and associated heating and cooling arrangements were housed, a sensitive current detector, a temperature controller and the associated power supplies for polarisation of the films.

4.2.2.1 The Cryostat, Sample Holder and Vacuum System

All measurements were carried out in a cryostat as shown in figure 4.10 which was evacuated to a pressure of about 1×10^{-5} torr.

Fig.4.8 Temperature Calibration plot for the PVB films during Surface Potential measurements. Actual temperature of sample is deduced from the solid line.

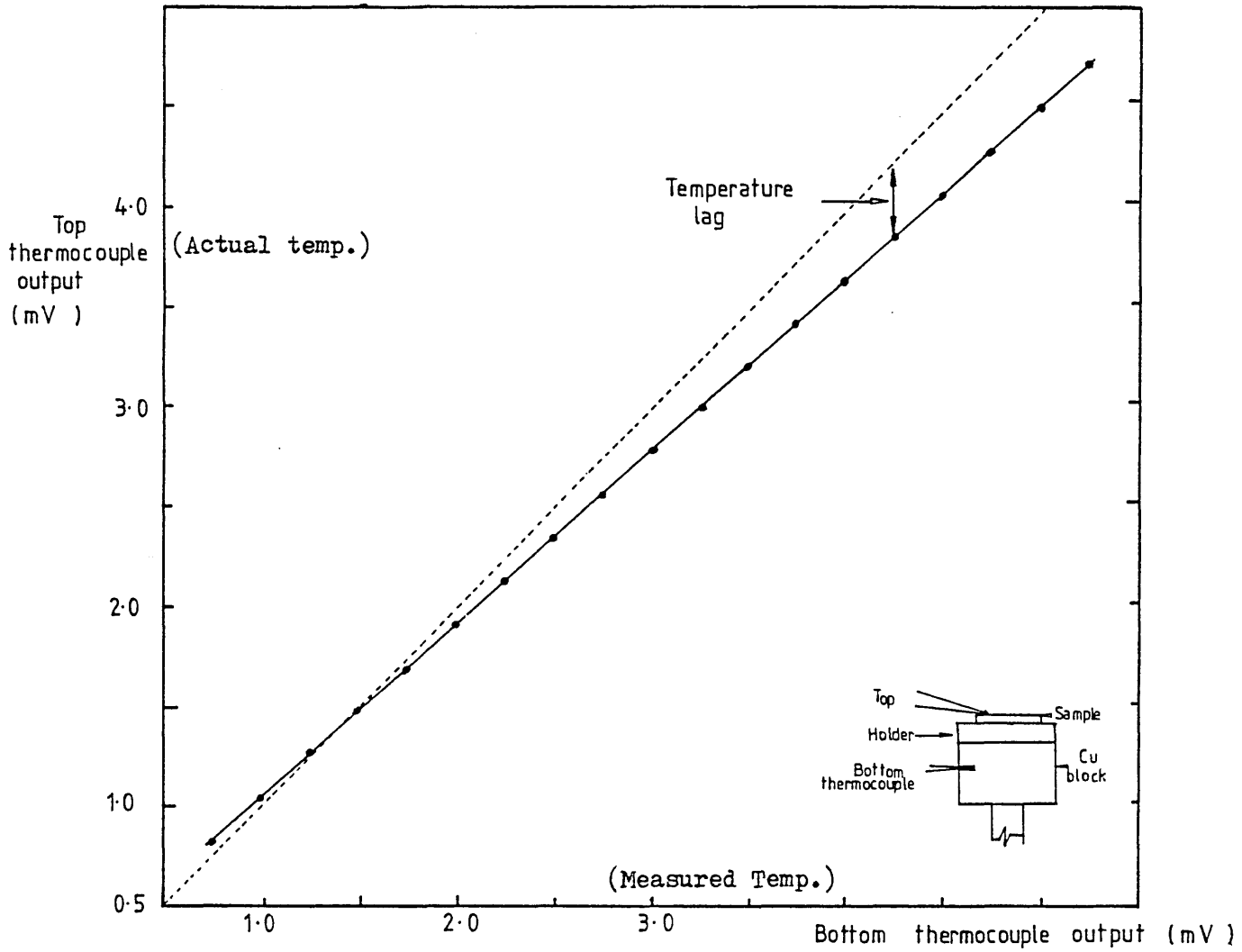
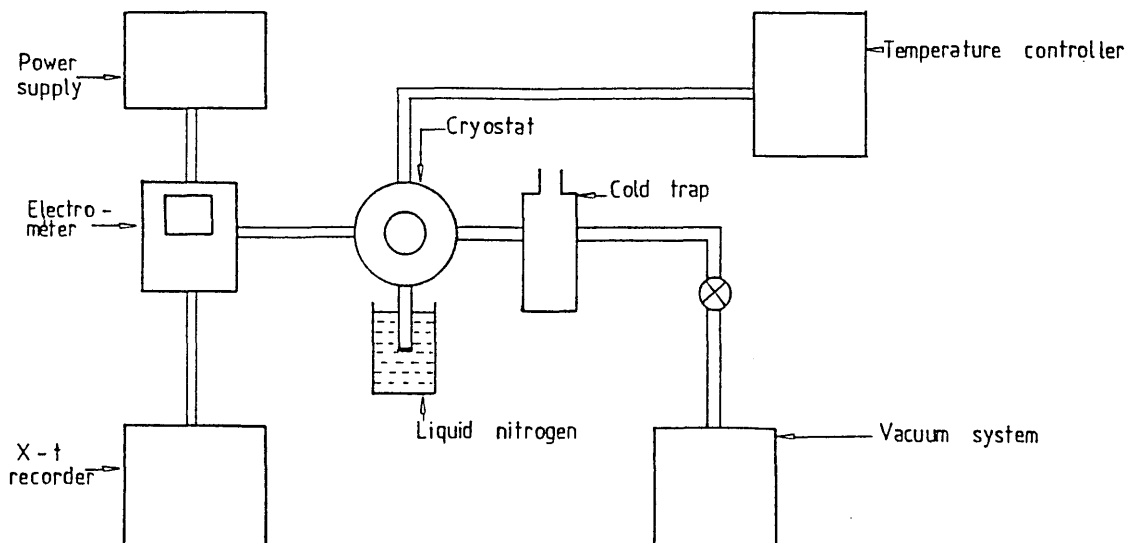


Figure 4.9 Schematic lay-out of TSD apparatus.



The cryostat was constructed out of aluminium (Dural) and has an internal diameter of 15.0 cm. A stainless steel sheath of thickness 2.0 mm. was screwed down to the bottom section of the cryostat through which a copper rod of external diameter 1.9 cm. was silver soldered at its end to form a vacuum seal. The copper rod acted as the cold finger of the heat source/sink. At the top end of the copper rod a rectangular copper block measuring 3.8 cm. x 3.0 cm. x 2.2 cm. was attached and this acted as the sample holder. The samples were mounted on to the sample holder by using thermal joint compound (Thermacote, Thermalloy Company Texas). External electrical connections were made by using thin strands of copper wire attached to the fabricated electrodes of the sample by Aquadag (Acheson Colloids Company, Plymouth).

The cryostat was evacuated by the conventional system of oil diffusion and rotary pumps. A liquid nitrogen cold trap was also incorporated into the vacuum system to facilitate a fast pump down of the cryostat. With this arrangement the cryostat could be evacuated to $\sim 10^{-5}$ torr in about 10 minutes.

4.2.2.2 Temperature Control

A length of heater wire (Phillips thermocoax, nichrome) was coiled through holes that were pre-drilled into the copper block via which controlled pulses of current were passed through to act as the heat source. Temperature control was achieved by using a Stanton Redcroft temperature controller (model 681). The necessary feedback temperature measured was supplied to the temperature controller by a

platinum resistance temperature detector embedded in the copper block. Linear temperature heating rates ranging from $1^{\circ}\text{C min}^{-1}$ to $6^{\circ}\text{C min}^{-1}$ could easily be obtained this way.

For fast cooling of the sample, the cold finger of the heat source/heat sink was dipped into a dewar of liquid nitrogen enabling cooling rates of up to $20^{\circ}\text{C min}^{-1}$ to be achieved. By using this set-up, the temperature of the sample holder could be varied, with full control, between -180°C to $+200^{\circ}\text{C}$. External temperature measurements were made by utilising chromel-alumel thermocouples placed in the vicinity of the sample.

4.2.2.3 Current Detection and Recording

The detector used for current measurements was a Keithley 610C electrometer capable of detecting currents which may range from 10^{-14} to 0.3 amperes (Keithley, 1972). The simplified electrical circuit diagram is shown in figure 4.11. A protection resistor R_p of value $22\text{ k}\Omega$ was connected in series in the charging branch of the circuit. The polarising DC field was applied by using a regulated voltage supply (Fluke model 412B).

Usually currents in the range of 10^{-12} to 10^{-8} amperes may emanate after thermal stimulation of the polarised, short circuited samples. No pertinent noise problems were encountered by using short, low-noise coaxial signal cables. The thermally stimulated currents were then recorded by a Bryans x-t recorder (model 2700).

Fig.4.10
Details of
the Cryostat

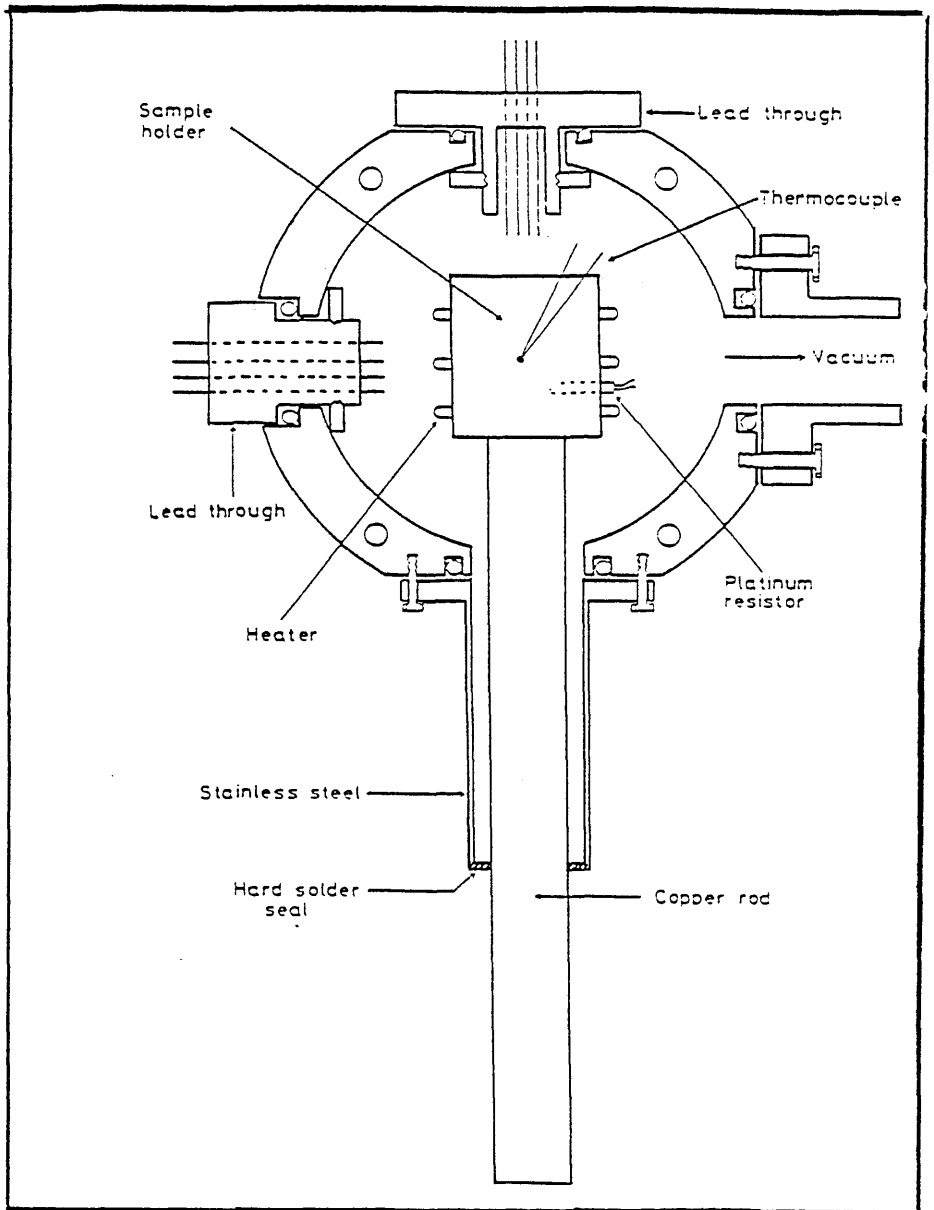
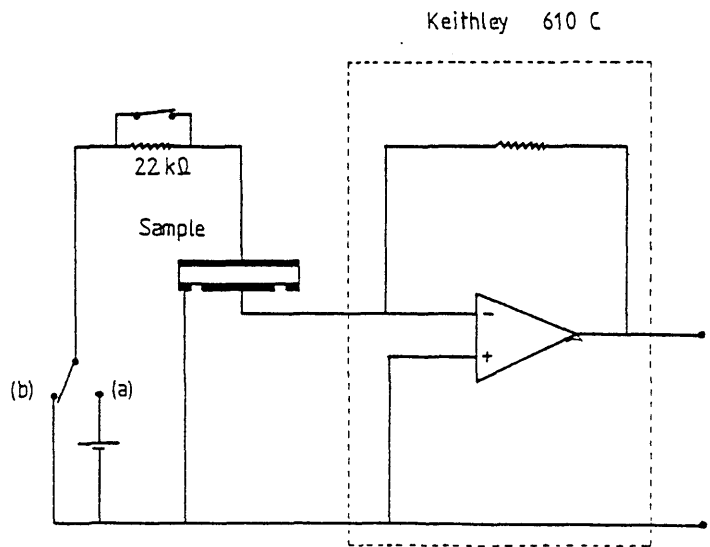


Figure 4.11 Simplified measuring circuit
for current measurement.



- (a) Charging
- (b) Discharging

4.3 Materials Characterisation

Several other experiments were carried out on the samples, viz Differential Thermal Analysis and Infra-red spectrophotometry. These supplementary experiments were carried out in order to characterise the composition as well as the glass transition temperature of the sample.

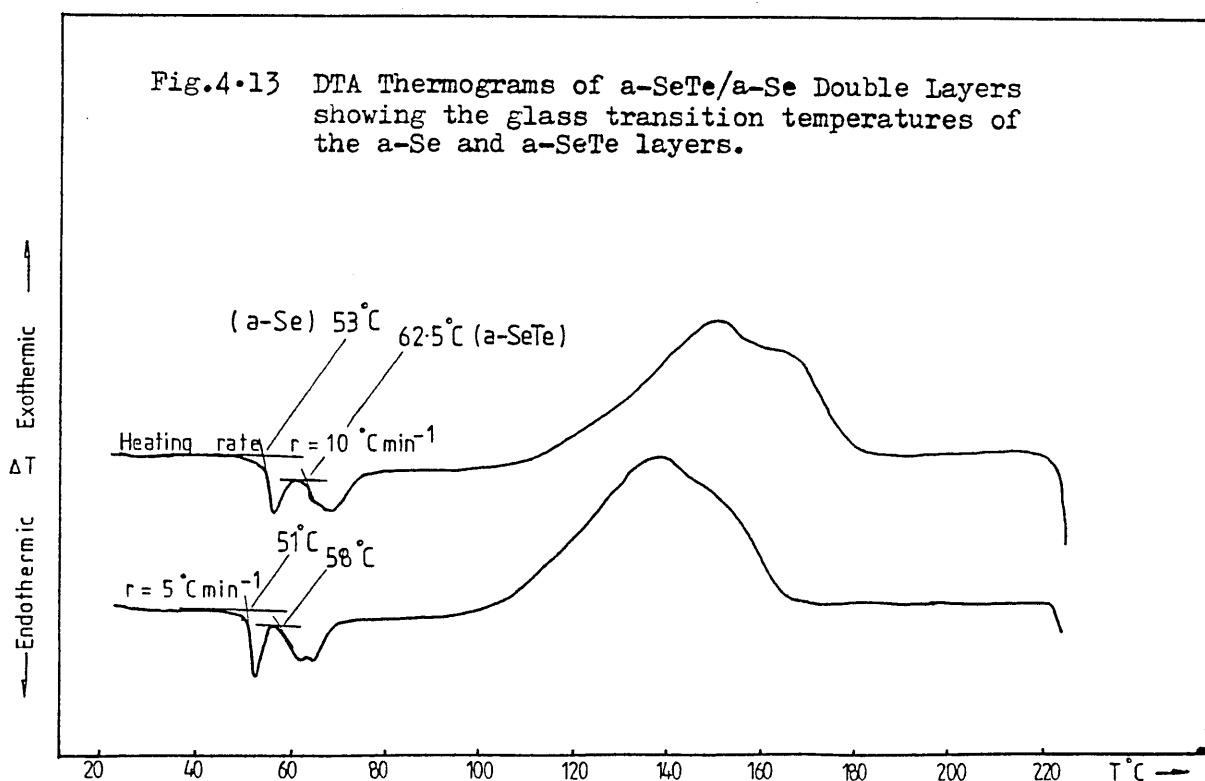
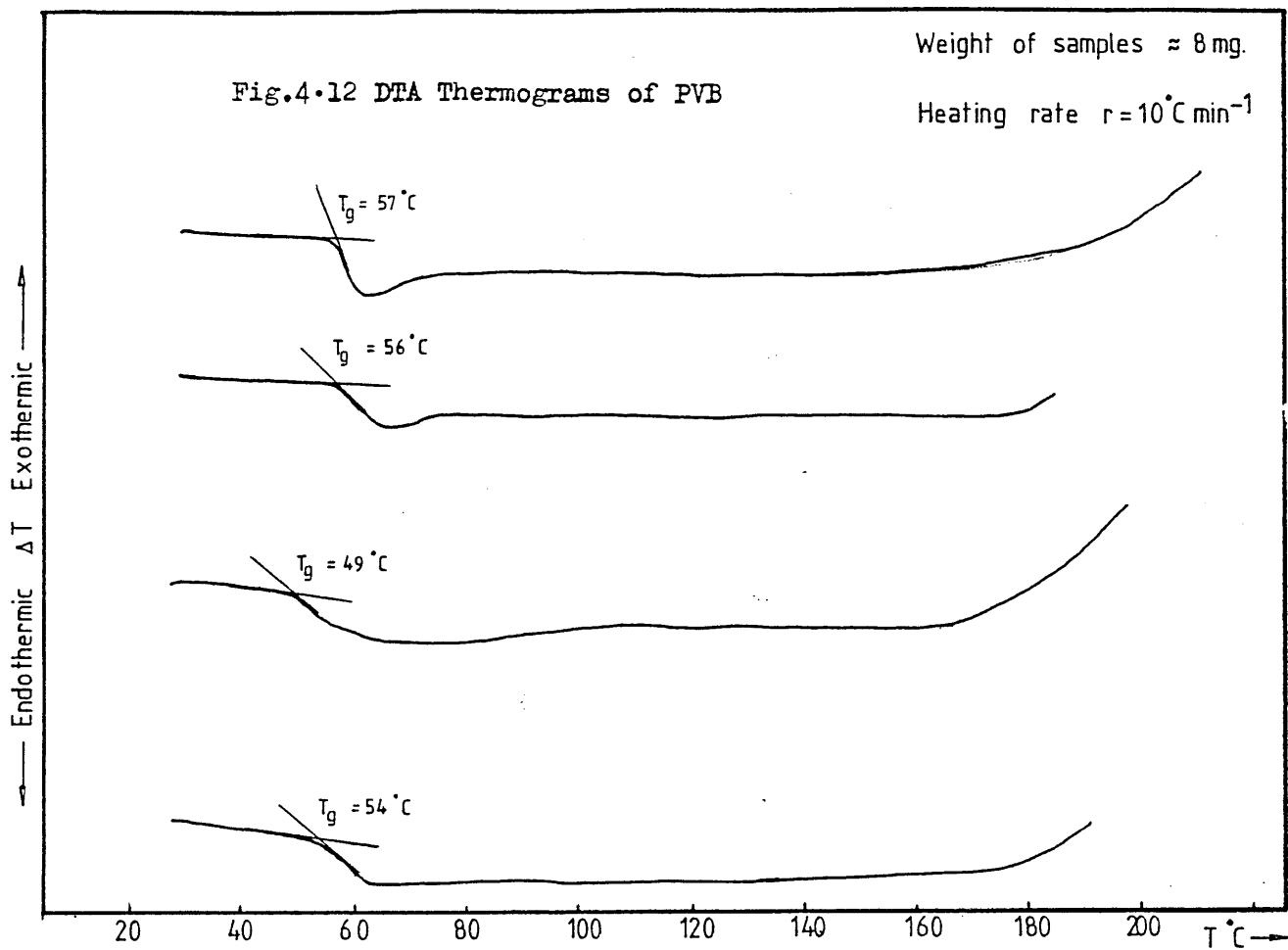
4.3.1 Differential Thermal Analysis

The thermal transitions of the PVB polymer and the a-SeTe/a-Se photo-receptor films were observed by using a DuPont 900 differential thermal analyser. Sample mass of about 10 mg were normally used, with an empty aluminium pan acting as the reference material.

For PVB, the samples were prepared from the polymer solution, which was then left to dry at room temperature and pressure for about 24 hours. The samples were then placed in a vacuum of $\sim 1 \times 10^{-2}$ torr to drive off any remaining solvent. For a-SeTe/Se samples, flakes of the film were first peeled from the photoreceptor drums by using pliers before being placed into the aluminium pans.

The DTA thermograms of PVB and a-SeTe/Se films are shown in fig. 4.12 and fig 4.13 respectively. For PVB, the approximate values of T_g as evidenced from the DTA thermograms carried out at a heating rate of $10^\circ\text{C min}^{-1}$ were found to vary between 57°C to 49°C . These values agreed very well with those quoted by the manufacturer (table 3.1 of chap.3)

The thermograms for the a-SeTe/Se multilayers showed 2 glass transition temperatures T_g and T_g' which we believed were due to the structural relaxations in the bulk a-Se and bulk a-SeTe respectively.



It is a known fact that the effect of alloying Se glasses with Te is to displace its glass transition temperature to a higher value. This was believed to be due to the inhibiting effect of the heavier and physically larger Te atoms on the structural relaxations of the glass towards equilibrium. The effect of Te alloying on the glass transition temperature and crystallisation kinetics of xerographically important Se glasses has been studied by several authors (Leder L 1982, Kasap et al 1984). It could also be seen that T_g and T'_g exhibited a shift with heating rates.

4.3.2 Infra-Red Spectrophotometry

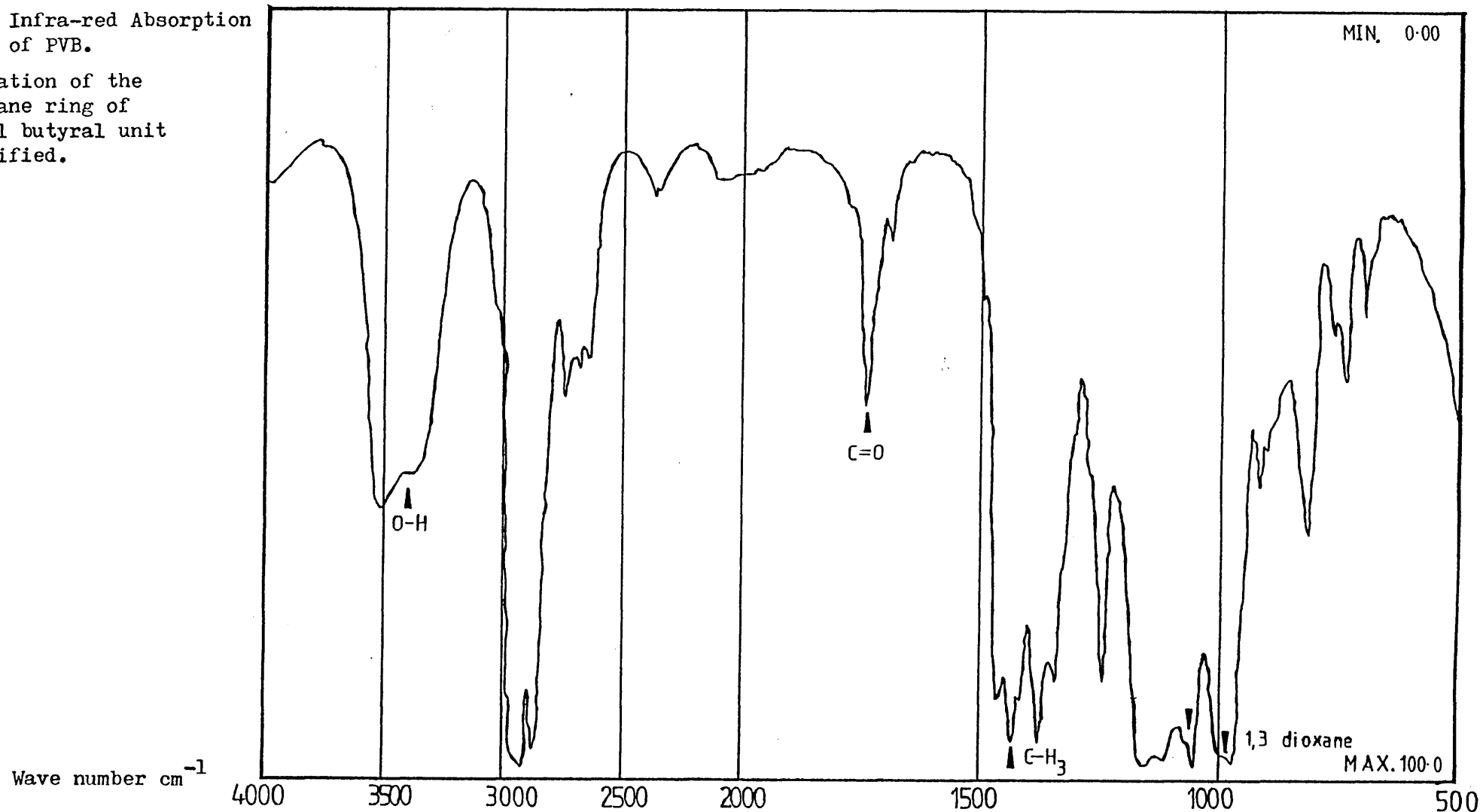
The spectrophotometer used in this work was a Perkin Elmer 580 B. Films of PVB about 20 μm thick were rod coated onto aluminium glass slides which acted as the reflective element in the set-up.

Before the measurements were carried out, it was ensured that a complete solvent removal from the films was achieved. The infra-red absorption spectrum of the films is shown in figure 4.14. Comparison with the "standard" spectra from Hummel and Scholl 1971 (spectra 1015 and 1017) reveal that small amounts of vinyl alcohol and vinyl acetate structures were present in our films. The presence of these groups were identified by absorption bands at 2.9 μm (3448.3 cm^{-1}) due to O-H stretchings in vinyl alcohol, 5.75 μm (17391.1 cm^{-1}) due to C = O stretchings in vinyl acetate and also at 7.28 μm (1373.6 cm^{-1}) due to bendings of the C-H₃ bonds in vinyl acetate.

The presence of very strong absorption band complexes at 8.9 μm (1123.6 cm^{-1}) and 10.1 μm (990.1 cm^{-1}) confirmed that the films investigated were dominated by vinyl butyral units.

Fig.4.14 Infra-red Absorption
of PVB.

The vibration of the
1,3-dioxane ring of
the vinyl butyral unit
is identified.



CHAPTER 5

RESULTS AND DISCUSSIONS

5.1 Introduction

The previous chapters have briefly described the sample preparation and the experimental procedures. This chapter is divided into two main sections, each discussing the results of the different material systems investigated. In the next section results on the films of PVB will be presented followed by the results of the work carried out on a two-layer a-Se based xerographic photoreceptor.

5.2 Poly vinylbutyral

Thermally stimulated discharge current measurements were carried out on sample films that had been previously polarised with a static electric field as well as those that had been polarised with a DC corona discharge. Isothermal as well as thermally stimulated surface potential measurements of unmetallised corona charged films were also carried out. The results of these experiments will be discussed under the appropriate sub-sections below.

5.2.1 TSD of DC charged PVB films

5.2.1.1 Preliminary

In this sub-section the short-circuit TSD current measurements carried out on aluminium electroded PVB films of about 20 μm thick are discussed. All measurements were carried out on virgin samples at

pressures of about 1×10^{-5} torr and in the dark. The sample films were first short-circuited and heated up to the desired polarisation temperature T_p and held there for about 1 minute before being polarised by a static field E_p for a period t_p . The samples were then subsequently cooled down to a temperature T_d ($\sim -20^\circ\text{C}$) at a fast rate of about $-20^\circ\text{C min}^{-1}$. The field E_p was then switched off and the samples short-circuited. After a further period ($t_d - t_s$) of about 1 minute the temperature of the sample was raised at a rate $r = 4^\circ\text{C min}^{-1}$ to about 120°C . Heating beyond this temperature was not carried out as the samples tended to deteriorate physically and yielded unreliable results.

5.2.1.2 Results

The TSD current thermograms of samples that had been polarised at $T_p = 70^\circ\text{C}$ for a period of $t_p = 10$ minutes with both positive and negative applied voltages, V_p , are shown in figures 5.1(a) and 5.1(b) respectively. Two TSD relaxation current peaks are clearly discernible, centred around 60°C and 78°C . These peaks are designated as the α -peak and ρ -peak respectively. We believe the mechanisms responsible for the occurrence of these peaks are markedly different and as such the discussions of the results will be carried out separately for reasons of brevity. Only the results of samples with evaporated aluminium electrodes are discussed in this thesis as no significant differences were detected when evaporated silver electrodes were used.

5.2.1.3 The α -peak

The TSD current spectra of the PVB films which had been polarised with the different applied voltages all exhibit a prominent

α -peak centred around 60°C. Reproducibility of this peak is found to be good. The temperatures at which the TSD currents are maximum, T_m , are found to be independent of the magnitude and the polarity of the polarising voltage. The magnitude of the peak current, I_m , exhibits a linear dependence on the magnitude of the polarising voltage. This is plotted in figure 5.2.

The area under the α -peak (taken between $T = 0^\circ\text{C}$ to $T = +70^\circ\text{C}$) which yielded the amount of charge released during the relaxation also exhibit a linear dependence on the magnitude of the applied field as shown in fig.5.3. Similar results are obtained for both positively and negatively charged samples.

The initial rising portion of the α -peaks in the thermograms of figures 5.4(a) and 5.4(b) were used to estimate the apparent activation energy of the relaxation process. The plots of $\ln I(T)$ vs $\frac{1}{T}(\times 10^{-3})\text{K}^{-1}$ are linear, allowing the activation energy to be calculated. From these plots (figure 5.5) the average activation energy is found to be 0.65 eV. The plot of the relaxation frequencies, $\tau(T)^{-1}$, obtained by a graphical integration of the TSD current peaks, vs $\frac{1}{T}(\times 10^{-3})\text{K}^{-1}$ (BFG plot, sect.2.7.2.2) are also reasonably linear (figure 5.6). The slope of this plot defines an activation energy and this is found to be of the order of 1.00 eV. From the plot of figure 5.6, it could also be seen that the relaxation frequencies of the α -peak lie in the region of 10^{-4} to 10^{-3} Hz.

From the TSD current thermograms (figs.5.1(a,b) and 5.4(a,b)) it could be seen that the α -peaks exhibit a characteristic asymmetric shape. Chen (1976) has suggested that this particularity in the shape of the TSD thermogram is a good indication of relaxation processes obeying

first order kinetics (see also chap.2,sect.2.4.1). Assuming that the observed thermograms followed a first order process also allows the calculation of the activation energy by the method which was recently proposed by Christodoulides (1985 a). This method is based on using the values of the temperatures at the corresponding 1/4, 1/2 and 3/4 heights of the current maximum of the thermogram. Table 5.1 summarises the equations that were used and the calculated values of the activation energy. The average value of the activation energy is found to be 1.70 eV.

4.2.1.4 Origin of the α -peak

The appearance of the α -peak at a similar temperature range to that of the glass transition (as determined by Differential Thermal Analysis, fig.4.12, chap.4) suggests that the relaxation is closely related to structural re-arrangements and micro-Brownian movements in the polymer bulk.

The linear dependences of the current maxima, I_m and the total charge collected, Q_α on the applied voltage V_p (figs.5.2 and 5.3) is a strong indication of a dipole depolarisation mechanism. This view is also supported by the experimental observation that the general characteristics of the current peaks (position and shape) are independent of the polarity of the forming electrode. For a TSD current peak which is due to a space charge drift or diffusion, the amount of charge released during the thermally stimulated relaxation will not be a linear function of the magnitude of the applied field as was discussed in section 2.4.3.2. For a space charge drift, the positions of the current maxima would also be expected to exhibit a shift towards lower temperatures for higher applied fields. These experimental characteristics were not observed thus consolidating the view that a mechanism involving dipolar disorientation is the dominant process responsible for the TSD current peaks observed.

The presence of molecular groups bearing permanent dipole

Fig.5.1(a)

TSD current thermograms of DC charged films of PVB, 20 μm thick.

$T_p = 70^\circ\text{C}$, $r = 4^\circ\text{C min}^{-1}$; $t_p = 10$ mins.

The values of the polarisation voltages are shown in the inset.

Two current peaks are observed. The α -peaks are observed at 60 C while the ρ -peaks are centred at about 78 $^\circ\text{C}$.

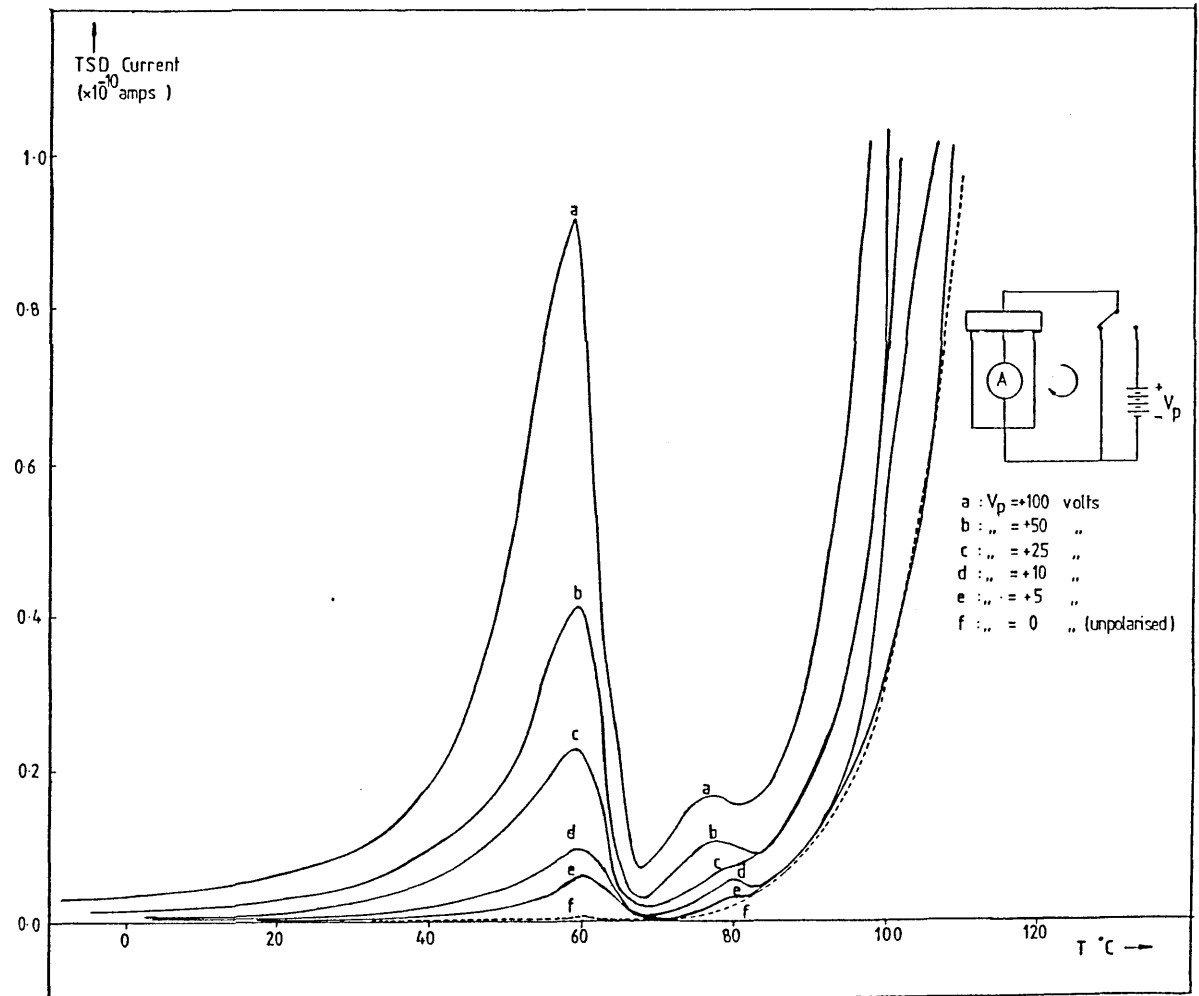


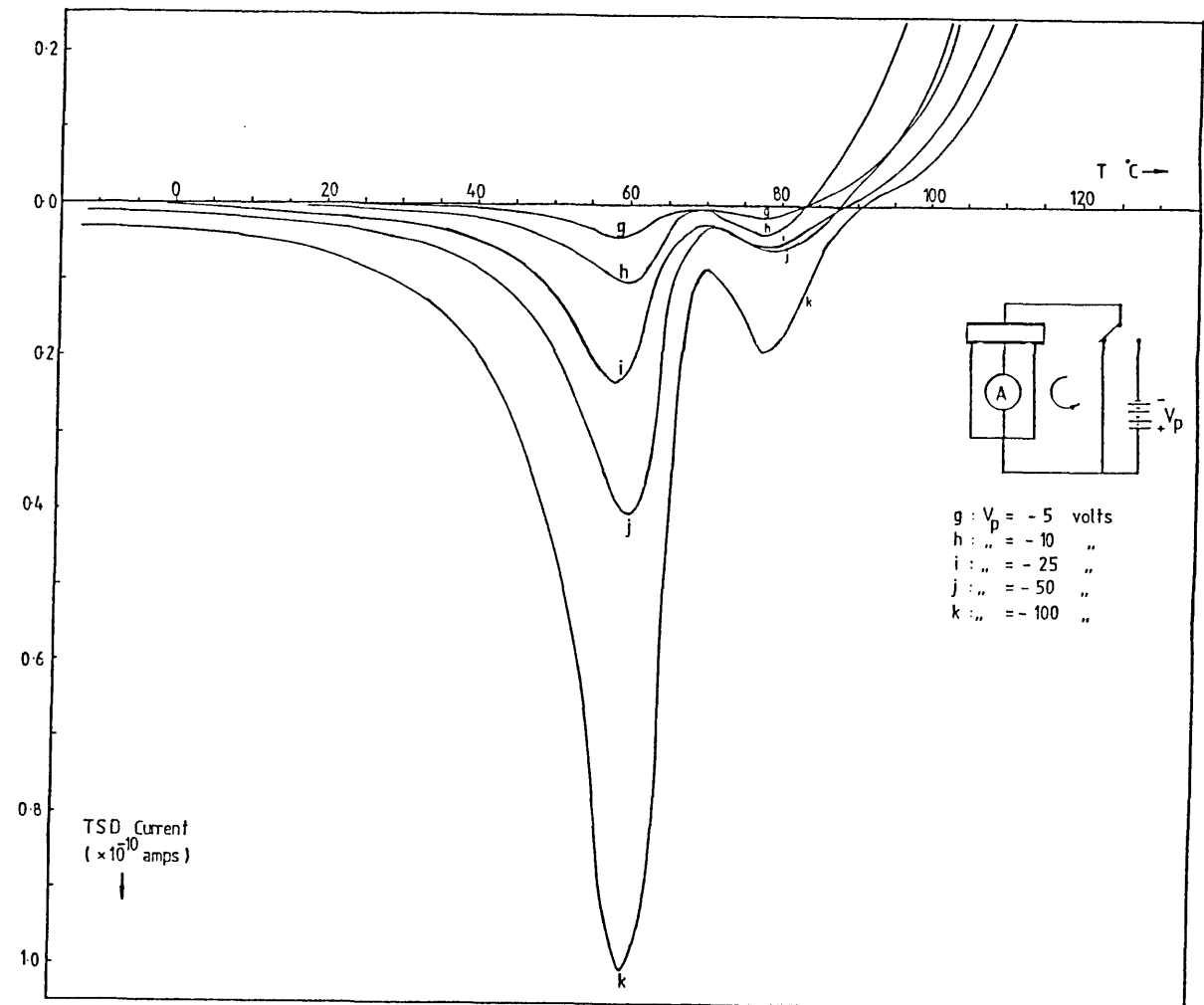
Fig 5.1(b)

TSD current thermograms of DC charged films
of 20 μm thick PVB films.

$T_p = 70^\circ\text{C}$, $r = 4^\circ\text{C min}^{-1}$, $t_p = 10$ mins

Inset shows values of the polarisation
voltages. The values are of opposite sign
to those shown in fig.5.1(a)

The α -peaks and ρ -peaks are clearly visible.



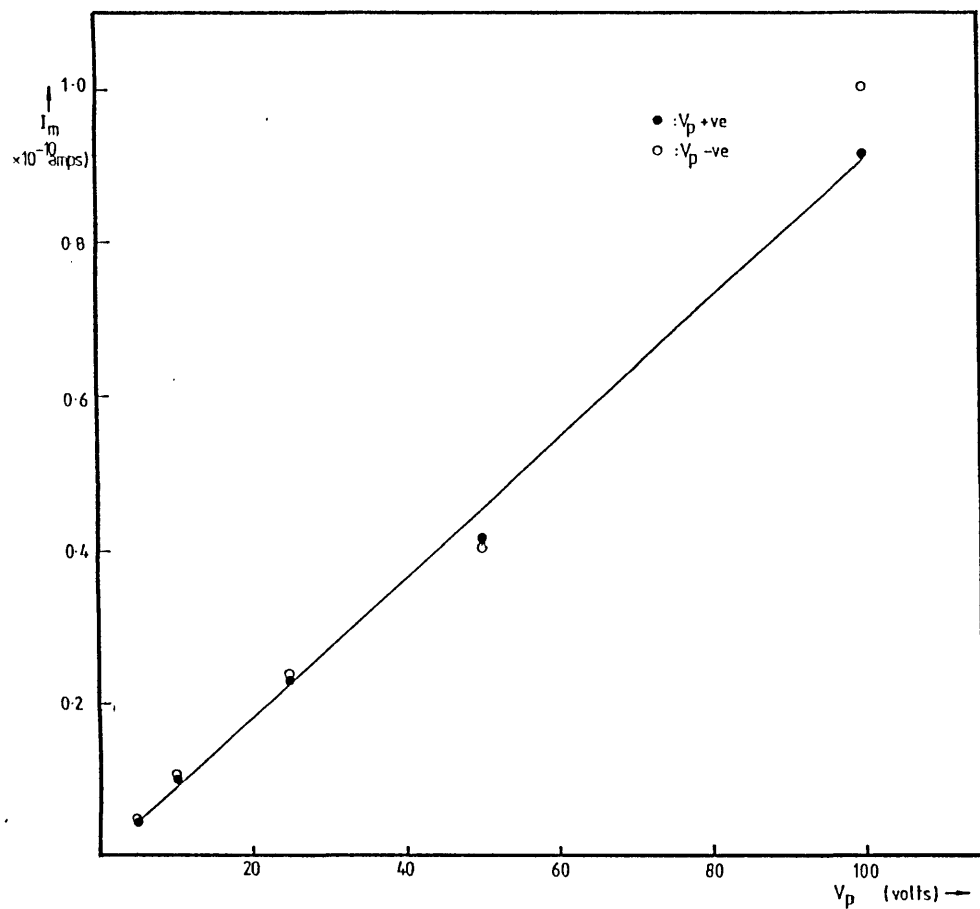


Fig.5.2 Dependence of the α -peak current, I_m , on the magnitude of the polarisation voltage.

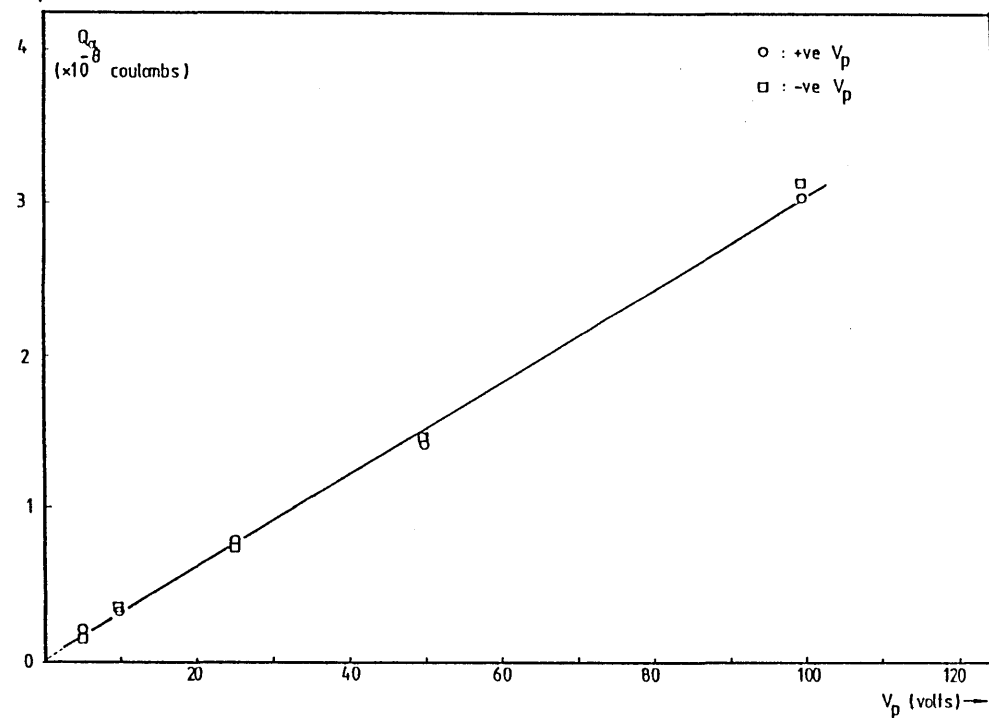
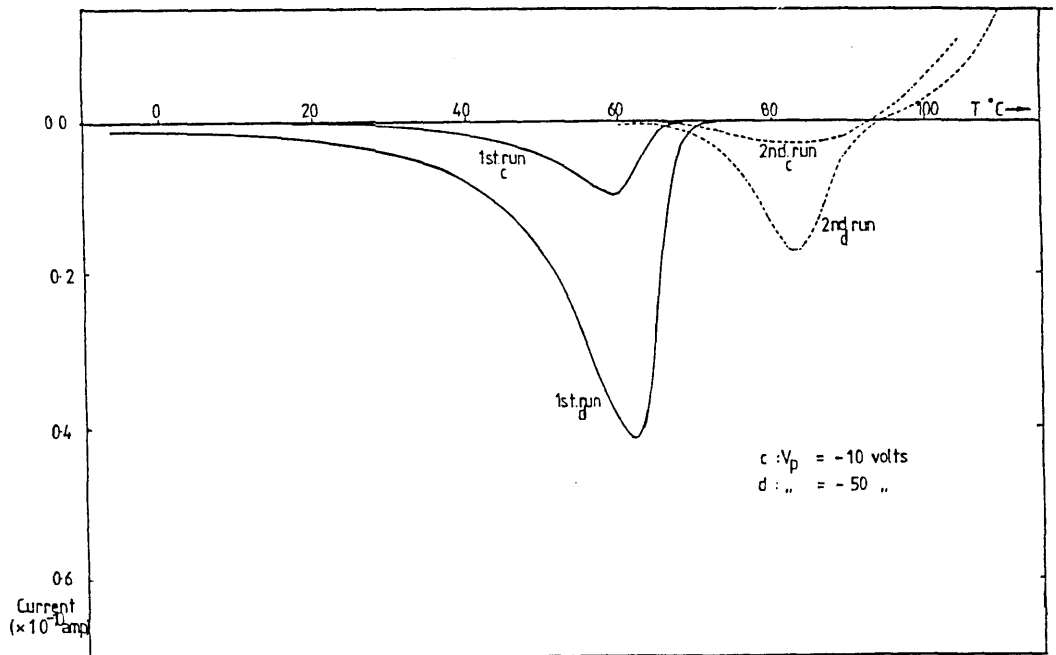
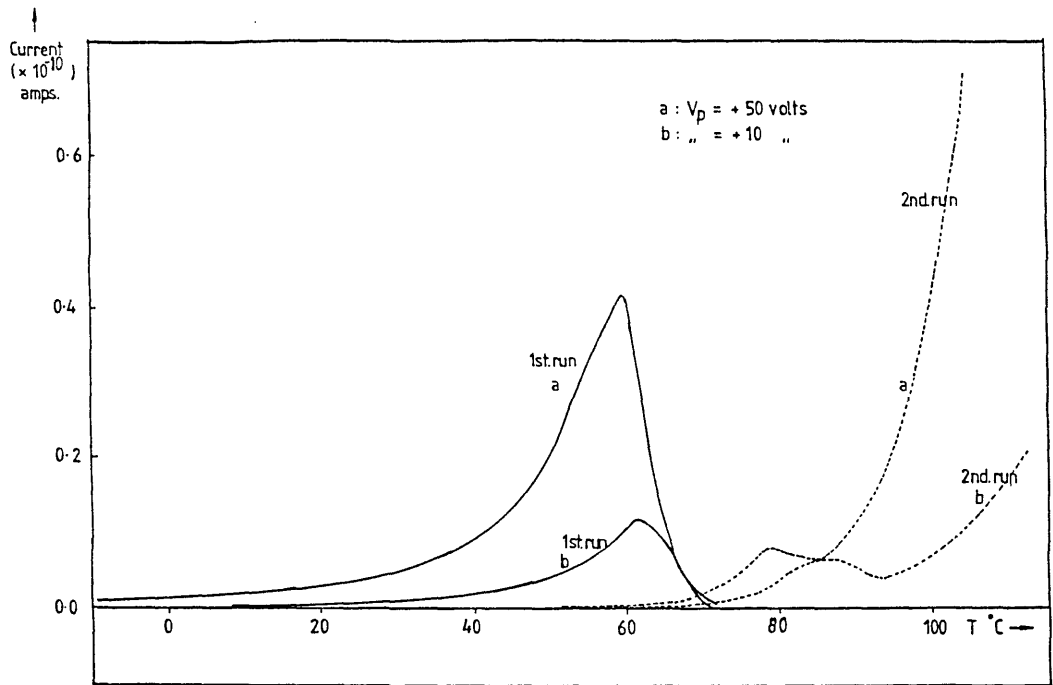


Fig 5.3 Released charge during the α -relaxation vs. magnitude of polarisation voltage. The released charge is found from a graphical integration of the area beneath the α -peak.



Top fig.5.4(a)
Bottom fig.5.4(b)

TSD current thermograms carried out with a two-stage heating programme. The samples are first discharged up to about 65°C then immediately cooled to room temperature before being re-heated and fully discharged. No overlap of the current peaks are observed.
 $T_p = 70^\circ\text{C}$, $r = 4^\circ\text{C min}^{-1}$, $t_p = 10$ mins

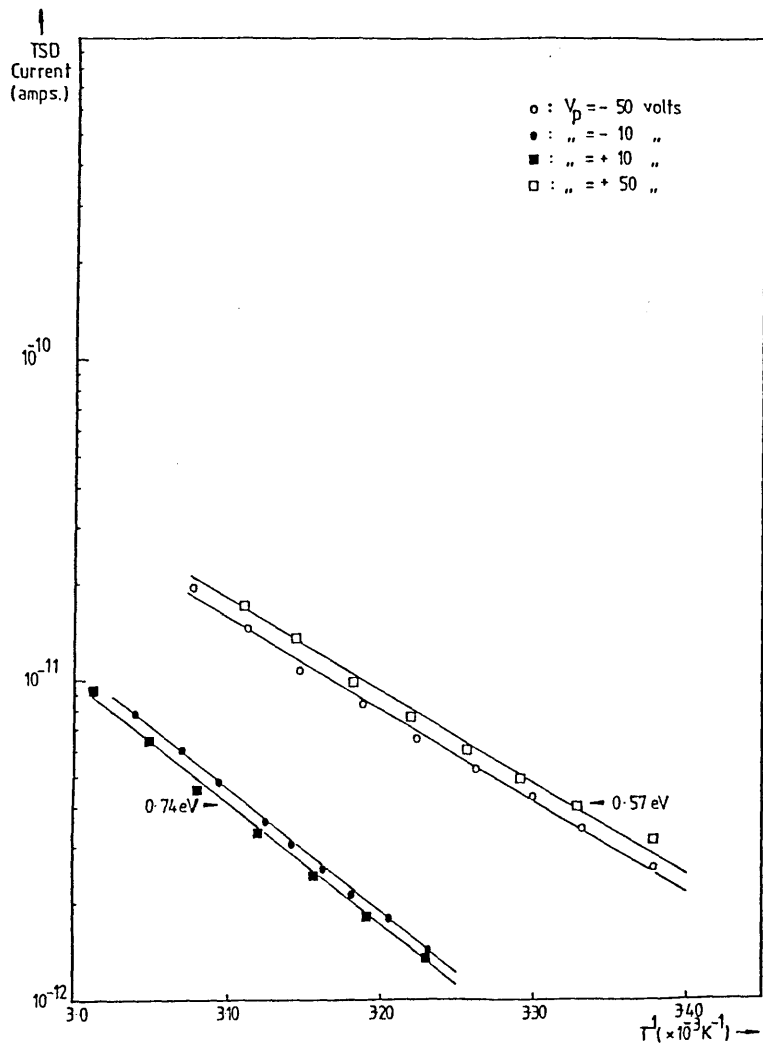


Fig. 5.5 Initial Rise plots of the -peak yielding the activation energy for the relaxation.

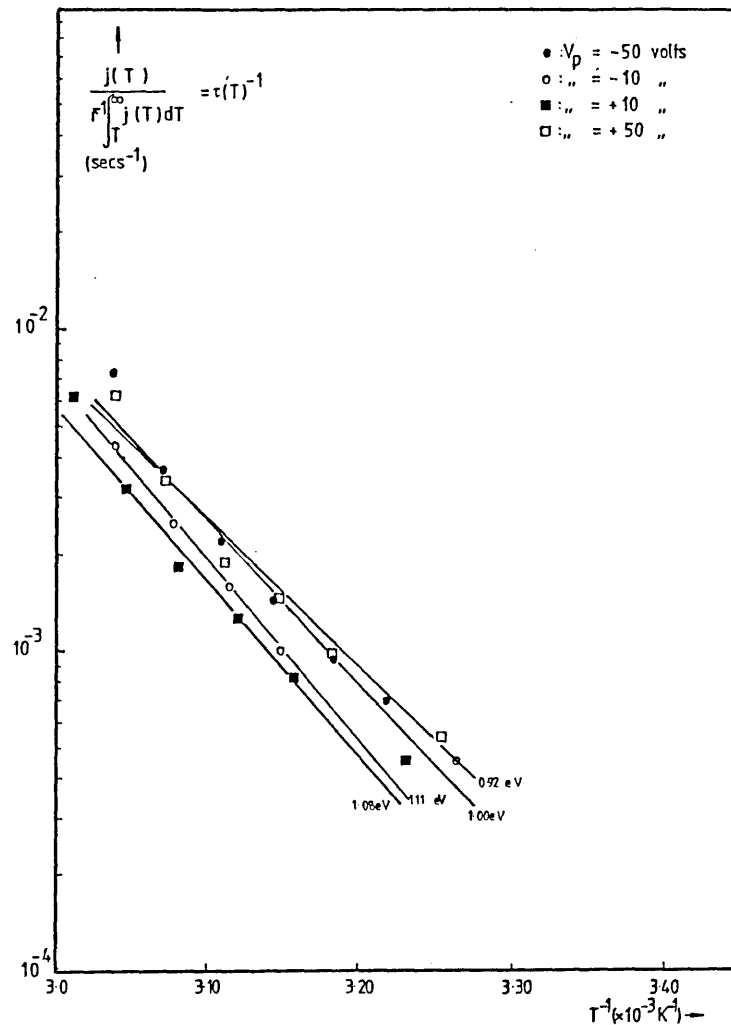


Fig. 5.6 BFG plots of the -peak. The slopes of the plots define an apparent activation energy for the relaxation.

| V _p | +100 volts | +50 volts | +10 volts | -100 volts | -50 volts | -10 volts |
|--------------------|------------|-----------|-----------|------------|-----------|-----------|
| S ₁ (K) | 316.31 | 314.5 | 315.80 | 317.0 | 316.09 | 316.25 |
| T ₁ " | 323.03 | 323.25 | 323.88 | 325.06 | 323.85 | 323.85 |
| U ₁ " | 326.65 | 328.17 | 327.95 | 329.19 | 328.36 | 328.30 |
| T _m " | 331.80 | 332.61 | 332.85 | 333.99 | 333.06 | 333.23 |
| U ₂ " | 334.56 | 335.58 | 335.76 | 336.89 | 336.48 | 335.91 |
| T ₂ " | 335.62 | 336.72 | 337.02 | 338.17 | 337.74 | 336.98 |
| S ₂ " | 339.34 | 338.05 | 338.28 | 339.55 | 339.00 | 338.22 |
| Eqn.1 | 1.52 eV | 1.42 eV | 1.49 eV | 1.51 eV | 1.45 eV | 1.43 eV |
| Eqn.2 | 2.44 eV | 2.28 eV | 2.25 eV | 2.26 eV | 2.01 eV | 2.51 eV |
| Eqn.3 | 1.79 eV | 1.68 eV | 1.73 eV | 1.74 eV | 1.63 eV | 1.73 eV |
| Eqn.4 | 1.30 eV | 1.12 eV | 1.20 eV | 1.21 eV | 1.20 eV | 1.20 eV |
| Eqn.5 | 1.65 eV | 2.29 eV | 2.30 eV | 2.26 eV | 2.11 eV | 2.51 eV |
| Eqn.6 | 1.42 eV | 1.37 eV | 1.45 eV | 1.45 eV | 1.42 eV | 1.48 eV |
| Eqn.7 | 1.21 eV | 0.91 eV | 1.03 eV | 1.03 eV | 1.02 eV | 1.04 eV |
| Eqn.8 | 1.26 eV | 2.47 eV | 2.42 eV | 2.31 eV | 2.43 eV | 2.64 eV |

Average value for energy of activation = 1.70 eV

* Equation (1) : $A = \frac{T_1 T_m}{7940(T_m - T_1)} - \frac{T_1}{14866}$

* Equation (2) : $A = \frac{T_2 T_m}{11780(T_2 - T_m)} - \frac{T_m}{10010}$

* Equation (3) : $A = \frac{T_1 T_2}{4738(T_2 - T_1)} - \frac{T_1}{11616}$

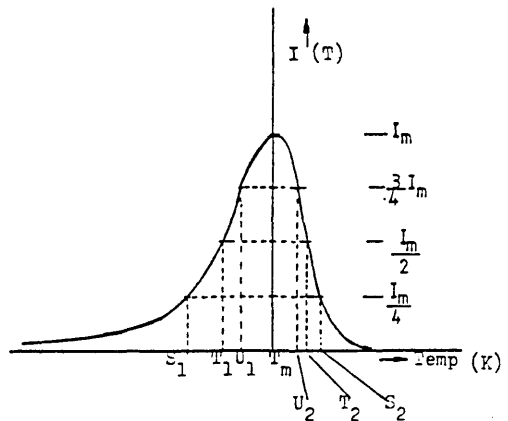
* Equation (4) : $A = \frac{S_1 T_m}{5077(T_m - S_1)} - \frac{S_1}{16813}$

* Equation (5) : $A = \frac{S_2 T_m}{8881(S_2 - T_m)} - \frac{T_m}{9439}$

* Equation (6) : $A = \frac{S_1 S_2}{3225(S_2 - S_1)} - \frac{S_1}{11797}$

* Equation (7) : $A = \frac{S_1 U_1}{8192(U_1 - S_1)} - \frac{S_1}{22121}$

* Equation (8) : $A = \frac{S_2 U_2}{18351(S_2 - U_2)} - \frac{U_2}{9018}$



* A is in eV when temp. is in Kelvin.
After Christodoulides(1985 a)

Table 5.1 Calculation of the activation energy for the dipole peaks using the method suggested by Christodoulides (1985 a)
The equations used are listed .

moments were already shown by our measurements of infra-red absorption (figure 4.14 of chapter 4). Attached to the main $-\text{CH}-\text{CH}_2$ chains are polar acetate ($-\text{CH}_3\text{CO}$), hydroxyl ($-\text{OH}$) and butyral ($-\text{CH}_2\text{CH}_2\text{CH}_3$) groups (fig. 3.1 of chapter 3). The application of a polarising field across the electrodes at a temperature where the polymer chains have had sufficient segmental mobilities to undergo conformational movements had resulted in an overall polarisation of the sample caused by the preferential alignments of the dipole groups. The loss of this internal polarisation due to the gradual disorientation of the dipoles upon thermal stimulation had resulted in the release of an external current between the electrodes. Since the rate of the dipole disorientations was highest as the glass transition region was approached, the TSD current released correspondingly display a peak at this temperature region.

The view that the α -peaks are due to a dipole mechanism is also confirmed by the results of a thermally stimulated polarisation experiment (TSP) carried out following the principles of McKeever and Hughes 1975. Briefly, the virgin samples were first heated up to 70°C and after a period of about 10 minutes, were cooled down to about -20°C at a rate of $-20^\circ\text{C min}^{-1}$. This was to ensure that the samples undergo a similar pre-conditioning as those in a normal TSD run. Throughout this pre conditioning period, the electrodes were short-circuited. A polarising field was then applied at this low temperature and the sample was gradually heated up at a linear rate.

An example of a TSP plot is shown in figure 5.7 where it is evident that a single peak is present at about 60°C . This is then followed by a sharp current rise commencing at about 65°C . The equivalent TSD thermogram is also plotted and from this it could be seen that the current peaks (the α -peaks) of both experiments coin-

side. The current peak in the TSP run could not have been due to a space charge relaxation as the sample was short circuited and pre-conditioned under a zero field condition. Since the samples are likely to be electrically neutral before the start of the run, the TSP current peaks could only have arisen via dipolar orientations. As the temperature is linearly raised, the dipole groups in the sample bulk gradually orientate under the influence of the applied field. A current peak is observed in the external circuit when the rate of dipole orientation is maximum, the current then diminishes when the number of dipoles to be orientated becomes gradually exhausted. As the temperature is raised further, the TSP current quickly becomes dominated by the increased electrical conductivity of the sample which explains the large increase in the current at about 65°C. The equation describing the TSP current density could be written as

$$j(t) = \frac{dP(t)}{dt} + \sigma(T)E \quad (5.1)$$

with the first term on the right hand side accounting for the increase in the dipole polarisation and the second term for the electrical conductivity. Comparison of eqn. 5.1 with the equation describing the decay of a dipole polarisation (eqn 2.5 through to eqn. 2.11 of chapter 2) also show that the TSP current peak will be characterised by the same position, height and shape as the corresponding TSD current peak, the only difference being that the polarisation current is of the opposite direction.

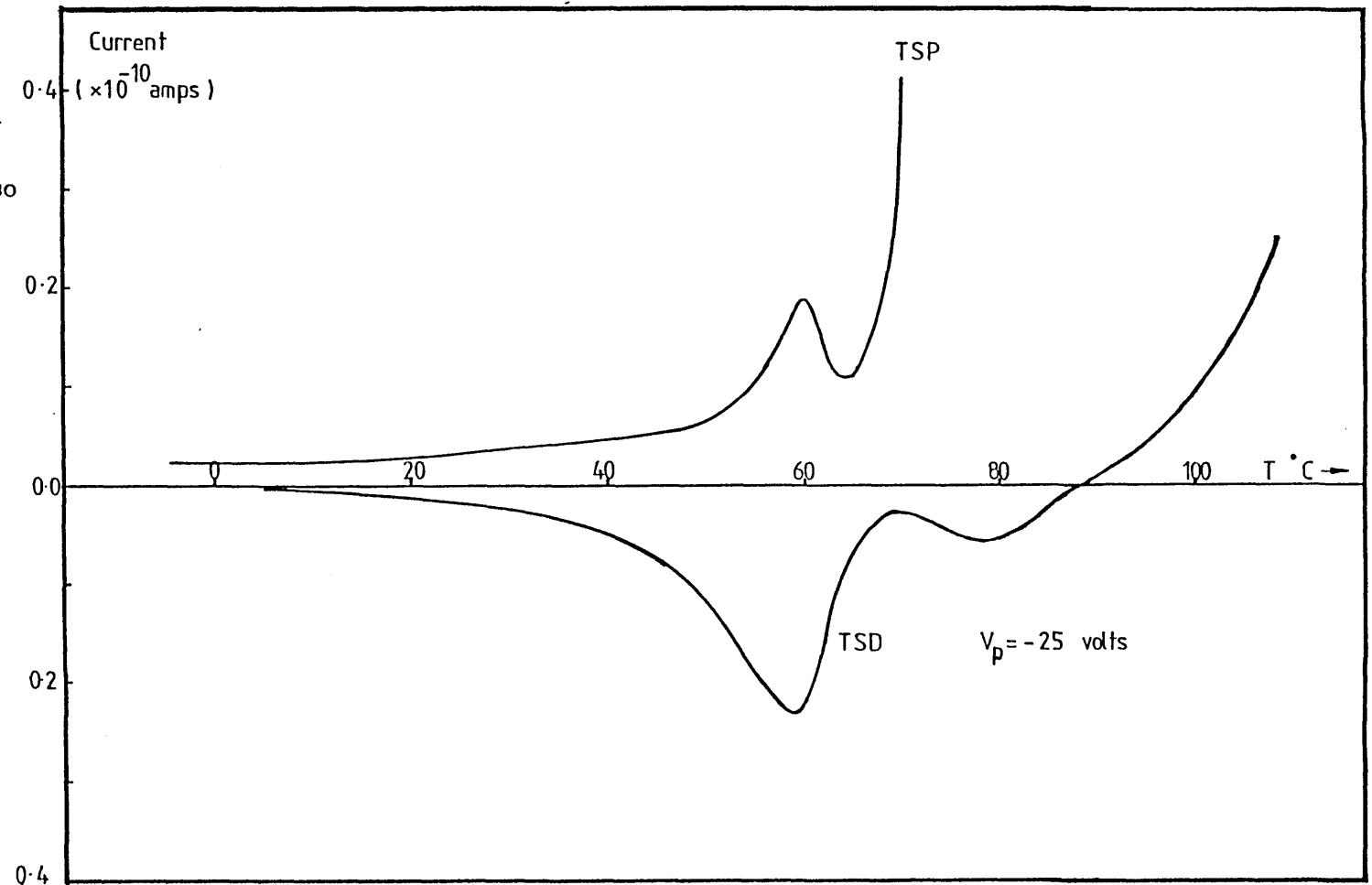
Apart from consolidating the view that the α -peaks are indeed due to a dipole relaxation, the TSP thermogram also facilitated in the determination of an optimum polarisation temperature T_p and helped to avoid unnecessary overheating of the sample. The TSP run also revealed the temperature at which the bulk electrical conductivity of the sample becomes significant.

'Fig.5.7

A Thermally Stimulated Polarisation plot (TSP) of a 20 μm thick PVB film. The polarisation voltage is -25 volts. Heating rate $r = 4^\circ\text{C min}^{-1}$

An equivalent TSD current plot is also shown.

The TSP plot also evidences the temperature at which electrical conductivity of the film becomes significant. This is about 65°C .



5.2.1.5 Estimation of Other Relaxation Parameters

Apart from the determination of the apparent activation energy, other parameters for the relaxation may also be estimated. The area underneath the TSD current peaks was also used to find the relaxation strength, $\Delta\epsilon$, of the α -relaxation. If it is assumed that equilibrium polarisation has been achieved during the formation stage of the TSD and that the detected TSD current is solely due the depolarisation of this polarisation state, then the use of equation 2.78 (section 2.7.3) would yield $\Delta\epsilon$ from the TSD current peak. The values of $\Delta\epsilon$ obtained from several TSD current thermograms are tabulated in table 5.2.

Knowing the value of $\Delta\epsilon$ also allows the estimation of one of the molecular parameters, N , the density of dipole entities undergoing the relaxation, or p , its electric moment via eqn. 2.79, provided that one of the quantities is known previously. An estimate of N could be found by using the values of the specific gravity of the sample bulk and the molecular weight of the monomeric repeat unit. Taking the specific gravity of Butvar B79 to be 1.083 (table 3.1), the average molecular weight of the monomeric repeat unit to be 119 (noting that Butvar B79 contains 88% vinylbutyral, 10% vinyl alcohol and 2% vinyl acetate) and using Avogadro's number, the density of monomer units of PVB is about 5.48×10^{21} per cm^3 . If it is further assumed that each monomer unit contain a single dipole group, then the density of dipoles N , in the sample will be $5.48 \times 10^{21} \text{ cm}^{-3}$. Substituting this value of N and using the value of $\Delta\epsilon$ calculated from the area of the TSD α -current peaks, eqn. 2.79 yields an average value of 2.98D for p , the effective electric moment of the dipoles. The calculated values of p are tabulated in table 5.2

The estimated value of 2.98D can be considered to be quite reasonable, noting that a value of 2.72D was quoted (Sherman 1978) for the vapour phase butyraldehyde. We also note here that the use of eqn. 2.79 to calculate p is based on the assumption that the equilibrium polarisation P_e has been adequately described by the Langevin function for freely rotating dipoles in the temperature range investigated and that the contribution of any space charges to the overall sample polarisation could be neglected.

5.2.1.6 The ρ -peak

TSD current peaks are also observed at temperatures higher than the dipole or α -relaxation peaks. These peaks, which we will call as the ρ -peaks, are centred at about 78°C and are observed for both positive and negative polarisation voltages (figure 5.1(a) and 5.1(b)).

No significant overlap of the ρ -peak with the α -peak is observed. The thermograms of 5.4(a) and 5.4(b), which were obtained by a two-stage heating program shows this more clearly. During these runs the samples were first discharged up to a temperature just beyond the temperature at which the α -relaxation peaks diminished (about 65°C) after which they were cooled down to room temperature at a rate of about $-20^\circ\text{C min}^{-1}$. The samples were then re-heated at the original rate of heating up to a temperature of about 120°C. As shown in the thermograms, the relative positions of the individual peaks in the two-step thermograms are identical to those where the heating was continuous. This observation is also a good indication that the current peaks detected are due to two distinctly different relaxation processes.

One feature of the ρ peaks is that its reproducibility in

terms of peak height and width can only be considered as moderate when compared to the well-characterised dipole relaxation peaks. The ρ -peak heights are also much smaller than their corresponding α -counterpart and also do not show any significant increase when the polarisation field is increased. The magnitude of the current maxima, I_m , plotted against the polarisation voltage do not exhibit a linear dependence (fig. 5.8). The amount of charge released during the ρ -relaxation (area under the curve between 70°C to 82°C) also do not depend linearly on the magnitude of the applied voltage (fig. 5.9). It can also be seen that the positions of the ρ -peaks exhibit a slight shift towards lower temperatures as the polarising voltage is increased.

The apparent energy of activation calculated from the initial rise portion of the peaks yield values in the range of 1.20 eV to 1.92 eV. The initial rise plots are shown in fig. 5.10. The BFG plots for the ρ peaks (fig. 5.11) yielded values of about 2.14 eV and 2.37 eV. It can be said that both plots exhibit reasonable linearities. Using the method based on the TSD current values at 1/4, 1/2 and 3/4 heights of the peak maxima (after Christodoulides 1985a), an average value of 2.36 eV is found (table 5.3).

5.2.1.7 Origin of the ρ -peak

The appearance of the ρ -peaks at a temperature where the bulk electrical conductivity had become significant indicate that these peaks are closely related to the said sample property. The electrical conductivity of the samples had only become significant at a temperature of about 65°C as was shown by the TSP thermogram of figure 5.7. Below this temperature, the current flowing across the sample under the influence of the applied field and linearly rising temperature had been negligibly small.

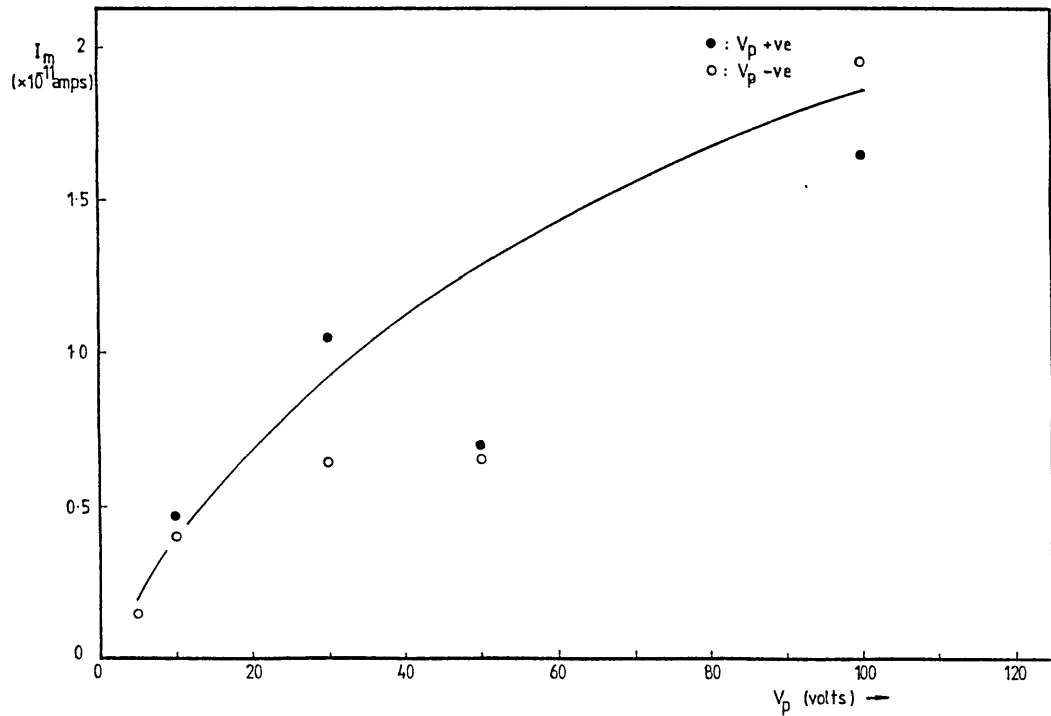
Table 5.2 Some calculated parameters for the dipole relaxation.

| Applied Voltage V_p volts | Equilibrium Polarisation $P_e \text{ C m}^{-2}$ | Dipole Moment p Debye |
|--------------------------------|--|----------------------------|
| + 5 | 1.24×10^{-5} | 3.32 |
| + 10 | 2.03×10^{-5} | 3.00 |
| + 25 | 4.91×10^{-5} | 2.95 |
| + 50 | 8.73×10^{-5} | 2.78 |
| + 100 | 1.87×10^{-5} | 2.85 |

1 Debye = $3.36 \times 10^{-30} \text{ C m}$

Estimated density of dipole units = $5.48 \times 10^{27} \text{ dipoles m}^{-3}$

Fig.5.8 Dependence of the I_m peak currents on the magnitude of the polarisation voltage. A non-linear relationship is observed.



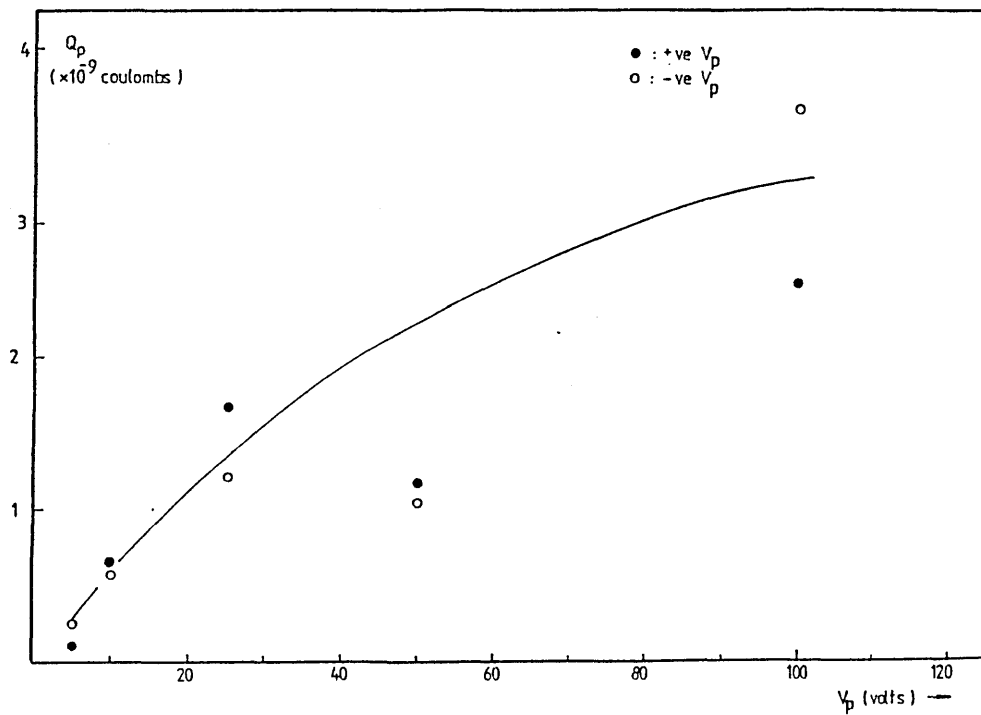


Fig.5.9

Released TSD charges for the space charge relaxation as a function of the magnitude of the polarisation voltage.

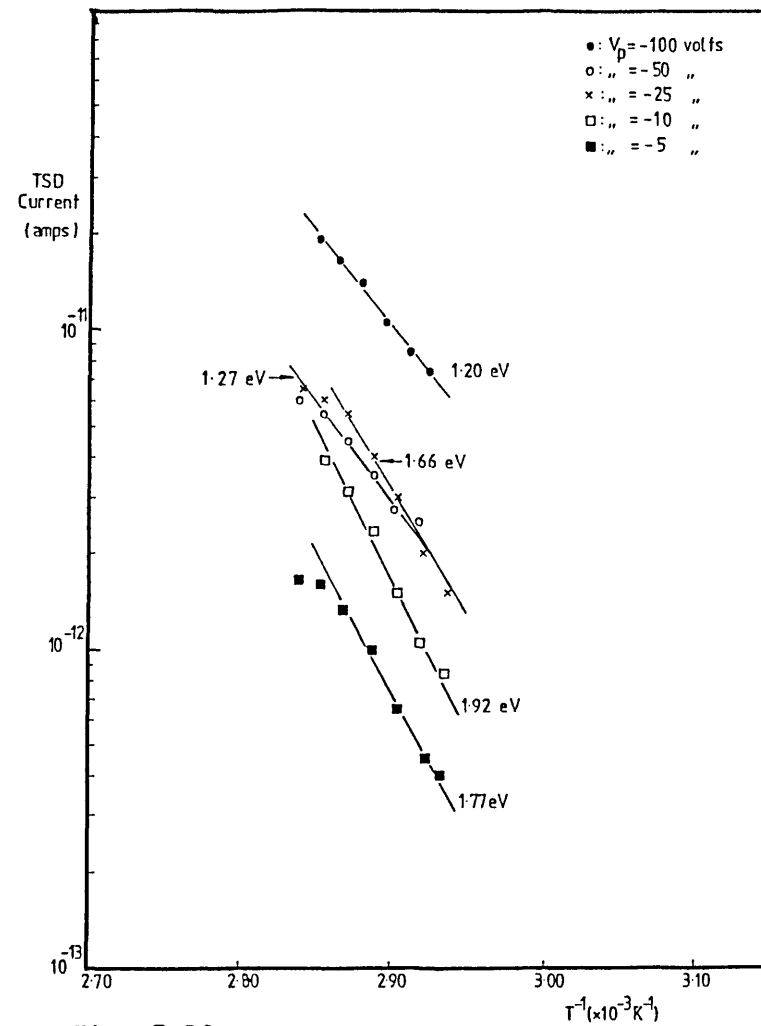


Fig. 5.10

Initial Rise Plots for the ρ -peaks of the TSD current thermograms.

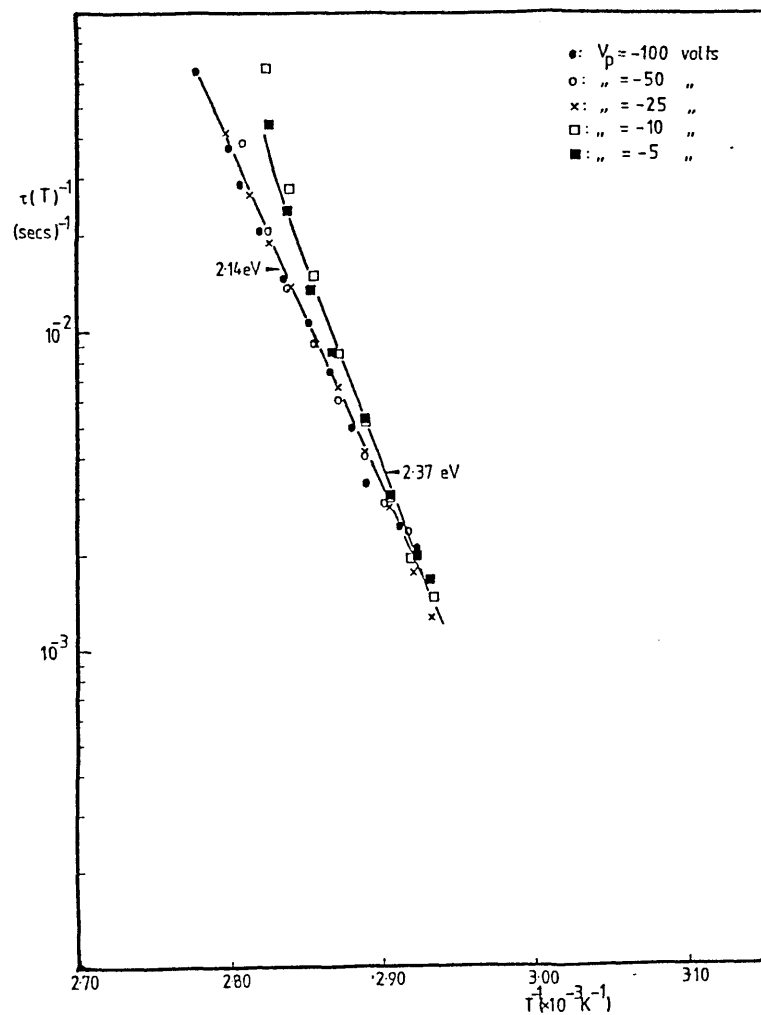


Fig.5.11

BFG plots for the Space charge peaks. The slopes of the plots yield the activation energy for the relaxation.

| | | | | |
|-----------|------------|------------|------------|------------|
| V_p | + 50 volts | + 10 volts | - 10 volts | - 50 volts |
| S_1 (K) | 342.56 | 349.50 | 343.23 | 346.26 |
| T_1 " | 346.14 | 352.62 | 346.33 | 349.72 |
| U_1 " | 349.00 | 355.15 | 349.05 | 352.63 |
| T_m " | 352.84 | 359.13 | 353.88 | 356.00 |
| U_2 " | - | 363.29 | 361.45 | 359.06 |
| T_2 " | - | - | - | 360.87 |
| S_2 " | - | - | - | 362.92 |
| Eqn.1 | 2.27 eV | 2.42 eV | 2.02 eV | 2.47 eV |
| Eqn.2 | - | - | - | 2.20 eV |
| Eqn.3 | - | - | - | 2.35 eV |
| Eqn.4 | 2.29 eV | 2.55 eV | 2.23 eV | 2.47 eV |
| Eqn.7 | 2.25 eV | 2.67 eV | 2.50 eV | 2.32 eV |

Average value for energy of activation = 2.36 eV

For description of equations used see table 5.1

Table 5.3 Calculation of the activation energy for the ρ -peaks using the method suggested by Christodoulides (1985 a)

Before proceeding with the discussions, it would be worthwhile for us to consider the possible origin of charge carriers in an organic polymer like PVB. The presence of ionic carriers in the samples can be considered to be highly probable due to the highly polar nature of the vinyl butyral as well as the residual vinyl alcohol and vinyl acetate side groups. The hygroscopic behaviour of the PVB bulk will undoubtedly cause an increase in the electrical conductivity due to the absorption of water. The dissociation of absorbed water molecules has been known to cause a significant change in the bulk electrical conductivity in many organic polymers (e.g. Crowley et. al. 1979).

It would also be reasonable to assume that ionic products in the sample could also have originated from impurities left from the original acetalisation process during the PVB manufacture, fragments of polymerisation catalysts, as well as thermal degradation products of the PVB itself. On this basis, the PVB would contain cations like H^+ , H_3O^+ , Na^+ , K^+ and anions of SO_4^{2-} , OH^- , and Cl^- , although this would be experimentally difficult to verify.

Apart from the proximity of the ρ -peaks to the temperature where the bulk electrical conductivity had first become significant, several other characteristics of the TSD current peaks also point to the conclusion that space charges are involved in the relaxation. The non-linear dependences of the peak currents and the total amount of charge released to the external circuit on the applied voltage give a strong indication that a dipolar-type of disorientation processes can be ruled out. As had been discussed in section 2.4.3.2, the overall shift of the current maxima to lower temperatures as the polarisation voltage is increased is characteristic of a space charge relaxation proceeding via a self-drift motion.

It has been observed that intrinsic space charges generally tend to collect at regions near the metal electrodes when a field is applied (e.g. Croitoru 1965, Walker and Jefimenko 1973). Charges may also accumulate at heterogeneties in the sample bulk, i.e. at amorphous/crystalline interfaces. However, this can be considered to be effectively absent due to the completely amorphous nature of our samples. PVB, by virtue of it having a large side group, could be considered to be highly uncrystallisable (Shen and Eisenberg 1966). Studies on PVDF electrets have shown that piezoelectric activity is found to be greater at regions that were nearer to the electrodes due to space charge accumulation during the poling stage (Sussner and Dranfeld 1978). Sectioning experiments carried out on PMMA electrets also reveal that 90% of the intrinsic space charges resided at regions near the electrodes (Van Turnhout 1975).

Obviously, a significant heterocharging of the samples could only have occurred when there is an abundance of intrinsic carriers in the sample bulk. The fact that the polarisation was performed at a temperature above T_g and hence when the electrical conductivity of the sample was large enough to supply the intrinsic charges is important for the appearance of peaks in the final TSD spectrum. In fact, the TSD current spectra of PVB samples that were polarised at low temperatures (-3°C and 30°C) did not exhibit any ρ -peaks which emphasised the role of the intrinsic space charges in the formation of the polarisation. For these samples the electrical conductivity of the samples had been too low to successfully cause any space charge polarisation. As expected, well-defined dipole relaxation peaks are not observed due to the failure of the formation of any significant dipole orientation during the electret formation at the low temperatures (fig. 5.12). The thermograms also exhibit broad and weak current peaks observable at low temperatures which are probably due to the neutralisation of the electrode injected charges (i.e. extrinsic

charges which were relatively loosely trapped at the electrode/polymer interfaces). Electrode effects are important for low conductivity solids (e.g. Lewis 1984), however for our samples which were polarised above T_g , the overwhelming effects of the high bulk conductivity had probably swamped any electrode injection effects. It is believed that this was also responsible for the lack of any difference in the overall TSD current thermograms when different electrode materials are used. Differences in the characteristics of the space charge relaxation peaks in organic polymers attributable to electrode effects has been reported but these were observed in relatively high resistivity polymers (Hickmott 1975, Kojima et.al. 1976, Vanderschueren and Gasiot 1979).

During the polarisation of the PVB films at 70°C, the intrinsic (equilibrium) charges gradually accumulate at regions near the electrodes. These charges are then immobilised when the temperature is reduced. During the TSD, the charges are thermally activated and regain their mobilities and drift, under their own field, towards their opposite counterparts in the sample bulk. Some of the charges may also drift towards the electrodes, finally getting neutralised by the image charges residing on the electrodes. This bi-directional internal motion of the charges releases some of the induced charges at the electrodes, finally leading to a TSD current peak. The drift of the charges in the sample bulk is basically a conductive motion, thus the temperature dependence of the space charge decay is closely related to that of the intrinsic bulk conductivity of the sample.

It has been discussed that a good test for the decay of the space charge polarisation as described above would be the linearity of the so-called "Charge Ratio" plot (chap.2, sect.2.7.5). It was observed that other TSD decay processes such as dipole disorientations or trap emptying with slow retrapping would not exhibit this linearity (Van Turnhout 1975). Fig.5.13 shows the plot for the ρ -peaks. A good linearity is observed, thus strongly suggesting that

the decay of the polarisation is indeed due to the self-drift of the previously immobilised charges. The slope of fig. 5.13, which defines an activation energy, yields a value of 3.90 eV. This is considered to be a large value for what is basically a conductive motion.

In general, it has been found that the activation energy for the ρ -peaks range from 1.20 to 3.90 eV. It has been suggested by Jonscher (1967) that it is possible to distinguish between electronic or ionic conduction mechanisms by their respective values of the activation energies. On this basis, it could be considered that due to the large values of the apparent activation energies, the dominant type of charge carriers involved would most likely be ions.

The view that the electrical conductivity of the PVB films is dominantly ionic is also supported from a consideration of the relatively large value of the static dielectric constant of the polymer associated with its strong polar groups. A large value of ϵ_s will greatly enhance the dissociation of any ionisable groups in the solid, thus increasing the overall ionic conductivity of the polymer. The effect of a large ϵ_s on the ionic conductivity has been described by eqn. 1.8 of chapter 1.

5.2.1.8 Ionic conduction and the free volume

The experimental observation that the ρ -peak appears at a temperature above T_g , (i.e. in the "rubbery" phase of the solid) has underlined the close relation between the space charge relaxation process with the increase in the free volume of the bulk solid. If it is assumed that the dominant charge carriers were indeed ions and that the relaxation proceeded via the drift of these ions through the sample bulk, then this experimental observation would be expected.

The movement of these ions could be viewed as a series of hops from one equivalent position to another in the bulk solid. The frequency of these

Fig. 5.12

TSD current thermograms of PVB films charged at temperatures below T_g . No dipole peaks are observed.

Space charge peaks are ill-defined.

$r = 4 \text{ C min}^{-1}$

TSD plots are generally difficult to be characterised.

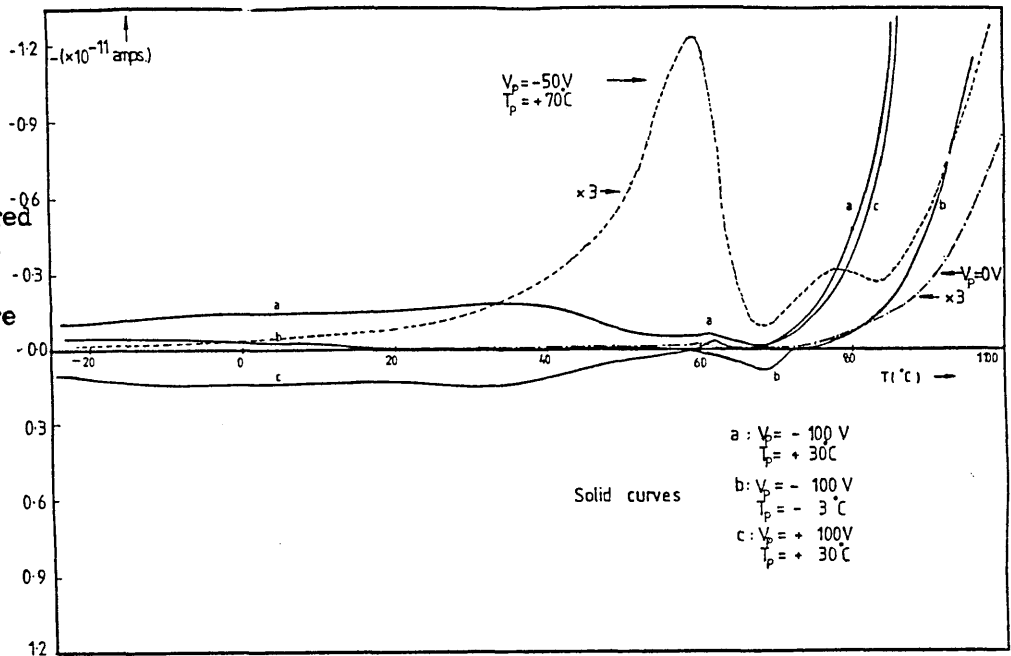
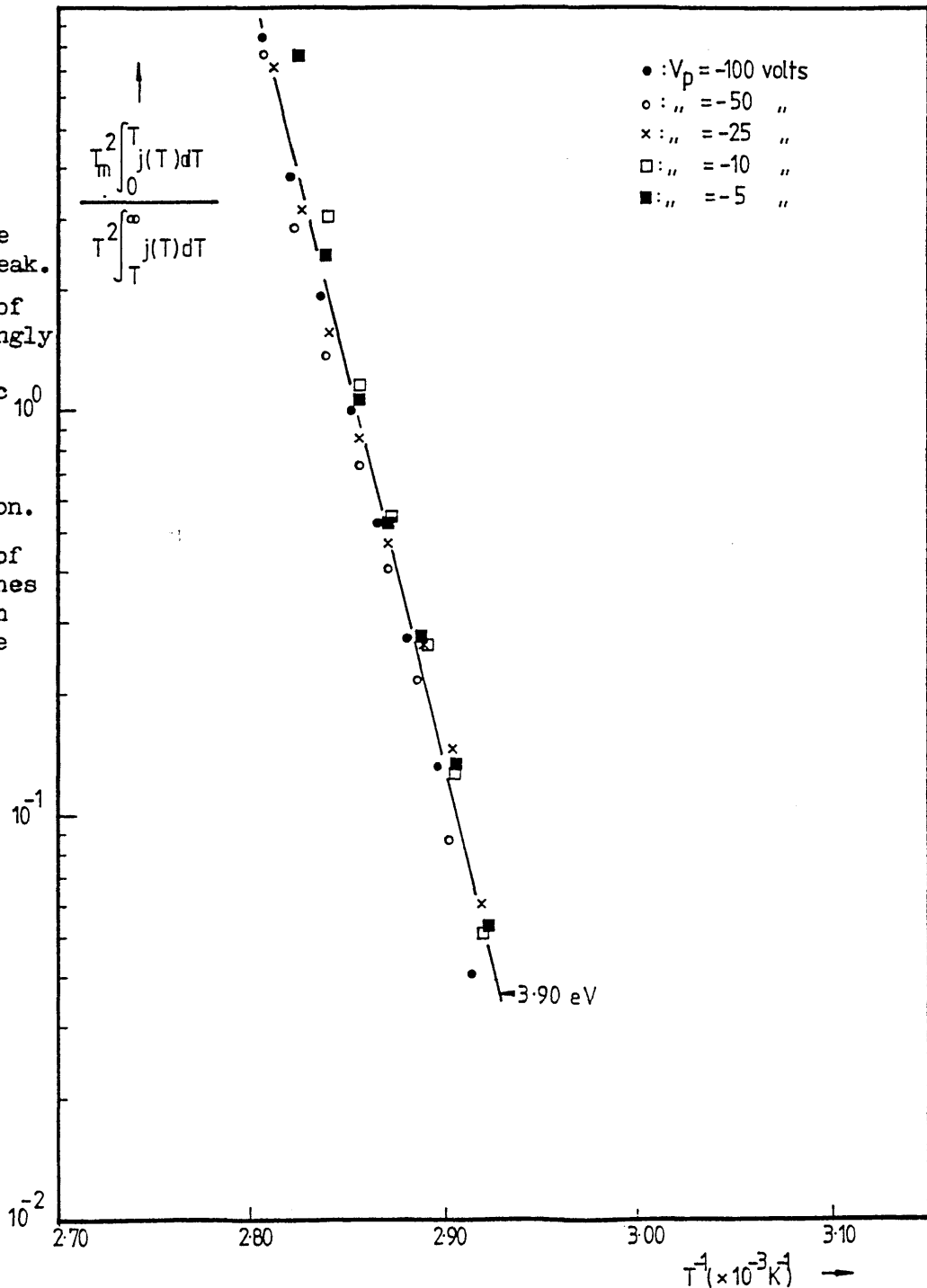


Fig. 5.13

"Charge Ratio Plots" for the space charge peak.

The linearity of this plot strongly supports the view that ionic self-drift is the main decay mechanism of the polarisation.

The gradient of the plot defines the activation energy for the ionic drift motion.



hops would depend on firstly, finding a physical void or hole of a critical size to accomodate the incoming ion and secondly, on the probability of jumping into that available hole. The free volume model of Cohen and Turnbull (1959) Turnbull and Cohen (1961) has expressed the probability, per second, for the formation of a void of a critical size v_i^* by the structural re-arrangements of the chain segments at a temperature above a so-called critical temperature T_∞ as,

$$P_h \sim \exp \left[- \frac{\gamma v_i^*}{v_f} \right] \quad (5.1)$$

where γ is a constant ($0.5 \leq \gamma \leq 1$) accounting for the overlap of the free volume and v_f is the free volume. T_∞ is a temperature which marks the onset where any free volume added to the bulk could be distributed without an energy cost. The probability per second of a successful jump into the available hole v_i^* could be expressed as (according to the rate theory of processes, Glasstone and Eyring 1947)

$$P_j \sim \exp \left[\frac{-\Delta U}{kT} \right] \quad (5.2)$$

where ΔU is the energy barrier that has to be surmounted. Thus the frequency of the transitions, i.e. ionic jumps in the bulk could be written as

$$f \sim \exp \left[\frac{-\gamma v_i^*}{v_f} \right] \cdot \exp \left[\frac{-\Delta U}{kT} \right] \quad (5.3)$$

Miyamoto and Shibayama 1973 has expressed the ionic conductivity in a solid at a temperature, T , above T_g and in an electric field F as

$$\sigma_{\text{ionic}} \sim \exp \left[- \left(\frac{\gamma v_i^*}{v_f} + \frac{\Delta U}{kT} + \frac{\Delta W}{2e_s kT} \right) \right] \sinh \left\{ \frac{eaF}{2kT} \right\} \quad (5.4)$$

where ΔW is the dissociation energy of the ion, e_s is the static dielectric constant of the medium, e the charge on the ion and a is the average distance of the available sites for the ionic jumps. Eqn.

5.4 is actually an extension of eqn. 1.9 of chapter 1 where ~~now the free~~ volume of the solid above T_g is taken into account. As can be seen, the exponential dependence of the ionic conductivity on both the temperature T and on the available free volume v_f as expressed in eqn.5.4 emphasises the importance of both these quantities in the formation and subsequent decay of a space charge polarisation in our samples.

According to the freevolume model of Cohen and Turnbull (1959) the free volume v_f could be written as

$$\begin{aligned} v_f &= \alpha \bar{v}_m (T - T_\infty) & \text{for } T > T_\infty \\ v_f &= 0 & \text{for } T < T_\infty \end{aligned} \quad 5.5$$

where α is the average coefficient of expansion of the medium and \bar{v}_m is the average value of the "occupied" or molecular volume, ($\bar{v}_m = v_0$ at 0 K). The fractional free volume f could then be expressed as

$$\begin{aligned} f &= \frac{v_f}{v_0} = \alpha \frac{\bar{v}_m}{v_0} (T - T_\infty) & 5.6 \\ &= \alpha_f (T - T_\infty) \end{aligned}$$

where $\alpha_f = \alpha \frac{\bar{v}_m}{v_0}$ is the coefficient of expansion of the free volume.

By assuming that $P_j = 1$ (effectively saying that a jump will take place as long as a void is available), the inverse of eqn. 5.3 will define an average relaxation time, $\tau(T)$. Using the relations in 5.5 and 5.6 this can be expressed as, assuming $\gamma \frac{v_1^*}{v_0} \sim 1$

$$\tau(T) = \tau_0 \exp \frac{1}{\alpha_f (T - T_\infty)} \quad 5.7$$

Lacabanne and Chatain (1973) has proposed that the relaxation time obtained from the ratio $\frac{P(T)}{J(T)}$ from the TSD current data could represent the relaxation time for the structural relaxations of the free volume model. Applying this assumption to the ρ -peaks of the PVB films, the values of $\frac{P(T)}{J(T)}$ obtained from the thermograms would then represent the structural relaxation times for void formations in the sample bulk. These values would also equal the relaxation times of the ionic motion since the jump probability was taken to be unity. It can also be shown that eqn. 5.7 will exhibit a temperature shift identical to the WLF eqn. (eqn. 1.2 of sect. 1.3.3) by choosing the parameters C_1 and C_2 as

$$C_1 = \frac{1}{2.303 \alpha_f (T_g - T_\infty)}, \quad C_2 = T_g - T_\infty \quad 5.8$$

From eqn. 5.7, a plot of $\ln \tau(T)$ vs $\frac{1}{(T - T_\infty)}$ would be linear with a gradient of $\frac{1}{\alpha_f}$ from which the average coefficient of expansion of the free volume could be found. Fig. 5.14 shows the plot of $\tau(T)^{-1}$ vs $\frac{1}{(T - T_\infty)}$ for the TSD ρ peaks with T_∞ chosen as 278.4K (i.e., $T_\infty = T_g - C_2 = 330 - 51.6K$). The gradients of the linear portions of the plots yield values of α_f as 9.0×10^{-4} and $10.0 \times 10^{-4} K^{-1}$. Knowing α_f , the fractional free volume f of the samples could also be found from eqn. 5.6. The use of this equation yields values of 0.046 and 0.052 at T_g (=330K). For organic polymers in general, Roberts and White 1973 has noted that the values of α_f range from $2.9 \times 10^{-4} K^{-1}$ to $7.0 \times 10^{-4} K^{-1}$ yielding corresponding free volumes of 0.015 and 0.036 respectively.

5.2.1.9 Conclusions

Short-circuit TSD current measurements carried out on aluminium electroded PVB samples which were polarised with a

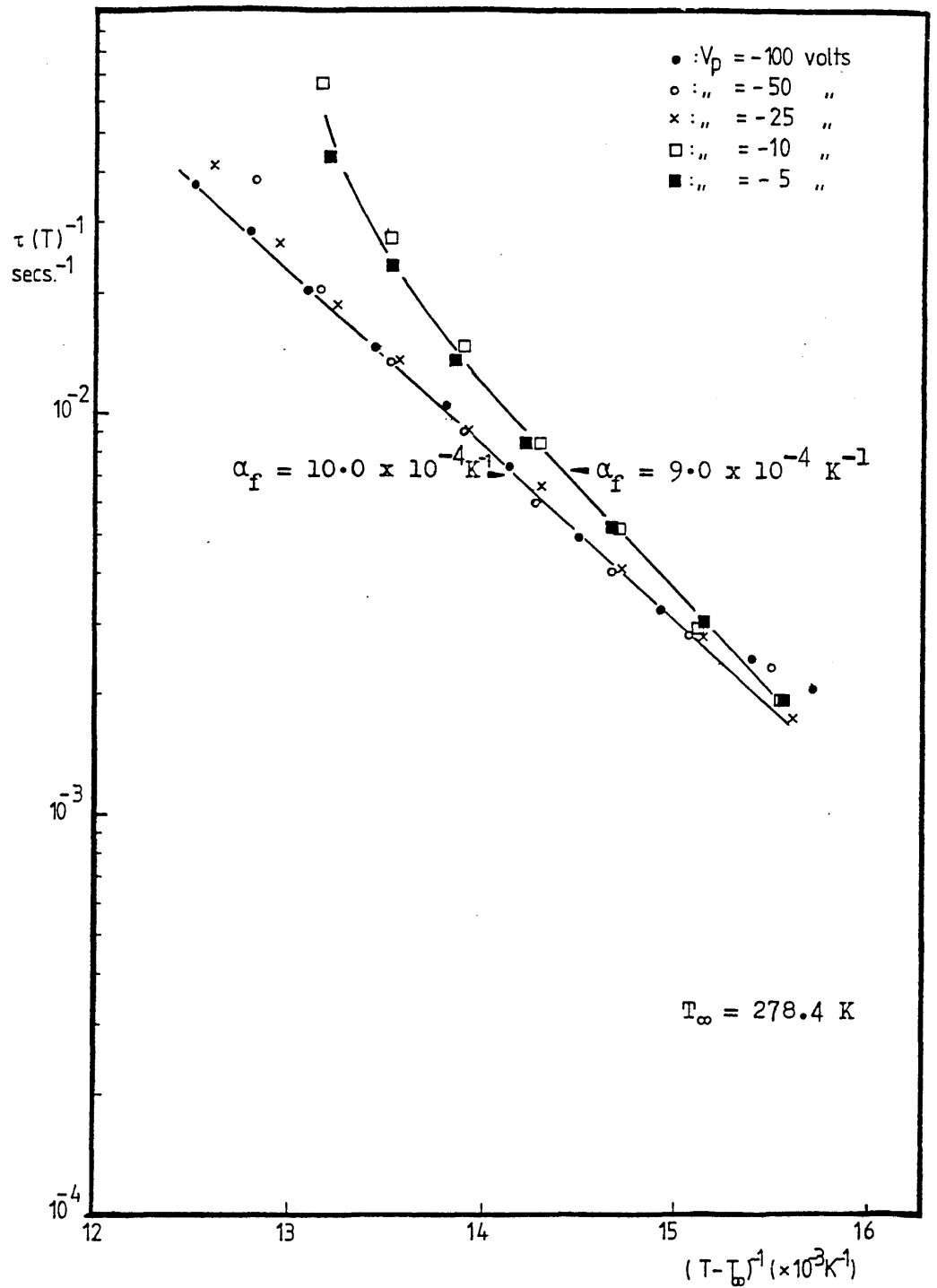


Fig.5.14 Plots of the relaxation frequencies of the space charge relaxation vs. $(T - T_\infty)^{-1}$ where $T_\infty = T_g - C_2$; $T_g = 330 \text{ K}$, $C_2 = 51.6 \text{ K}$. The linear portions of the plots yield the coefficient of expansion of the free volume.

static electric field at 70 °C reveal the presence of heterocharge polarisations of two different kinds in the sample bulk.

Well-defined current peaks attributed to the disorientation of dipole groups are observed at about 60 °C. This also coincides with the calorimetrically determined glass transition temperature of the polymer (~57 °C), signifying the close relationship of the disorientation of the oriented dipoles with the structural re-arrangements of segments of the main polymer chains. The apparent activation energy for the relaxation is estimated to be between 0.65 to 1.70 eV by the different methods of analyses. The relaxation frequency of the dipoles is of the order of 10^{-4} to 10^{-3} Hz. A simple estimate yields a dipole density of the order of 10^{21} cm⁻³, each with an effective moment of about 2.98 Debyes. This is attributed to the polar butyraldehyde groups which are attached to the carbon atom flanked by the two oxygen atoms of the 1,3-dioxane structure.

Another depolarisation peak due to the drift of intrinsic space charges which were previously frozen-in at regions near the electrodes is also observed at about 78 °C in the TSD current spectrum. The formation of the space charge polarisation is dependent on the temperature of formation of the electret. A charging temperature above T_g is required so that a significant density of charges could be frozen-in and thus lead to a relatively well-defined peak.

The relatively large values of the activation energy for the relaxation (1.20 to 3.90 eV) and the appearance of the current peak in the rubbery phase of the sample strongly suggests that the space charges involved are dominantly ions. The ions are most likely to be the dissociation products of absorbed water (H^+ , H_3O^+ and OH^-) in view of the hygroscopic nature of the polar polymer.

The structural parameters of the bulk solid are also estimated by correlating the average relaxation times obtained from the TSD current data

with the relaxation time for structural re-arrangements as defined in the free volume model of Cohen and Turnbull (1959). It is found that the average coefficient of expansion of the free volume is about $(9.0 \text{ to } 10.0) \times 10^{-4} \text{K}^{-1}$ corresponding to fractional free volumes of 0.046 to 0.052 respectively (at T_g). Both of these structural parameters are of a similar order to those that has been dilatometrically observed in amorphous organic polymers in general.

5.2.2 TSD of Corona Charged PVB films

5.2.2.1 Preliminary

In view of the wide use of corona charging in the study of the electret effect in organic polymers, it was decided to apply the technique to the films of PVB. Corona charging has been found to be a reliable and quick way of producing electret foils for use in transducer applications (see, for e.g. Perlman (ed.) 1973, Wada et al. (ed.) 1979, Sessler (ed.) 1980 and references therein). However and more importantly, it was thought that the polarisation achieved in the PVB films via exposure to the corona discharge would be more representative of the situation where the polymer is being used as one of the components of a xerographic photoreceptor material system. In addition to this, the non-contacting type of charging technique would also allow a higher degree of persistent internal polarisation to be achieved (due to the higher charging voltages that could be afforded without the electrode-induced sample break-downs) and hence, better defined TSD current signals be recorded.

In this section the short circuit TSD current measurements of corona charged PVB films will be discussed. Prior to metallisation, the free surface of the virgin PVB films were charged with a DC corona in an ambient laboratory atmosphere (15 to 25% relative humidity). The temperature of the samples, T_p , were maintained at 70°C throughout the charging period of $t_p = 1$ minute. The use of charging times longer than 1 minute did not result in higher surface potentials being achieved.

Uniform surface potentials were obtained by using a wire mesh grid between the corona charging unit and the surface of the films. By applying a biasing voltage, the magnitudes of the initial surface potential could also be controlled. These were varied from +1000V to -1000V.

After exposure to the corona discharge, the samples were immediately transferred into a metallisation unit where they were coated with aluminium top electrodes. The samples are then ready for depolarisation in the short-circuit mode in the cryostat. The heating rate used was $4^{\circ}\text{C min}^{-1}$. All measurements were carried out in the dark up to a temperature of about 120°C .

5.2.2.2 Results

The values of the initial surface potential achieved for the different magnitude of the grid voltages is shown in fig. 5.15. It is also noted that the sign of the effective surface potential is similar to that of the mesh grid, i.e. corona charging resulted in an overall homocharging of the polymer surface. The results of the short-circuit TSD current measurements are shown in figs. 5.16(a) and 5.16(b) for the positive and negative grid voltages respectively. It could be observed that only a single, well-defined peak centred at about 60°C is present in each of the current thermograms. The positions of the peaks are independent of the magnitude and polarity of the surface voltage.

The magnitude of the released charges, as found from a graphical integration of the areas beneath the TSD current peaks, exhibit a linear dependence on the magnitude of the grid voltage (fig. 5.17). The height of TSD current peak is also linearly dependent on V_g (fig. 5.18). The initial rise plots show that the apparent activation energy for the depolarisation ranged from 1.09eV to 2.68 eV (figs. 5.19(a) and 5.19(b)).

5.2.2.3 Discussions

The position of the TSD current peaks in the vicinity of the glass transition region, the linear dependences of the released charge

Fig.5.15 Attainable magnitude of the surface Potential as a function of the grid voltage after a charging period of 1 minute.

Charging times longer than 1 min. do not result in higher surface potentials.

An overall homocharging of the PVB film surface is obtained. The charging temp. is 70°C.

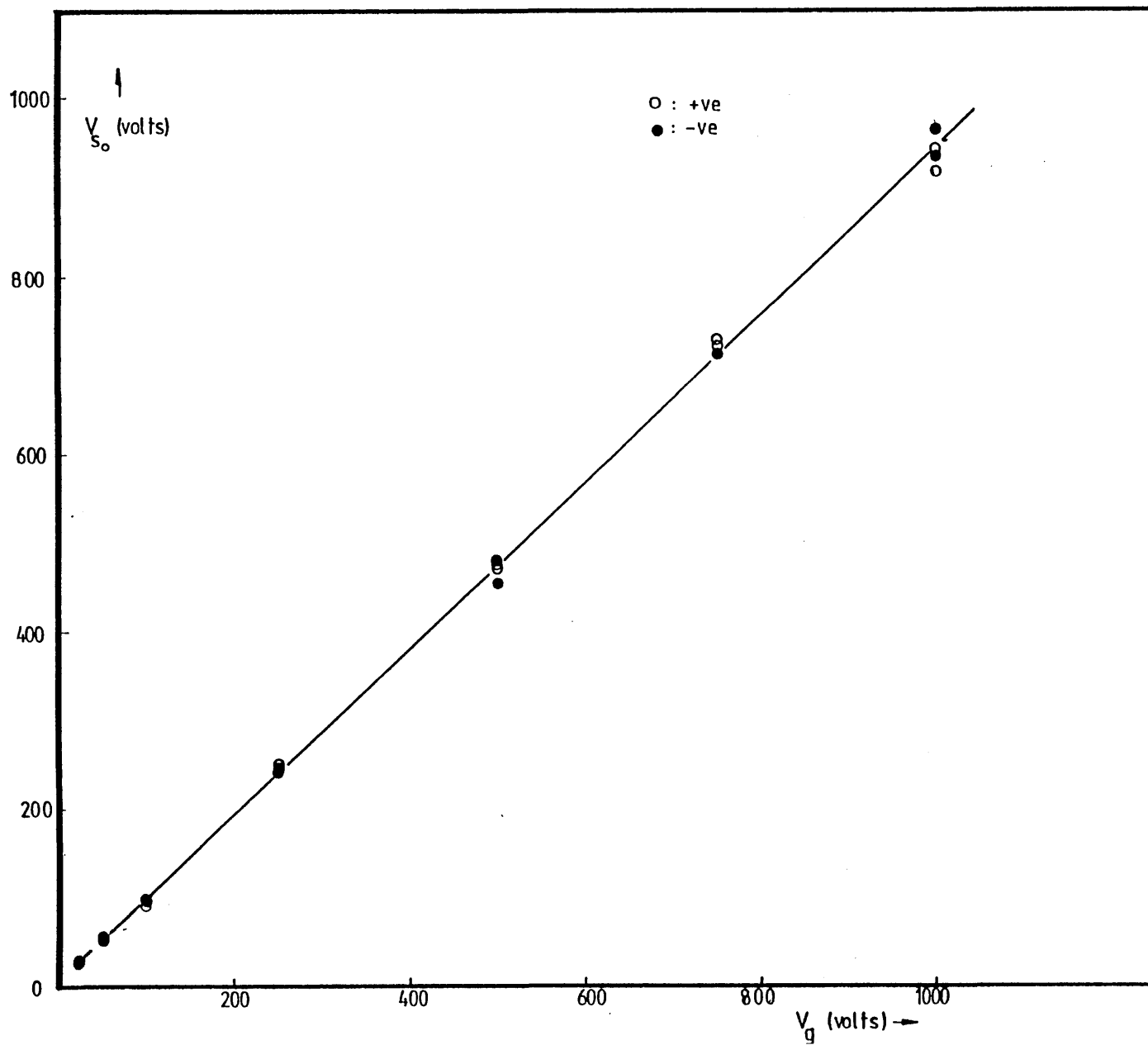


Fig.5.16(a)

Short circuit TSD current thermograms of corona charged 20 μ m films of PVB.

$T_p = 70^\circ\text{C}$, $r = 4^\circ\text{C min}^{-1}$, $t_p = 1 \text{ min}$.

The values of the grid voltages during corona charging are shown in the inset.

A dipole peak can be clearly seen, however the space charge peak above T_g is not observed at all.

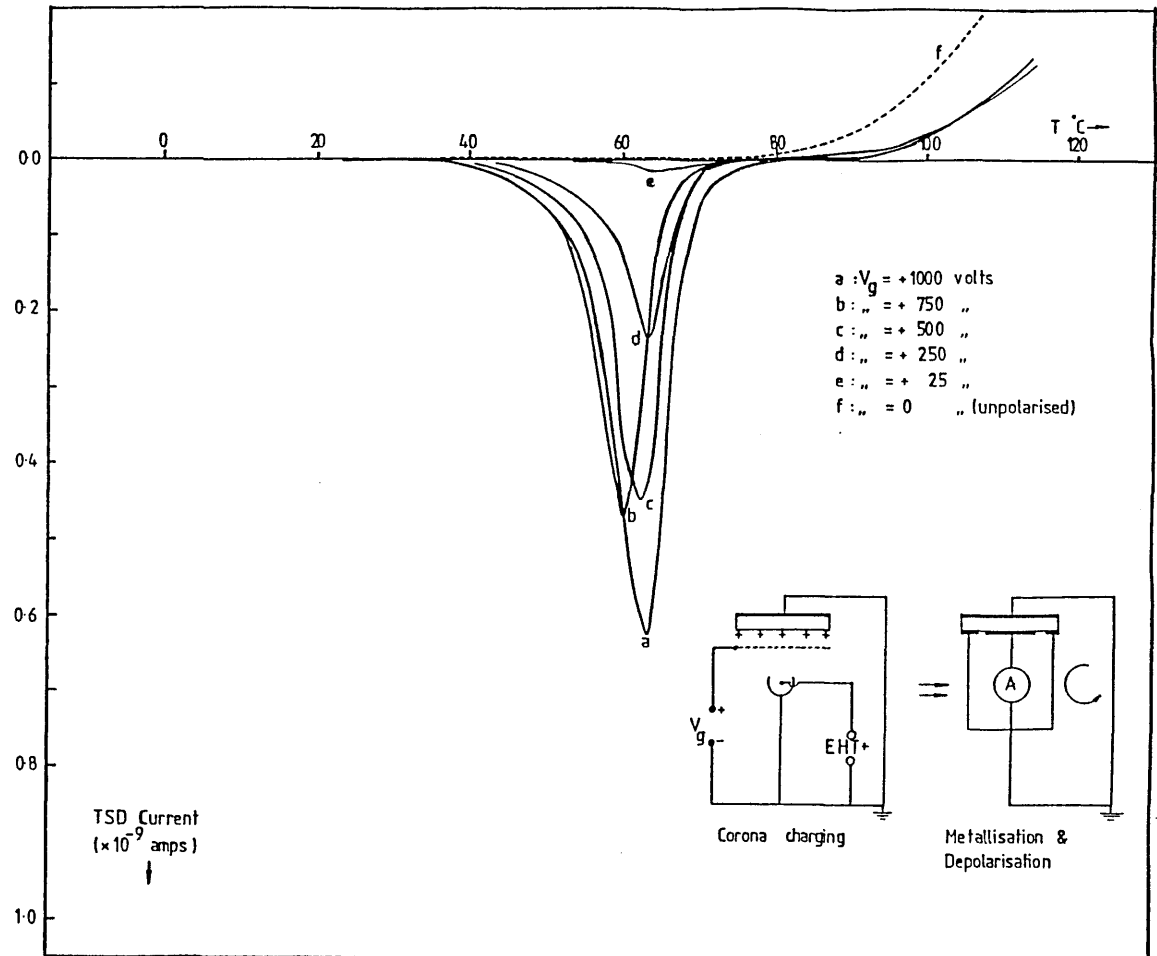


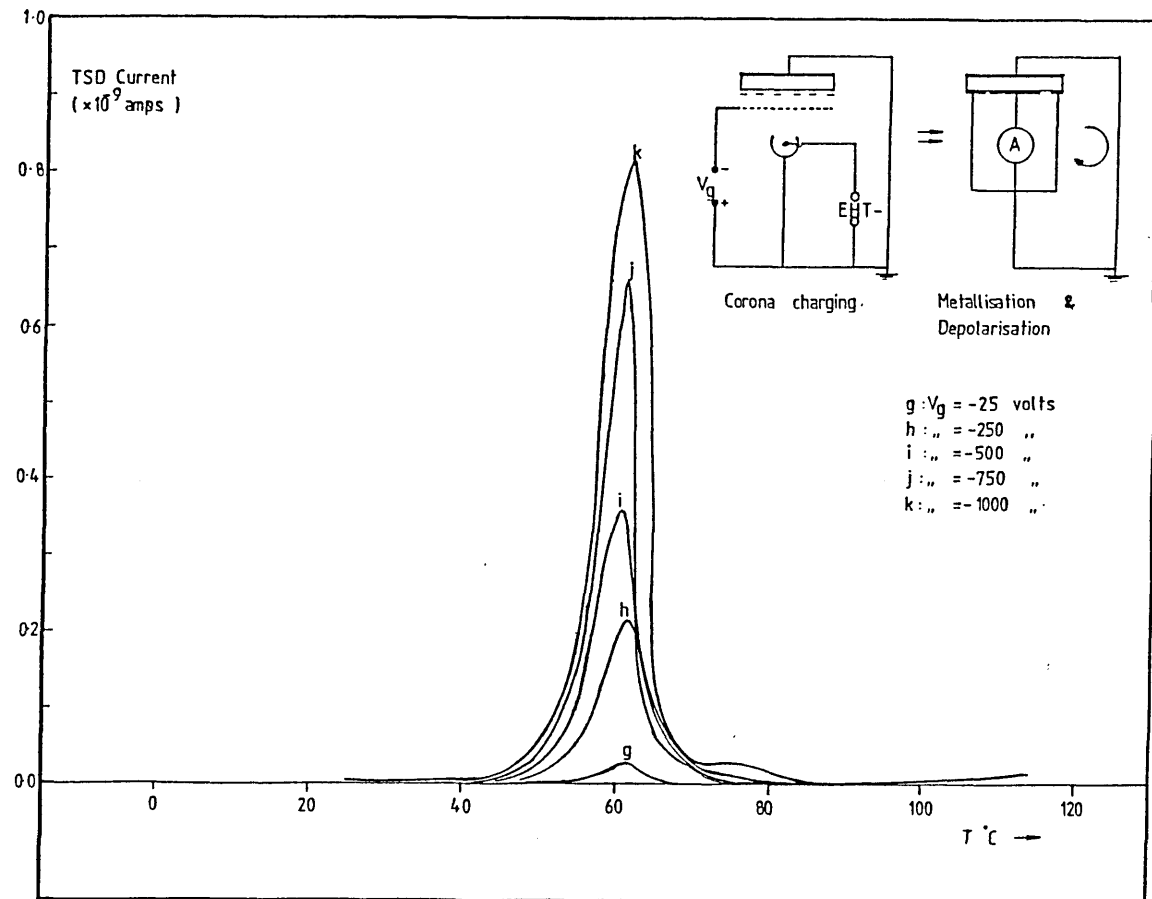
Fig.5.16(b)

Short circuit TSD current thermograms of corona charged PVB films.

$T_p = 70^\circ\text{C}$, $r = 4^\circ\text{C min}^{-1}$, $t_p = 1 \text{ min}$.

Values of the grid voltages are shown in the inset.

Clear and well-defined dipole peaks are observed. Space charge peaks are absent.



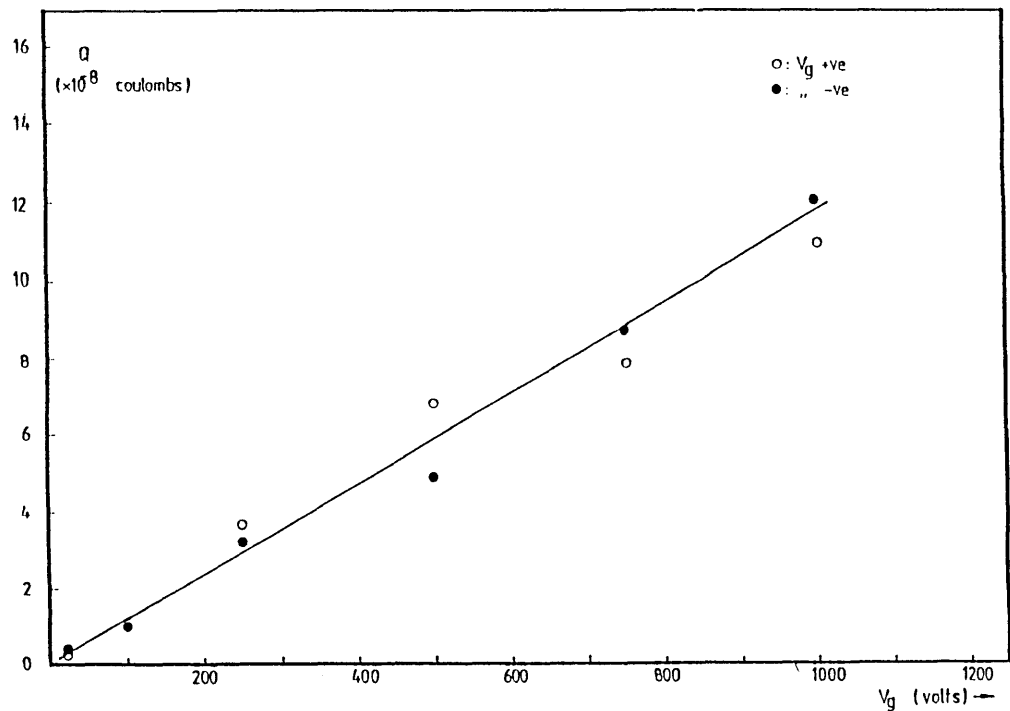


Fig.5.17 Released TSD charges obtained by the graphical integration of the TSD peak as a function of the magnitude of the grid voltage.

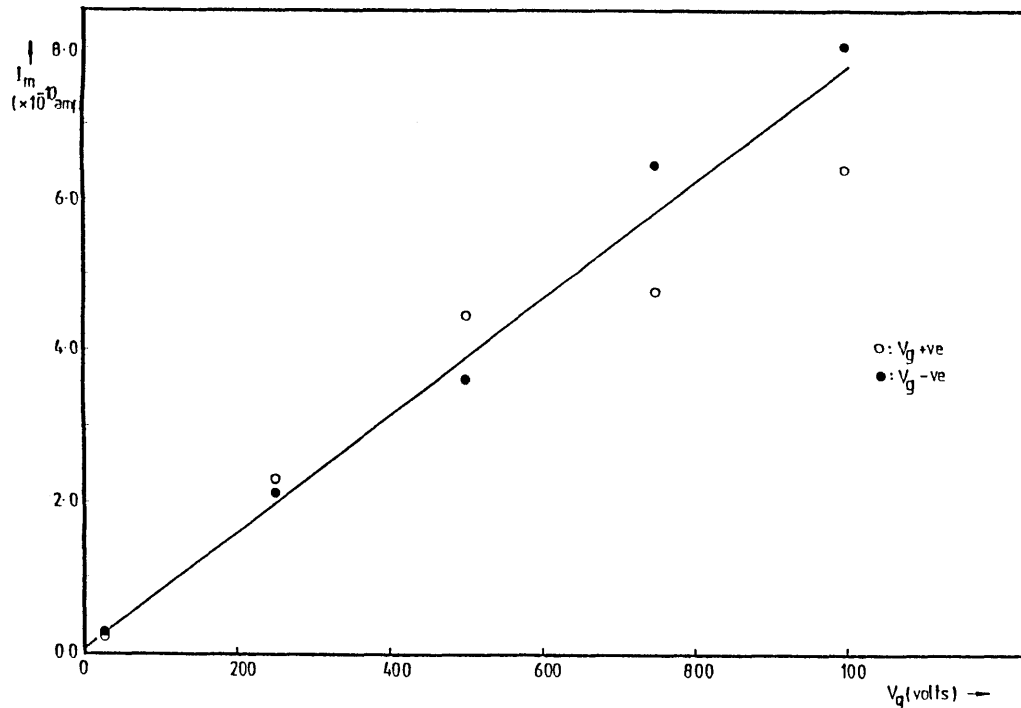


Fig.5.18 Magnitude of the TSD peak currents as a function of the grid voltage .

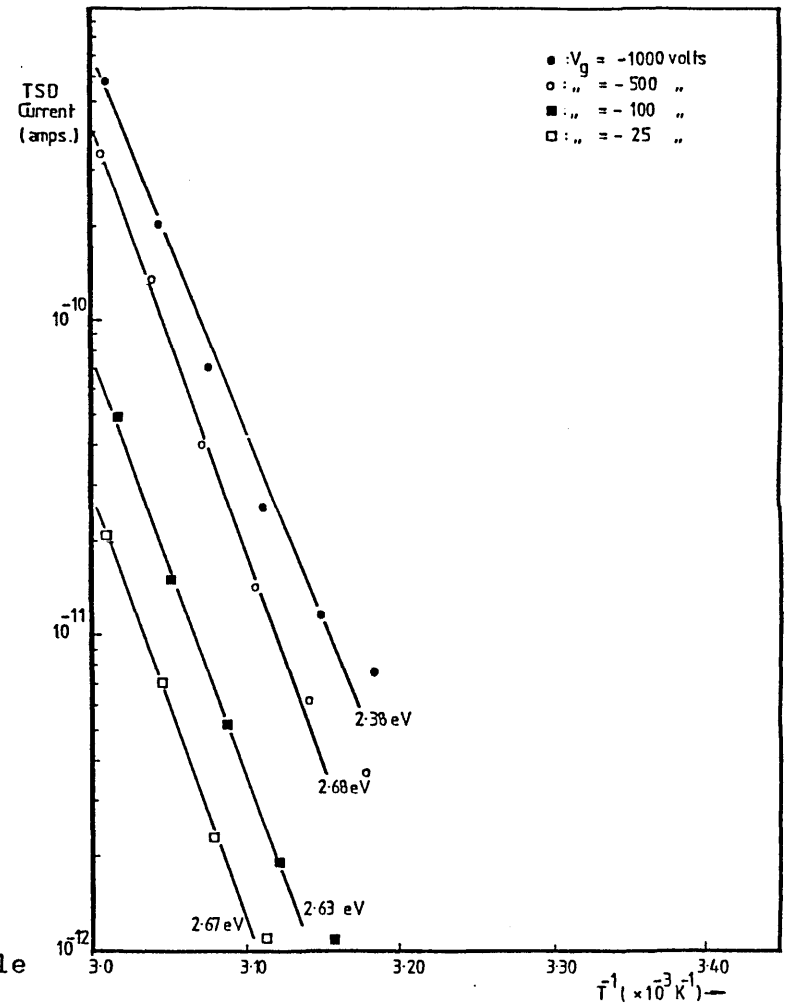
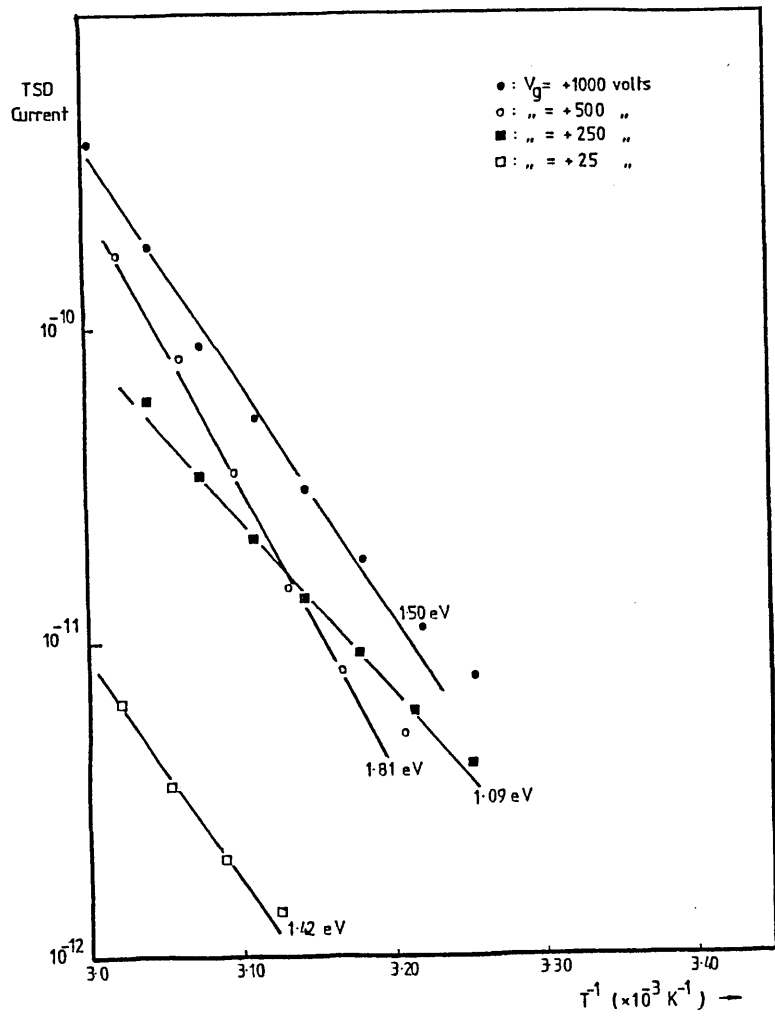


Fig.5.19 (a,b)

Initial Rise Plots of the Dipole peaks.

- a) positive V_g 's ,left
- b) negative V_g 's ,right

and the peak currents on the magnitude of the grid voltage all indicate that dipole disorientations **is** the dominant relaxation process responsible for the appearance of the current peaks. Comparison with the TSD current thermograms of the metallised DC charged films (section 5.2.1) shows that the peaks detected **are** actually similar to the α -relaxation peaks, thus confirming that **they are of a dipolar** origin.

The relaxation peaks of the corona charged films are also relatively sharper than those of the DC charged films. The apparent energies of activation calculated by the initial rise method for the former are also of a higher value than the latter. These two observations are consistent with the view that a significant truncation of the dipole relaxation peaks has occurred during the time lapse between coronacharging and final depolarisation in the short - circuit mode. In the present experimental set-up the sequence of corona charging, top electrode metallisation and the final depolarisation in the cryostat required a time lapse of about 60 to 80 minutes. It is believed that this have sufficiently allowed the disorientation of the relatively fast, low activation energy dipoles before the sample could be depolarised through the electrometer. Therefore, at the start of the TSD run only the long-lived dipoles would be available to contribute to the final depolarisation current.

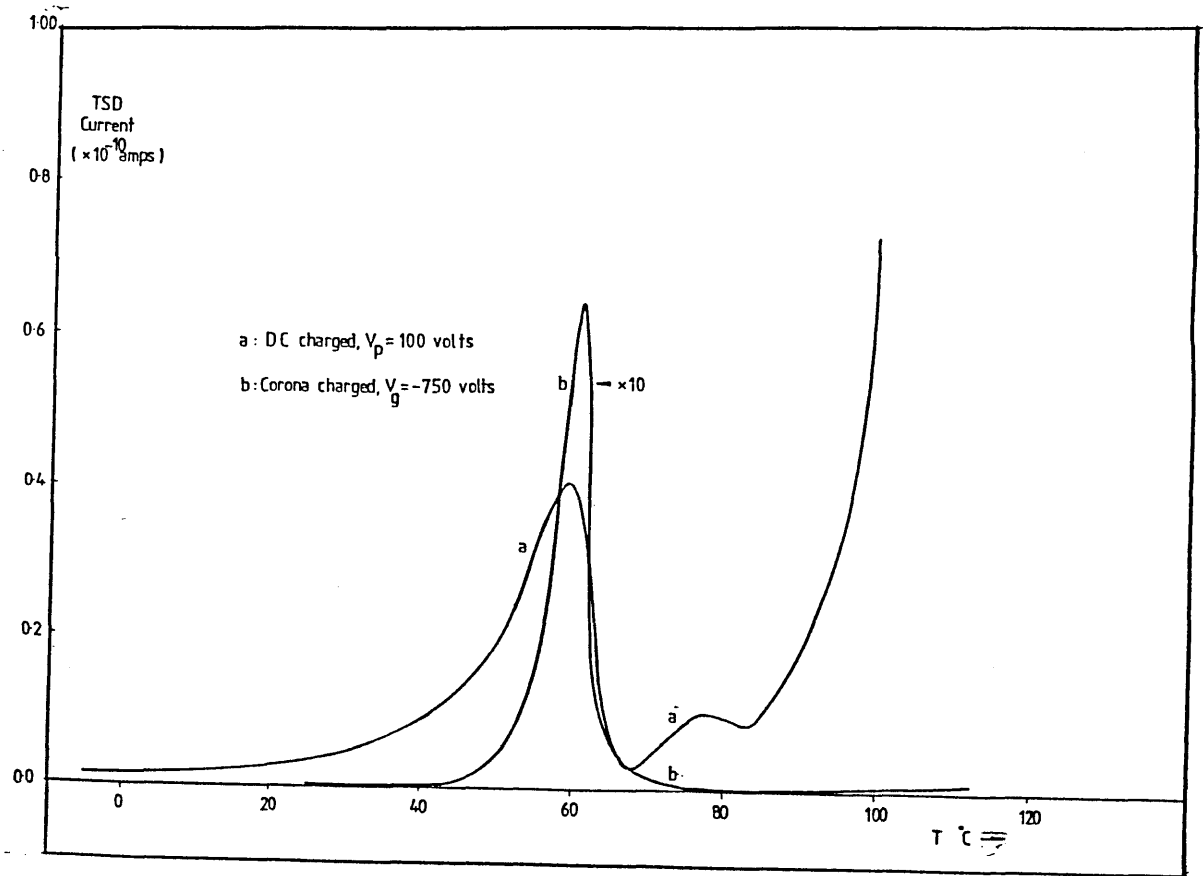
Absence of the Space Charge (ρ) peaks

Another interesting result for the corona charged films is that the high temperature peaks expected at about 78 °C **are** conspicuously absent from the current thermograms. A comparison with a thermogram of a DC charged sample clearly demonstrate this observation (fig.5.20). The absence of a current peak due to a space charge process in the corona charged PVB film is initially considered to be a surprising experimental observation in view of the large amount of reported work on the study of surface and bulk trapping states in a variety of organic polymer films (for e.g., Creswell and Perlman 1970,

Fig.5.20 Comparison between the short-circuit TSD current thermograms of a DC charged and corona charged sample.

The dipole peak of the corona charged sample is relatively sharper than the DC charged counterpart.

For the corona charged sample, the space charge peak above T_g is absent.



Kao et.al 1979, Gross 1981, Von Seggern 1981a, 1981b and Von Seggern and West 1984). A closer examination of the of the actual processes involved during the corona charging would be helpful in an attempt to elucidate the observed behaviour of the PVB films.

A detailed discussion of the physico-chemical interactions between the corona ions and polymer surface is beyond the scope of this thesis, nevertheless there are several points that are worth noting. Shahin (1966, 1969) has shown that the dominant species in a positive DC corona discharge in ambient laboratory air are hydrated protons, $(H_2O)_nH^+$ where $n = 1, 2, \dots, 9$, depending on the relative humidity. For a negative corona, the dominant ionic species are CO_3^- and its hydrated derivative $CO_3^-(H_2O)_{1,2}$. Gallo (1969) has also suggested that hydrated electrons $(H_2O)^-$ may also be present in negative corona discharge. The interactions of these ions with the surface would be determined primarily by the recombination energy (RE) of the ion and the work function ϕ_s of the polymer surface. For a positive ion, surface reaction would occur if $RE > \phi_s$ and this may involve a charge exchange with a surface atom resulting in the charge being trapped by a surface state. If $RE < \phi_s$, then no charge exchange is possible. The ions then stay on the surface, being held only by electrostatic forces. In addition to the possibilities previously mentioned, physical changes like pitting or removal of oxidised layers from the polymer surface may also take place (Blais et. al. 1971, Schomhorn et. al. 1974).

Vibrationally excited neutral molecules of NO_2 , N_2 and O_2 may also play an important part in the charging of the polymer surface. Haridoss et. al. 1982 has observed that the excited neutral molecules could act as efficient injectors of any previously surface trapped negative charges (electrons) into energetically shallower bulk states of several polymers, like low density polyethylene, polypropylene and poly tetra fluoroethylene. Charge injection is however not detected

for the case of positive charging of the polymers quoted. Moreno and Gross 1976, in their work on films of poly fluoroethylene propylene however observed charge injection only for the case of positive corona charging. Charge injection by negative coronas was reported to be absent.

It seems that the physical extent of charge injection by corona ions into a polymer surface is highly dependent on the type of polymer, the polarity of the corona ions and specific physical conditions of the surface (Von Seggern 1979, Haridoss and Perlman 1984). Based on the discussions above it would be difficult to ascertain whether there was any injection of charges into the PVB films. The lack of knowledge about the actual ions and other physical variables that were involved does not allow any proper consideration to be made. However, it could generally be said that the physical extent of the injected charges would be limited to regions near the surface and as such, any post-treatment of the charged surface could have a significant effect on the final TSD characteristics of the film.

Top electrode metallisation of the polymer surface would destroy any loosely held ions and this may lead to a significant modification to the eventual short-circuit TSD current thermograms. For the injected charges, the heat of condensation of the gaseous metal atoms may cause a significant change to their trapping behaviour, leading to an overall modification to the polarisation of the film itself.

It is worth noting that Baba and Ikezaki 1982, 1985 and Ikezaki et al. 1984 have reported the observation of significant modifications to the current thermograms of partially crystalline films of polypropylene and polyethylene which were directly attributable to the metallisation process. It was concluded that the heat released by the condensation of the metal atoms was so large that the degree of crystallinity of the surface region was changed. The changes in the crystallinity of the surface resulted in the final changes to the TSD current thermograms of the films.

Apart from the effects of the top electrode metallisation which may have annihilated the loosely held charges on the PVB film surface, any injected charges residing at the near surface regions (which have survived the effects of the metallisation) could also be quickly neutralised by thermally generated carriers from the bulk of the film before the TSD run. In view of the large electrical conductivity of the sample, this mode of "pre-neutralisation" of the space charge polarisation would also be highly probable. This internal conduction current effectively limits the degree of attainable space charge polarisation by supplying oppositely charged carriers to the surface region where they neutralise the corona injected charges.

Finally, it has to be noted that the non-appearance of the high temperature peak in the short-circuit current thermogram does not necessarily indicate that a space charge polarisation is not present in the film before the start of the TSD run. It has been pointed out in section 2.3, chapter 2, that the neutralisation of a space charge layer in the bulk of a short-circuited and homogenous sample by the internal conduction current would not be observed. It is thus still possible that a space charge layer may be present at the near-surface region of the film and be neutralised without being observed by the external circuit.

5.2.2.4 Conclusions

The short-circuit TSD current spectra of PVB films that were corona charged at 70°C reveal that a dipole polarisation was achieved during the charging period, however, due to the necessary time lapse required for the top electrode metallisation, a significant number of the aligned dipoles became disoriented before they could be depolarised in a TSD run. The truncation of the dipole polarisation results in sharp TSD current peaks due to the absence of the contribution of the dipoles with short relaxation times. The apparent activation energy of the dipole relaxation found from the initial rise plots range from 1.09 to 2.68 eV.

It is found that the use of a short-circuit TSD current measurement utilising evaporated metal electrodes on samples that were corona charged would not yield a complete account of all the known depolarisation characteristics of the polymer. It is believed that the process of top electrode metallisation may have caused a significant modification to the original corona-induced polarisation. This also contributed to the non-appearance of the known space charge peak.

The inherent inefficiency of the short-circuit measurement in detecting the decay of the space charge polarisation is also a contributory factor to the non-appearance of the TSD current peak. Due to the reasons cited above, it was decided to carry out measurements on the corona charged films by an electrode-less technique which will be described in the next section.

5.2.3 TSD of Surface Potential - " Charge " TSD

5.2.3.1 Preliminary

It has been discussed in chapter 2 (sect.2.3) that the decay of a space charge polarisation in a short-circuited, metallised electret would not be efficiently observed. In particular, the decay of the frozen-in space charges in a homogenous sample by internal ohmic conduction during the TSD would not be observed at all. This is considered to be a serious experimental limitation, since in a polymer with a high electrical conductivity (e.g PVB) internal conduction could be a dominant mechanism in the restoration towards overall electrical neutrality.

The results of the TSD of samples carried out in the short-circuit mode (DC charged and corona charged) of the previous sections have revealed that the current peaks associated with the neutralisation of a space charge layer are relatively not well-defined and are of small magnitudes. For the corona charged samples, the combination of top electrode metallisation and high bulk conductivity even resulted in the complete absence of the known space charge peaks.

In this section the results of the "Charge" TSD measurements will be discussed. The measured quantity is the persistent surface potential of the PVB films. Since a top electrode metallisation is not required, any effects associated with the metallisation process that may have contributed to the loss of the corona induced polarisation can thus be avoided.

The samples were first charged by a DC corona using the usual experimental arrangement for a period t_p of 1 minute. The temperature of the samples, T_p was chosen as 30 °C or 70 °C depending on the experiment. The samples were immediately discharged at a rate r of 4 °C min⁻¹. The effective surface potential was measured with a non-contacting electrostatic voltmeter. The aluminium substrate remained grounded throughout the course of the measurement.

5.2.3.2 Results

The sign of the observed surface potential of the films were similar to the grid voltage V_g , i.e overall homocharging were achieved. There was also no reversal in the sign of the surface potential throughout of the course of the TSD run.

The thermally stimulated surface potential decay curves of films polarised at $T_p = 30^\circ\text{C}$ are shown in fig.5.21. The decay curves display a characteristic two-step like drop which is believed to be indicative of two different processes contributing to the overall loss of electrical polarisation in the films. It could be seen that there are two distinct temperature regions centred at about 60°C and 85°C where the rates of surface potential decay are high. Similar results are obtained for positively charged samples.

The dependence of the decay of the surface potential on $V_g(0)$, its initial value, is shown in fig.5.22 and 5.23 for positive and negative polarisation voltages respectively. The plots are normalised to their respective initial surface potentials, $V_g(0)$, which is taken immediately after each corona charging. Only the individual decay curves for $V_g = +25, +1000$ volts and $V_g = -25, -1000$ volts are shown in the respective figures. For samples that were charged with intermediate values of V_g , it was found that their decay plots fell in the shaded regions of the plots. In the high temperature region, the higher charged samples exhibit a slightly higher rate of surface potential decay.

In fig.5.23 the isothermal decay curves of samples charged at $T_p = 30^\circ\text{C}$ and 70°C with $V_g = -500$ volts are also shown. From a comparison of the general shapes of the isothermal and thermally stimulated decay curves, it is clear that apart from considerably speeding up the loss of the overall electrical polarisation, the TSD curves are also more structured and hence, are more informative with regards to revealing the decay mechanisms involved.

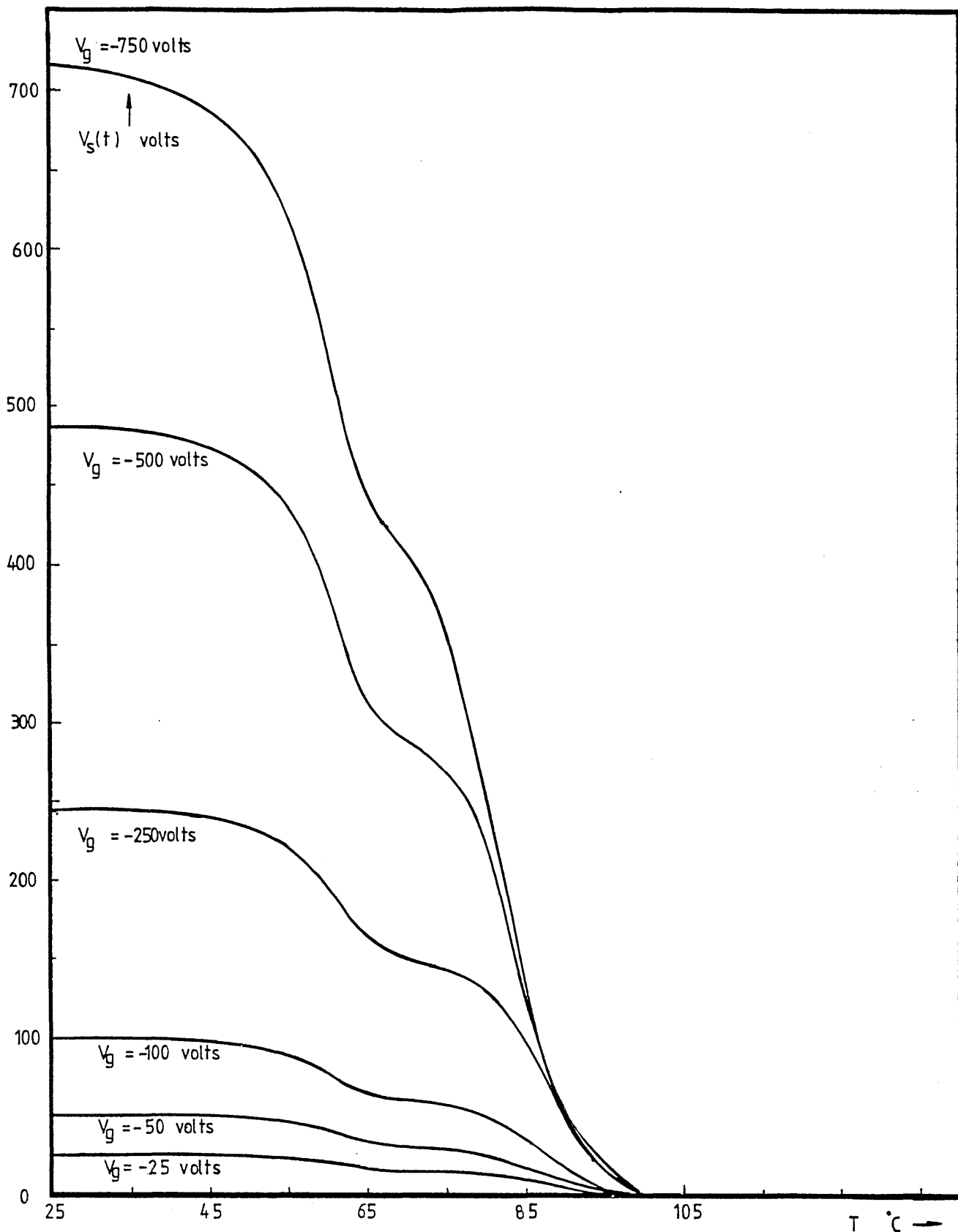


Fig.5.21

Thermally Stimulated Surface Potential Decay of unmetallised 20 μ m thick PVB films.

$T_p = 30$ °C, $r = 4$ °C min^{-1} , $t_p = 1$ min.

Values of the grid voltages used during the corona charging are noted. The decay curves exhibit a characteristic 2-step like drop indicative of two internal mechanisms.

Similar plots are obtained for positive values of V_g .

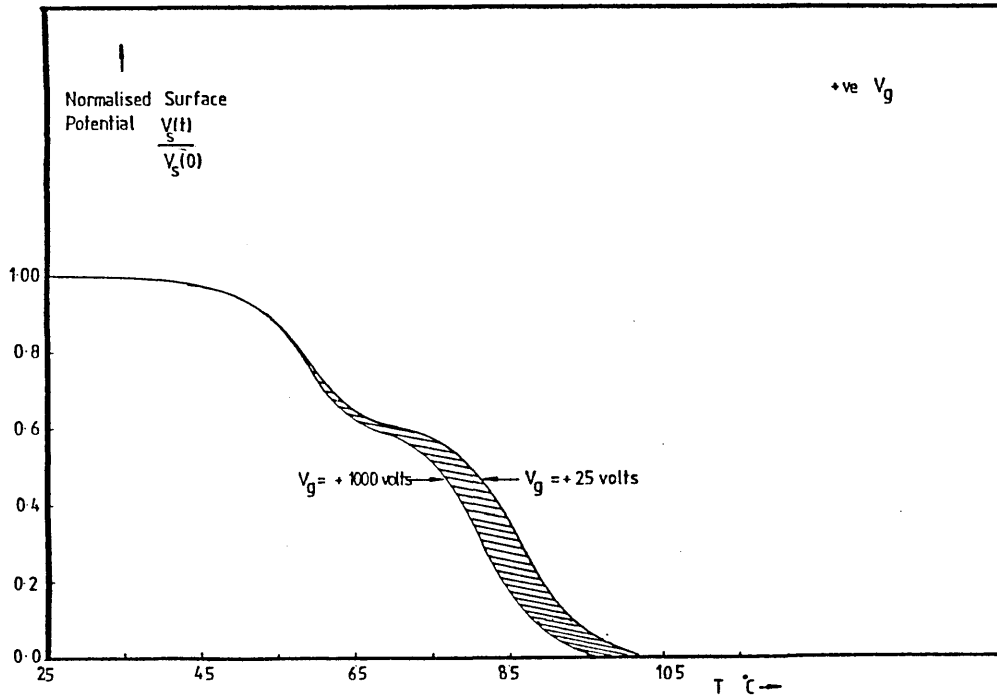


Fig.5.22 Normalised Thermally Stimulated Decay plots for positive surface potentials. The values of the surface potential are normalised to the initial values before the start of the TSD. Decay plots for intermediate values of V_g are enveloped between the V_g plots for $V_g = +1000$ and $+25$ volts.

$$T_p = 30^\circ\text{C}, r = 4^\circ\text{C min}^{-1}, t_p = 1 \text{ min.}$$

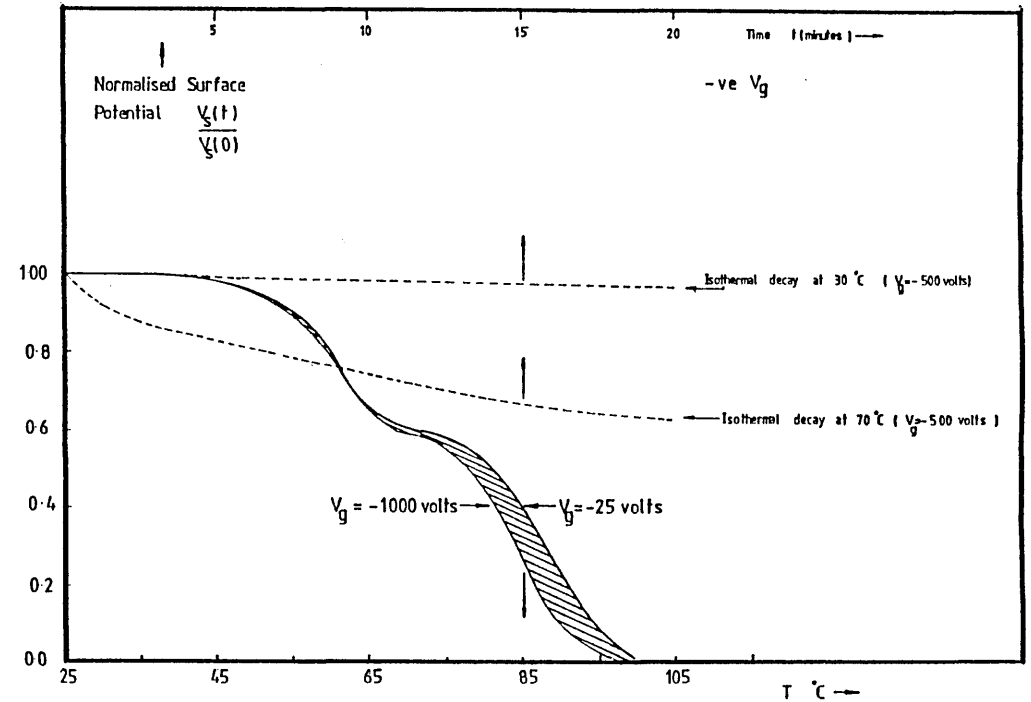


Fig.5.23 Normalised Thermally Stimulated Surface Potential decay plots for negative surface potentials. Data is similar to that of fig.5.21.

TS decay plots for intermediate values of V_g 's are enveloped by the plots of $V_g = -1000$ and -25 volts.

The Isothermal decay plots for samples charged with $V_g = 500$ volts are also shown. These plots are less structured compared to the thermally stimulated decay plots.

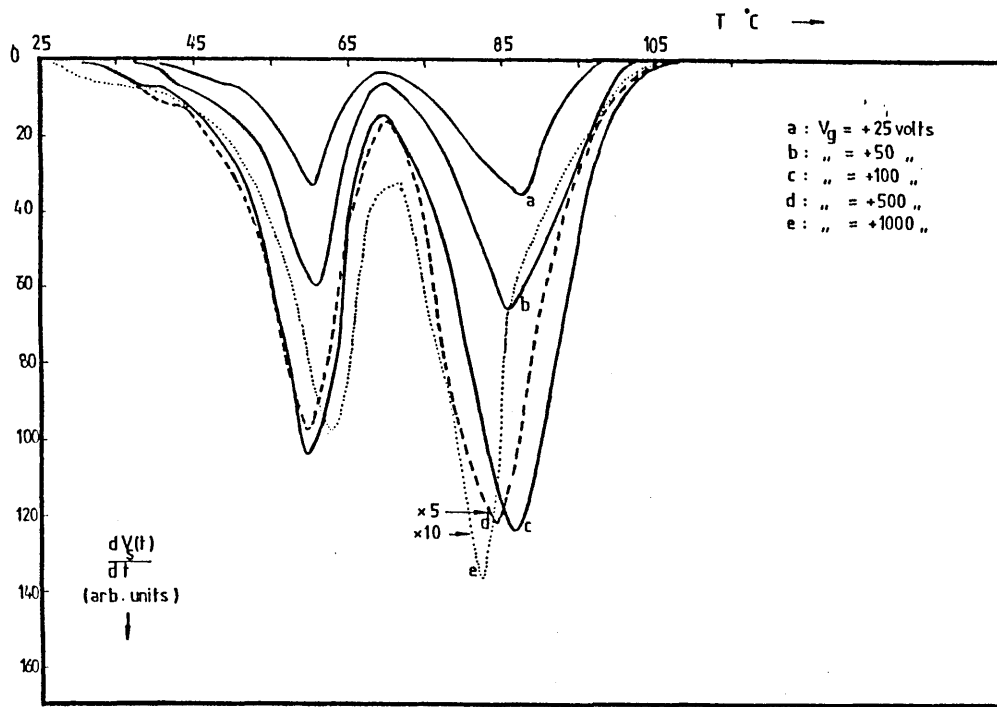


Fig.5.24 Time derivative of the thermally stimulated surface potential decay plot for positive V_g 's. This open-circuit TSD displacement current thermogram evidences two distinct processes operating during the surface potential decay. $T_p = 30^\circ\text{C}$, $r = 4^\circ\text{C min}^{-1}$, $t_p = 1 \text{ min}$.

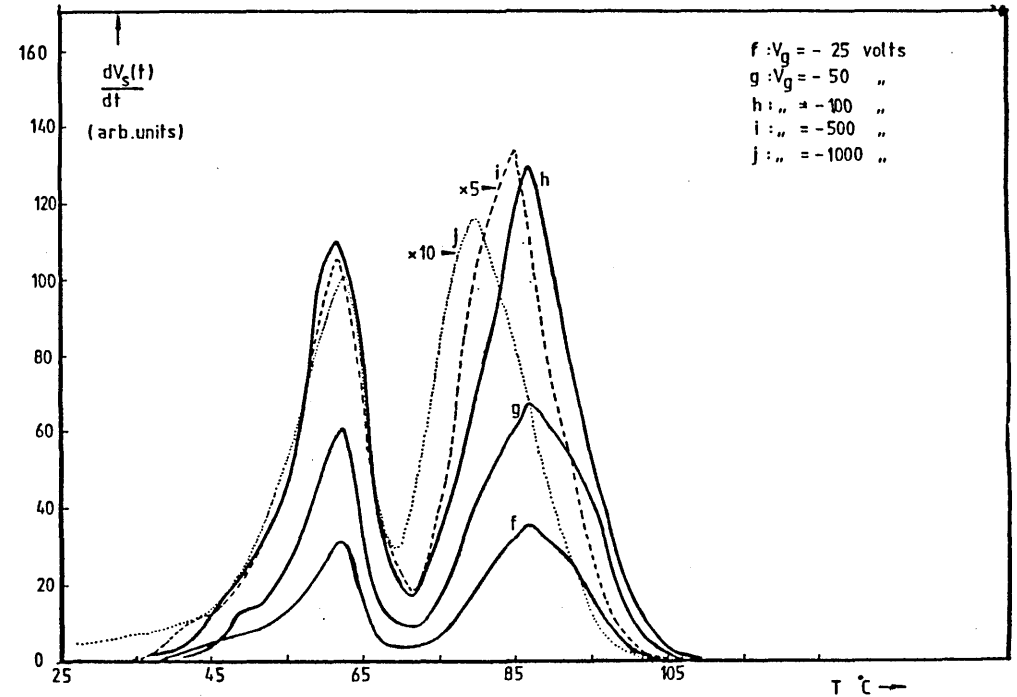


Fig.5.25 Time derivative of the thermally stimulated surface potential decay plot for negative V_g 's. Two distinct peaks are observed. For large values of V_g , a shift in the high temperature displacement current peaks towards lower temperatures are observed. The reason for this shift is unclear.

The time derivative of the surface potential decay plots are shown in fig.5.24 for positive V_g 's and in fig.5.25 for negative V_g 's. The plots, which are proportional to the displacement current, clearly reveal the presence of the two temperature regions within which the rates of surface potential decay had been greatest. These two regions are shown by the corresponding peaks in the plots. The plots also show the slight temperature shifts of the high temperature peaks towards lower temperatures as the grid voltage were increased. The temperature shifts are more noticeable for the large V_g curves.

5.2.3.3 Discussions

Since the upper surface of the films were not metallised, it could be assumed that apart from the injected charges that were trapped by atoms of the surface molecules, some electrostatically held charges may also be present on the surface. Also, since the samples were polarised at 30°C, which was well below T_g , it is expected that the majority of the dipoles in the sample bulk has had no chance to be oriented (it is noted that dipole polarisation could be achieved in room temperature charged samples as was shown by Southgate 1976 and Das-Gupta and Doughty 1978).

The surface potential that is observed $V_s(t)$, is proportional to the algebraic sum of $Q(t)$, the effective density of the surface charges due to ions and electronic carriers representing the nett homocharges and $P(t)$, the induced dipole polarisation which is the heterocharge. The equation describing the observed surface potential has been written in chapter 2, eqn.2.63. This is reproduced below.

$$V_s(t) = \left[Q(t) - P(t) \right] \frac{l}{\epsilon_0 \epsilon_\infty}$$

where l is the thickness of the FVB film.

The decay of the surface potential during the TSD run would depend on the individual responses of $P(t)$ and $Q(t)$ to the temperature rise. It has already been known from the previous sections that in general dipolar

processes respond at a lower temperature than the processes involving the gross motion of space charges. This is understandable because the former involves only the re-orientation of groups of atoms while the latter involves the dissociation and the translational displacement of ionic groups through the sample bulk.

For the samples polarised at $T_p = 30^\circ\text{C}$ (figs. 5.21 and 5.23), the initial decay of the observed surface potential is caused by a transient dipole polarisation. As the temperature of the sample is raised, the random dipoles become orientated as they gain increased rotational mobilities. This situation is similar to that of a thermally stimulated polarisation (sect. 5.2.1.4) but in this case, the polarisation field is caused by the space charge layer residing on the surface of the films. The temperature at which the rate of surface potential decay was highest also coincided with the glass transition temperature of the films. The derivative of the surface potential decay curve clearly indicate this correspondence with T_g (fig. 5.24 and 5.25). This correspondence consolidates the view that dipole orientations is the dominant mechanism responsible for the drop in the observed surface potential.

The decay of the observed surface potential could also be described by eqn. 2.63 . With increasing $P(\tau)$, the value of $V_s(t)$, the effective surface potential drops accordingly. It is assumed that in this temperature range, the bulk conductivity of the sample is still too low to supply the carriers to neutralise the space charge layer on the surface of the film. Thus, it is believed that the initial drop in the surface potential is solely due to the dipole orientation.

The increase in the dipole polarisation gradually ceases as the number of still-random dipoles becomes exhausted. This also retards the rate of decay of the observed surface potential. As the temperature is raised further, the increased electrical conductivity of the sample bulk also results in more thermally generated carriers being transported to the surface region

where they neutralise the homocharges. The decrease in $Q(t)$ also weakens the internal field causing the oriented dipoles to randomise quickly as now the magnitude of the thermal agitations is also significant. This dynamic equilibrium of the processes described above is manifested by the plateau regions in the surface potential decay curves.

Beyond this plateau region, the decay of surface potential is due to the final neutralisation of the surface homocharges. It is believed that the dominant mechanism responsible for this decay is the internal ohmic conduction of carriers from the sample bulk in view of the large electrical conductivity of the sample at these temperatures ($\sim 70^\circ\text{C}$). Other decay processes such as the diffusion and the self-drift of the homocharges will both assist in the eventual decrease in the surface potential but their respective contributions would most probably be masked by the strong internal conduction.

The plots of the time derivative of the surface potential vs. the temperature (figs. 5.24 and 5.25) both show two peaks corresponding to the mechanisms described. The first peak is due to the orientation of the dipoles while the second peak is due to the decay of the surface charges. It is interesting to note that this latter peak would not be observed if the measurements were carried out in a short-circuit configuration. The increased efficiency of the measurement in the open-circuit mode is due to the presence of the air gap which blocks any charge exchange between the detecting electrode (the electrostatic voltmeter probe) and the polymer surface. With this arrangement, all the induced image charges on the non-contacting probe could only be eventually released by processes within the sample.

As was discussed in sect. 2.6.3, the plot of $\ln \left[V_s(T) \cdot \frac{dV_s(T)}{dT} \right]$ vs. T^{-1} for the second region of the decay curves would be linear from which the apparent activation energy of the ohmic conduction in the sample bulk could be found. The plots for several values of V_g are shown in fig. 5.26. The average value of the activation energy was found to be about 2.03 eV. The activation energy calculated from the charge decay plot could also be compared

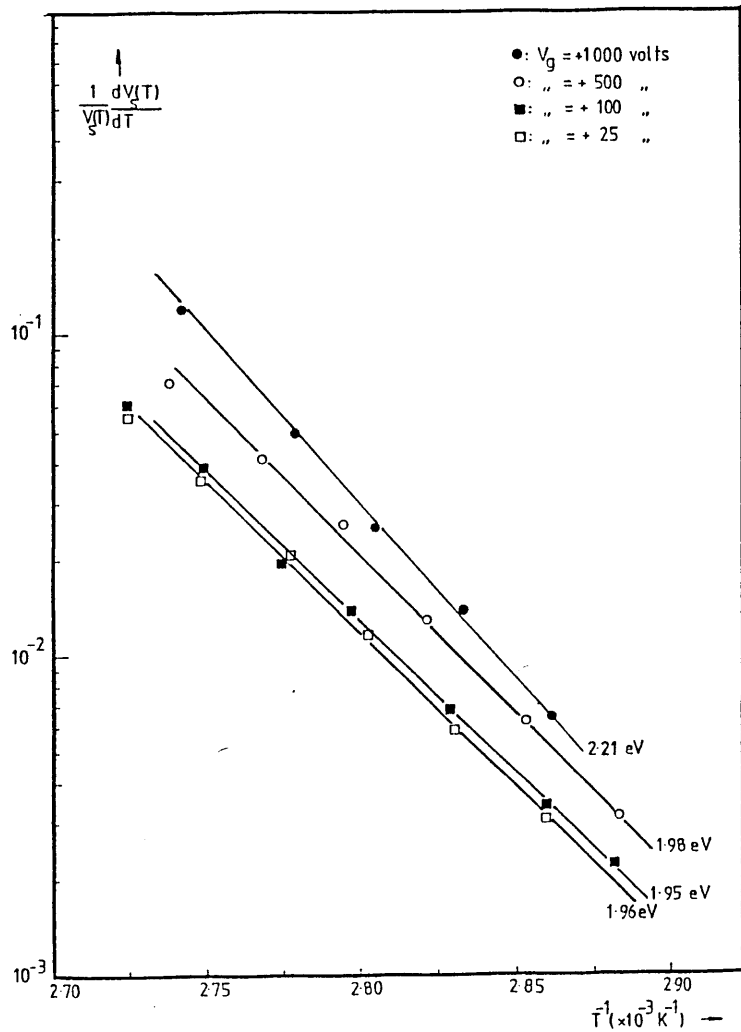


Fig.5.26 Calculation of the activation energy for the decay of the surface homocharges by the internal bulk conduction of the PVB film. The slopes of the plots define the apparent activation energy. Plot are for the samples charged at $T_p = 30^\circ\text{C}$.

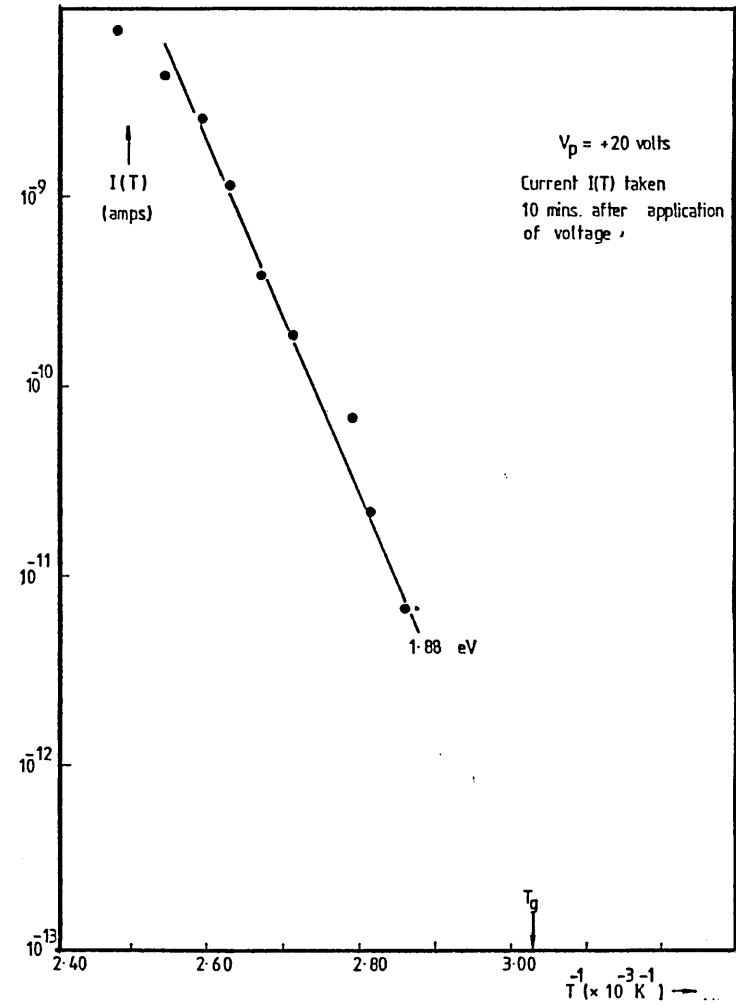


Fig.5.27 $\ln I(T)$ vs. $T^{-1} (\times 10^{-3} \text{K}^{-1})$ for $20\mu\text{m}$ thick PVB film. "Steady state" current values are taken 10 mins. after application of field. Measurements are carried out above T_g .

with a typical value from a conventional current-voltage-temperature plot of the PVB film (fig.5.27).The activation energy calculated from the slope of this plot was found to be about 1.88 eV.In this measurement the values of the currents were taken 10 minutes after the application of the voltage.It has to be noted that the values of the currents taken at this time lapse were only approximate steady-state values.The measurements were carried out at temperatures above T_g to minimise the contribution of the displacement current due to dipole orientations.

Samples Charged at 70 °C

In order to verify that the initial decay of the observed surface potential was indeed due to dipole orientations rather than an identified charge decay process such as lateral charge spreading or surface ion compensation by air-borne molecules,* several runs were carried out on samples charged at $T_p = 70^\circ\text{C}$.It is believed that charging at this temperature would allow a significant number of dipoles to be orientated.However due to the large electrical conductivity at this high temperature,the deposited charges would also be less stable due to the increased neutralisation by the bulk carriers.

Fig.5.28 shows the results of the TSD decay of the 70 °C corona charged samples.The dotted curves in the figure depicts the initial surface potential decay of the samples before the start of the TSD run.It could be seen that the surface potential immediately decays at the cessation of the corona charging due to the combined effects of dipole polarisation and ohmic neutralisation of the deposited homocharges.The samples were left to stabilise

* Studies on surface charge decay by this mechanism (Anderson et.al 1973, Van Turnhout et.al 1976) has showed that this effect could be quite significant if the decay measurements are carried out in an open environment where constant replenishment of cosmic generated ions are available.In a closed-box environment such as was carried out in our work,this effect was found to be negligible

for a period of 10 minutes after which they were cooled to room temperature at a rate of about $10^{\circ}\text{C min}^{-1}$ before the start of the TSD run.

During the TSD the surface potential apparently increased up to about 65°C after which it finally decreased to zero. This increase in the observed surface potential could only arise from dipole disorientations. The decrease in $P(t)$ causes an apparent increase in $V_s(t)$ as described by eqn. 2.63. This increase in the observed surface potential is temporary since with the gradual increase in the temperature of the sample, the surface homocharges are also neutralised by the internal conduction. The decaying portion of the surface potential plot was also used to estimate the apparent activation energy for the internal conduction. A value of 2.07 eV is found from fig. 5.29.

The derivative of the surface potential decay plot is shown in fig. 5.30. Corresponding to the apparent increase in $V_s(t)$, the initial portion of the plots is of opposite sign to the overall direction of the main space charge decay peak. This is because, unlike the case for samples that were charged at $T_p = 30^{\circ}\text{C}$, the initial response of the dipoles in the sample is their overall disorientation instead of orientation.

It is also noted that in common with the samples that were charged at 30°C , the high temperature peaks of the displacement current curves also exhibit a shift towards lower temperatures, especially for large values of V_g . The shifts that were observed however do not seem to show any regular behaviour. The decay of the surface charges via a pure ohmic decay would not exhibit this behaviour, therefore in order to account for these observations, it is believed that at large initial surface potentials, some of the injected surface charges may become mobile and drift towards the bottom electrode. Due to the higher driving fields, the higher charged sample decays at a faster rate than a relatively weakly charged one.

The irregularity of the observed behaviour and its appearance only in the higher charged samples underline the influence of the large bulk

electrical conductivity in determining the overall decay characteristics of the homocharges. It is believed that due to the high rate of recombination of the drifting charges with the thermally generated carriers, the effect only becomes noticeable when there is a large density of drifting carriers. Unlike the case for the short-circuited DC charged samples where the charges did not have to drift far to reach the appropriate electrode, the drifting charges in the unmetallised film have to effectively traverse the whole thickness of the sample to be finally neutralised. Due to this increased distance, the probability of neutralisation by thermally generated carriers also increases, thereby reducing the impact of the self-drift of the charges on the observed decay of the surface potential.

5.2.3.4 Conclusions

The TSD of the persistent surface potential of unmetallised corona charged films of PVB evidences two different types of decay mechanisms. There exist two temperature regions where the rate of surface potential decay were high, resulting in distinctive shapes of the eventual decay curves.

The observed surface potential is the algebraic sum of two quantities of the opposite sign, namely the corona deposited ions and injected charges which constitute the homocharges and the dipole orientation which is a hetero-charge. The presence of a space charge layer at the surface of the film creates an internal electric field which caused interesting dipolar responses during the TSD run. Depending on the state of polarisation of the dipoles at the start of the TSD run, either dipole disorientations or their orientations could be observed. The temperature at which these dipolar processes exhibit their maximum rates of response also coincide with the glass transition temperature of the polymer ($\sim 57^{\circ}\text{C}$). These dipolar responses dominate the overall behaviour of the observed surface potential in the first temperature region.

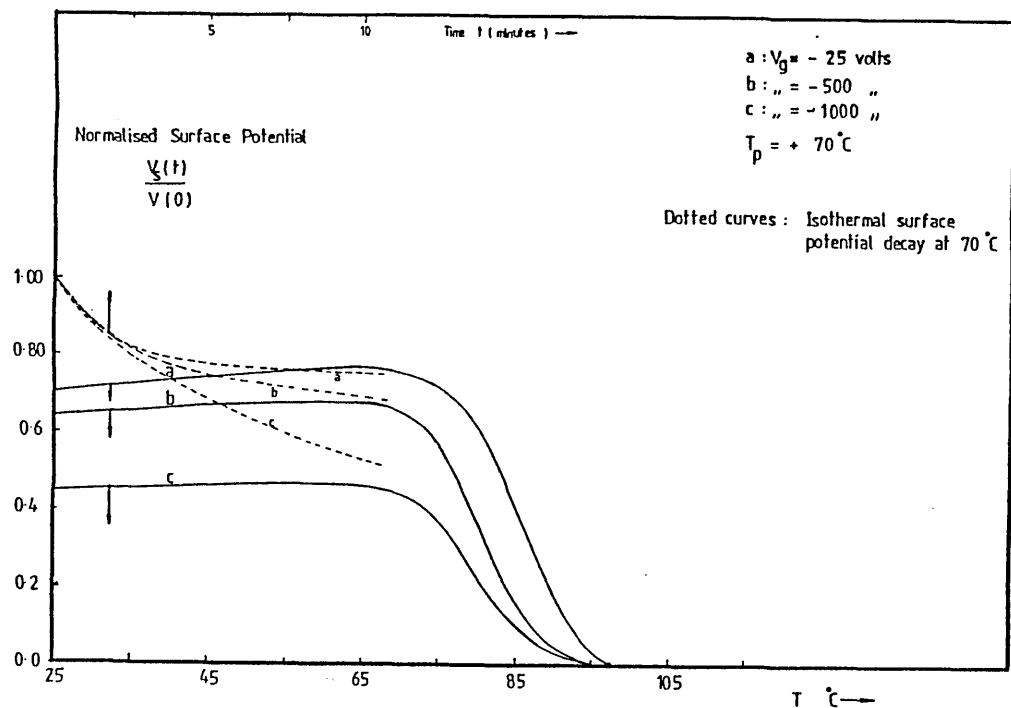


Fig.5.28 Normalised plot for the thermally stimulated surface potential decay of films corona charged at $T_p=70$ C.

The transient increase in the observed surface potential is due to dipolar disorientations, causing a decrease in the heterocharge polarisation. This results in the overall increase of the homocharge polarisation.

The dotted curves show the initial isothermal decay of the surface potential.

Heating rate $r = 4\text{C min}^{-1}$.

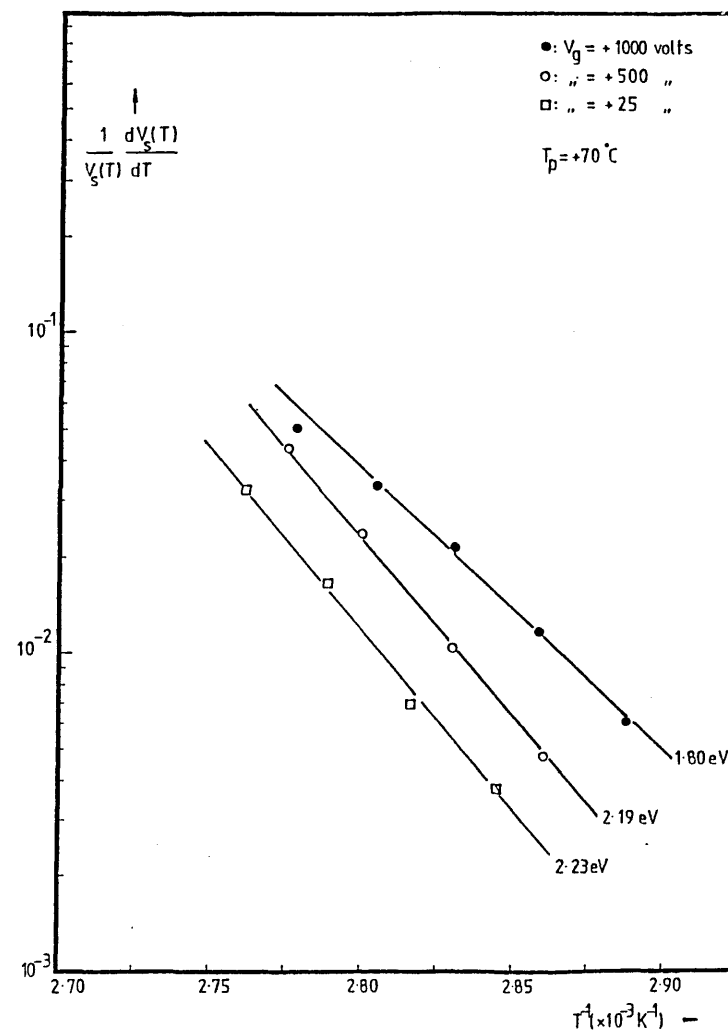
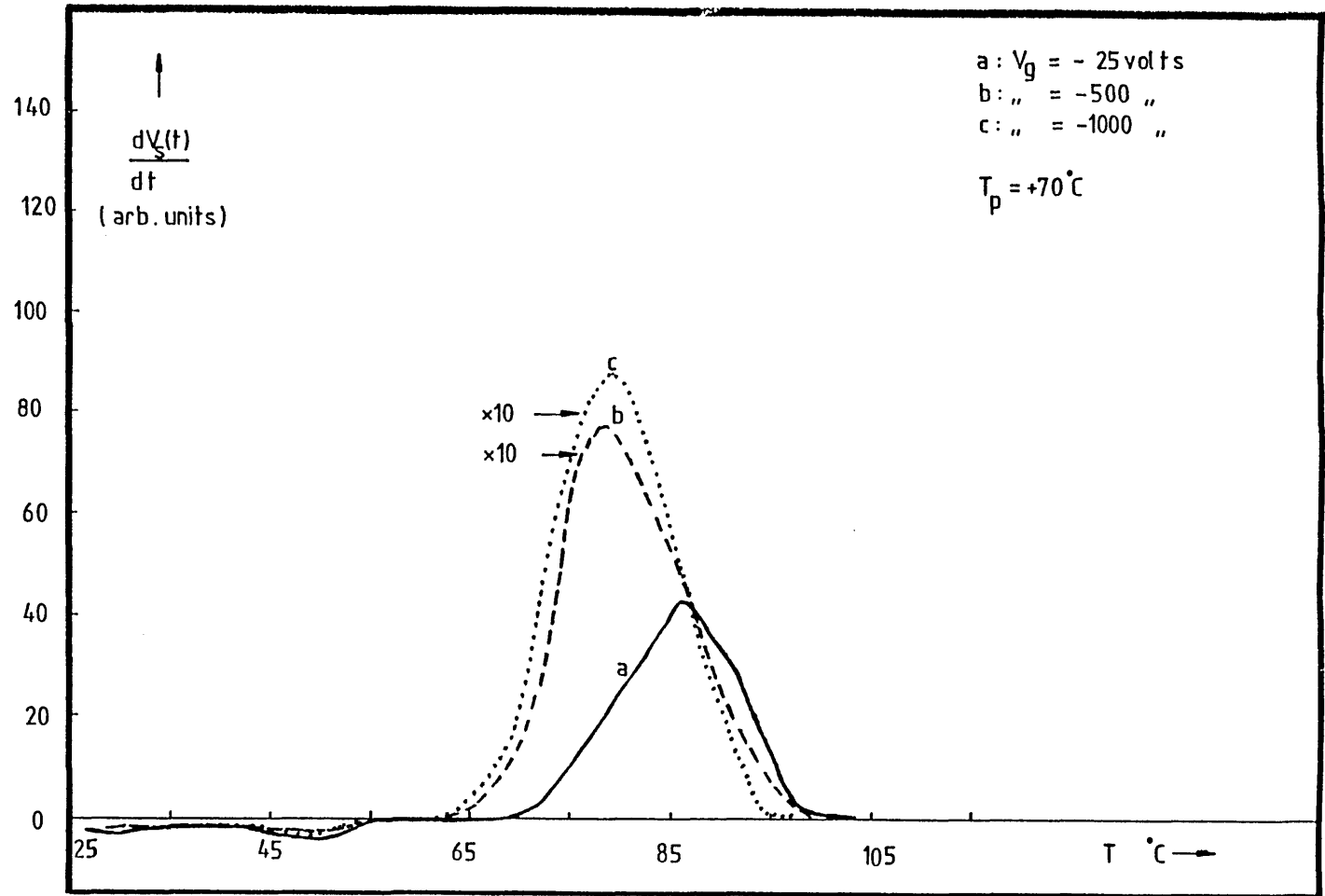


Fig.5.29 Activation energy for the decay of the surface potential in the high temperature region. Decay of the homocharge polarisation is due to the intrinsic electrical conductivity of the sample bulk.

Fig. 5.30 Time derivative of the surface potential decay plots of fig.5.28.

The plots evidence the presence of heterocharge and homocharge polarisations in the corona charged PVB films.

The initial portion of the plot is of opposite sign to main space charge decay peak. It corresponds to dipole disorientations in the film.



The decay of the dipole polarisation is then followed by the final neutralisation of the surface homocharges by carriers thermally generated within the sample bulk. This internal conduction current would normally be not observed if the TSD measurement is carried out in a short-circuit configuration with contacting electrodes. This presents a considerable advantage in view of the high electrical conductivity of the polymer. In high conductivity polymers it could be said that the overall TSD behaviour (excluding dipolar processes) involving space charges would be dominated by the large value of this intrinsic property. Other processes which may lead to TSD peaks are normally masked by the large internal conduction currents.

The activation energy for the internal conduction current in the sample bulk obtained from the charge decay plots is about 2.03 to 2.05 eV. As was discussed in a previous section (sect. 5.2.1.7) the space charges involved would most likely be products of water dissociation due to the hygroscopic behaviour of the polymer. The value of the activation energy calculated from the surface potential decay data also agrees with the value found from a conventional "steady state" DC current vs. temperature measurement.

5.2.4 Summary

A summary of the results of the experiments carried out on the films of PVB is presented below. Three different types of TSD measurements were carried out, namely the TSD of short-circuited DC charged samples, the TSD of short-circuited corona charged samples and the TSD of the surface potential of the (unmetallised) corona charged films. Representative thermograms of the three different types of TSD runs are plotted in fig. 5.31. A good general correspondence of the positions of the peaks can be observed, however care is needed in their interpretation.

The Dipole peak (α - peak)

All three variants of the thermograms display a peak which has been identified as being due to a dipolar process. The positions of the peaks of the TSD thermograms coincide with the calorimetrically determined value of the glass transition temperature of the polymer. This value is centred at about 60°C.

Curves a and b of fig. 5.31, which are the short-circuit thermograms of a DC charged and Corona charged sample respectively, both exhibit well-defined peaks corresponding to the disorientation of a previously induced dipole polarisation. These samples were polarised at $T_p = 70^\circ\text{C}$. Curve c, which is a displacement current thermogram obtained from the time derivative of the decay of the persistent surface potential, also displays a peak in the same temperature range as the previous short-circuit thermograms. However, the actual process leading to the peak with a direction as plotted is opposite to that of the previous short-circuit thermograms. In this particular plot, the peak of the displacement current curve is due to the orientation of

permanent dipoles instead of their disorientation. The sample in this case was polarised at 30 °C.

The overall dipolar response of the sample films to the electret formation cycle is believed to have mainly originated from the polar butyraldehyde groups which are attached to the two carbon atoms of the 1,3-dioxane structure. A schematic representation of this structure has been suggested in fig. 3.4. Several preliminary TSD runs carried out on the samples did not indicate the presence of any other dipolar peaks which could have originated from residual vinyl alcohol and vinyl acetate groups in the film.

The apparent activation energy for the dipole relaxation obtained from the analyses of the short circuit current thermograms range from 0.65 to 1.70 eV with a relaxation frequency of about 10^{-4} to 10^{-3} Hz. It has to be said that the values of the relaxation parameters that are quoted represent average values only, considering the nature of the dipole groups involved. Since the dipole groups could not re-orientate independently of the main vinyl chain, the dipole relaxation process would most likely be distributed. This is due to the differences in the lengths of the relaxing segments to which the dipole groups are attached and to the differences in the actual energy barriers that the chain segments have to overcome. It would also be reasonable to assume that the relaxing segments would undertake some sort of a cooperative behaviour in view of the major structural rearrangements that is associated with the glass transition.

Gil-Zambrano 1981 reported that the dipolar relaxation peak of the PVB^{*} films investigated display a distribution in both the natural frequency and apparent activation energy. Although a proper attempt was not made to

*

PVB type was Monsanto Butvar B 76

investigate this behaviour further, evidence of a distribution in the activation energy of the dipolar relaxation was shown by the current thermograms of the corona charged samples. The activation energy calculated for the corona charged samples were consistently higher than those of the DC charged samples. This was due to the truncation of the fast polarisations in the samples before the actual TSD run, leaving the slow, high activation energy dipoles to account for the final released current.

The density of the dipole groups was estimated to be about $5.48 \times 10^{21} \text{ cm}^{-3}$ with an effective electric moment of 2.98 Debyes per dipole. It has to be noted that the calculation of the effective dipole moment was carried out with the assumption that the equilibrium polarisation obtained at the start of the TSD run was adequately described by the Langevin function.

The Space Charge peak

A second peak was observed at about 78°C in the short-circuit current thermogram of the DC charged sample (curve a). For the corona charged samples this peak was not observed when the measurement was carried out in the short-circuit mode (curve b) but was however clearly displayed in the displacement current thermogram (curve c).

It is believed that the peaks that are observed in the thermograms are both essentially conductivity determined relaxation peaks i.e., they are actually manifestations of the temperature dependence of the bulk electrical conductivity of the sample. For the DC charged sample, the space charge polarisation arose from the intrinsic charges that were transported to the near-electrode regions and subsequently frozen-in when the temperature of the sample was cooled to a value where their rate of transport becomes low. Upon being short-circuited and linearly heated up, the immobilised charges are thermally activated and drift towards their opposite counterparts in the sample bulk. The gross motions of these charges which precede their eventual neutralisation causes a current to flow in the external circuit.

In the DC charged samples, some of the immobilised charges may also be neutralised by fresh, thermally generated carriers which effectively reduces the density of polarisation. The neutralisation of the frozen-in space charges by this mode however does not release an external current due to the spatially independent nature of the internal current and the short-circuit condition during the TSD. As a result of this, part of the decay of the space charge polarisation is obscured.

The situation that is described above is believed to have been responsible for the absence of a space charge relaxation peak in the short-circuit thermogram of the corona charged sample (curve b). The strong internal conduction current may have acted to neutralise the space charge polarisation during the TSD run so much so that no external current was detected. It is also believed that the effects of the top electrode metallisation carried out after the corona charging may have significantly reduce the attained space charge polarisation by annihilating the weakly held corona-deposited ions and promoting the neutralisation of the surface trapped charges by providing the activation energy needed through the local heating effects caused by the condensation of the metal atoms. The latter mechanism could not, however, be substantiated without further work being carried out.

The neutralisation of the corona induced space charge polarisation can be clearly observed in the TSD displacement current thermogram of the unmetallised film (curve c). The space charge layer at the surface of the film sets up an internal field which drives an internal neutralisation current that increases as the temperature of the sample is raised. The increased efficiency of the technique in observing the decay of the space charge layer is evident by the better defined peak of the displacement current plot compared to the plots of the short-circuited samples.

The apparent activation energy of the relaxation peak of the DC charged sample range from 1.20 to 3.90 eV as found by the different methods of analyses. Due to the relatively large value of this quantity, it is strongly believed

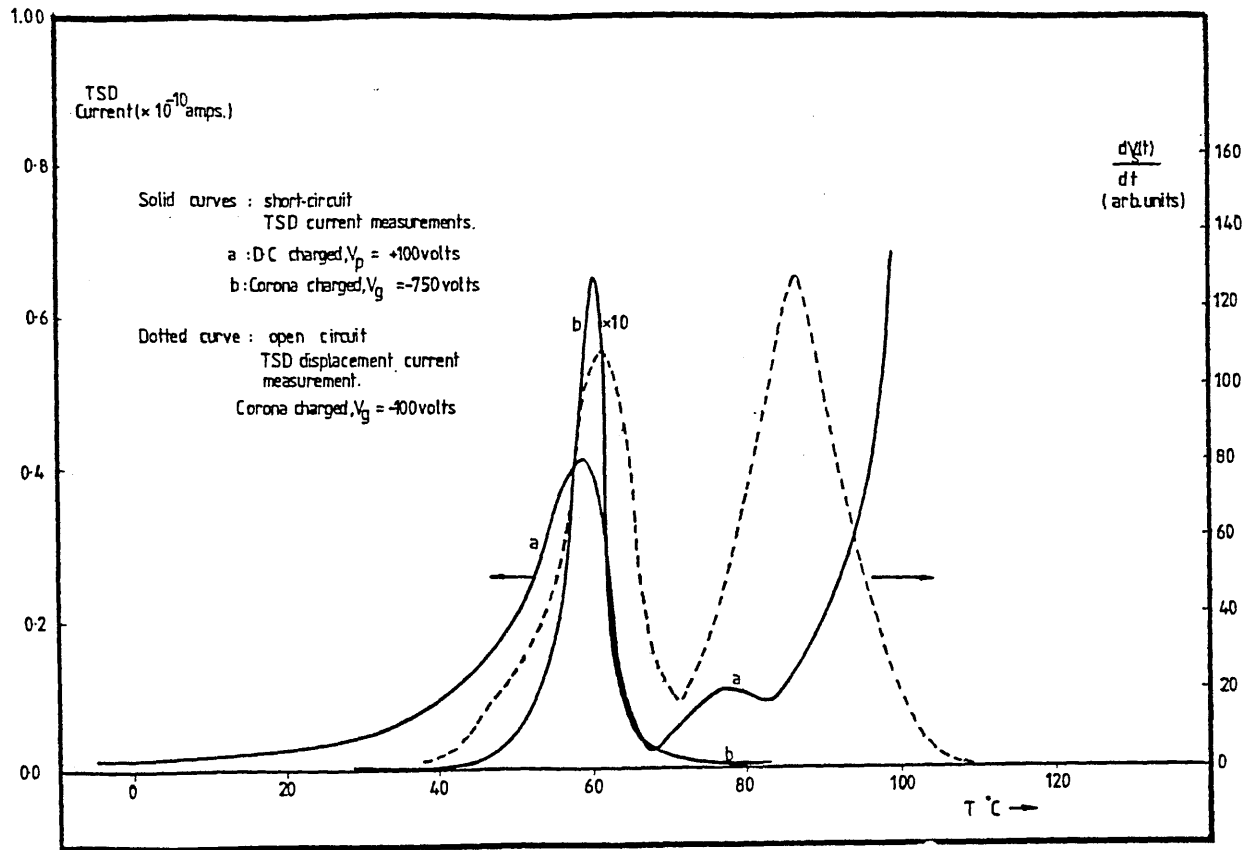


Fig.5.31 The TSD response of 20 μm thick PVB films (Butvar B79).

A dipolar relaxation is exhibited by all three types of measurements. The temperature at which the response is maximum coincides with the glass transition region of the polymer.

Above $T_g (=57\text{ C})$, a space charge peak related to the self-drift of intrinsic ions is observed in the short-circuited, DC charged thermogram (curve a).

For corona charged samples (curve b), the space charge peak is absent due to the combined effects of top electrode metallisation and "invisible" neutralisation by the electrical conductivity of the film.

The effect of the neutralisation by the conduction of the sample bulk is reflected by the relatively better defined peak of the displacement TSD current thermogram (curve c).

Overall, the intrinsic electrical conductivity (or rather, its temperature dependence) of the film is the dominant parameter in determining the build-up and eventual decay of any space charge polarisation in the sample.

that the space charges involved are ions. This view is supported by the observation that all the TSD peaks occurred in the rubbery phase of the solid, i.e. a region where the transport of ions is enhanced due to the increase in the available free volume.

The ionic species involved are believed to be the products of water dissociation although the contribution of other species could not be ruled out. These "other" ions are most likely to be the products of the chemicals used in the commercial manufacture of the polymer. In this work no attempt was made to specify the impurity ions nor was the polymer further purified.

The average relaxation time for the decay of the space charge polarisation found from the TSD current peaks was also taken as to be representative of the structural relaxation time that was defined by the free volume theory of Cohen and Turnbull (1959). Following this, the fractional free volume of the bulk PVB as well as the coefficient of expansion of the free volume was found to be 0.046 to 0.052 (at $T_g = 57^\circ\text{C}$) and $(10.0 \text{ to } 9.0) \times 10^{-4} \text{ K}^{-1}$ respectively. These values of the structural parameters are also of the same order to the (dilatometrically determined) values found for organic amorphous polymers in general.

The activation energy for the decay of the corona-induced space charge polarisation found from the open-circuit circuit measurements was about 2.03 to 2.05 eV. This value would correspond to the activation energy for the internal ionic conduction of the polymer bulk since this was taken to be the dominant decay mechanism of the polarisation. A conventional current-voltage-temperature measurement carried out above T_g yielded a value of 1.88 eV, signifying a close agreement between the two methods.

It is also noted that the value of the activation energy calculated from the open-circuit TSD measurement is also similar to that calculated from the short-circuit measurement. Although the decay mechanisms of the space charge polarisation are different (the former is due to an internal conduction

while the latter is due to the drift of the space charges themselves) the similarity in the activation energies is to be expected. In the short-circuited DC charged samples, the space charge polarisation originated from carriers which had taken part in the internal conduction and which were then immobilised when the temperature of the sample was reduced. Therefore, the ions involved are similar and as such, their activation energy for transport (self-drift) through the sample upon re-mobilisation will closely resemble that of the ohmic conduction mechanism.

In general, it can be said that the formation and decay of a space charge polarisation in the PVB films is determined primarily by the bulk electrical conductivity of the sample. It was found that the space charge peaks were not affected by a change in the electrode material, underlining the overwhelming nature of the bulk conductivity in determining the overall TSD behaviour of the material.

A comparison with the few known TSD results on PVB films confirms the orientation of dipole groups as a source of persistent electrical polarisation. The decay of this polarisation is intimately related to the glass transition temperature of the samples used. However, the reported results on the appearance and identification of the origin of the high temperature peak needs further comment. Jain et al. 1974, 1979 and Mehendru 1980 all reported the presence of a peak at about 150 to 170 °C which, significantly, was far above the respective glass transition temperatures of the samples used. In this work no such high temperature peaks were observed and furthermore, frequent problems with sample stability was encountered at these temperatures. Samples that were fabricated as sandwich structures often show visible physical deterioration especially at the polymer/electrode interface.

Although a large TSD current was observed in the samples that did survive the high temperature runs, none displayed any peak or any identifiable current formation. The large currents that were observed is believed to be

due to a combination of effects which may involve the release of charges associated with thermally induced chemical degradations (Stupp and Carr 1977) and electrochemical effects at the polymer/electrode contacts (Furukawa et.al. 1968, Sharma and Sud 1981).

A more detailed discussion of the results of Jain et.al.1974,1979 and Mehendru et.al.1980 has been given in chapter 3 (sect.3.1.4.4 and table 3.2) and at best suggests that the large discrepancy between the results of this work and of the above authors can only be due to the actual grade of PVB used. Differences in the T_g of the samples will have a strong impact on the dipole polarisation and on the ionic transport of carriers in the sample. The actual carriers involved is also sensitive to the type and amount of impurities in the sample. It is also interesting to note that the high temperature peaks of Jain et.al.1979 and Mehendru et.al.1980 were attributed to the release of electronic carriers from the sample bulk while Jain et.al. 1974 attributed the high temperature peaks to dipolar disorientation. It is thought that the latter interpretation is erroneous considering the T_g 's of the samples used lie between 77 to 85°C while the peak temperatures occurred at 157°C.

5.2.4.1 Significance to Xerography

Apart from being the physical binder in the pigment-resin-dye type photoreceptor, the PVB is required to provide the charge retention properties of the overall photoreceptor and be able to retain the corona-induced polarisation prior to being discharged through the conducting channels that are provided by the photoconductive pigment. The important factor in determining the performance of the PVB is the time lapse between the xerographic processes of corona charging and photo-discharge. This time lapse is of the order of seconds in a typical practical system (Schaffert 1975). It has been found in this work that the limiting factor in determining the corona-induced polarisation is the intrinsic conductivity of the polymer and that a significant decay of the surface potential proceeds over a period of

minutes (for e.g., it will take 30 minutes for $\frac{V_s(t)}{V_s(0)}$ to reach 0.5 for an isothermal decay at 70°C ($V_g = -500$ volts) as shown in fig.5.23). From the isothermal decay curves of fig.5.23, it can be said that the performance of the PVB polymer will be adequate.

As a toner particle however, the tribo-electrically induced polarisation needs to be retained over a longer period in order to allow time for the physical transfer of the particles and their final fusion on to the paper (seconds). Although the increase in the time lapse between the xerographic processes is not critical in the context of the ability of the PVB to retain its charge, the effects of carbon black impregnation (which will increase the overall conductivity) and the high temperature working environment will both impose a more critical limitation on the temporal ceiling available for the processes involved. Several other factors which may limit the applicability of the polymer as an effective toner particle are its impact strength (for the particulating of the polymer into finer entities, low impact strength is required, i.e. high T_g is desirable) and ease of fusion and wettability of the polymer on to the paper (the former requires a low T_g while the latter requires a low surface energy for the molten polymer compared to the critical surface energy of the paper). Aspects of toner particle requirements for xerographic use has been discussed by O'Reilly and Erhardt 1973.

5.3 Double-Layer Xerographic Photoreceptor

5.3.1 Introduction

TSD current measurements were carried out on a xerographic photoreceptor having a physical configuration as shown in figure 4.4 of the previous chapter. All the experimental steps carried out on the sample during the TSD run were performed in the dark, with the sample having been short circuited and dark-rested in the cryostat for a period of about 12 hours prior to the measurement. Virgin samples were used for each run as the samples were all inevitably destroyed after being heated to temperatures far beyond their glass transition temperatures during each run.

After being poled at a temperature $T_p = 30.5^\circ\text{C}$ for a period $t_p = 30$ minutes, the sample was subsequently cooled down to -50°C at a rate of about $-7.5^\circ\text{C min}^{-1}$ (with the applied voltage still on). The value of the poling voltage V_a was varied from -50 volts to $+50$ volts, with respect to the polarity of the aluminium substrate, i.e. the electrode bordering the SeTe layer.

The heating rate used was 2°C min^{-1} as this was found to yield reasonably large currents being released during the TSD. Higher heating rates were found to cause a high occurrence of sample failure during a run. The thin and brittle ($\sim 50 \mu\text{m}$) photoreceptor layers had a tendency to flake off the aluminium substrate ($\sim 0.5 \text{ cm}$ thick). This was probably due to the different rates of thermal expansions of the photoreceptor layers and of the substrate.

5.3.2 Results and Discussions

The short circuit TSD current spectra of the photoreceptor layers exhibited very different characteristics when the polarity of the forming electrode was reversed. To aid our analysis, this section will be divided into two sub-sections based on the polarity of V_a , the applied voltage.

5.3.2.1 V_a Positive

The TSD current spectra for a series of positive poling voltages are shown in figure 5.32. From the plots, it could be observed that well-defined current peaks are present in the temperature region of about -8°C , followed by the appearance of several irregular TSD current peaks over a broad temperature region between $+30^\circ\text{C}$ to $+50^\circ\text{C}$. This latter temperature range incidentally also spanned the glass transition temperature of the a-Se and a-SeTe layers as had been shown by our DTA results (fig. 4.13 of chapter 4). The low temperature peaks will first be discussed followed by the high temperature peaks.

Similar TSD runs were also carried out on samples with a homogeneous structure. The Te concentration of the single layer a-SeTe photoreceptor is shown in fig. 5.33. A representative TSD current thermogram of the sample is shown in fig. 5.34. As can be seen, no current peaks are observed even though the samples were polarised under identical conditions. It is thus established that the observed current peaks in the thermograms of fig. 5.32 are indeed due to the interfacial nature of the 2-layer photoreceptors.

The low temperature current peaks displayed an asymmetric shape which is reminiscent of dipole disorientation peaks undergoing a Debye relaxation. The plot of the maximum TSD current, I_m , vs. the applied voltage is shown in fig. 5.35. A linear relationship is found. The plot of the total charge released, Q , as a function of the applied voltage is also linear (fig. 5.36, plot a.). The TSD current peaks also exhibit a slight shift towards higher temperatures as the polarising voltage is increased.

It has been discussed in chapter 2 that a space charge polarisation would occur in an electrically heterogeneous sample when an electric field is applied across its electrodes. This Maxwell-Wagner polarisation is caused by the accumulation of charge carriers at the boundaries or interfaces of the regions of the different media. Upon cooling and removal of the applied voltage, this layer of space charges would decay at a very slow rate due to the relatively high resistivities of the media at the low temperature. When the temperature is raised, the frozen-in charges will be gradually neutralised by the thermally generated carriers from the bulk of the media bordering the interface. It was shown in sect. 2.6.1 that the decaying density of the frozen-in charge would respond to a linear temperature rise in a manner similar to that of a dipole depolarisation. This model for the decay of the frozen-in interfacial charges would be used for the analysis of the low temperature peaks.

The sign as well as density of the charges stored at the interface, $Q(\infty)$, could be estimated by the use of eqn. 2.45. As was described in sect. 2.6.1 the ratio $\frac{\epsilon_1 \sigma(T)}{\epsilon \sigma_1(T)}$ would play an important part in determining the magnitude and sign of the charges. Using approximate room temperature values for the electrical conductivities and static dielectric constants as $\sigma(T) = \sigma_{Se}(T) \sim 10^{-11} \Omega^{-1} \text{cm}^{-1}$, $\sigma_1(T) = \sigma_{SeTe}(T) \sim 10^{-9} \Omega^{-1} \text{cm}^{-1}$, $\epsilon = \epsilon_{Se} \sim 6.8$ $\epsilon_1 = \epsilon_{SeTe} \sim 7.5$ (Mehra et. al. 1977, 1979), the sign of $Q(\infty)$ is found to be positive

(i.e. holes), for positive V_a 's. The theoretical density of charges that could ultimately be stored for the different applied voltages are plotted in fig.5.36 (plot b). A comparison with the actual magnitude of the charges released as found by a graphical integration of the TSD current peaks reveals that this quantity is consistently less than the former. Eqn. 2.52 has shown that the released TSD current is an algebraic sum of the two opposite currents in the respective a-Se and a-SeTe layers. In fact, using the values of the material constants that were noted previously, the external TSD current as described by eqn. (2.52) would be dominated by the component in the a-SeTe layer. Hence the density of charges as determined by the graphical integration of the TSD current peaks could not have fully accounted for the total density of frozen-in charges.

Using the method of initial rise, the apparent activation energy derived from the peaks centred at about -8°C is found to range from 0.31 eV to 0.38 eV. These plots are shown in fig.5.37. The BFG plots (fig.5.38) also yield values ranging from 0.39 eV to 0.48 eV. The apparent energies of activation that were calculated from the TSD current peaks would actually be a hybrid value of the energies of activation for ohmic conduction in the a-SeTe and of the a-Se layers. However, since the electrical conductivity of a-SeTe layer was about 2 orders of magnitude larger than that of the pure a-Se layer throughout the temperature range of the current peak, then it would be reasonable to assume that the calculated apparent activation energies would correspond to the of conduction in the a-SeTe layer. The values of the activation energy for low field DC conduction in amorphous alloys of SeTe (10 to 30 wt.% Te) lie in a range between 0.40 to 0.80eV (Mehra et. al. 1977, 1979 and Parthasarathy 1984). These values were determined via conventional current-voltage-temperature measurements.

Fig.5.32

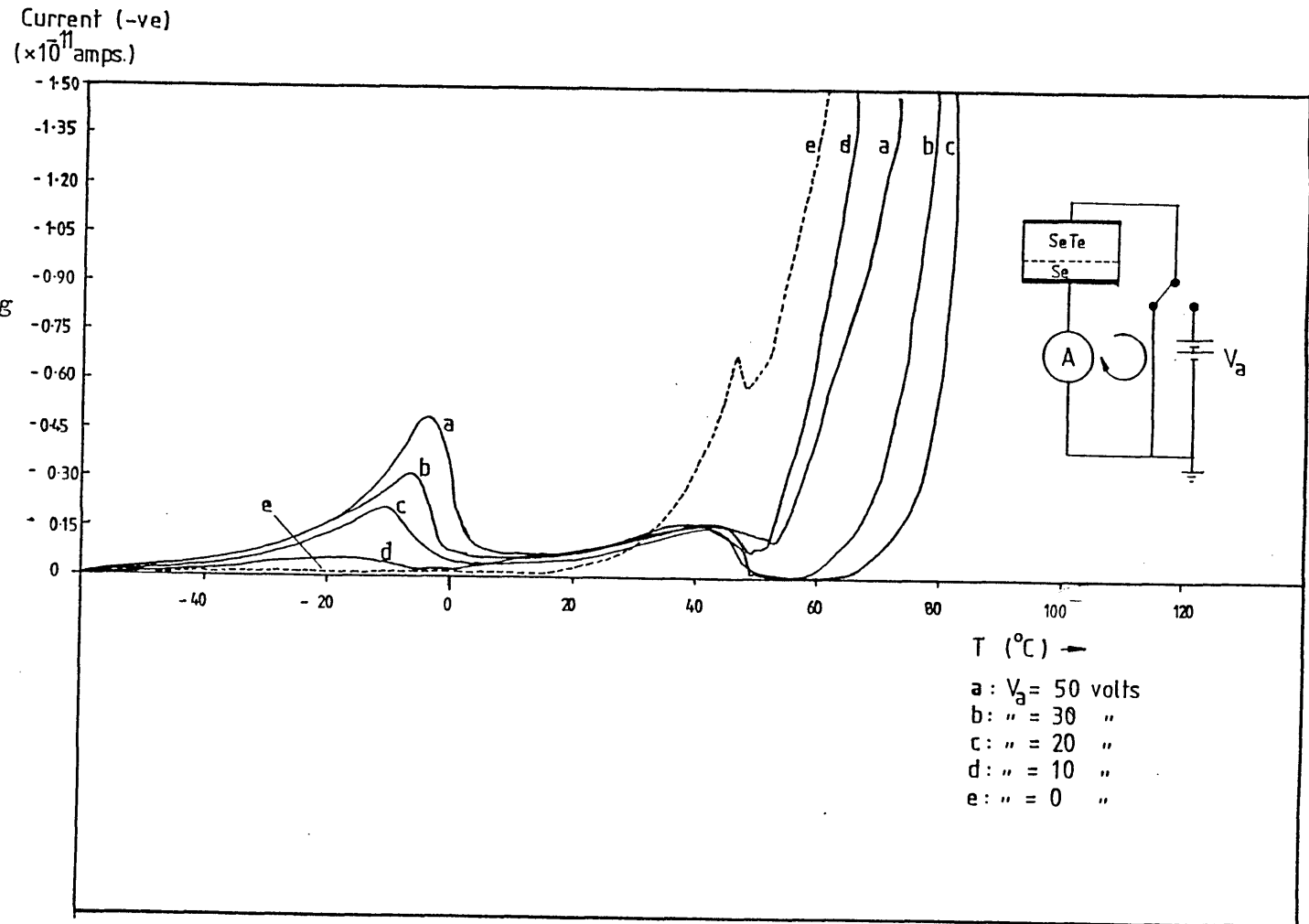
TSD current thermograms of a-SeTe double-layer photoreceptor.

$T_p = 30.5^\circ\text{C}$, $r = 2^\circ\text{C min}^{-1}$, $t_p = 30$ mins.

Two current peaks are observed.

A well-defined peak at about -8°C is observed followed by a broad peak spanning between 30 and 50°C .

All measurements are carried out in the dark.



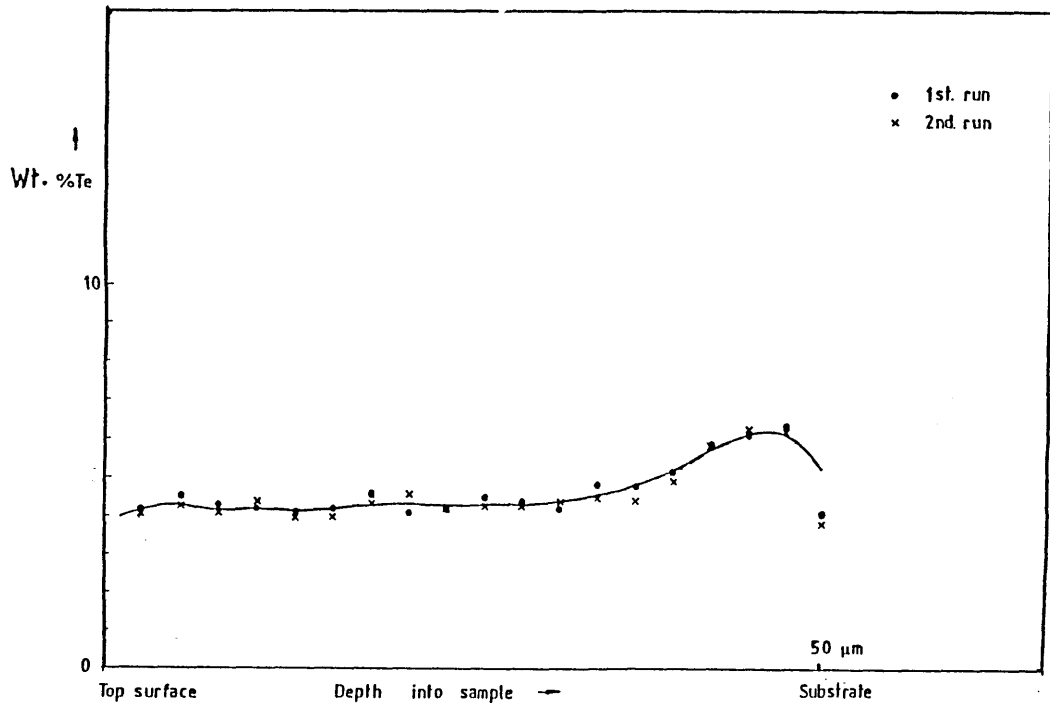


Fig.5.33

Te concentration profile in the single layer a-SeTe photoreceptors

The Te atoms are homogenously distributed throughout the thickness of the sample.

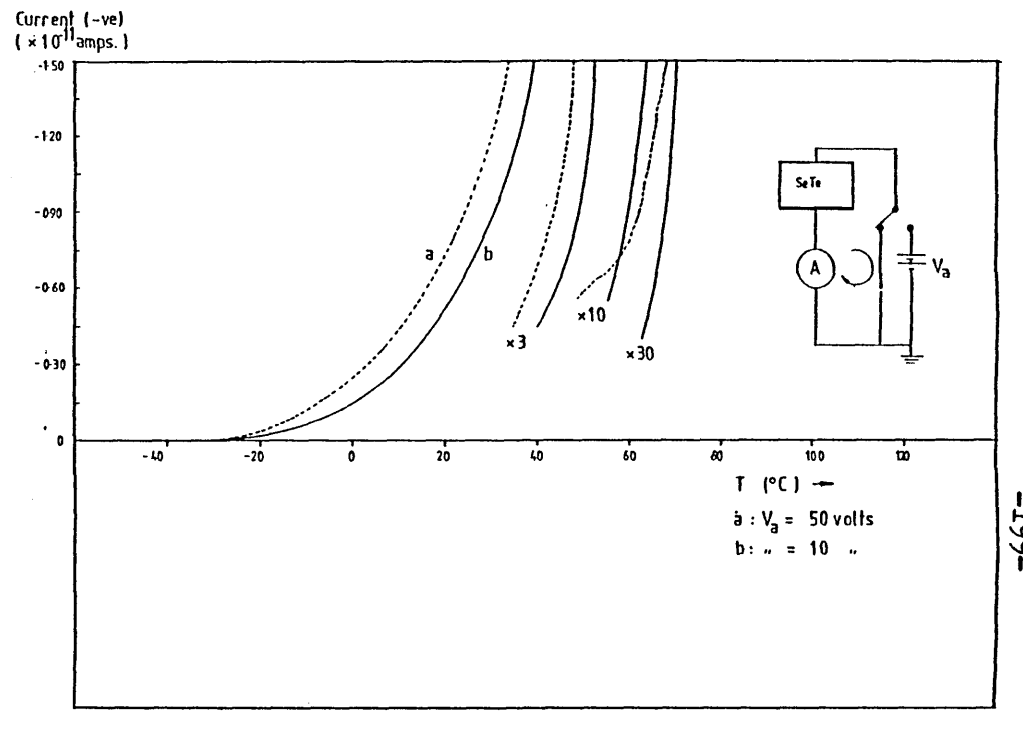


Fig.5.34 TSD current thermograms of a homogenous single layer a-SeTe photoreceptor. $T_p = 30.5^\circ\text{C}$, $r = 2^\circ\text{C min}^{-1}$, $t_p = 30$ mins. No current peaks are observed for the samples that had been polarised under identical conditions to those of fig.5.32

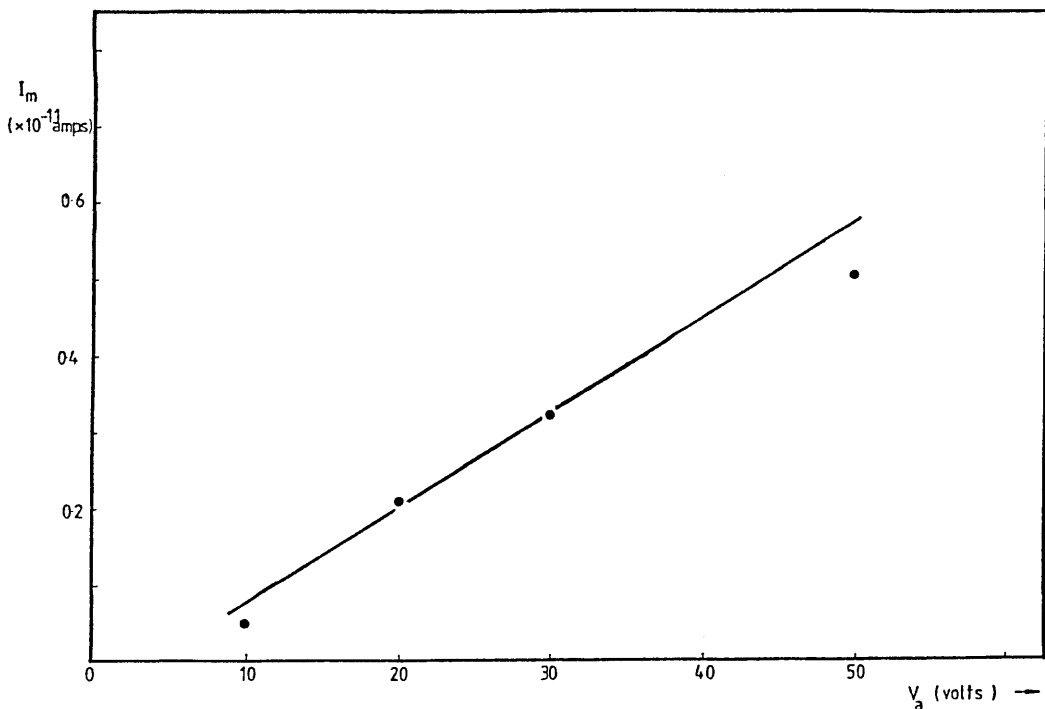


Fig.5.35 Peak current maxima as a function of the applied polarisation voltage for the low temperature Maxwell-Wagner peaks. A linear relationship is observed.

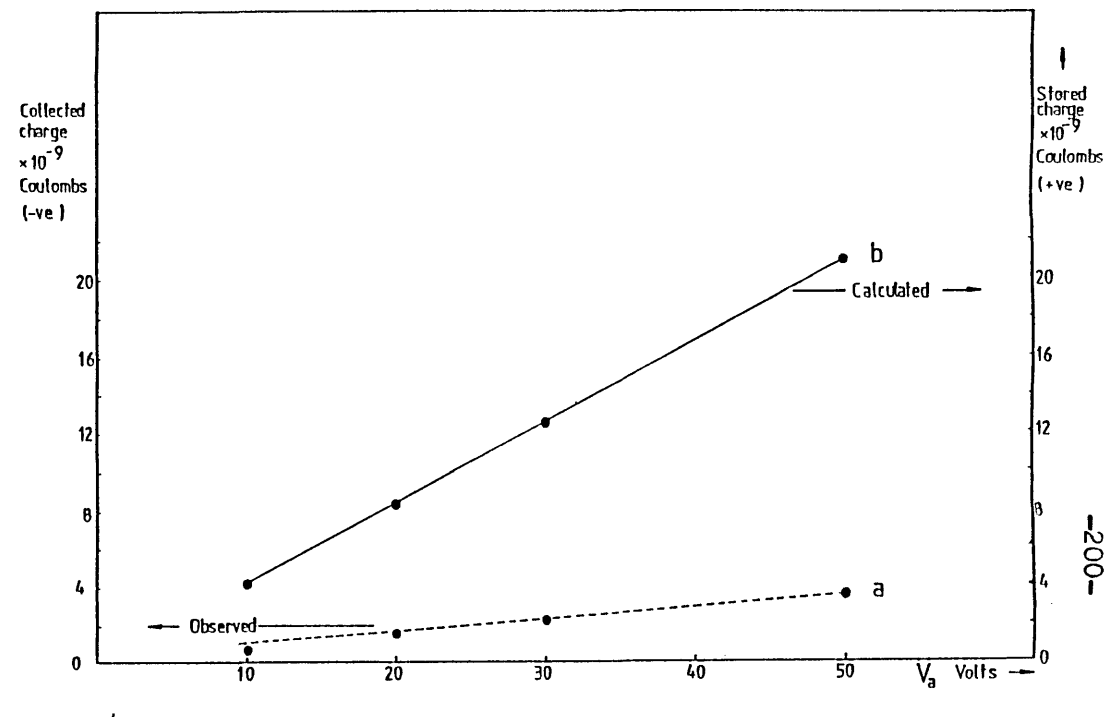


Fig.5.36

Plot (a) : Released TSD charges as a function of the applied polarisation field. The observed values are obtained by a graphical integration of the area underneath the TSD peak.

Plot (b) : Theoretically stored charges as a function of the polarisation field. The values of the stored charges are calculated using eqn.2.45.

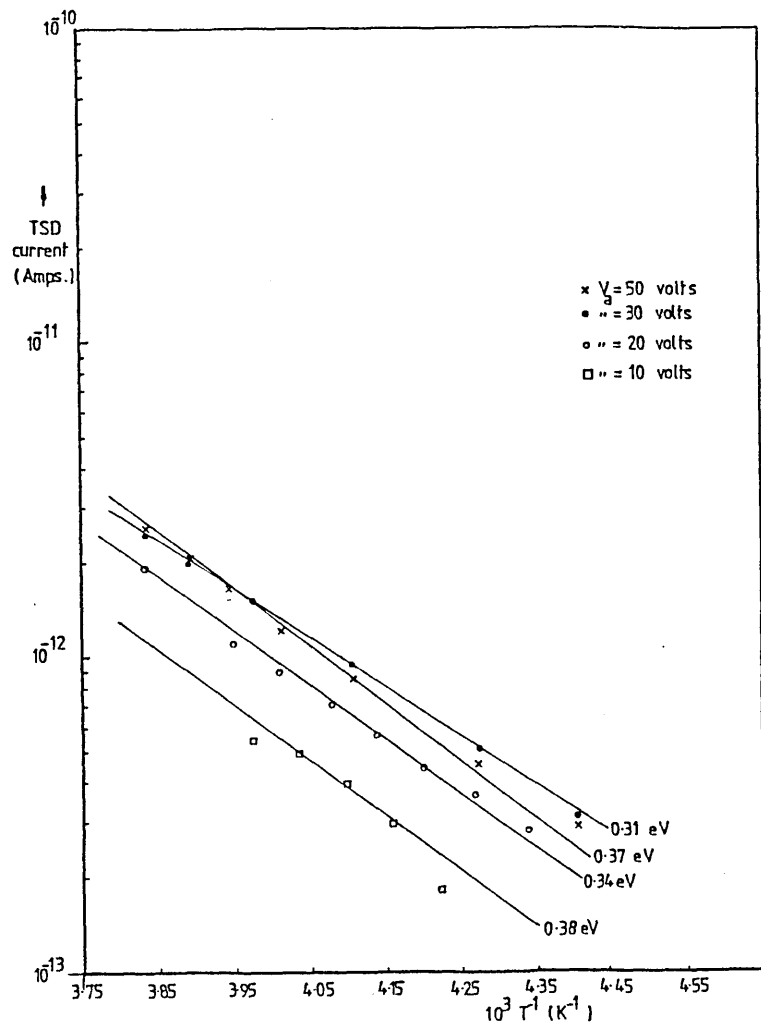


Fig.5.37 Initial Rise Plots of the low temperature Maxwell-Wagner peaks .

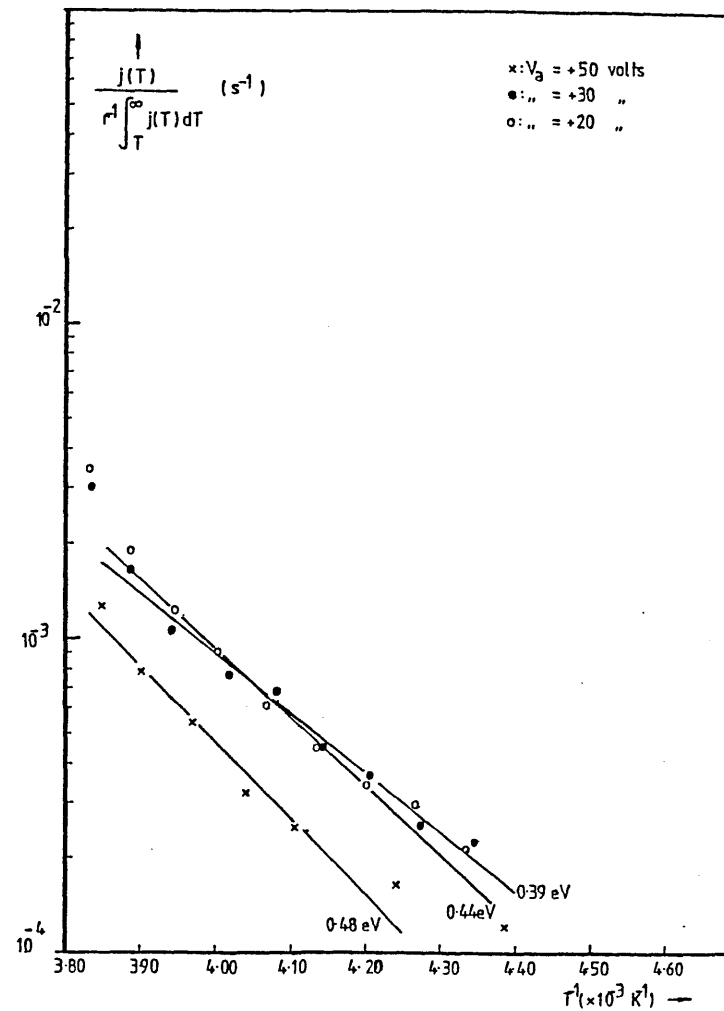


Fig.5.38 BFG plots of the Maxwell-Wagner peaks of the a-SeTe/a-Se layers.

As the samples were heated further, broad TSD current peaks are observed. The temperature range within which the peaks are observed coincided with the glass transition regions of the a-Se and a-SeTe layers. This observation strongly suggests that these current peaks are closely related to the onset of major structural relaxations in the samples.

It is expected that due to the mismatch in the amorphous lattices of the a-Se and a-SeTe layers at the junction, defect states would be present. These states at the interface could act as traps for any mobile carriers traversing across the junction. During the polarisation stage of the TSD run these states could be filled and remain so before being discharged.

As the temperature of the sample is raised, the individual rates of structural relaxations of the a-Se and a-SeTe layers would cause a dramatic change in the physical characteristics of the interface which could easily lead to the release of the trapped carriers. The trapped carriers are "shaken out" of the interfacial states as the system re-adjusts to the changing physical stresses. The rate of release of the trapped carriers would be greatest as the glass transition is approached.

The TSD current peaks also exhibited a saturation effect, i.e. the amount of released charge as found from the area underneath the peaks are independent of the magnitude of the charging voltage, V_a . This observation is believed to be due to the finite nature of the density of the interfacial traps that were filled during the polarisation. The graphical integration of the TSD peaks yields an average value of about $1.53 \times 10^{-9} \text{ C.cm}^{-2}$ which corresponds to a density of $9.56 \times 10^9 \text{ cm}^{-2}$ of released electronic charges.

At this point it would also be interesting for us to consider a simple estimate for the density of interfacial states that may arise from the mismatch in the packing order of the atoms at the junction of the layers.

Taking the bulk density of a-Se to be 4.3 gm.cm^{-3} (Zingaro and Cooper 1974) and that for a-SeTe (10 atomic % Te) as 4.4 gm.cm^{-3} (Das et. al 1972), it can be shown that the number of atoms of Se or SeTe units in the solid would be about $3.28 \times 10^{22} \text{ cm}^{-3}$ and $3.07 \times 10^{22} \text{ cm}^{-3}$ respectively. This would correspond to a surface density of $1.02 \times 10^{15} \text{ cm}^{-2}$ and $0.98 \times 10^{15} \text{ cm}^{-2}$ for the respective layers*. If the difference between these two quantities is taken as the surface density of available sites for the lattice defects, then it could be said that an upper limit of about $4.0 \times 10^{13} \text{ cm}^{-2}$ states would then be present at the interface of the two layers.

A comparison with the density of released charges obtained from the TSD current peaks shows that about 1 in 4.1×10^3 interfacial states were actually filled when the sample was polarised in the experimental conditions used.

The apparent activation energy for the TSD peaks calculated from the initial rise plot (fig.5.39) is found to be 0.54 eV. This would correspond to the effective depth of the interfacial states at the junction. The actual interpretation of the apparent activation energy calculated from the TSD peak would be difficult in view of the absence of any detailed knowledge regarding the physical processes that were operative during the structural relaxations. It is noted that activation energy of structural relaxations associated with the glass transition of films of a-Se is of the order of 2.50 eV (Matsuura and Suzuki 1979, Kasap, Juhasz and Hardwick 1985) and of a-SeTe (5.5 wt.% Te, 26 ppm Cl) is about 2.26 eV (Kasap et. al 1985). It also has to be pointed out that the values above were obtained for homogenous single layer films of the materials. To the best of the author's knowledge, no work has yet been carried out for the layered structures. By

*
If n_b is the number of units in the bulk,
then n_s , the corresponding number of units
on the surface is,

$$n_s = (n_b)^{2/3} \quad (\text{for a uniform distribution in a cubic array})$$

relating the values of the activation energies for the structural relaxations with that of the activation energy of the TSD relaxation current, it could be said that a "full-blown" structural re-adjustment (involving the breaking of bonds and also micro-Brownian motions) would not be required in releasing the trapped carriers.

The broadness of the peaks also suggests that the relaxation is a distributed one. Unfortunately, our attempts to resolve the peaks following the "peak cleaning" principle (Perlman and Unger 1974) did not result in clear, well-defined sub-peaks from which further inference could be made. This experimental difficulty is believed to be directly attributable to the heterogenous nature of the sample. Repeated sequences of heating and fast cooling as required by the technique may have caused irreversible changes to the state of the still frozen-in polarisation making the results of subsequent TSD runs uncharacteristic of the total polarisation state that would have been revealed. However, it is clear that from the very broad observed peaks and their close proximity with the glass transition regions of the individual layers, the actual relaxation involved would be governed by some form of cooperative behaviour.

5.3.2.2 V_a Negative

The TSD current thermograms for negative applied voltages are shown in fig. 5.40. No clear or well-defined peaks that could be attributed to a Maxwell-Wagner mechanism could be observed. Instead, several small and broad peaks are present followed by current reversals as the T_g region was approached. Only a qualitative discussion of these peaks are possible as attempts to increase the magnitudes of the peaks by using larger poling voltages or higher heating rates resulted in frequent sample failure. The use of longer t_p , the polarisation time also did not significantly affect the final results.

It is clear that the use of eqn. 2.52 is not adequate in describing the observed TSD behaviour. It appears that a space charge polarisation due

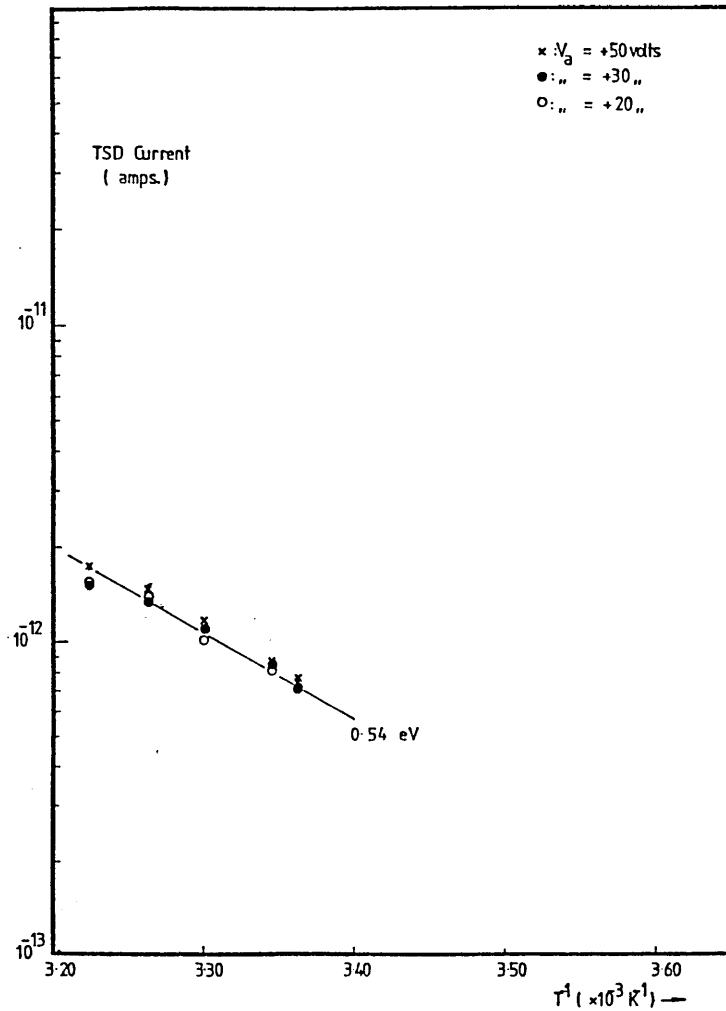


Fig.5.39 Initial Rise Plot of the broad detrapping peak of the a-SeTe/a-Se layers.

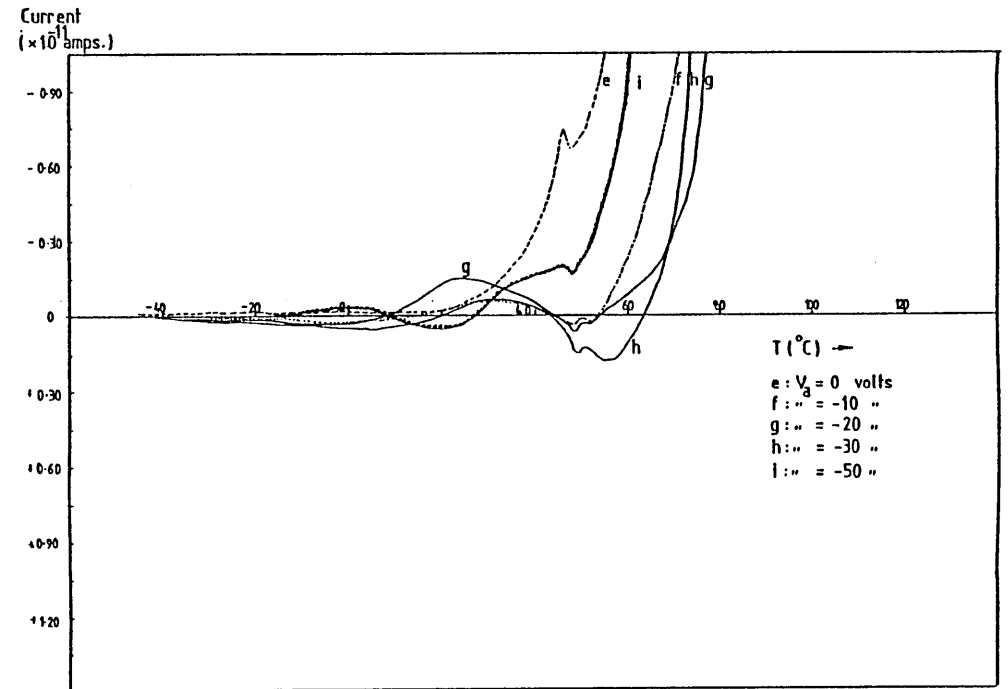


Fig.5.40 TSD current thermograms of a-SeTe/a-Se double layers for negative applied polarisation voltages.
 $T = 30.5^{\circ}C, r = 2^{\circ}C \text{ min}^{-1}$
 $t_p^D = 30 \text{ mins.}$

A Maxwell-Wagner polarisation was not achieved under the experimental conditions.

The small current peaks between 40 and 60°C is believed to be due to the detrapping of carriers from the interface of the layers.

to the Maxwell-Wagner effect was not successfully achieved when the polarity of the forming electrode was reversed. It has to be stated that the successful formation of a space charge layer at the interface of two media depends on whether the incoming conduction current is greater or smaller than the outgoing one. It has been established that the D.C. conductivity of certain alloys of a-SeTe can be about 10^2 times higher than that of a-Se (details of the variation of the dark conductivity with Te concentration can be found in the works of Lanyon 1964, Mehra et al. 1977, 1979). It was also found from thermoelectric measurements that a predominantly p-type of conduction is exhibited by a-Se (Vengris et al. 1972, Juska et al. 1974). The isoelectronic addition of Te would not affect this property.

For the case of positive V_a 's, the requirement that is outlined above was easily satisfied. This has resulted in holes being immobilised at the interface of the layers. For negative V_a 's however, the outgoing hole current was greater than the incoming current. This has resulted in an insignificant density of charges being immobilised with the final consequence of small current peaks being released during the TSD run. It is also believed that the inter-play of the small neutralisation currents and the ubiquitous parasitic background current was responsible for the current reversals detected.

5.3.3 Conclusions

It has been shown that the short circuit TSD current behaviour of a DC polarised a-SeTe/a-Se double layer photoreceptor is dependent on the polarity of the forming electrodes. For negative polarities of the aluminium substrate, no distinct TSD current peaks which could be attributed to the neutralisation of a layer of previously frozen-in interfacial space charges could be observed. However, distinct TSD current peaks were observed when positive charging voltages were employed.

Two current peaks, directly attributable to the presence of a heterogeneity in the samples, were observed. The low temperature peak, centred at about -8°C , is essentially a dielectric relaxation peak. It was due to the response of the intrinsic electrical conductivities of the component layers of the laminate to the linear temperature rise. The high temperature peak, which spanned a broad temperature range between $+30^{\circ}\text{C}$ and $+50^{\circ}\text{C}$, is believed to be due to the release of trapped carriers from states associated with the mismatch in the amorphous lattices of the layers.

From the direction of the released TSD currents and by the use of the Maxwell-Wagner model to describe the isothermal charging of the a-SeTe/a-Se junction, it is believed that a layer of positive space charges (holes) were accumulated when the forming electrode was made positive. During the subsequent TSD, thermally generated carriers (electrons) from both sides of the interface were driven to the interface where they neutralised the immobilised holes. From a consideration of the relative magnitudes of the DC conductivities and the dielectric constants of the individual layers, it is also concluded that the TSD neutralisation current that was externally detected would be dominated by the component in the a-SeTe layer.

The decay of the space charge layer at the interface is caused by intrinsic conduction rather than by the redistribution i.e self-drift of the charges. Several experimental observations consolidate this view. The positions of the TSD current peaks did not shift towards lower temperatures as the polarising field was increased. For a decay via self-drift of the charges, it is expected that a lowering of T_m , the peak temperature would be observed due to the speeding up of the decay caused by the higher driving field. The "charge-ratio" plots of the TSD current peaks (fig.5.41) are also non-linear. A linear plot would be characteristic of the decay of the space charges

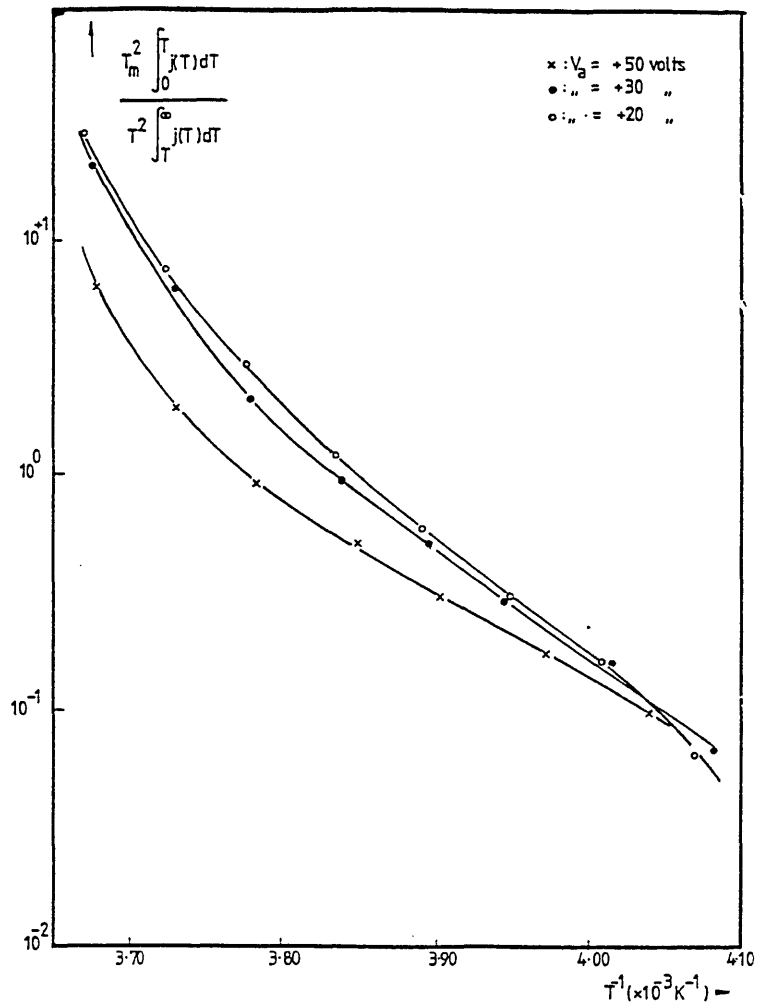


Fig.5.41 "Charge Ratio Plots" of the low temperature (-8°C) peaks of the a-SeTe/a-Se photoreceptors. The non-linearity of plots suggests that the space charges at the interface are neutralised by the internal conduction of the sample bulk, i.e., the interfacial charges are immobile and are eventually neutralised by carriers of the opposite sign from within the sample bulk.

Compare with the equivalent plots of the space charge peaks of the PVB films (fig. 5.13)

via a self-drift (compare fig.5.13 for the results on PVB films). The average relaxation time of the decay determined from the TSD current peaks were of the order of 10^3 to 10^4 seconds (see fig.38). If the decay of the interfacial charges were to occur via a drift towards the electrodes and the times quoted above were to represent the average time taken for the majority of the carriers to reach the electrodes, then unrealistically low values for the effective drift mobilities of the carriers would result. Using the simple relation for the drift mobility as $\mu = \frac{L^2}{t.V}$ where L is the distance to be traversed and V is the driving voltage (taken to be ~ 50 volts), then the effective drift mobility μ would be of the order of 10^{-12} to $10^{-11} \text{ cm}^2 \text{ V}^{-1} \text{ s}^{-1}$. These values would be too low compared to known values of effective drift mobilities for holes or electrons in a-Se or a-SeTe alloys in the temperature range of the TSD peak currents (-25 to -5°C). Time-of-flight experiments on a-Se and certain a-SeTe alloys (Te < 18 wt.%) yielded values of the order of 10^{-2} to $10^{-4} \text{ cm}^2 \text{ v}^{-1} \text{ s}^{-1}$ (Kasap and Juhasz 1982, 1985, Abkowitz and Markovics 1982) for holes or electrons.

The apparent activation energy for the relaxation was about 0.38 to 0.48 eV. This would correspond to the activation energy for the conduction of intrinsic, thermally generated electrons in the a-SeTe layer. The values calculated from the TSD current thermograms are of the same order to those that were determined via more conventional methods.

The magnitude of the charges ultimately recovered is found to be less than the theoretical value of charges that were frozen-in at the interface. This experimental finding is in agreement with the general TSD behaviour of heterogenous physical systems involving space charges whereby the so-called Gross charge invariance principle (Gross 1972a, 1972b) is violated. Only in the unlikely case where the a-Se

layer is fully insulating would the principle be obeyed and the magnitude of the theoretically stored charges be fully recovered (in accord with eqn. 2.45).

Broad current peaks observed in the T_g regions of the layers are believed to be due to the emptying of filled traps. It is assumed that defect states at the interface could act as traps for the mobile carriers. These defect states probably arise from the misfits and stresses of the a-SeTe and a-Se lattices at their contact interface and as such, the occupancies and the actual densities of these states can dramatically change when the glass transition is approached. The density of the defect states, found from the TSD current peaks, is about $9.56 \times 10^9 \text{ cm}^{-2}$.

It is found that the emptying of the defect states is a distributed process as evidenced by the broad TSD current peaks. This is due to the close dependence of the kinetics of the trapping states to the structural relaxations of the layers in the sample at the glass transition. Assuming a simple thermally activated behaviour for the relaxation, an apparent activation energy of 0.54 eV was found. This value would represent the effective energy required for the release of trapped holes from the interface states.

Here it is also acknowledged the caution that is needed in the interpretation of the observed current peaks in the TSD of heterogenous semiconductor device structures that utilise various layers of semiconductor materials and insulators in general. As has been found for the a-SeTe/a-Se structure, the presence of a TSD peak does not necessarily entail the presence of any particular set of trapping levels that could be attributed to a component layer of the device or to the device as a whole. It is possible that an interpretation that is based on the Maxwell-Wagner type of polarisation is adequate in accounting for the peaks observed. This cautionary note has in fact been pointed out by Agarwal 1974 and Muller 1974, 1976.

5.3.3.1 Significance to Xerography

The impact of a Maxwell-Wagner polarisation to the overall transport of the excess, photogenerated charges through a heterogenous xerographic photoreceptor is dependent on the time delay between sensitisation of the photoreceptor (corona charging) and the photo-discharge. This delay is usually of the order of seconds or less (Schaffert 1975). The time needed for the build-up of the equilibrium charges at the interface is essentially determined by the effective ohmic relaxation time of the sample, which for a two-layer structure is expressed by eqn. 2.41 in chapter 2. Using typical values for the room temperature conductivities, dielectric constants and the thicknesses involved, the relaxation time is found to be of the order of several minutes.

Thus it can be said that a Maxwell-Wagner polarisation will not be a significant problem to the xerographic performance of the photoreceptor as long as the sensitisation/photo-discharge delay is short compared to the effective relaxation time of the heterogenous structure. However it has to be noted that the relaxation time is a temperature dependent quantity, being considerably shorter if the temperature is increased. This effect may be a significant factor to be considered if high temperature working environments are encountered.

Results from recent Time-of-Flight experiments on multi-layer photoreceptors (Okamoto and Nakamura 1979, Kiyota et al. 1980 and Tateishi and Hoshino 1984) all did not report the observation of any effects that may be attributed to the presence of a space charge layer at the interfacial regions of the samples. The time delay between the application of the driving field and the photogenerating flash that was employed in the above works was of the order of 10^{-6} seconds and thus it is envisaged that the times involved had been too short to cause any significant build-up of a Maxwell

-Wagner polarisation.

It is believed that the deep interface states that were revealed by the TSD results will have a significant effect on the long term cyclic property of the photoreceptor. A build-up of trapped charges at the interface of the layers of the heterogenous structure will lead to undesirably high values of the so-called residual potential which in turn will cause a significant degradation to its xerographic performance.

Analysis of the observed surface (residual) potential and its cyclic build^{-up} will yield information on the available trapping states in the photoreceptor (for e.g. Abkowitz and Enck 1982) but as yet there has been no reported works on multilayer photoreceptors. The reason for this is not clear, but it can be said that the use of the TSD technique to study trapping states of the heterogenous photoreceptor structures can reveal vital information regarding the characterisation of the long term properties of the photoreceptor.

CHAPTER 6

FINAL CONCLUSIONS

The brief discussion on the electrical properties of polymeric solids has shown that the subject is inter-disciplinary in nature. The understanding of the wide range of electrical phenomena in these solids is important in view of their increasing technological use. Apart from their essential usefulness as insulators, materials belonging to this class of solids are also used in the micro-electronics industry (as photo- and electron-beam resists and encapsulants) and in transducer arrangements (piezo- and pyroelectric polymers). In the field of electrophotography they have been used not only as photo-sensitive elements but also as charge and pigment transfer agents.

In this thesis, the charge storage behaviour of two materials systems which are used in xerography are investigated by the technique of thermally stimulated discharge. The materials are a) Poly vinylbutyral, a polar polymer which has been widely used as a binder resin in the pigment-resin-dye type of photoreceptors and also when impregnated with carbon black, as toner particles for image reproduction and b) a two-layer photoreceptor based on a laminate of amorphous Selenium and amorphous Selenium-Tellurium alloy. This is a relatively recently developed type of photosensitive element which has been designed to operate with the semiconductor-laser printers.

Phenomenological theories of TSD current and surface potential measurements are described. Due to the simplifying assumptions made, the resulting expressions describing the functional dependences of the released TSD current on the temperature for the different types of polarisation are always nearly similar. This also stresses the importance of carrying out additional diagnostic experiments to complement the TSD results. Correlations with the results of Infra-red spectrophotometry and Differential Thermal Analysis are found to be helpful in elucidating the polarisation mechanisms involved.

The TSD of metallised and homogenous films of PVB (20 μm thick) which were polarised with a static electric field (between 2.5×10^3 and $5.0 \times 10^4 \text{ V cm}^{-1}$) reveals the presence of two distinct mechanisms which are responsible for the persistent internal polarisation. A peak in the TSD current thermogram which is centred at about 60°C is attributed to the disorientations of dipole groups in the solid. It is believed that the main contribution to the dipolar polarisation comes from the polar butyraldehyde groups which is attached to the 1,3 dioxane structure. It is estimated that there are about 5.48×10^{21} per cm^{-3} of such dipole units, each with an effective electric moment of 2.98 D.

The temperature at which the rate of dipole disorientation is maximum, revealed by the maximum in the TSD current thermogram, coincides with the calorimetrically determined glass transition temperature of the polymer ($\sim 57^\circ\text{C}$). This observation underlines the close relationship between the structural relaxations undertaken by segments of the vinyl main chains with the disorientations of the dipole groups. It is also noted that the dipole groups are attached to two points along the main chain, a physical arrangement which will prevent any possible independent movements of the dipole groups during the TSD run.

The apparent activation energy for the dipolar relaxations ranges from 0.65 to 1.70 eV as was found by several methods of analyses that were based on the assumption that the relaxations follow a Debye-like behaviour. The corresponding relaxation frequencies fall between 10^{-4} to 10^{-5} Hz in the temperature range between 30 and 60°C . It is however expected that the relaxations involved are distributed in both the natural frequencies and activation energies.

The second peak in the short-circuit current thermogram which is centred at about 78°C is attributed to the drift motion of intrinsic space

charges that were previously immobilised during the electret formation cycle. The space charges involved are believed to be ions which were introduced, by default, into the polymer during its commercial manufacture. In particular, the products of water dissociation are thought to be the dominant types of ions involved, in view of the additional water absorption caused by the hygroscopic nature of the polar polymer.

The apparent activation energy for the ionic drift is found to range from 1.20 to 3.90 eV as determined by several different methods of analyses. The appearance of the space charge peak in a temperature region which is immediately above T_g also underlines the close dependence of the ionic transitions on the available free volume in the polymer bulk. A correlation of the average relaxation times of the space charge relaxation that was obtained from the TSD thermogram with the structural relaxation times of the free volume theory of Cohen and Turnbull (1959) yields two structural parameters for the PVB bulk. It is found that at the glass transition temperature of the polymer ($\sim 57^\circ\text{C}$), the fractional free volume is about 0.046 to 0.052 and that the coefficient of expansion of the free volume is about $(9.0 \text{ to } 10.0) \times 10^{-4} \text{ K}^{-1}$. It is interesting to note that this means that the TSD technique can be used to investigate some aspects of the structural properties of amorphous solids, especially those that exhibit a significant ionic conduction. The fact that the technique is an alternative to the dilatometric or differential calorimetric measurements in determining T_g has been quite well established.

In general, it can be said that the relatively large magnitude of the bulk ionic conductivity of the PVB film dominates any other space charge relaxation process that may be present in the charged polymer. Corona charging, which allows higher polarisation fields to be used (up to $5.0 \times 10^5 \text{ V cm}^{-1}$), did not reveal any new mechanism of space charge polarisation such as bulk or surface trapping of electronic carriers that is often reported for the highly insulating organic polymers. Open circuit, thermally stimulated surface potential measurements confirms that the internal conductivity of the solid

is the dominant parameter in determining the decay of any induced space charge polarisation.

The activation energy for the ionic conduction, found from the thermally stimulated surface potential measurements, is about 2.03 eV. This value is also similar to the values that were found from the short-circuited TSD current measurements although the actual mechanisms for the decay of the space charge polarisations in the two cases are different. This similarity also confirms that the space charge carriers that are involved are similar and that they are intrinsic to the polymer bulk.

The short-circuit TSD current thermograms of a DC charged and heterogeneous a-SeTe/a-Se double layer xerographic photoreceptor display two peaks which are believed to be due to two distinctly different types of space charge polarisation. Both of these peaks however owe their appearance to the presence of a heterogeneity in the sample structure.

The well-defined low temperature peak which is centred at about -8°C is a consequence of the difference in the dielectric constants and electrical conductivities of the two member layers of the laminated sample structure. The application of an electric field (positive polarity applied to a-SeTe) results in the build-up of a space charge layer (holes) at the interface of the layers due to the unequal conduction currents arriving and leaving that interface (the Maxwell-Wagner effect).

The decay of this polarisation is essentially governed by the individual responses of the electrical conductivity of the layers to the linear temperature rise during the TSD run. In the samples investigated, it is believed that the TSD current peak that is observed is dominated by the neutralisation current in the a-SeTe layer. The apparent activation energy for the relaxation calculated from the TSD current peaks range from 0.31 to 0.48 eV. This corresponds to the conduction of intrinsic, thermally generated electrons in the a-SeTe layer.

The broad high temperature peak which is observed between +30 to +50° in the thermogram is believed to be due to the release of carriers (holes) from trapping states associated with the physical discontinuity of the a-SeTe/a-Se junction. These states originate from the stresses and misfits of the amorphous lattices of the layers at their interface and as such are sensitive to any structural changes that may occur during the TSD run. This accounts for the proximity of the TSD current peak to the glass transition regions of the a-Se and a-SeTe layers.

From the TSD current peaks, it is estimated that the density of hole traps at the interface is about $9.56 \times 10^9 \text{ cm}^{-2}$. The activation energy for the relaxation, which corresponds to the effective energy for the detrapping of holes from the interface states, is found to be about 0.54 eV. The actual relaxation process is distributed as evidenced by the broad current peaks observed. Attempts to resolve this by the peak cleaning method was however not very successful due to the sensitive nature of the physical structure of the interface to repeated heating/cooling sequence of the technique.

In this work, the versatility of the TSD technique in studying the various origins of the persistent internal polarisation in amorphous dielectric materials has been demonstrated. The TSD current peaks due to the decay of different types of polarisation have been identified. Dipole disorientation and the self-drift of ions has been responsible for the peaks observed in the homogenous PVB samples. In the heterogenous sample structures (PVB/air-gap, a-SeTe/a-Se), bulk conductivity induced space charge relaxation peaks are observed. The release of carriers from trapping states are also identified in the heterogenous samples of a-SeTe/a-Se.

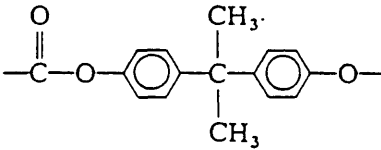
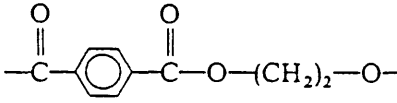
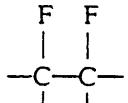
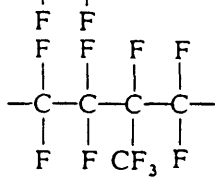
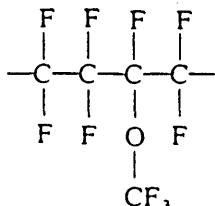
Future Work

The effect of water absorption on the space charge polarisation peaks of the PVB films need to be investigated further. This is considered

to be important in view of the use of the polymer in xerography. Water absorption due to prolonged exposure to humid conditions coupled to high temperature working environments may seriously degrade the charge retention properties of the polymer.

The high temperature TSD current peaks that are observed for the a-SeTe/a-Se layers should be further resolved into their component peaks in order to gain a proper understanding of the deep interface states that are present. It will be interesting to compare the TSD results of the heterogeneous layers with calorimetric measurements so that further insight can be obtained regarding the relationship between the structure of the interface and its trapping properties.

APPENDIX 1 : Chemical Name and Structure of
some Commercially Important Polymers.
(After Sessler 1980)

| Name | Abbreviation | Structure |
|--|--------------|--|
| | | $\begin{array}{c} \text{H} \quad \text{x} \\ \quad \\ -\text{C}-\text{C}- \\ \quad \\ \text{H} \quad \text{y} \end{array}$ |
| Polycyclohexyl methacrylate | PCHMA | $x = \text{CH}_3, y = \text{COO}-\text{C}_6\text{H}_{11}$ |
| Polyethyl methacrylate | PEMA | $x = \text{CH}_3, y = \text{COOC}_2\text{H}_5$ |
| Polymethyl methacrylate | PMMA | $x = \text{CH}_3, y = \text{COOCH}_3$ |
| Polyphenyl methacrylate | PPhMA | $x = \text{CH}_3, y = \text{COO}-\text{C}_6\text{H}_5$ |
| Polyethylene | PE | $x = \text{H}, y = \text{H}$ |
| Polypropylene | PP | $x = \text{H}, y = \text{CH}_3$ |
| Polyvinyl chloride | PVC | $x = \text{H}, y = \text{Cl}$ |
| Polyvinylidene chloride | PVDC | $x = \text{Cl}, y = \text{Cl}$ |
| Polyvinyl fluoride | PVF | $x = \text{H}, y = \text{F}$ |
| Polyvinylidene fluoride | PVDF | $x = \text{F}, y = \text{F}$ |
| Polybisphenol A carbonate | PC-n |  |
| Polyethylene terephthalate (Mylar) | PET |  |
| Polytetrafluoroethylene | PTFE |  |
| Tetrafluoroethylene-hexafluoropropylene copolymer | Teflon-FEP |  |
| Tetrafluoroethylene-perfluoromethoxyethylene copolymer | Teflon-PFA |  |

BIBLIOGRAPHY

- Abkowitz M, Enck R.C (1982) Phys.Rev.B25,2567
- Abkowitz M, Markovics J.M (1982) Solid State Comm. 44,1431
- Adamec V.A, Calderwood J.H. (1978) J.Phys.D ,11,781
- Agarwal S.C. (1974) Phys.Rev. B10,4340
- Anderson E.W., Blyler L.L., Johnson G.E., Link G.L. (1973) in "Electrets, Charge Storage and Transport in Dielectrics" Ed.by Perlman M.M, Electrochemical Soc., Princeton. pp.424
- Anderson P.W. (1978) Rev.Modern Phys.,50, 191
- Andre J.M., Ladik J.(Eds.) (1975) " Electronic Structure of Polymers and Molecular Crystals " Plenum Press, New York
- Baba A, Ikezaki K (1982) App.Phys.Lett.,40, 1027
- Baba A, Ikezaki K (1985) J.App.Phys.,57,359
- Bamji S.S (1982) J.Phys.D ,15,911
- Baird M.E. (1968) Rev.Modern Phys.,40, 219
- Batra J.P., Kanazawa K, Seki H (1970) J.App.Phys., 41, 3416
- Baum E.A, Lewis T.J, Toomer R (1972a) J.Phys.D 10,25
- " " " " " (1972b) J.Phys.D 10,487
- Berger S.B, Enck R.C, Scharfe M.E and Springett B.E (1979) in Gerlach and Grosse (Eds.) pp256
- Berger S.B and Enck R.C (1980) Proc.of Intl.Symp.on Industrial Uses of Selenium and Tellurium, Toronto, Canada. Selenium and Tellurium Development Assoc.Inc., Darien CT. pp 179.
- Blais P, Carlssen D.J, Wiles D.M (1971) J.App.Polym.Sc.,15, 129
- Blythe A.R (1979) "Electrical Properties of Polymers" Cambridge Univ Press.
- Bohun (1954) Czech.J of Phys., 4 ,91 . Bond (1954) see page 227
- Booth A.H (1954) Can.J of Chem.,32, 214
- Boyer R.F (1963) Rubber Chem.and Tech.,36,1303
- Bucci C, Fieschi R (1964) Phys Rev.Lett.,12,16
- Bucci C, Fieschi R, Guidi G (1966) Phys Rev.,148,816
- Bunn C.W. (1948) Nature,161, 929
- Calderwood J.H, Scaife B.K (1970) Phil.Trans.Royal Soc.,269, 217
- Chen R (1969a) J.App.Phys., 40, 570
- " (1969b) J.Electrochem.Soc., 116, 1254
- " (1976) J.Mat.Sc.,11, 1521
- Cheung L, Foley G.M.T, Fournia P, Springett B.E (1982) Photo.Sci.and Eng.,26,245
- Chiang C.K, Fincher C.R et.al (1977) Phys.Rev.Lett., 39, 1098
- Christodoulides C (1985a) J.Phys.D 18, 1501
- " (1985b) J.Phys.D 18, 1665

- Cohen M.H,Turnbull T (1959) J.Chem.Phys., 31, 1164
Cole K.S,Cole R.H (1941) J.Chem.Phys., 9, 341
Creswell R.A,Perlman M.M (1970) J.App.Phys., 41, 2365
Croitoru Z (1965) in "Progress in Dielectrics" Ed.by Birks J.B.,6, 105
Crowley J,Wallace R.A,Bube R.H (1976) J.Polym.Sc.:Polym.Phys.,14, 1769
Daniels T (1973) "Thermal Analysis" Kogan Page,London
Daniels V (1967) "Dielectric Relaxation" Academic Press, New York
Das G.C,Bever M.B,Uhlmann D.R,Moss S.C (1972) J.Non Crystalline Sol.,7,251
Das Gupta D.K,Joyner K (1976) J.Phys D, 8, 829
Das Gupta D.K,Doughty K (1978) J.Phys.D , 11, 2415
Dessauer J.H.,Clark H.E (1965) "Xerography and Related Processes",Focal Press
New York.
Deutsch K,Hoff E.A.W,Reddish W (1954) J.Polym.Sci., 13,565
Dolezalek F.K (1976) in "Photoconductivity and Related Processes" Ed.by Mort J
and Pai D.M.,Elsevier,Amsterdam.
Dreyfus G,Lewiner J (1974) J.App.Phys., 45, 721
Duke C.B. (1978) Surface Sci., 70, 674
Duke C.B,Salaneck W.R et.al (1978) Phys Rev., B18, 5717
Eyring H (1941) in "The Theory of Rate Processes" Ed. by Glasstone S,Landler K.J
and Eyring H.,Mc Graw-Hill,New York.
Elias H.G (1977) in " Macromolecules " Vol. 1,Structure and Properties,Plenum Press
New York
Fabish T.J (1979) C.R.C. Critical Rev.Solid State Sci.,December.
Fincher C.R ,Peebles D.L (1978) Solid State Comm., 27, 489
Flory P.J (1938) J .Am.Chem.Soc.,61, 1518
" (1953) "Principles of Polymer Chemistry " Cornell Univ.Press,Ithaca.
Fotland R.A (1960) J.App.Phys.,31, 1558
Fox T.G.,Flory P.J (1948) J.Am.Chem.Soc., 70, 2384
" " (1950) J.App.Phys.,21, 581
Frei H ,Groetzingler (1936) Phys. Z ,37, 720
Frohlich H (1958) " Theory of Dielectrics " Oxford Univ.Press.London
Funt B.L (1952) Can. J.of Chem., 30, 84
Furukawa T,Uematsu Y,Asakawa K and Wada Y (1968) J.App.Polym.Sci.,12,2675.
Gallo C.F,Germanos J.E,Courtney J.E (1969) App.Optics,Suppl 3-Xerography,111
Garlick C.F.J,Gibson A.F, (1948) Proc.Phys.Soc., A60, 574
Gee G (1970) Contemp.Phys., 11, 313
Gerlach E,Grosse P (eds.) (1979) " The Physics of Selenium and Tellurium "
Springer-Verlag,New York.
Gill W.D (1976) in " Photoconductivity and Related Phenomena" Ed.by Mort J and
Pai D.M ,Elsevier,Amsterdam.
Gil-Zambrano J.L and Juhasz C (1981) J.Phys.D , 14, 1661

- Gil-Zambrano J.L (1981) Ph.D Thesis, Univ. of London
- Glasstone S, Eyring H (1947) " The Theory of Rate Processes" McGraw-Hill, New York
- Golden D.M Benson S.W (1969) Chem.Rev., 69, 125
- Goodings E.P (1976) Chem.Soc.Rev., 5, 95
- Grammatica S, Mort J (1981) App.Phys.Lett., 38, 445
- Grant P.M, Batra I.P, (1979) Solid State Comm., 29, 255
- Greene R.L., Street G.B, Suter L.J (1975) Phys.Rev.Lett., 34, 577
- Gross B (1949) J.Chem.Phys., 17, 866
- " (1968) J.Electrochem.Soc., 115, 376
- " (1972a) J.Electrochem.Soc., 119, 855
- Gross B (1972b) J.Polym.Sci., Pt.A-2, 10, 1941
- Gross B (1980) in " Electrets ", Topics in Applied Physics. 33 Springer-Verlag, Berlin, Heidelberg, New York. Ed. by Sessler G.M.
- Gross B, Giacometti J.A, Leal Ferreira G.F (1981) IEEE Trans.on Nuclear Sci., 28, 4513
- Grossweiner L.I (1953) J.App.Phys., 24, 1306
- Guillaud G, Fornazero J, Maitrot M et.al. (1977) J.App.Phys., 48, 3428
- Gutmann F, Lyons L.F (1967) " Organic Semiconductors" Wiley and Sons, New York, London and Sydney.
- Halperin A, Braner A.A (1960) Phys.Rev., 117, 408
- Hamon B.V (1952) Proc.IEE., 99, 151
- Haridoss S, Perlman M.M, Carlone C (1982) J.App.Phys., 53, 6106
- Haridoss S, Perlmann M.M (1984) J.App.Phys., 55, 1332
- Heaviside O (1892) " Electrical Papers " Chelsea, New York, pp488
- Heijboer J (1978) in " Molecular Basis of Transitions and Relaxations " Ed. by Meier D.J, Gordon and Breach, London, New York. pp 75
- Hickmott (1975) J.App.Phys., 46, 2583
- Hino T (1975) J.App.Phys., 46, 1956
- Hoogenstraaten W (1958) Philips Res.Rep., 13, 515
- Hoshino Y (1981) J.App.Phys., 52, 5655
- Hoshino Y, Miyata H (1981) J.App.Phys., 52, 6214
- Hummel O, Scholl F (1971) "Infrared Analysis of Polymers, Resins and Additives : An Atlas." Vol.1, Pt.1 and 2. Wiley Interscience, New York, London.
- Huntsberger J.R (1981) J.Adhesion 13, 107
- Ikezaki K, Ishii T, Miura T (1984) Phys.Stat.Sol., A85, 615
- Ing S.W, Chiang Y.S (1967) J.Chem.Phys., 46, 478
- Ishiwata T, Fujimaki Y, Shimizu I, Kokado H (1980) J.App.Phys., 51, 444
- Jain K, Kumar N, Menendru P.C, (1979) J.Electrochem.Soc., 126, 1958
- Jain K, Rastogi A.C, Chopra K.L (1974) Phys.Stat.Sol., A21, 685
- Jonscher A.K (1967) Thin Sol.Films, 1, 213

- Juska G, Vengris A and Viscakas J.K (1974) in "Amorphous and Liquid Semiconductors", Proc. of the 5th. Intl. Conf. on Amorphous and Liquid Semiconductors, Garmish-Partenkirchen FDR, 1973. Ed. by Stuke J and Brenig W, Taylor and Francis, pp 363.
- Kao K.J, Bamji S.S and Perlman M.M (1979) J.App.Phys., 50, 8181
- Kasap S.O and Juhasz (1982) Photo.Sci.and Eng., 26, 239
- " " " (1985) J.Non.Cryst.Solids, 72, 23
- Kasap S.O, Juhasz C and Hardwick J.R (1985) Proc.3rd.Intl.Symp.on Industrial uses of Selenium and Tellurium, Stockholm. Darien CT: Selenium and Tellurium Development Assoc.
- Kao K.J, Bamji S.S, Perlman M.M (1979) J.App.Phys., 50, 8181
- Kasap S.O, Juhasz C (1982) Photo.Sci.and Eng., 26, 239
- " " (1985) J. Non Cryst.Sol., 72, 23
- Kato M, Nishioka Y (1985) App.Phys.Lett., 38, 445
- Kauzmann W (1948) Chem.Rev., 43, 219
- Keiss H (1978) R C A Rev., 40, 59
- Keith H.D (1963) in " Physics and Chemistry of the Organic Solid State " Vol. 1 Ed.by Fox D., Labes M.M, Weisberger A, Interscience Pub., New York, London. pp 462
- Kerr J.A (1966) Chem.Rev., 66, 465
- Kessler A, Caffyn J.E (1972) J.Phys.C 5, 1134
- Kimura A, Yoshimoto S, Akana Y, Hirata H et.al. (1970) J.Polym.Sci., A2, 643
- Kivits P, Hagebeuk H.J.L (1977) J. of Luminescence, 15, 1
- Kiyota K, Teshima A, Tanaka M (1980) Photo.Sci.and Eng., 24, 289
- Kojima K, Maeda A, Ieda M (1976) Jap.J. of App. Phys., 15, 2457
- Kolomietz B.T, Lyubin V.M, Averyanov V.L, (1970) Materials Res. Bull., 5, 655
- Kosaki M, Sugiyama K, Ieda M (1971) J.App. Phys., 42, 3388
- Kovacs (1958) J.Polym.Sci., 30, 131
- Lacabanne C, Chatain D (1973) J.Polym.Sci.: Polym.Phys., 11, 2315
- Laj C, Berge P (1966) C.R. Acad.Sci. Paris, B263, 380
- Lanyon H.P.D (1964) J.App.Phys., 35, 1516
- Leal Ferreira G.F (1974) J.Non Metals, 2, 109
- Leal Ferreira G.F, Gross B (1973) J.Non Metals, 1, 129
- Legros D, Lewiner J (1973) J.Acoust.Soc.Am., 53, 1663
- Lewis T.J (1984) IEEE Trans. on Electrical Insulation, EI 19, 210
- Lichtmann L.S, Fitchen D.B, (1979) Bull.Am.Phys.Soc., 24, 327
- Lindemann M.K (1971) in " Poly vinylacetals " Encyclo. of Polym. Sci. and Tech., Wiley, 14, 209
- Matsuura M, Suzuki K (1979) J.Materials Sci., 14, 395
- Mc Crum N.G, Read B.E, Williams G (1967) " Anelastic and Dielectric Effects in Polymeric Solids " Wiley, New York
- Mascarenhas S (1980) in Sessler (1980), chap. 6 .

- Mc Keever S.W.S, Hughes D.M (1975) J.Phys.D 8, 1520
- Mehendru P.C, Jain K, Kumar N (1980) Thin Solid Films,70, 7
- Mehra R.M, Mathur P.C, Kathuria A.K et.al. (1977) Phys.Stat.Sol.,A41, K189
- Mehra R.M, Radhey S, Mathur P.C (1979) Phys.Rev., 19, 6525
- Meier H (1974) " Organic Semiconductors " Verlag Chemie, Weinheim.
- Miyamoto T, Shibayama K (1973) J.App.Phys., 44, 5372
- Monsanto Co., (1977) Technical Bull., No.6070 D, St.Louis,MO.
- Moran P.R, Fields D.E (1974) J.App.Phys., 45, 3266
- Mort J (1972) Phys.Rev., B 5, 3329
- Mort J et.al. (1980) Photo.Sci.and Eng., 24, 241
- Mort J, Pfister G (1982) in " Electronic Properties of Polymers " Wiley and Sons, pp 215.
- Mort J et.al. (1984) J.App. Phys., 55, 3197
- Mott N.F, Gurney R.W (1948) "Electronic Processes in Ionic Crystals " Oxford Univ.Press
- Mott N.F, Davis E.A (1979) " Electronic Processes in Non Crystalline Materials " 2 nd. Edn., Clarendon Press, Oxford.
- Muller P (1974) Phys.Stat.Sol., A23, 165
- " (1976) Phys.Stat. Sol., A33, 543
- Murphy P.V (1963) J.Phys.Chem.Solids, 24, 329
- Nakamae K , Sumiya K (1984) J.Polym.Sci.:Polym.Symposia,71,109
- Natta G, Corradini (1960) Nuovo Cimenta, 15, Suppl. 1, 40
- Natta G, Corradini, Bassi I.W (1960) Nuovo Cimenta , 15, Suppl. 1, 68
- Nedetzka T, Reichle M, Mayer A, Vogel H (1970) J.Phys.Chem., 74, 2652
- Neyhart J.H (1966) Photo. Sci. Eng., 10, 126
- Ong P.H, van Turnhout J (1973) in " Electrets , Charge Storage and Transport in Dielectrics " Ed. by Perlman M.M , Electrochemical Soc., Princeton. pp 213
- O'Reilly J.M , Erhardt P.F (1973) in " Second International Conf. on Electrophotography " Ed.by White D.R., Society of Photo.Scientists and Engineers, Washington D C , pp 95
- Owen A.E , Spear W.E (1976) Phys. and Chem. of Glasses, 17, 174
- Parthasarathy G, Gopal E.S.R (1984) Phys.Stat. Sol., A85, K165
- Parthasarathy R, Rao K.J, Rao C.N.R (1983) Chem.Soc.Rev.,12, 361
- Perlman M.M and Creswell R.A (1971) J App.Phys.,42 ,531
- Perlman M.M (Ed.) (1973) "Electrets, Charge Storage and Transport in Dielectrics" Electrochemical Soc., Princeton.
- Perlman M.M, Unger S (1974) J.Appl.Phys., 45, 2389
- Pfister G (1979) Contemp. Phys., 20, 449
- Pfister G, Griffiths C.H (1978) Phys. Rev. Lett., 40, 659

- Pfister G, Scher H (1977) in " Amorphous and Liquid Semiconductors " Proc. 7th. Intl. Conf.on Amorphous and Liquid Semiconductors,Ed. by Spear W.E.,Grenoble.
- Pohl H.A (1962) in " Modern Aspects of The Vitreous State " Vol.1.,Ed.by Mac Kenzie J.D.,Butterworth,London.
- Randall J.T,Wilkins M.H.F (1945) Proc. Royal Soc. London, A184, 366
- Ranigar J.H, Fleming R.J (1972) J.Polym.Sci.:Polym.Phys., 10, 1979
- Reiser A, Lock M.W.B,Knight J (1969) Trans.Faraday Soc., 65, 2168
- Renecker D.H, Geil P.H (1960) J.App.Phys.,31, 1916
- Ritsko J.J (1982) in "Electronic Properties of Polymers" Ed.by Mort J and Pfister G,John Wiley and Sons,New York.pp.13
- Roberts G.E ,White E.F.T (1973) in " The Physics Of Glassy Polymers " Ed. by Haward R.N., App.Sci. and Publishers Ltd.,London ,pp.153
- Rombach L.H (1964) U.S. Pat. No.3,153,009 to du Pont de Nemours and Co.Inc.
- Saito S,Sasabe H,Nakajima T,Yada K (1968) J.Polym. Sci.Pt.A2, 6, 463
- Salaneck W.R. (1978) Phys.Rev.Lett.,40,60
- Sharma R,Sud V (1981) J.Phys.D, 14, 1671
- Schaffert R.M (1975) " Electrophotography ",Focal Press,London ,New York.
- " (1978) Photo.Sci.and Eng., 22,149
- Schmidlin F.W (1976) in "Photoconductivity and Related Phenomena " Ed.by Mort J and Pai D.M ,Elsevier New York,Chap. 11
- Schonhorn H ,Ryan F.W (1974) J.App.Polym.Sci., 18, 235
- Schottmiller J.C, Tabak M.D,Lucovsky G,Ward A (1970) J.of Non Cryst.Sol.,4,80
- Schulz G,Muller G (1952) Kunststoffe, 42, 298
- Schwarzl F.R and Struik L.C.E (1967-1968) Adv.Mol.Relaxation Processes, 1, 201
- Sessler G.M (1977) in "Intl. Symposium on Electrets and Dielectrics " Acad.Brasil de Ciencias,Rio de Janeiro,pp. 321
- Sessler G.M (1980) Ed. " Electrets " Topics in App.Phys.,Vol 33,Springer Berlin Heidelberg.
- Sessler G.M, West J.E (1962) J.Acoust.soc.Am., 34,1787
- " " (1976) J.App.Phys., 47, 3480
- Shahin M.M (1969) Applied Optics, Suppl. 3,106
- " (1966) J.Chem.Phys.,45, 2600
- Shahbazian S.M (1984) The Journal of Photo. Sci., 32, 111
- Shen M.C Eisenberg A (1970) Rubber Chem.and Tech.,43,95
- Sherman P.D (1978) in " Butyraldehyde " Encyclopaedia of Chem.Technology 3rd. Edition,Wiley. Vol. 4.
- Shimizu I,Komatsu T,Inoue E (1980) Photo Sci. and Eng., 24, 251
- Silins E.A (1980) "Organic Molecular Crystals " Springer-Verlag,Berlin
- Simmons J.G, Taylor G.W (1972) Phys.Rev., B 6, 4804
- Smith R.A (1978) " Semiconductors " 2nd.Edn.,Cambridge Univ.Press.
- Sodolski H (1984) Phys.Stat.Sol., A 86, 703

- Southgate P.D (1976) App.Phys.Lett.,28, 250
- Street R.A,Yoffe A.D (1972) Thin Sol.Films, 11, 161
- Street R.A,Clarke T.C (1981) IBM J.Res.and Dev., 25, 51
- Stroupe J.D,Hughes R.E (1958) J.Am.Chem.Soc.,80, 2341
- Stupp S.I,Carr S.H (1977) J.Polym.Sci.: Polym.Phys.,15, 485
- Sussner H, Dransfeld K (1978) J.Polym.Sci.:Polym.Phys.,16, 529
- Tabak M.D ,Hillegas W.J (1971) J.Vac.Sci.and Tech.,9, 387
- Takahashi Y (1961 a) J.Phys.Soc.Japan, 16,1024
- " (1961 b) J.App.Polym.Sci., 5, 468
- Takamatsu T ,Fukada E (1970) Polym. J., 1, 101
- Taniguchi Y, Yamamoto H et.al. (1981) J.App. Phys., 52,7261
- Tateishi K, Hoshino Y (1984) IEEE Trans. on Elec. Devices, ED 31, 793
- Thurzo I, Barancok B et.al. (1975) J.Non Cryst. Sol.,18, 129
- Toyoshima K (1973) in "Poly vinylalcohol " Ed.by Finch C.A,Wiley,London.pp. 17
- Turnbull T, Cohen M.H (1961) J.Chem .Phys., 34, 120
- Vanderschueren J,Gasiot J (1979) in "Thermally Stimulated Relaxation in Solids" Edited by Braunlich P .Topics in Applied Physics,Vol.37,Springer-Verlag Berlin,Heidelberg,New York .Chap.4
- van der Ziel (1968) " Solid State Physical Electronics "2nd.Edn.,Prentice Hall,N.J.
- van Turnhout J (1971) Polym.J., 2, 1973
- " (1973) in "Electrets,Charge Storage and Transport in Dielectrics" Ed. by Perlman M.M, Electrochem.Soc.,Princeton.pp230
- van Turnhout J (1975) " Thermally Stimulated Discharge of Polymer Electrets " Elsevier, Amsterdam
- van Turnhout J, Ong P.H (1975) IEE Conf. on Dielectric Measurements and Applications,Cambridge. pp.68
- van Turnhout J et.al. (1976) Staub-Reinhalt Luft., 36,36
- van Turnhout J,Klaase P.T.A,Ong P.H,Struik L.C.E (1977) J.Electrostatics, 3, 171
- Vengris S.A,Viscakas J.K ,Sakalas A.P,Juska G (1972) Soviet Phys.Semicon.,6,903
- von Seggern H (1979) J.App. Phys., 50, 7039
- " (1981 a) J.App. Phys., 52, 4081
- " (1981 b) J.App. Phys., 52, 4086
- von Seggern H ,West J.E (1984) J.App. Phys.,55, 2754
- Vosteen R.E (1974) Proc. 9 th. Ann. Meeting,IEEE Industry Appn.Soc.,ES-WED-AM1 799-810.
- Voss A,Starck W (1930) German Pat.No. 737,630 to I.G Farben Industrie A.G
- Wada Y,Perlman M.M,Kokado H (Eds.) (1979) "Charge Storage,Charge Transport and Electrostatics with their Applications" ,Elsevier Amsterdam and Kodansha Ltd. Tokyo.

- Walatka V.V, Labes M.M, Perlstein J.H (1973) Phys. Rev. Lett., 31, 1139
- Walker D.K, Jefimenko O (1973) in "Electrets , Charge Storage and Transport in Dielectrics " Ed. by Perlman MM , Electrochemical Soc., Princeton, pp.455
- Watson P.K (1979) in " Electrostatics 1979 " Inst of Phys. Conf. Series No. 48, Bristol, London.
- Wendlandt W.W (1974) "Thermal Methods of Analysis" Wiley, New York
- Williams E.M (1984) "The Physics and Tech.of Xerographic Processes" John Wiley and Sons, New York, Chichester, Toronto.
- Weiehe A (1941) Kunststoffe, 31, 52
- Williams M.L, Landel R.F, Ferry J.D (1955) J.Am.Chem.Soc., 77, 3701
- Wintle H.J (1971) J. Appl.Phys., 42, 4724
- " (1974) J.Non Cryst. Sol., 15, 471
- Yamaguchi T, Takahashi K, Kokado H, Inoue E (1961) Denshi Shashin (Electrophotography Japan), 3, 12
- Young R.J (1981) " Introduction to Polymers " Chapman and Hall, London, New York
- Zielinski M ,Kryszewski M (1977) Phys.Stat.Sol., A 42, 305
- Zingaro R.A ,Cooper W.C (1974) Editors, " Selenium " van Nostrand Rheinhold, New York
- Bond W L (1954) J. Opt. Soc. Am 44, 429
- Booth G L (1968) " The Sci. and Tech. of Polymer Films " Ed. by Sweeting OJ Interscience N York , Vol.1, Chap.11